DISSERTATION

VULNERABILITY OF U.S. RIVER BASINS TO WATER SHORTAGE OVER THE 21ST CENTURY

Submitted by

Hadi Heidari

Department of Civil and Environmental Engineering

In partial fulfillment of the requirements

For the Degree of Doctor of Philosophy

Colorado State University

Fort Collins, Colorado

Spring 2021

Doctoral Committee:

Advisor: Mazdak Arabi

Travis Warziniack
Thomas C Brown
Ryan Bailey
Christopher G. Goemans

ABSTRACT

VULNERABILITY OF U.S. RIVER BASINS TO WATER SHORTAGE OVER THE 21ST CENTURY

Future changes in climate and population across the United States may cause a decrease in freshwater availability and an increase in water demand. These trends may lead to more frequent water shortage conditions when water demand exceeds water supply. The enhanced characterizations of changes in both long-term anomalies such as aridity and evaporative indices and short-term anomalies such as multi-year and interannual water shortage events in a changing environment are requisite to the appropriate management and planning of future water resources, and improved implementation of regional adaptation and mitigation strategies. The main goal of this dissertation is thus to assess shifts in hydroclimatic conditions and water shortage (IDF) relationships across the conterminous United States (CONUS) over the 21st century.

To achieve this goal, first, the effects of climate change on the regional hydroclimatology of U.S. river basins were assessed over the 21st Century to determine regions with prolonged dry or wetting periods. This analysis shows that U.S. river basins within the CONUS can be clustered into seven groups with unique hydroclimatic behaviors in response to climate change that are highly associated with regional landform, climate, and ecosystems of river basins. The South United States is more likely to experience warmer and drier conditions meaning higher chances of aridification. Second, the impact of climate change on hydroclimatic conditions of U.S. national forests (NFs) and national grasslands (NGs) was investigated. The results of this study indicate that NFs and NGs are more likely to experience larger changes in hydroclimatic variables

compared to the average of the United States. The findings help environmental scientists and forest managers to mitigate the negative consequences of climate change on forest and grassland resources. Third, shifts in hydroclimatology of U.S. megaregions in response to climate change were investigated. This analysis reveals that Houston may experience more arid climatic conditions with higher evaporative loss of freshwater resources in the future. These steps provide an improved understanding of the effects of climate change on the regional aridification or desertification across the CONUS.

To accomplish the goal of the study, fourth, a probabilistic approach was developed to improve the characterization of both within-year and over-year socioeconomic droughts in a changing environment. The proposed approach provides a procedure to update sub-annual socioeconomic drought IDF relationships while taking into account changes in water supply and demand. Fifth, the developed probabilistic approach was applied to examine the effects of urban development patterns, i.e., sprawl versus high-density development, on the socioeconomic drought characteristics. The results of this study highlight that urban regions under the sprawl development pattern are likely to experience more frequent socioeconomic drought events with higher intensity and longer duration compared to the high-density development pattern. Finally, the developed approach was implemented across the CONUS to characterize vulnerability of U.S. river basins to water shortage from 1986-2015 to 2070-2099 periods. The results show that prolonged water shortage conditions in drier basins and interannual water shortage events in wetter basins are likely to be the main concerns in the future and should gain more attention in future water resource planning and management.

ACKNOWLEDGMENTS

I would like to thank my advisor, Professor Dr. Mazdak Arabi, for providing me with this great opportunity to pursue my Ph.D. at Colorado State University (CSU). His knowledge and deep understanding were greatly influential and helpful for me to conduct my Ph.D. research. Without his comprehensive support and encouragement, I would have not been able to finish this journey. I would also like to thank my committee member, Dr. Travis Warziniack, who provided continuous support and guidance during development of my research. I would like to thank my committee members, Drs. Thomas C Brown, Ryan Bailey, and Christopher G. Goemans, for their valuable feedback and insightful comments. Also, I would like to thank Dr. Shih-Chieh Kao, and Dr. Sybil Sharvelle for sharing their valuable thoughts and ideas that greatly influenced the work presented in this dissertation.

In memory of Dr. Jorge Ramirez and Dr. Andre Dozier, I would like to offer special thanks to them, who, although no longer with us, continue to inspire by their dedication to the students they served over the course of their career.

This work was funded by NSF Sustainability Research Network (SRN) Cooperative Agreement 1444758 as part of the Urban Water Innovation Network (UWIN) and a cooperative agreement with US Forest Service Research and Development, Rocky Mountain Research Station.

I would like to thank my friends and colleagues at our research lab whose company, assistance, and friendship was always heartwarming. I would also like to thank my parents who have always supported and respected my decisions throughout my life and have always been there for me through thick and thin.

Last but not least, I have to thank my lovely wife, Shadi, for her patience, encouragement, and continuous and unconditional love and support throughout the completion of this program and dedicate this dissertation to her as a gesture of my appreciation and gratitude towards her kindness and support. Without her unconditional support, this dissertation would not have been accomplished.

TABLE OF CONTENTS

LIST OF TABLES

LIST OF FIGURES

CHAPTER 1.

INTRODUCTION

Water Shortage is an inevitable and complex phenomenon that has plagued civilization throughout history by affecting water and natural resources (Cook et al., 2015; Greve et al., 2015; Hagenlocher et al., 2019; Redmond, 2002). The water shortage conditions (or socioeconomic drought) occurs when water demand exceeds water supply (Yevjevich, 1967; Salas et al., 2005). Future changes in climate and population can beget shifts in water supply and demand (Naz et al., 2016; Wang et al., 2016; Mahat et al., 2017; Brown et al., 2019). As the balance between water supply and demand becomes more unequal, water shortage characteristics may shift at various spatial and temporal scales (Mehran et al., 2015, 2017; Rajsekhar et al., 2015; Salas et al., 2018).

This dissertation aimed to characterize the effects of climate change in both long-term anomalies such as aridity and evaporative indices and short-term anomalies such as sub-annual water shortage events across the United States over the 21st century. The assessment of future water shortage condition and understanding mechanisms behind that can play an important role in future water resource management and planning that is requisite to the appropriate drought monitoring, early warning systems, and adaptation strategies (Andreadis & Lettenmaier, 2006; Hagenlocher et al., 2019; Svoboda et al., 2002; Tu et al., 2018).

Recent water shortage events across the conterminous United States (CONUS) have shown that severe water shortage events can develop very rapidly if climate change leads to shifts in hydroclimatic conditions in a region (Andreadis & Lettenmaier, 2006; Piemontese et al., 2019). Assessing shifts in regional hydroclimatic conditions of river basins across the CONUS can be a different way of approaching future water resource management (Maliva & Missimer, 2013).

Long-term changes in the relationship between climate and water budgets of river basins may lead to aridification or desertification.

This dissertation first investigated shifts in regional hydroclimatic conditions of U.S. river basins in response to climate change over the 21st Century (Heidari et al., 2020b). The integrated effects of climate change on the hydrology of a river basin were assessed using the Budyko framework by the combination of changes in aridity and evaporative indices. Other objectives of this study were to identify regions with unique hydroclimatic behavior in response to climate change; assess the most important factors which differentiate the hydroclimatic responses; and determine most prone regions for hydroclimatic changes across the CONUS over the 21st century. This study provides insights for decision-makers and water planners to prepare for changes in factors that influence the vulnerability to water shortage.

Future shifts in regional hydroclimatic conditions may have severe impacts on natural resources such as national forests (NFs) and national grasslands (NGs) across the United States (Allen et al., 2010; Astigarraga et al., 2020; Bonan, 2008; Esquivel-Muelbert et al., 2019; Jeong et al., 2016; Jump et al., 2017; McIntyre et al., 2015). NFs and NGs provide a wide range of services that have broadened to hydrological, ecological, social, economic, recreational, and aesthetic (Bonan, 2008; Duan et al., 2016; Yannian, 1990). Long-term shifts in hydroclimatology of NFs and NGs may cause a decrease in freshwater availability and changes in the structure and composition of forests and grasslands (Allen et al., 2010; Astigarraga et al., 2020; Bonan, 2008; Esquivel-Muelbert et al., 2019; Jeong et al., 2016; Jump et al., 2017; McIntyre et al., 2015).

This dissertation specifically assessed the effects of climate change on hydroclimatic conditions and basin characteristics of NFs and NGs across the CONUS over the 21st century. Although significant progress has been made in understanding the effects of climate change on

U.S. forests and grasslands (Bonan, 2008; Esquivel-Muelbert et al., 2019; Fekety et al., 2020; Littell et al., 2012; Rehfeldt et al., 2009; Yannian, 1990), there is a lack of comparative studies for characterizing the effects of climate change on regional hydroclimatology and basin characteristics of NFs and NGs at the local and national scales (Littell et al., 2012). Improved assessments of potential shifts in hydroclimatic conditions of NFs and NGs can help forest managers to mitigate the negative consequences of climate change such as deforestation (Peterson et al., 2011).

Future shifts in regional hydroclimatology of the United States may furthermore significantly affect U.S. megaregions. The megaregions are large contiguous geographical regions across the CONUS that encompasses most population and economic growth of the United States (Hagler, 2009; Nelson, 2017; Nelson and Rae, 2016). Hydroclimatic change may exacerbate existing problems in the U.S. megaregions by negative consequences on energy sources, water supply, air quality, habitat preservation, ecosystem, and natural resources (Ashfaq et al., 2013; Ponce Campos et al., 2013; Greve et al., 2014).

This dissertation specifically investigated the effects of climate change on the hydroclimatic conditions of fourteen U.S. megaregions including Seattle, San Francisco, Los Angeles, San Diego, Denver, Phoenix, Chicago, Miami, Washington D.C., Philadelphia, New York, Boston, Houston, and Atlanta. The improved understanding of future shifts in long-term hydroclimatology of U.S. megaregions may help urban planners to attenuate the potential consequences of climate change on cities and strengthen economic prosperity (Brown et al., 2019; Butler et al., 2017; McDonald et al., 2011).

By the improved understanding of the effects of climate change on the hydroclimatology of U.S. river basins, national forests, national grasslands, and megaregions, we assessed changes in future water shortage properties across the United States in this dissertation. Climate change

combined with population growth can cause water shortage conditions at various scales from short-time (interannual) to long-time (decadal drought) events (Evans & Sadler, 2008; Jaeger et al., 2017; Wang et al., 2019). Both sub-annual and annual events may lead to significant consequences and disrupt water supply and agricultural systems (Foti et al., 2014a; Hao et al., 2018; Mehran et al., 2015; Otkin et al., 2018; Rajsekhar et al., 2015).

This dissertation developed a novel probabilistic approach to simultaneously improve characterization of within-year and over-year socioeconomic drought intensity-duration-frequency (IDF) relationships in response to shifts in water supply and demand conditions. We addressed three important considerations in this approach. First, shifts in both water supply and demand conditions were considered. Second, socioeconomic drought properties were characterized at a sub-annual scale. Third, a mixture Gamma-Generalized Pareto (Gamma-GPD) model was proposed to enhance the characterization of both non-extreme and extreme socioeconomic droughts (Heidari et al., 2020a).

We first evaluated the application of the proposed approach in the City of Fort Collins, Colorado, water supply system. The enhanced characterization of sub-annual socioeconomic drought IDF relationships undergoing climate and socioeconomic changes allows the implementation of effective adaptation and mitigation strategies to reduce the impact of droughts on communities (Brown et al., 2019; Gutzler & Nims, 2006; Warziniack & Brown, 2019).

Although urban regions are being threatened by water shortage conditions due to climate change and rapid population growth, the role of urban development patterns on future socioeconomic droughts is rarely investigated (Bounoua et al., 2020; Forrest et al., 2020; Hemmati et al., 2020; Saraswat et al., 2017). The development of urban areas in the west and southwest of the United States has been exacerbated at a significant rate (Hummel, 2020). While the rapid

urbanization seems inevitable in the United States, understanding a sustainable way to mitigate potential negative consequences on urban water resources in the future is an important challenge (Butler et al., 2017; Forrest et al., 2020; Saraswat et al., 2017).

In this dissertation, we investigated and compared future changes in socioeconomic drought IDF relationships under the sprawl development pattern versus the high-density development pattern for the City of Fort Collins, Colorado as a representative region that is rapidly developing over the last decades. Understanding how urban development patterns may affect municipal water shortage leads to developing an adaptive path to save water supply, meet future water demand, and mitigate drought impacts.

Although diverse definitions, classifications, and methods have been used in previous studies for monitoring and assessing drought events in the United States, a few studies discussed the effects of shifts in both water supply and water demand on the intensity, duration, and frequency (IDF) relationships of water shortage conditions across the United States at various spatial and temporal scales (Guo et al., 2019; Heidari et al., 2020a; Salas et al., 2018; Tu et al., 2018). More research is needed to support actionable managements to mitigate negative impacts.

This dissertation applied the developed probabilistic approach across the CONUS at the 4-digit hydrologic unit code (HUC4) basin scale to characterize changes in IDF relationships in response to shift in water supply and water demand in light of population growth and climate change. The findings of this study can help decision-makers and water managers to assess and improve the ability of different U.S. water supply systems to future water shortage and address the considerations in water resource planning and management under considerable shifts in water supply and demand conditions.

Overall, the main goal of this dissertation was to assess future shifts in both hydroclimatic conditions and water shortage IDF relationships across the conterminous United States (CONUS) over the 21st century. Specifically, the objectives are to: 1) investigate shifts in regional hydroclimatic conditions of U.S. river basins in response to climate change over the 21st century; 2) assess the impacts of climate change on the hydroclimatology of national forests (NFs) and national grasslands (NGs); 3) evaluate shifts in hydroclimatology of U.S. megaregions; 4) develop a probabilistic approach to improved characterization of sub-annual socioeconomic drought IDF relationships in a changing environment; 5) investigate the role of urban development patterns on changes in future drought IDF relationships; and 6) characterize shifts in water shortage IDF relationships of U.S. river basins from the interannual to decadal scales under shifts in both water supply and water demand conditions.

These steps can provide an improved understanding of the effects of climate change on future water shortage across the United States to help decision-makers, urban planners, and water, land, and forest managers to be prepared and appropriately react to future water shortage conditions in the United States.

CHAPTER 2.

ASSESSING SHIFTS IN REGIONAL HYDROCLIMATIC CONDITIONS OF U.S. RIVER BASINS IN RESPONSE TO CLIMATE CHANGE OVER THE 21ST CENTURY

Characterization of shifts in regional hydroclimatic conditions helps reduce negative consequences on agriculture, environment, economy, society, and ecosystem. This study assesses shifts in regional hydroclimatic conditions across the continental United States in response to climate change over the 21st Century. The hydrological responses of five downscaled climate models from the Multivariate Adaptive Constructed Analogs (MACA) dataset ranging from the driest to wettest and least warm to hottest were simulated using the Variable Infiltration Capacity (VIC) model. Shifts in regional hydroclimatic conditions at 8-digit hydrologic unit scale (HUC8) were evaluated by the magnitude and direction of movements in the Budyko space. HUC8 river basins were then clustered into seven unique hydroclimatic behavior groups using the K-means method. A tree classification method was proposed to illustrate the relationships between hydroclimatic behavior groups and regional characteristics. The results indicate that hydroclimatic responses may vary from a river basin to another, but basins in the same neighborhood follow a similar movement in the Budyko space. The systematic hydroclimatic behavior of river basins is highly associated with their regional landform, climate, and ecosystem characteristics. Most HUC8s with Mountain, Plateau and Basin landform types will likely experience less arid conditions. However, most HUC8s with Plain landform types behave differently according to the regional ecosystem and climate. This study provides a potential roadmap of shifts in regional hydroclimatic conditions of U.S river basins, which can be used to improve regional preparedness and ability of various sectors to mitigate or adapt to the impacts of future hydroclimate change.

2.1. Introduction

Climate change may significantly beget shifts in long-term hydroclimatic conditions of river basins (Jaramillo et al., 2018; Xing et al., 2018; Piemontese et al., 2019; Zaninelli et al., 2019) and cause serious impacts on the environment, agriculture, economies and ecosystems (Ashfaq et al., 2013; Ponce Campos et al., 2013; Greve et al., 2014; Hemmati et al., 2020). Characterization of shifts in regional hydroclimatic conditions can help water managers and decision-makers to mitigate potential consequences of climate change on various sectors (Destouni et al., 2013). This study investigates future shifts in regional hydroclimatic conditions of river basins across the conterminous United States (CONUS) in response to climate change over the 21st century.

In the CONUS, hydroclimatic parameters such as precipitation, temperature, evaporation, water yield (or total runoff), and potential evapotranspiration have been projected to change over the 21st century (Sankarasubramanian & Vogel, 2003; Hay et al., 2011; Sanford & Selnick, 2013; Mahat et al., 2017). The CONUS covers broad physiographic, ecological, and climatic conditions. Thus, regional hydroclimatic shifts in response to climate change can be quite different from one region to another (Abatzoglou & Ficklin, 2017). Regional characterization of hydroclimatic changes is vital to improve implementation of region-specific adaptation and mitigation strategies (Piemontese et al., 2019; Zaninelli et al., 2019).

Most previous studies that discussed changes in hydroclimatiology of river basins within the CONUS focused on particular basins or individual parameters (e.g., streamflow, precipitation, evaporation) (Wang & Hejazi, 2011; Renner et al., 2012; Ashfaq et al., 2013; Weiskel et al., 2014; Naz et al., 2016). A few studies have assessed the integrated shifts in hydroclimatic conditions of river basins as the combination of changes in aridity and evaporative indices across the CONUS

to understand how different river basins with varying climatic, ecological and physiographical characteristics respond to climate change (Abatzoglou & Ficklin, 2017; Piemontese et al., 2019).

One effective way to evaluate the combined hydroclimatic changes is through the Budyko framework (Van der Velde et al., 2014; Piemontese et al., 2019; Zaninelli et al., 2019). The Budyko framework describes a relationship between evaporative and aridity indices (Budyko, 1974, 1982). A number of previous studies have used the Budyko framework to estimate actual evaporation and streamflow from long-term water and energy balances (McKee, 1993; Yang et al., 2006; Reis et al., 2013; Rouholahnejad Freund & Kirchner, 2017; Zhang et al., 2017; Deng et al., 2018; Xing et al., 2018; Li et al., 2019). A river basin can move over time in the Budyko space due to a combination of shifts in aridity and evaporative indices (Van der Velde et al., 2014; Piemontese et al., 2019; Zaninelli et al., 2019). Additionally, movement in the Budyko space can be characterized by a magnitude and direction (Jaramillo et al., 2018; Piemontese et al., 2019; Zaninelli et al., 2019). Direction can determine regional differentiation and magnitude can characterize the most sensitive regions under climate change (Van der Velde et al., 2014).

This study assesses regional hydroclimatic changes induced by shifts in the Budyko space across the CONUS over the 21st Century at an 8-digit hydrologic unit code (HUC8) basin scale under a range of possible climate change models. Specifically, the objectives are to: 1) evaluate changes in combined hydroclimatic variables in response to climate change using Budyko space; 2) identify regions with unique hydroclimatic behavior in response to climate change using the K-means clustering method; 3) assess the most important factors which differentiates the hydroclimatic responses using the tree classification method; and 4) determine hotspot regions of hydroclimatic changes across the CONUS over 21st century. This study provides a potential roadmap of changes in regional hydroclimatic conditions across the CONUS, which can help

decision-makers and water managers to implement region-specific adaptation and mitigation strategies for regional water resource management.

2.2. Material and Methods

Future changes in climatic variables were obtained from the downscaled Multivariate Adaptive Constructed Analogs (MACA) datasets. The projected climatic variables were then used as inputs to the Variable Infiltration Capacity (VIC version 4.1) model to evaluate the hydrologic responses of future climate projections. The Budyko space was applied to estimate changes in hydroclimatic conditions of the CONUS at HUC8 river basin scales. HUC8 river basins across the CONUS were clustered into groups with unique hydroclimatic behavior in response to climate change using the K-means method. Then, the association between hydroclimatic behavior groups and basin characteristics such as regional climate, landform, and ecosystem was assessed using the tree classification method. The 1986-2015 period was used as the baseline to represent current conditions while the 2070-2099 period represented the future conditions.

2.2.1. Hydroclimatic Projections

Raw global climate model (GCM) outputs cannot be used for regional hydroclimatic assessments due to the coarse resolution of grid cells, approximately on the order of 150-200 km (Naz et al., 2016). Thus, the downscaled MACA datasets were used to provide possible future climate change models in this study (Abatzoglou & Brown, 2012). The MACA climate dataset includes 20 models that were downscaled for the entire CONUS at the grid size of ~4 km (1/24 degree) under the RCP 4.5 and RCP 8.5 emission scenarios. Joyce and Coulson (2020) selected five MACA climate models for the CONUS to represent a possible range of temperature and precipitation over the 21st century including the wettest, driest, hottest and the least warm models, and one model located near the middle of these ranges (Table 2.1) (Joyce and Coulson, 2020). In

this study, we used these five selected MACA models to study the shifts of combined hydroclimate conditions. It should be noted that HOT, WARM, WET, and DRY, respectively, indicate the MACA climate models that are on average the hottest, warmest, wettest, and driest models at the conterminous scale. For example, the DRY climate model is not always the driest in all river basins across the CONUS.

Table 2.1. Projected MACA climate models (Joyce and Coulson., 2020).

	HOT	**WARM**	**WET**	**DRY**	**MIDDLE**
Name	HadGEM2-ES365	MRI-CGCM3	CNRM-CM5	IPSL-CM5A-MR	NorESM1-M
Model Agency	Met Office Hadley Center, UK	Meteorological Research Institute, Japan	National Centre of Meteorological Research, France	Institute Pierre Simon Laplace, France	Norwegian Climate Center, Norway

The MACA climate dataset includes forcing data such as the maximum daily temperature near surface (tasmax), the minimum daily temperature near surface (tasmin), the average daily precipitation amount at surface (pr), the average daily eastward component of wind near surface (uas), and the average daily northward component of wind near surface (vas). The total wind speed was calculated in this study as the combination of the eastward and northward winds ($\sqrt{uas^2 + vas^2}$).

A good representation of the current climate is indeed a necessary condition required to realistically simulate future climate changes. Figure A-1 compares the 30-yr average of annual precipitation for each HUC8 river basin over the historical period (1986-2015). The 30-yr average values for each HUC8 river basin are approximately the same meaning that the variation between climate models is not significant at the 30-year average scale. Additionally, 30-yr average of all selected climate models over the historical period has a high correlation with the selected baseline historical model that is the combination of Daymet and PRISM. The MIDDLE climate model with

RCP 4.5 shows the strongest linear correlation (0.9964) between the 30-year average of the observed and simulated mean annual water yield.

We used the term baseline to denote a historical period from 1986 to 2015 as a basis for comparison with future climate. The historical climate data were obtained from a combination of Daymet (Thornton et al., 1997) and the Parameter-elevation Regressions on Independent Slopes Model (PRISM, Daly et al., 2008) datasets. Precipitation and daily maximum and minimum temperature were calculated by Daymet and biased corrected with PRISM at the monthly scale. Additionally, wind speed was calculated from the North American Regional Reanalysis (NARR) dataset (Mesinger et al., 2006). Readers are referred to Oubeidillah et al. (2014) and Naz et al. (2016) for the details about this historic forcing dataset.

In addition to the selected MACA models, we also conducted VIC simulation using this forcing dataset to estimate the baseline hydrologic conditions. The VIC version 4.1 hydrologic model (Liang et al., 1994) was set up at the grid size of ~4 km (1/24 degree) to simulate the hydrologic responses driven by different forcing datasets. The VIC model is a semi-distributed macroscale model that solves full water and energy balances using the variable infiltration capacity curves (Cherkauer & Lettenmaier, 2003). The VIC model has been widely used to simulate streamflow over a number of large river basins in North America (Andreadis & Lettenmaier, 2006). Topography, soil characteristics, vegetation, land surface classification, and meteorological forcing are key hydrological inputs to the VIC model. Required meteorological forcing includes daily minimum and maximum temperature, precipitation, and wind speed. The VIC model uses the Penman–Monteith equation to estimate potential evapotranspiration.

We obtained the VIC model parameters also from Oubeidillah et al. (2014) and Naz et al. (2016), which were calibrated using the historic monthly runoff from the USGS WaterWatch

runoff dataset (Brakebill et al., 2011) at each HUC8 unit. The aggregated monthly runoff obtained from the USGS National Water Information System gauge observations (WaterWatch dataset) (Brakebill et al., 2011) was used to calibrate the VIC model for each HUC8 basin. The naturalized streamflow routed to gauge locations has been traditionally used to calibrate hydrological models. However, calibrating the VIC model using the WaterWatch monthly runoff data leads to the homogenous application of the VIC model for all grid cells with the same resolution, and the parameter transfer to ungauged basins is not required.

To calibrate the VIC model, the simulated monthly total streamflow (surface runoff plus baseflow) of each HUC8 basin was matched with the monthly runoff from the USGS WaterWatch runoff dataset. It should be considered that the historical human impairments might result in a biased estimation of HUC8s runoff. The VIC model was run in full energy mode. Readers are referred to Oubeidillah et al. (2014) and Naz et al. (2016) for the detailed description of the VIC model set up, calibration and evaluation. The daily hydroclimatic outputs were then aggregated to annual values at each HUC8 unit for evaluation.

2.2.2. Movements in the Budyko Space

Changes in hydroclimatology of each HUC8 river basin across the CONUS were characterized as a function of shift in the Budyko space (Budyko, 1974, 1982). The Budyko framework describes an empirical relationship between the evaporative index and aridity index. The evaporative index is defined as

$$Evaporative\ index = \frac{P - Q}{P} \tag{2.1}$$

where P is precipitation, and Q is water yield (or total runoff) in the river basin. Water yield is the average of freshwater that runs off in a basin (Foti et al., 2012; Kumar et al., 2018). $P - Q$ can be simplified to actual evapotranspiration. The aridity (or dryness) index is defined as

$$Aridity\ index = \frac{PET}{P} \tag{2.2}$$

where PET is potential evapotranspiration. The aridity index is a ratio of long-term average potential water demand (i.e., PET) to long-term average water supply (i.e., P) (Yang et al., 2006; Q. Zhang et al., 2017). The interaction between aridity and evaporative indices can be defined as the Budyko space (Figure 2.1) (Jaramillo et al., 2018). Aridity and evaporative indices have been commonly used to combine these hydroclimatic variables to assess changes in long-term hydroclimatic conditions of river basins. Characterization of changes in long-term anomalies such as aridity and evaporative indices is a different way of approaching the extreme events assessment rather than characterization of temporary anomalies such as floods (Ghanbari et al., 2019, 2020) and droughts (Maliva & Missimer, 2013; Heidari et al., 2020a).

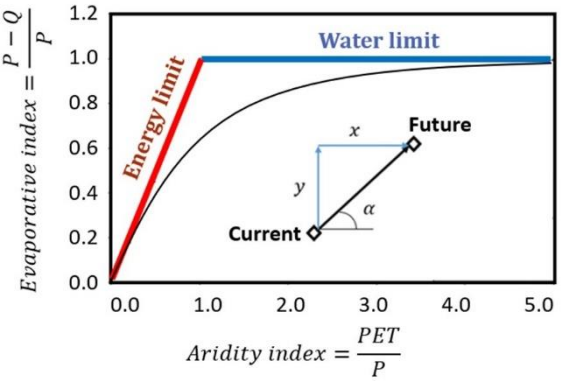

Figure 2.1. Characterization of magnitude and direction of movements in the Budyko space.

A river basin may move in the Budyko space over time due to a combination of changes in the aridity and evaporative indices (Van der Velde et al., 2014). The combination of shifts in the Budyko space can be identified by the direction and magnitude of movements (Jaramillo et al., 2018; Piemontese et al., 2019; Zaninelli et al., 2019). The direction of movement can be defined by

$$Direction\ (D) = arctan(\frac{\Delta y}{\Delta x}) \tag{2.3}$$

where Δy is change in the evaporative index and Δx is change in the aridity index (Figure 2.1). Subsequently, the magnitude of change in the Budyko space can be obtained as follows:

$$Magnitude\ (M) = \sqrt{x^2 + y^2} \tag{2.4}$$

The direction represents regional differentiation and the magnitude of change identifies the most sensitive regions (Van der Velde et al., 2014). Movements in the Budyko space are constrained by physical limits on energy demand when the aridity index is equal to the evaporative index (red line in Figure 2.1), and water demand when the evaporative index is equal to one (blue line in Figure 2.1). Moving to the right means warmer and drier climatic conditions and moving to the left means less arid conditions. Besides, moving downward indicates higher rates of river discharge or wetter conditions while moving upward indicates less water yield or streamflow for a given HUC8 river basin.

2.2.3. Hydroclimatic Behavior Groups

River basins in close vicinity may follow systematic and similar movements in the Budyko space. Systematic movements are meaningful and represent a common water and energy balance adaptation to regional climate change (Jaramillo et al., 2018; Piemontese et al., 2019; Zaninelli et

al., 2019). We used cluster analysis with the K-means method to identify unique hydroclimate behavior groups in response to climate change across the CONUS based on the direction and magnitude of movements in the Budyko space. The CONUS was subdivided into seven hydroclimatic behavior groups with similar direction and magnitude.

The United States landform (Figure A-2), ecoregion (Figure A-3) and climate classifications (Figure A-4) were applied to explain the differentiations in hydroclimatic behavior groups in response to climate change. Figure A-2 represents five major types of landforms within the CONUS including Basin, Lake, Mountain, Plain and Plateau (ESRI, 2014). Figure A-3 illustrates the spatial map of U.S. ecoregions provided by the Environmental Protection Agency (EPA) and the Commission for Environmental Cooperation (CEC) (Omernik & Griffith, 2014). Each ecoregion group specifies a unique ecosystem across the United States, which specifies type, quality, and quantity of environmental resources. The ecoregion classification uses four levels. Level I is shown in Figure A-3. Figure A-4 shows the main groups of the U.S. Koppen climate classifications including Dry, Temperate, Continental and Tropical (Chen & Chen, 2013). This classification is based on the seasonal precipitation and temperature patterns. In addition, these main climate groups are based on vegetation types in a given climate classification region (Chen & Chen, 2013).

Pearson's Chi-squared test was used to assess the statistical significance of the association between the aforementioned regional basin characteristics and the assigned hydroclimatic behavior groups as two categorical variables. Classifications with p-values less than 0.05 would suggest significant association. In addition, the statistical Goodman and Kruskal tau measure (Goodman & Kruskal, 1954) was also applied to determine the strength of associations. Classifications with higher values from the Goodman and Kruskal tau measure have higher strength of association to

the seven hydroclimatic behavior groups. Finally, a tree classification method was applied to test for relationships between each hydroclimatic behavior group and the regional landform, ecosystem, and climate types.

2.3. Results and Discussion

The study reveals that shifts in U.S. regional hydroclimatic conditions in response to climate change vary from a region to another. However, HUC8 river basins in the same neighborhood can generally follow a similar and systematic movement in the Budyko space. The CONUS can be subdivided into seven groups with similar changes in direction and magnitude in the Budyko space. These hydroclimatic behavior groups are highly associated with the regional types of climate, ecosystem, and landform. This study suggests a potential roadmap of shifts in regional hydroclimatic conditions to improve the preparedness and ability of river basins across the United States to mitigate or adapt to the impacts of hydroclimate change over the 21st century. We further used the nine U.S. climate regions defined by the National Climatic Data Center (NCDC) (National Oceanic and Atmospheric Administration (NOAA), 2014) to explain regional shifts in hydroclimatic conditions across the United States through this section. This U.S. climate regions are regularly used in climate summaries.

2.3.1. Changes in Hydroclimatic Variables

Changes in five hydroclimatic variables including precipitation, temperature, evaporation, water yield and potential evapotranspiration were first evaluated. Figure A-5 provides the 30-year baseline climatology maps of these five variables. Besides, Figure A-6 show the temporal evolution of the five selected MACA models under RCP 4.5 and 8.5 emission scenarios. Figures A-7, A-8 and A-9 represent the spatial patterns of the five selected MACA models under RCP 8.5 emission scenario for precipitation, potential evapotranspiration, and water yield, respectively. It

should be noted that the estimated potential evapotranspiration highly depends on calculation method. The Penman–Monteith equation was used in the VIC model to estimate potential evapotranspiration. The projections under all five climate models are highly variable. The DRY model with RCP 8.5 has the highest decreases in precipitation and evaporation, and the highest increases in potential evapotranspiration and temperature. Conversely, the WET model with RCP 8.5 has the highest increases in precipitation, water yield and evaporation and the highest decrease in potential evapotranspiration. Note that temperature increases across all climate projections though the magnitude of temperature increases varies.

The West United States has the highest increase in precipitation and water yield and the highest decrease in potential evapotranspiration. However, the South United States has the highest decrease in precipitation and water yield and the highest increase in potential evapotranspiration from current conditions to future conditions.

Water yield, precipitation and potential evapotranspiration have the primary control on water and energy balance (Yang et al., 2006; Zhang et al., 2017). Figure 2.2.a shows the 30-yr average of annual aridity index during the baseline period (1986-2015). The majority of river basins in the Northeast, Central, Northwest, and Southeast United States with lower aridity indices have been limited by available energy, while most river basins located in the West and Southwest United States with higher aridity indices have been limited by water availability. In addition, Figure 2.2.b illustrates the 30-yr average of evaporative index during the baseline period. River basins in the West North Central, South, and Southwest United States with higher evaporative index have comparatively less water yield.

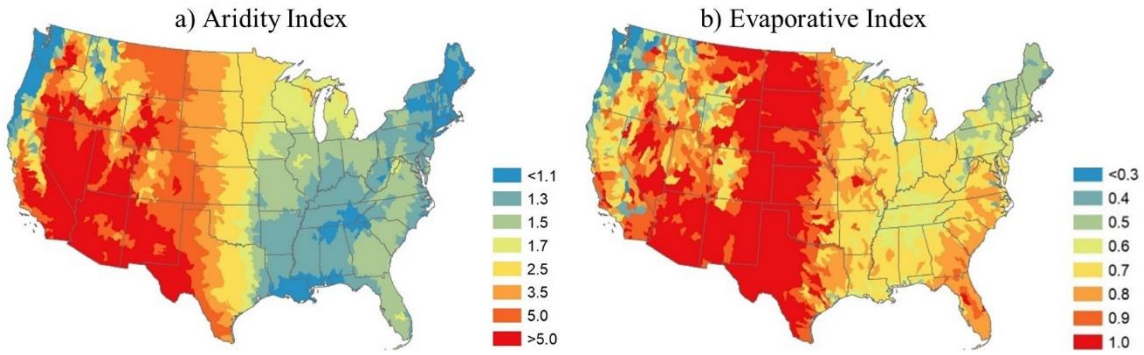

Figure 2.2. Maps of current (a) aridity index, and (b) evaporative index for the baseline period (1986-2015).

Figure 2.3 provides the 30-yr normal annual aridity and evaporative indices across all HUC8 river basins from 1980 to 2099 under RCPs 4.5 and 8.5 scenarios for the historic baseline and five selected MACA models. The historical period obtained from the combination of Daymet and PRISM from 1986 to 2015 was shown as a baseline in black. Under RCP 4.5, DRY and WET climate models are approximately representative of upper and lower bounds of future aridity and evaporative indices, respectively. However, there is not a substantial and consistent trend. Under RCP 8.5, the DRY climate projection foresees a substantial increase in aridity and evaporative indices over the 21st century. However, the WET and WARM models consistently project decreases in aridity and evaporative indices over the 21st century. Under the MIDDLE and HOT models, aridity and evaporative indices show slight changes compared to the baseline period.

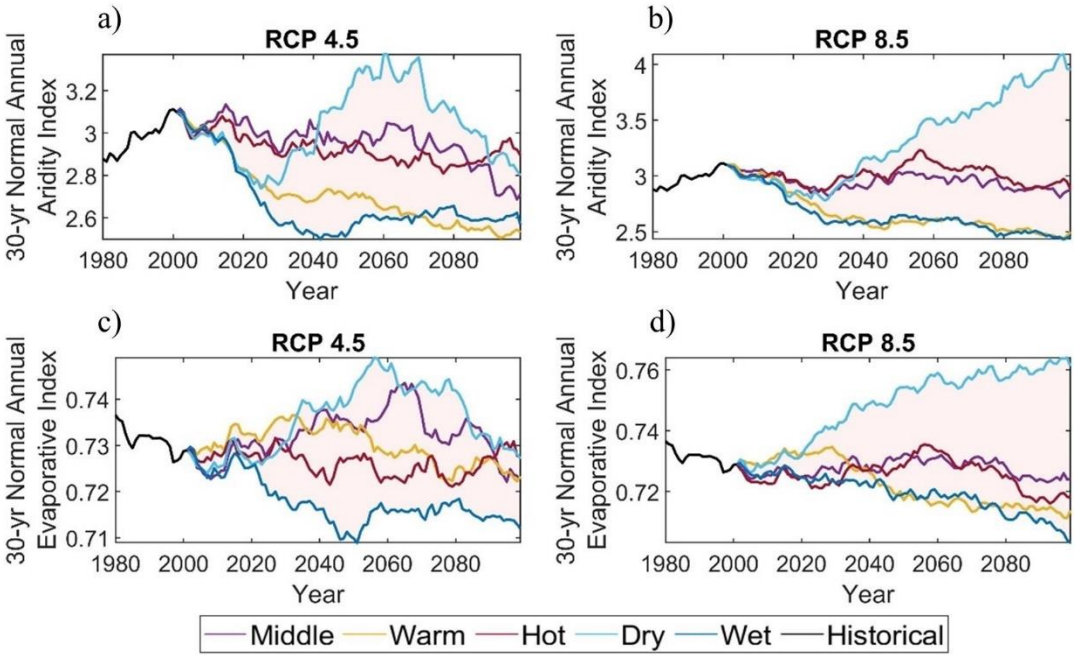

Figure 2.3. Timeseries of annual aridity index and evaporative index under RCPs 4.5 and 8.5 emission scenarios.

For a detailed assessment of hydroclimatic changes across the CONUS, we further used DRY, WET and MIDDLE climate models under RCP 8.5 to capture a wide range of potential future climate change across the entire CONUS. Figure 2.4 shows spatial changes in the aridity and evaporative indices of these three climate projections from baseline (1986-2015) to future (2070-2099) periods. Changes indicates the value of future indices minus the value of current indicis.

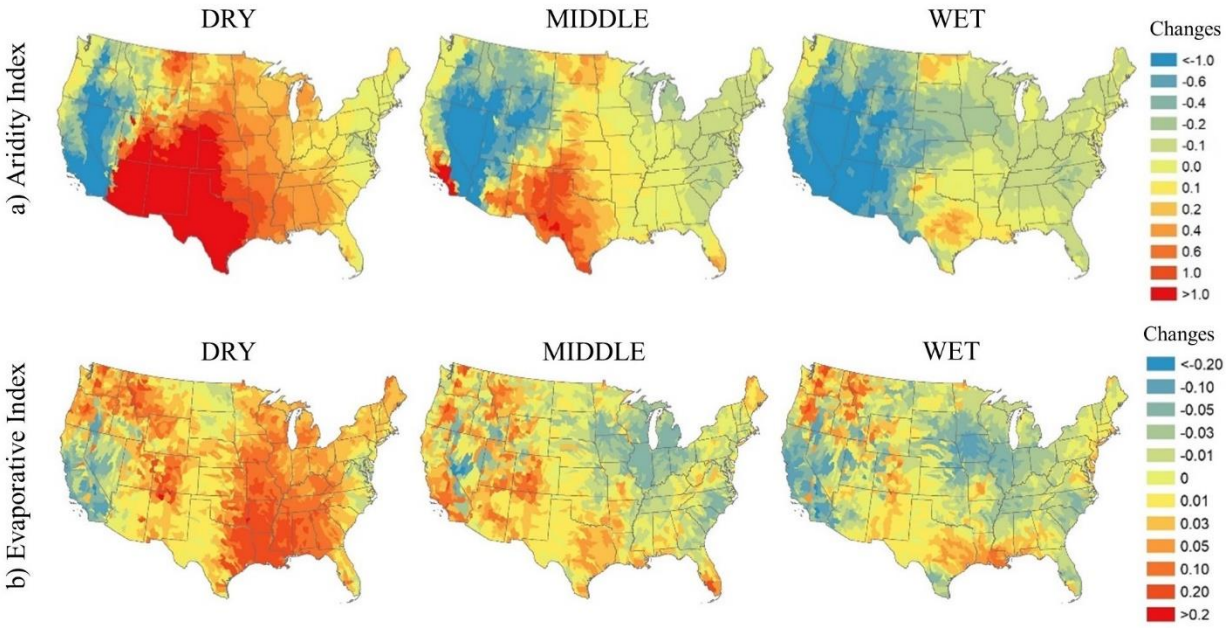

Figure 2.4. Spatial changes in (a) aridity and (b) evaporative indices from baseline (1986-2015) to future (2070-2099) periods (RCP 8.5).

Under DRY, MIDDLE and WET climate projections, the majority of HUC8 river basins located in the West United States show decreases in evaporative and aridity indices. Decreases in evaporative and aridity indices suggest increases in the chances of higher river discharges in these regions (Piemontese et al., 2019). Most river basins located in the South United States will have higher aridity and evaporative indices under all three climate projections indicating the likelihood of prolonged droughts in these regions (Piemontese et al., 2019). These findings are in line with the projections for precipitation, potential evapotranspiration, and water yield (Figures A-7 to A-9).

2.3.2. Movements in the Budyko Space

Direction of movement in the Budyko space characterizes regional differentiation, while the magnitude of movement reveals the most sensitive regions (Van der Velde et al., 2014). Here,

we projected shifts of each HUC8 in the Budyko space from baseline (1986-2015) to future (2070-2099) periods across the CONUS under DRY, MIDDLE and WET climate projections with RCP 8.5 emission scenario.

Under the DRY climate projection (Figure 2.5), most river basins deviate from the energy limit line (red line in Figure 2.1) meaning that the ratio of potential evapotranspiration to precipitation (i.e., aridity index) is increasing. In other words, most river basins are becoming more water limited. However, some HUC8 river basins in the West and Northwest United States move closer to the energy limit line. Additionally, most river basins in the Central and East North Central United States move to the upper-right meaning that the evaporative index is also increasing in these regions. Wind rose diagram in Figure 2.5 visualizes the summary of movements in the Budyko space including direction, magnitude, and frequency for all HUC8 river basins. This type of diagrams has been used in global hydroclimatic change assessments (Destouni et al., 2013). Based on the wind rose diagram in Figure 2.5, river basin movements are more likely to occur in the directions represented by the right, right-upper and left quadrants of the rose diagram, respectively. The results indicate that most river basins in the West and Southwest United States have high magnitude of changes meaning that the hydroclimatology of these regions is more sensitive to climate change.

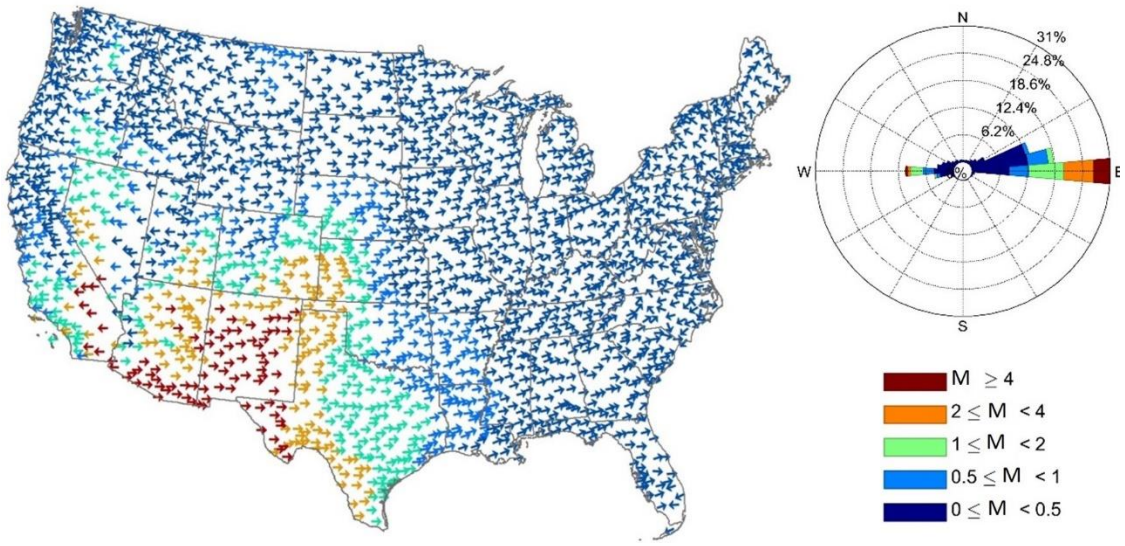

Figure 2.5. Movements in the Budyko space under the DRY climate model with RCP 8.5.

Under the MIDDLE climate projection (Figure 2.6), river basins in the West, Northwest, Northeast, and Southeast United States move closer to the energy limit line meaning that the aridity index is decreasing. However, most HUC8 river basins in the South US deviate from the energy limit line meaning that the climate is getting warmer and drier in this region. The majority of river basins do not show an increase or decrease in the evaporative index. There is only a slight decrease in evaporative indices of river basins located in the Central United States. According to the wind rose diagram in Figure 2.6, river basin movements are more likely to occur in the directions represented by the left, right and left-lower quadrants of the rose diagram, respectively.

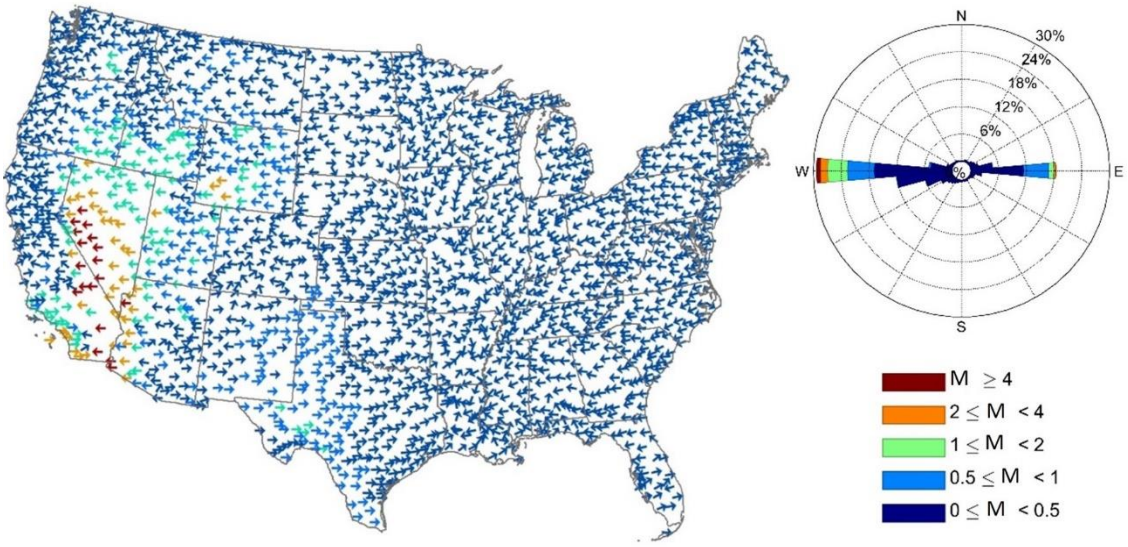

Figure 2.6. Movements in the Budyko space under the MIDDLE climate model with RCP 8.5.

Under the WET climate projection (Figure 2.7), a significant number of river basins moved towards left meaning that the aridity of river basins is decreasing. The HUC8 river basins in the WEST and Southwest United States have higher magnitude of changes meaning that the hydroclimatology of these regions is more sensitive to climate change compared to other regions. In addition, the majority of river basins in the Central and East North Central United States deviate from the water limit line (blue line in Figure 2.1) meaning that the evaporative index is decreasing in this region. In other words, the ratio of streamflow to precipitation is increasing, which resulted in higher river discharges. According to the wind rose diagram in Figure 2.7, river basin movements in the Budyko space are more likely to occur in the directions represented by the left and left-lower quadrants of the rose diagram, respectively.

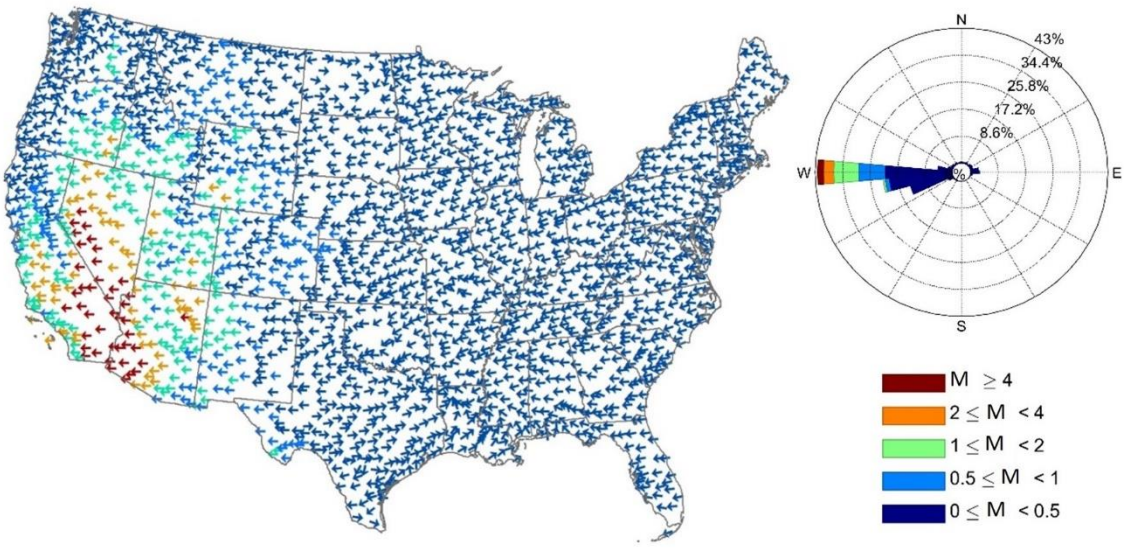

Figure 2.7. Movements in the Budyko space under the WET climate model with RCP 8.5.

Under all three climate projections, the systematic movements of HUC8 river basins in the Budyko space indicate that the CONUS will experience nonstationary changes in water and energy cycling over time. Figure A-10 compares changes in direction and magnitude across the three climate projections. As a common pattern across all three climate projections, climate change will cause a wetting trend over the western and eastern CONUS but a drying trend over the central and southern CONUS. A consistent pattern of changes in direction and magnitude was found across the three climate changes projections for the South and West United States, respectively. These river basins are likely to experience a similar hydroclimatic change regardless of the future climate projections. The magnitude of the change is particularly large along the West and Southwest United States under all three climate projections. The magnitude of change characterizes the most sensitive areas. Thus, hydroclimatic conditions of the West and Southwest United States are the most sensitive to climate changes over the 21st century. Direction determines regional differentiation. Most river basins in the South United States will likely get drier and warmer under

all three climate projections. Note that the movements in the Budyko space were projected to tend to be along the horizontal axis in most regions as shown in Figures 2.5 to 2.7 because the range of the evaporative index may be much smaller than the aridity index.

2.3.3. Hydroclimatic Behavior Groups

HUC8 river basins with systematic and similar magnitude and direction of movements in the Budyko space can be clustered to a hydroclimatic behavior group in response to climate change. To better understand the pattern of shifts across the CONUS, we clustered movement in the Budyko space under the MIDDLE model which can have potential implications for regional adaptation and mitigation strategies. The K-means method was used to cluster HUC8 river basins to the seven regions with unique hydroclimatic behavior. Table 2.2 and Figure 2.8 provide the ranges of direction and magnitude of each hydroclimatic behavior group that are in line with the wind rose diagram in Figure 2.6.

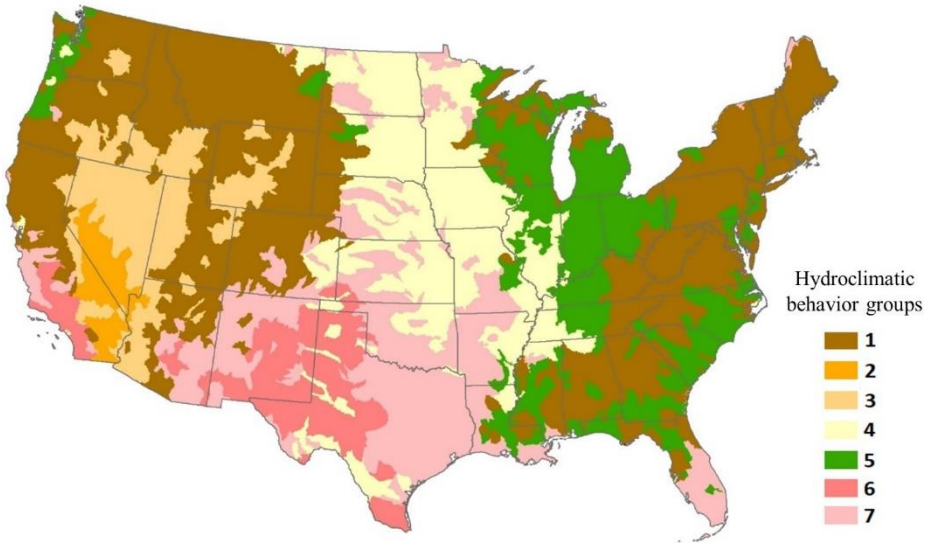

Figure 2.8. Regional hydroclimatic behavior groups of the United States under the MIDDLE climate model with RCP 8.5.

Table 2.2. Hydroclimatic behavior group.

Behavior Group	Direction (D) and Magnitude (M)
1	D (135-190) with M (<0.095)
2	D (135-190) with M (>3.4)
3	D (135-190) with M (0.95-3.4)
4	D (220-360)
5	D (190-220)
6	D (0-45) with M (>0.5)
7	D (0-45) with M (<0.5)

Groups 1, 2 and 3 have the same direction (moving to the left). However, they have different magnitude of changes. Groups 2 and 3 have higher magnitude than group 1. In addition, Groups 6, and 7 have the same direction (moving to the right-upper). However, Group 6 has higher magnitude of changes than Group 7. Group 6 and 7 are more likely to experience prolonged drought, while Group 5 with movement to the left-lower is likely to experience higher river discharge under wetter conditions. Group 4 includes a wide range of direction from 220 to 360 degree with more frequent movements to lower and lower-right.

Regional landform, climate, physiology, ecology and landcover play important roles in the hydroclimatic behavior of a river basin in response to climate change. In this regard, Koppen climate classifications, ecoregions, and landform (Figures A-2 to A-4) were used to relate systematic movements in the Budyko space to the regional river basin characteristics. Based on the Pearson's Chi-squared test, all regional classifications have p-values close to zero meaning that they are associated to the hydroclimatic behavior groups. Table 2.3 shows the p-value and chi-square values of each classification. In addition, the Goodman and Kruskal tau measure was used to determine strength of association between each classification with hydroclimatic behavior groups. Landform zones, ecoregion zones and climate zones have respectively higher associations.

A tree classification method was then used to find a relationship between hydroclimatic behavior groups and hydroclimatic factors based on the combination of these basin characteristics. Figure 2.9 illustrates the relationship between each hydroclimatic behavior group and its regional landform, ecosystem, and climate.

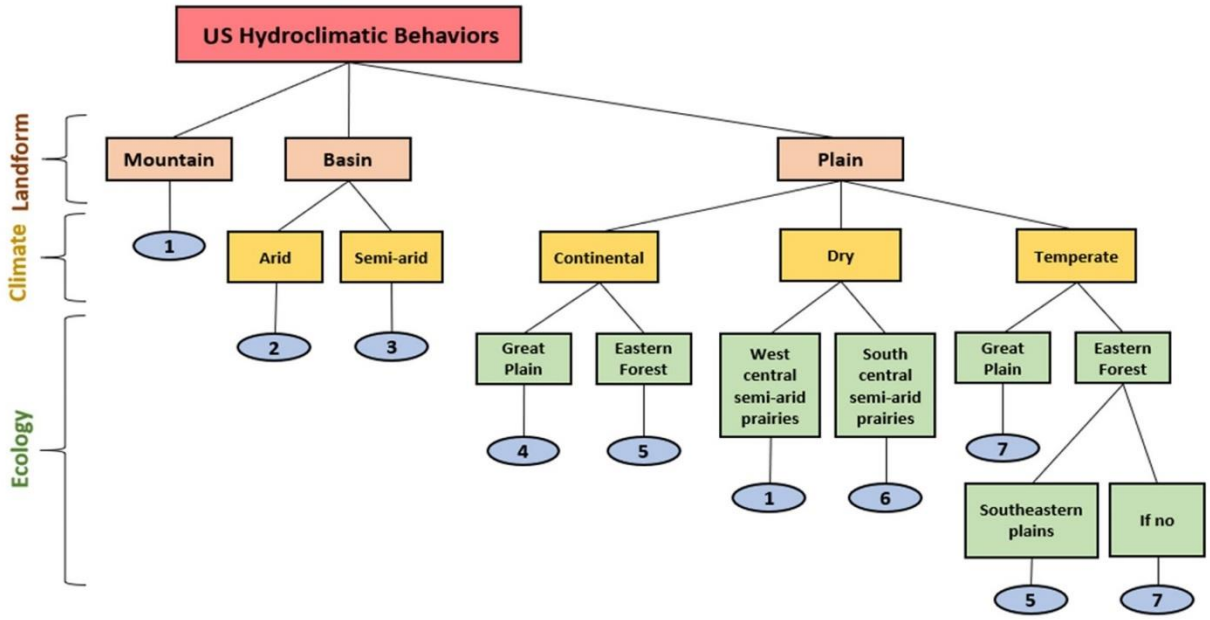

Figure 2.9. A tree classification to explain relationship between U.S hydroclimatic behavior groups and regional basin characteristics (landform, climate, ecosystem) under the MIDDLE climate model with RCP

Table 2.3. Statistical test for association between hydroclimatic behavior groups and regional climate, ecoregion, and landform classification of the United States.

Classification	**Pearson's P-value**	**Pearson's Chi-squared**	**Goodman and Kruskal tau measure**
Climate zones-Level1	p-value < 2.2e-16	707.83	0.157
Climate zones-Level2	p-value < 2.2e-16	1160.4	0.13
Climate zones-Level3	p-value < 2.2e-16	1580.3	0.118
Ecoregion zones-Level1	p-value < 2.2e-16	1944.2	0.238
Ecoregion zones -Level2	p-value < 2.2e-16	3173.3	0.128
Ecoregion zones -Level3	p-value < 2.2e-16	5213.2	0.045
Landform zones	p-value < 2.2e-16	1410.5	0.245

Figure 2.10 shows projected hydroclimatic behavior groups based on the tree classification method. It shows an acceptable accuracy for the spatial pattern of hydroclimatic behavior groups in comparison with Figure 2.8, which is useful to make a prediction for regional characteristics of each hydroclimatic behavior group. The tree classification method has the lowest accuracy for Group 6, though it has captured its spatial trend.

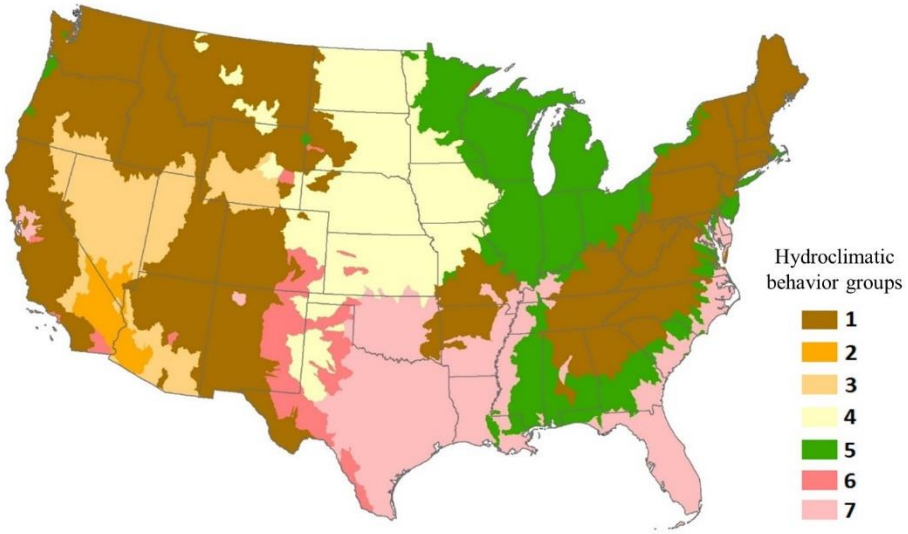

Figure 2.10. Estimation of U.S hydroclimatic behavior groups based on the tree classification under the MIDDLE climate model with RCP 8.5.

The majority of Group 1 is within the Mountain and Plateau types of landform. Group 2 includes basin regions with a Dry climate, and Group 3 is related to basin regions with a Semi-arid climate. Group 4 includes some parts of Great Plain with Continental climate type. Group 5 comprises most Plains which are located in the Eastern Forest type of ecosystem with both Continental and Temperate climate. Group 6 comprises Plains with Dry climate located in the South Central Semi-arid Prairies type of ecosystem, and majority of Group 7 is related to Plains with Temperate climate within the Great Plains.

Overall, the aridity in the Mountain, Plateau and Basin types of landforms is decreasing over the 21st century. Aridity will decrease more in the Basin region compared to Mountain and Plateau types of landform, meaning that the hydroclimatology of the Basin region is more sensitive to climate change than that of the Mountain region. In addition, within the Basin regions, Basin regions with Dry climate have larger declines in aridity than Basin regions with Semi-arid climates.

However, river basins with the Plain landform type behave differently in response to climate change according to their ecosystem and climate. Some river basins in the Plains with Dry climates inside the West Central Semi-arid Prairie ecosystem behave like Mountains and will have wetter climate conditions. Plains with Eastern Forest ecosystems are more likely to experience wetter climate conditions over the 21st century. The evaporative indices of these regions will also decrease significantly compared to Mountain and Basin types of landforms, meaning that the rate of discharge will be higher in the future.

Both aridity and evaporative indices will increase in Plains regions with Dry climate in the South Central Semi-arid Prairies ecosystems, and in Plains regions with Temperate climates in the Great Plains. These regions will experience less streamflow under drier climate conditions. However, some parts of the Great Plains with Continental climates experience decrease in their evaporative index with increase in aridity index, meaning that this region will experience higher streamflow even under drier climate conditions.

It can be concluded that river basins inside the Great Plains are getting warmer and drier in terms of climate conditions. However, some parts of the Great Plains which are located in the Continental climate will have higher rates of streamflow in the future while other parts of the Great Plains with Temperate climates and Dry climates (located in South Central Semi-arid Prairies) will experience lower rates of streamflow.

These findings highlight the need for regional differentiation in adaptation and mitigation strategies according to regional climate, landform, and ecosystem of river basins in the United States to protect vulnerable resources and reduce potential consequences on agriculture, environment, economy, society, and ecosystem.

The results of this study were subjected to a variety of uncertainties associated with climate models, emission scenarios, downscaling methods, hydroclimatic projections, and hydrological models. The uncertainty includes those introduced by the selection of the climate models and the hydrological models. The MACA climate models are highly uncertain because they depend on future anthropogenic and forcing scenarios. Additionally, future climate projections can be affected by the existence of internal climate variability and incomplete understanding and imprecise climate models (Wyard et al., 2020; Collins et al., 2020).

We focused on a range of possible future climate conditions, from driest to wettest, to account for current uncertainty about long-term future climatic conditions. Although variability in the projection of future climate conditions can be affected by some sources of uncertainty and variability in climate change scenarios, projected shifts in hydroclimatic conditions of river basins showed some consistency across climate change models in terms of the direction and magnitude of changes.

In addition to the uncertainty in the choice of climate models, some uncertainties remain, related to the hydrological model. The VIC model may not capture all physical basin characteristics, water management regulations, landcover changes (Naz et al., 2016). Furthermore, there are some uncertainties associated with the parameters of the VIC model and structural deficiencies of the model simulation (Gharari et al., 2019, 2020; Melsen et al., 2016).

Given the high uncertainty in the MACA climate projections, VIC hydrological modeling, K-means clustering and tree classification methods, this study is aimed to provide a general overview of future shifts in the regional hydroclimatic conditions of U.S. river basins in response to possible range of changes in climate variables. The findings can be used as a roadmap for decision-makers to implement adaptation and mitigation strategies at an improved and modified regional scale.

2.4. Summary and Conclusions

Climate change can alter hydroclimatology of river basins at various spatial and temporal scales. This study evaluates the potential impact of climate change on hydroclimatic conditions of U.S. river basins over the 21st century. Five sets of hydroclimatic projections were conducted using the VIC hydrologic model driven by the downscaled MACA datasets. Shifts in the long-term hydroclimatic conditions at the HUC8 river basin scale were expressed by magnitude and direction of movements in the Budyko space. Hydroclimatic responses vary from one river basin to another. However, a consistent pattern of changes in direction and magnitude was found across the climate change projections. Overall, six important conclusions can be made here:

1) HUC8 river basins can be clustered into seven hydroclimatic behavior groups with a similar, unique, and systematic movement in the Budyko space indicating that there should be common regional water and energy balance adaptations to climate change.
2) This finding challenges the stationary assumption of long-term water and energy cycles meaning that climate change may lead to shifts in long-term water and energy balances and changes in hydroclimatic conditions.
3) The hydroclimatic behavior of U.S river basins in response to climate change are highly associated with basin characteristics such as regional landform, climate, and ecosystems.

These findings highlight the need for regional differentiation in adaptation and mitigation strategies to protect vulnerable resources and reduce negative consequences of hydroclimatic shifts on various sectors.

4) The aridity index in the Mountain, Plateau and Basin types of landforms will decrease over the 21st century with higher rates in Basin compared to Mountain and Plateau regions. Additionally, both aridity and evaporative indices will decrease in the Plains with Eastern Forest ecosystems.
5) The aridity will increase over 21st century in Plains with Dry climates in the South Central Semi-arid Prairies, Plain with Temperate climates in the Great Plains and some parts of the Great Plains with Continental climates. The evaporative index also decreases in river basins inside the Great Plains with Continental climates, meaning that the rate of river discharge increases even though the climate gets warmer and drier.
6) The South and Southwest United States are the hotspots for shifts in long-term hydroclimatic conditions. The majority of river basins in the South United States move to the right-upper with high magnitude indicating that this region is likely to experience warmer and drier conditions with higher chances of prolonged droughts. Most river basins in the West United States move to the left-lower with high magnitude indicating that this region is likely to experience wetter conditions and increased river discharges.

These findings have potential implications for human and agricultural activities. Adaptation and mitigation strategies are best designed at a modified and improved regional scale to protect vulnerable ecosystems and freshwater resources. This study can help decision-makers to assess and improve the ability and preparedness of various resources to mitigate or adapt to the impacts of climate changes across the United States over 21st century.

CHAPTER 3.

IMPACTS OF CLIMATE CHANGE ON HYDROCLIMATIC CONDITIONS OF U.S. MEGAREGIONS, NATIONAL FORESTS, AND NATIONAL GRASSLANDS

The conterminous United States includes national forests and grasslands that provide ecological, social, economic, recreational, and aesthetic services. Future climate change can alter long-term hydroclimatic conditions of national forests and grasslands and lead to negative consequences. Furthermore, most of the population and economic growth in the United States occurs in megaregions, whereas climate change may amplify negative impacts on water and natural resources. Thus, this study characterizes shifts in hydroclimatology and basin characteristics of US national forests (NFs), national grasslands (NGs) and megaregions in response to climate change over the 21st century under the DRY, MIDDLE and WET climate models with RCP 8.5 emission scenario.

The results indicate that NFs and NGs are likely to experience larger changes in basin characteristics compared to the average of the United States. In general, across the conterminous US, the NFs in mountainous regions are likely to have larger changes in hydroclimatic variables than NFs with lower elevation and NGs. Comparing Forest Service regions, Pacific Northwest, Intermountain, and Northern regions may have a less arid climate with lower freshwater availability. The Southwestern, Northern, Intermountain, and Rocky Mountain regions are likely to experience higher shifts in their basin characteristics.

The results at the megaregional scale indicate that Los Angeles, San Diego, and San Francisco are more likely to experience less arid conditions with some shifts from Continental to Temperate climate type while the hydroclimatology of Houston may become drier with some shifts

from Temperate to Continental climate type. Additionally, water yield is likely to decrease in Seattle. Change in the hydroclimatology of Denver and Phoenix highly depends on the selected climate model. However, the basin characteristics of Phoenix have the highest sensitivity to climate change. Overall, the hydroclimatic conditions of Los Angeles, San Diego, Phoenix, Denver, and Houston have the highest sensitivity to climate change.

This study can help environmental scientists, and land and water managers improve future land management plans. Understanding of future shifts in hydroclimatology of megaregions can also help decision-makers to attenuate negative consequences by implementing appropriate adaptation strategies, particularly in the water-scare megaregions.

3.1. Introduction

The United States National Forest System includes National Forests (NFs) and National Grasslands (NGs), which are divided into eight regions in the conterminous United States (CONUS) managed by the U.S. Forest Service (USFS) (Joyce et al., 2008). The USFS provides a wide range of services for present and future generations that have broadened to include hydrological, ecological, social, economic, recreational, and aesthetic services (Bonan, 2008; Duan et al., 2016; Yannian, 1990). A challenge for the agency is that climate change may lead to shifts in hydroclimatic conditions of NFs and NGs, such as a decrease in freshwater availability and may cause changes in the structure and composition of forests and grasslands at various spatial and temporal scales (Allen et al., 2010; Astigarraga et al., 2020; Bonan, 2008; Esquivel-Muelbert et al., 2019; Jeong et al., 2016; Jump et al., 2017; McIntyre et al., 2015). Assessments of potential shifts in hydroclimatic conditions of NFs and NGs can help decision-makers to mitigate the negative consequences of deforestation (Peterson et al., 2011).

Furthermore, the conterminous United States (CONUS) can be divided into large contiguous geographical regions referred to as 'megaregions' centered on major cities (Nelson and Rae, 2016). The megaregions represent clusters of cities across the CONUS in terms of economic structures, culture, history, topography, natural resources, ecosystem, climate, urban growth telecommunication, and institutions (Hagler, 2009; Nelson, 2017; Nelson and Rae, 2016). Most of the U.S. population and economic growth has been concentrated in megaregions (Ross, 2008). Improving policies, planning, and investments at the megaregional scale can address new challenges arising around the large metropolitan centers that can affect environment, economy, and society (Nelson, 2017; Ross, 2008).

Rapid population growth, expansion of suburban areas, social equity, strained ecosystems are key challenges that U.S. megaregions are currently experiencing (Ross, 2008). Climate change may further exacerbate existing problems in metropolitan and regional planning over the 21st century by negative impacts on energy sources, water supply, air quality, habitat preservation, ecosystem, and natural resources (Ashfaq et al., 2013; Ponce Campos et al., 2013; Greve et al., 2014).

Current megaregions planning strategies mostly focused to deal with issues such as transportations and underestimate the need to deal with future changes in climate and freshwater availability of megaregions (Dewar & Epstein, 2007). Improved characterization of future shifts in long-term hydroclimatology of U.S. megaregions may help planners, researchers, and decision-makers to attenuate the potential consequences of climate change on cities and strengthen economic prosperity (Brown et al., 2019; Butler et al., 2017; McDonald et al., 2011).

Thus, this study first characterizes changes in regional hydroclimatology and basin characteristics of NFs and NGs across the CONUS (Heidari et al., 2021). Climate change has

already affected forests and grasslands throughout the CONUS via changes in wildfire frequency, forest pathogens, insect populations, and timber resources (Fekety et al., 2020; Rehfeldt et al., 2009; Weed et al., 2013; Westerling et al., 2006). Although significant progress has been made in understanding the effects of climate change on US forests and grasslands (Bonan, 2008; Esquivel-Muelbert et al., 2019; Fekety et al., 2020; Littell et al., 2012; Rehfeldt et al., 2009; Yannian, 1990), there is a lack of comparative studies for assessing the impacts of climate change on regional hydroclimatic conditions and basin characteristics of NFs and NGs at the local and national scales (Littell et al., 2012).

Second, this study examines the effects of climate change on the hydroclimatic conditions of fourteen U.S. megaregions including Seattle, San Francisco, Los Angeles, San Diego, Denver, Phoenix, Chicago, Miami, Washington D.C., Philadelphia, New York, Boston, Houston, and Atlanta. Assessing changes in long-term anomalies such as shifts in hydroclimatology may provide insights to support future water resource planning and management. It is important because many megaregions may do not have sufficient natural resources to overcome hydroclimatic changes, particularly in water-scarce regions (Maliva & Missimer, 2013).

We applied the Budyko framework to compare shifts in the integrated hydroclimatic conditions of U.S. NFs, NGs, and megaregions. In addition, we used Fu's equation (Zhang et al., 2004) to assess how shifts in hydroclimatic conditions of NFs, NGs and megaregions can lead to changes in their integrative basin characteristics such as land cover, and vegetation cover.

We estimated future changes in hydroclimatology of U.S. NFs, NGs, and megaregions in response to climate change from current conditions (1986-2015) to future conditions (2070-2099) for eight-digit hydrologic subbasins (HUC8) containing all or part of NFs and NGs under the DRY, MIDDLE, and WET climate models with RCP 8.5 emission scenario. Specifically, the objectives

were to: 1) assess shifts in long-term hydroclimatic conditions of NFs and NGs using the Budyko space; 2) characterize changes in basin characteristics of NFs and NGs in response to hydroclimatic changes using the Fu's equation; 3) evaluate comparative responses of eight US Forest Service regions within the CONUS to climate change; 4) investigate the effects of climate change on hydroclimatic conditions of U.S. megaregions using the Budyko framework; 5) assess and compare shifts in basin characteristics of U.S. megaregions using Fu's equation; 6) characterize shifts in climate types of U.S. megaregions using the Fine Gaussian Support Vector Machine (SVM) method; and 7) determine the hotspots of megaregions which show consistent changing signals across all selected climate models.

Characterizing shifts in regional hydroclimatology of NFs and NGs can help forest managers adapt appropriately to impending stresses caused by climate change. Besides, improved understanding of future change in hydroclimatology of megaregions can play a major role in the future urban planning and water resource management under the sustainable growth.

3.2. Materials and Methods

The downscaled Multivariate Adaptive Constructed Analogs (MACA) datasets (Abatzoglou & Brown, 2012) were used to characterize changes in future climate variables under three climate models representing future wet, dry, and intermediate conditions. Then, the Variable Infiltration Capacity (VIC) model (Liang et al., 1994) was applied to simulate future hydrological variables driven with the future climate scenarios. Finally, the Budyko framework was used to project shifts in hydroclimatic conditions, and Fu's equation was used to help assess changes in integrative basin characteristics. In this study, the 30-yr average of hydroclimatic variables from 1986 to 2015 represents current conditions and the 30-yr average of hydroclimatic variables from 2070 to 2099 describes future conditions.

3.2.1. U.S. National Forests and Grasslands

The CONUS is divided into eight Forest Service Regions (Figure 3.1). Each region encompasses NFs and NGs with diverse landscapes, ecosystems, fauna, and flora (Bonan, 2008; Duan et al., 2016). Although the Southern region is the largest region, spanning from Texas to Virginia, most NFs and NGs are located in the western United States. The total NF+NG area is about 114 million ha that NFs account for nearly 98% of this total NF+NG area in the CONUS.

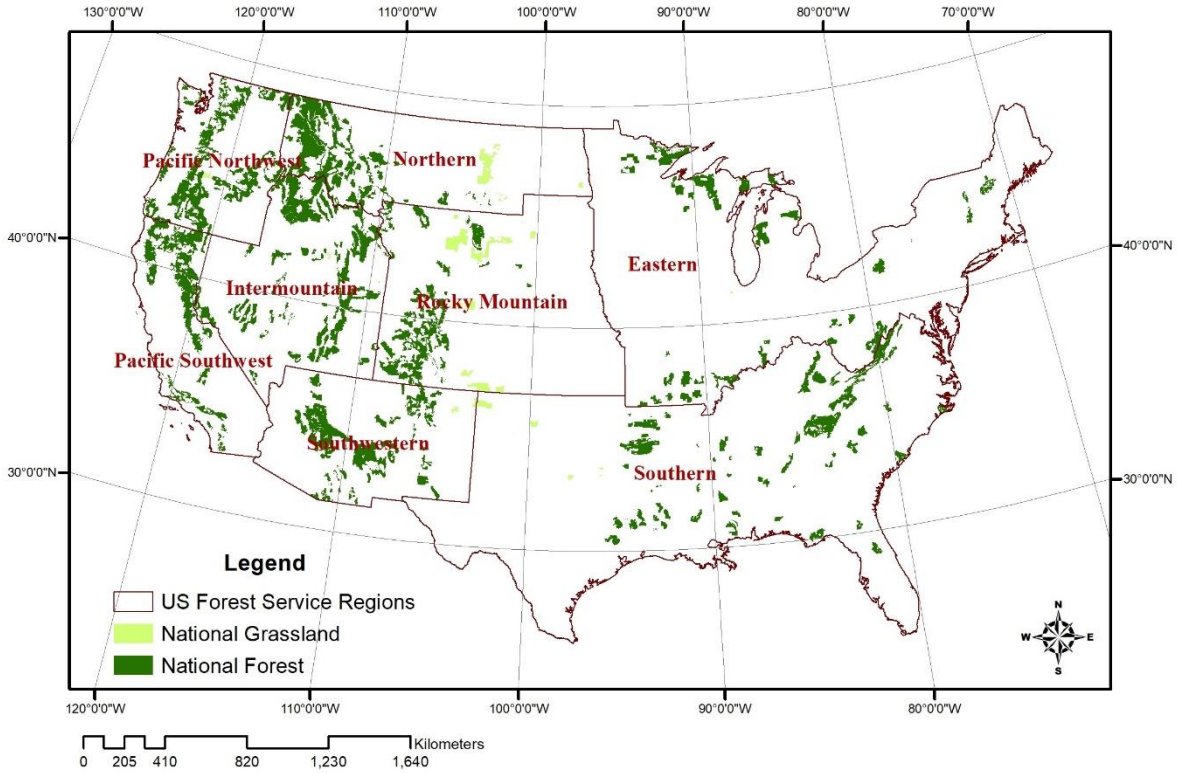

Figure 3.1. NFs and NGs of the CONUS divided to eight service regions.

3.2.2. U.S. Megaregions

The U.S. Megaregions are formed based on similar societal and geographical characteristics (Nelson and Rae, 2016). Cities inside each megaregion have common natural resources, ecosystem, settlement, and land use pattern. Fourteen U.S. megaregions were selected

from Nelson and Rae (2016) to assess the effects of climate change on hydroclimatology of U.S. megaregions (Figure 3.2). These megaregions were selected due to their importance and various eco-hydrologic and climatic regimes which represents a wide spectrum of climate, demographic, policy, and cultural settings (Todorovich, 2009). Boston, New York, Philadelphia, and Washington D.C. megaregions were merged as a large megaregion (WPHNB) given their geographical proximity. Similarly, Los Angeles and San Diego were combined to one LOS-SAN megaregion because of their similar hydroclimatic conditions.

Figure 3.2. The Selected U.S. Megaregions.

Nelson (2017) reported the projected population, and economy of the U.S. megaregions based on the Wood and Poole Economics (2016). Approximately, 76% of the U.S. population is concentrated in the megaregions, whereas the U.S. megaregions occupy only a small land area of the CONUS. Houston, Phoenix, and Miami megaregions were projected to experience the highest increase in population. The economic growth was measured by changes in gross regional product (GRP). Miami, Houston, and phoenix were estimated to experience double GRP (Nelson, 2017).

These regions encompass climate regimes from coastal moist mid-latitude climates of the Mid-Atlantic to the subtropical semi-arid deserts of the Southwest (Nelson and Rae 2016; Ross 2008). However, climatic conditions of megaregions are estimated to change faster than the global mean climate over the 21st century (America 2050, 2006; Nelson 2017).

3.2.3. Hydroclimatic Projections

Current climate variables (1986-2015) including minimum and maximum temperature and precipitation at the grid size of ~4 km (1/24 degree) were obtained from a combination of Daymet (Thornton et al., 1997a) and the Parameter-elevation Regressions on Independent Slopes Model (PRISM) datasets (Daly et al., 2008). The daily precipitation and temperature were derived from Daymet and biased corrected with PRISM at the monthly scale. The North American Regional Reanalysis (NARR) dataset (Mesinger et al., 2006) was used to obtain the historical wind speed data. Readers are referred to Oubeidillah et al. (2014), Naz et al. (2016), and Heidari et al. (2020b) for the detailed description of the historical climate dataset.

Future climate variables (2070-2099) were obtained from the downscaled Multivariate Adaptive Constructed Analogs (MACA) datasets (Abatzoglou & Brown, 2012). The MACA climate dataset provides CONUS-wide downscaled (to the grid size of ~4km, or 1/24 degree) climate projections for the RCP 4.5 and RCP 8.5 emission scenarios for twenty climate models. Three downscaled climate models were chosen to represent a range of possible climate scenarios, on average, ranging from wet to dry, plus one model that represents the middle of the range (Table 3.1) (Heidari et al., 2020b; Joyce & Coulson, 2020). The WET, DRY, and MIDDLE climate models under RCP 8.5 emission scenario were selected based on a range of changes in precipitation from current to future conditions. The use of these climate models allows to characterize the estimated range in projected annual precipitation across all projections for entire the CONUS.

Note, opposite patterns in individual ensemble members can originate from internal variability in the large-scale circulation (Deser et al., 2012, 2017; Kjellström et al., 2013).

A good representation of current climate is indeed a necessary condition required to realistically simulate future climate changes. Figure B-1 compares the 30-yr average of annual precipitation for each HUC8 watershed over the historical period (1986-2015). The 30-yr average values for each HUC8 watershed are approximately the same meaning that the variation between climate models is not significant at the 30-yr average scale. Additionally, 30-yr average of climate models over the historical period is close to the selected baseline historical model that is the combination of Daymet and PRISM.

Therefore, for the consistency over the historical period, we decided to use the combination of Daymet and PRISM models. The three climate models were able to reproduce current climate conditions with the same statistics. Although the 30-yr average values for the selected baseline is close to the historical MACA climate models, the performance, and skills of each selected GCM are not specifically evaluated in this study. Readers are referred to Naz et al. (2016), and Joyce & Coulson, (2020) for the detailed information about the climate models and historical projections.

Table 3.1. Projected MACA climate scenarios (Joyce & Coulson, 2020).

	WET	**DRY**	**MIDDLE**
Name	CNRM-CM5 (RCP 8.5)	IPSL-CM5A-MR (RCP 8.5)	NorESM1-M (RCP 8.5)
Model Agency	National Centre of Meteorological Research, France	Institute Pierre Simon Laplace, France	Norwegian Climate Center, Norway

The projected climatic variables were then used as inputs to the Variable Infiltration Capacity (VIC version 4.1) model (Liang et al., 1994) at the grid size of ~4 km (1/24 degree) to project precipitation, potential evapotranspiration, and water yield across the CONUS over the 21st

century at a HUC8 level scale. The VIC model is a macroscale semi-distributed hydrological model to simulate land-atmosphere fluxes and the water and energy balances at the land surface (Cherkauer & Lettenmaier, 2003). The VIC model has been widely used to simulate streamflow over a number of large river basins in North America (Andreadis & Lettenmaier, 2006).

The VIC model uses the variable infiltration capacity curve to solve full water and energy balances and estimate infiltration and surface runoff. The model takes into account snow processes. The land surface can be modeled as a grid of uniform cells at a daily or sub-daily time step. Each grid cell can represent the spatial variability of precipitation, topography, and vegetation (Cherkauer & Lettenmaier, 2003). Several key assumptions have been made in the VIC model, including that the atmosphere is the only source of incoming water for a grid cell, and that grid cells are independent of each other meaning that there are no horizontal water and energy exchanges between grid cells (Demaria et al., 2007).

Topography, soil characteristics, vegetation, land surface classification, and meteorological forcing are key hydrological inputs to the VIC model. Organized and calibrated VIC input data for the US Geological Survey (USGS) eight-digit hydrologic subbasins (HUC8) across the entire CONUS were obtained from Oubeidillah et al. (2014) (Oubeidillah et al., 2014). The VIC model uses the Penman–Monteith equation to estimate potential evapotranspiration.

Aggregated monthly runoff data from USGS National Water Information System gauge observations (WaterWatch dataset) (Brakebill et al., 2011) was used to calibrate the VIC model for each HUC8 basin. Calibrating the VIC model using the WaterWatch monthly runoff data allows the homogenous application of the VIC model to all relevant grid cells. To calibrate the VIC model, the simulated monthly total streamflow (surface runoff plus baseflow) of each HUC8 basin was matched with the monthly runoff from the USGS WaterWatch runoff dataset. Readers

are referred to Oubeidillah et al., (2014) and Naz et al. (2016) for the detailed description of the VIC model set up, calibration, and evaluation. The daily hydroclimatic outputs were then aggregated to annual values at each HUC8 unit for evaluation. Figure B-2 compares the observed versus simulated annual water yield for each NFs and NGs from 1986 to 2015 period. The VIC model shows a strong linear correlation (0.9799) between observed and simulated mean annual water yield.

3.2.4. Movements in the Budyko Space

The combined changes in hydroclimatic variables can be characterized by movements in the Budyko space (Budyko, 1974, 1982). The x-axis in the Budyko space shows the aridity index defined as:

$$Aridity\ Index = \frac{PET}{P} \tag{3.1}$$

and the y-axis in the Budyko space characterizes the evaporative index defined as:

$$Evaporative\ Index = \frac{P - Q}{P} \tag{3.2}$$

where PET, P, and Q are respectively potential evapotranspiration, precipitation, and water yield. $P - Q$ in Equation 3.2 can be simplified to actual evapotranspiration (Heidari et al., 2020b).

Movements in the Budyko space over time from current conditions to future conditions can be a combination of shifts in aridity index (Δx) and evaporative index (Δy). Improved understanding of the relative contribution of such drivers is a challenge to comprehensively characterize changes in future hydroclimatic conditions and basin characteristics in response to climate change. The movement can be described by a direction (D) and magnitude (M) defined as (Heidari et al., 2020a):

$$D = arctan(\frac{\Delta y}{\Delta x}) \tag{3.3}$$

$$M = \sqrt{x^2 + y^2} \tag{3.4}$$

where the direction of movements identifies regional differentiation and magnitude of movements describes sensitivity in response to climate change (Van der Velde et al., 2014).

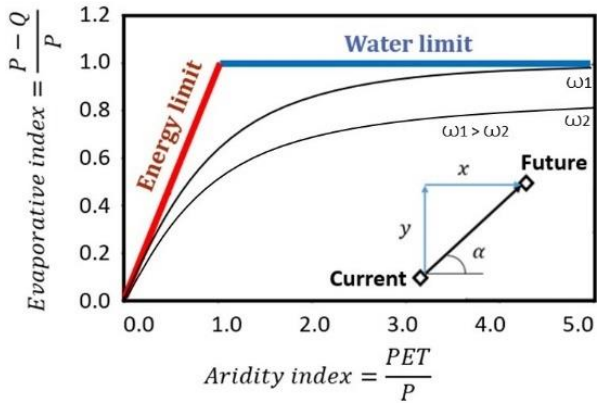

Figure 3.3. Characterization of magnitude and direction of movements in the Budyko space.

A river basin may move toward the right (D = 0) in the Budyko space over time by increase in the aridity index, meaning that the climatic condition gets more arid. Conversely, a river basin may move toward the left (D = 180) by decrease in aridity index, indicating that the climatic regime becomes less arid. Additionally, a river basin may move upward (D = 90) over time by increasing evaporative index indicating lower river discharge, or downward (D = 270) indicating higher freshwater availability and lower evaporation. Direction of movement in the Budyko space can be representative of regional differentiation in response to climate change.

Magnitude of change in the Budyko space can be representative of sensitivity of a river basin to climate change. Basins with high magnitude of change are more prone to experience

prolonged drought or long-term wetting period which can considerably affect their water and natural resources. Readers are also referred to Heidari et al., (2020b) for further explanation of movements in the Budyko space. In this study, we obtained the current and future PET, P, and Q from the VIC model and applied Equations 3.1 to 3.4 to estimate shifts in the Budyko space of NFs and NGs across the CONUS from current to future periods. Note that the PET obtained from the VIC model is potential evapotranspiration from open water. It was assumed that there is sufficient open water supply so that the PET values are the maximum (potential) evapotranspiration capacity.

3.2.5. Changes in Basin Characteristics

Previous studies have proposed several analytical equations describing relationships between the aridity and evaporative indices, including the Fu's one-parameter equation (Zhang et al., 2004). Fu's equation accounts for influencing factors such as basin size, seasonal variability, and soil and vegetation characteristics that can affect the relationship. Fu's equation is defined as:

$$\frac{P-Q}{P} = 1 + \frac{PET}{P} - \left[1 + \left(\frac{PET}{P}\right)^{\omega}\right]^{\frac{1}{\omega}} \tag{3.5}$$

where ω is a free parameter that has no physical meaning (Figure 3.3). The ω free parameter can represent an integrative property of the catchment that globally ranges between 1.3 to 4.6 with a median value at 1.8 (Yue et al., 2013). Previous studies reported that differences in ω are highly correlated with differences in land cover, vegetation cover, basin slope, and area (Coe et al., 2011; Zhang & Wei, 2012; Zhao et al., 2009; Zhou et al., 2015).

A Region with a sufficiently high ω is energy-limited, while a region with a sufficiently small ω is water-limited. In a water-limited region, forests have deeper and larger root systems that help them access more soil water (Zhou et al., 2015). The basin and vegetation characteristics of a region with small ω (i.e. a water-limited region) can be more affected by hydroclimatic changes (Li et al., 2019). Characterizing change in ω provides an understanding of how long-term climate and hydrological changes interactively affect forests, grasslands, and megaregions (Zhou et al., 2015). In this study, shifts in ω of NFs, NGs, and megaregions from current to future conditions was used to represent changes in integrative properties such as land cover, vegetation cover, and climate conditions.

Under stationary climatic conditions, the parameter Omega in Fu's equation is primarily governed by surface vegetation. However, long-term changes in climate normal (e.g., 30-yr average annual temperature, precipitation, relative humidity) beet changes in hydroclimatic indices in the Budyko space. Thus, the current study characterized these climatic influences while surface vegetation is kept the same as the control period. Significant changes in the integrative basin properties of U.S. megaregions may considerably affect future agricultural, economic, social, ecosystemic and environmental activities, especially in the megaregions with insufficient natural and water resources and rapid population and economic growth.

3.2.6. Changes in the Regional Climate Zones

The Koppen climate classification has been widely used to divide the United States to main climate groups including Arid, Temperate, Continental, and Tropical based on the empirical relationship between climate and vegetation (Chen & Chen, 2013). However, megaregions may shift from one type to another in the future. To understand this, we first determined the major regional climate zone of each HUC8 river basin (Figure B-3.a). Then, the Fine Gaussian SVM

(Cristianini & Shawe-Taylor, 2000) was applied to divide the Budyko space into three regions based on the Koppen Climate Classification and current aridity and evaporative indices. Koppen Climate Classification-Level1 has a high accuracy (76.2%) to classify Budyko space to three Regions. Figure B-3.b provides classification of the Budyko space based on the Koppen climate classification. Figure B-3.c illustrates the classified climate zones using the Fine Gaussian SVM.

Arid region is pretty close to the water limited condition while the temperate region is close to the energy limited condition, and the Continental region is somewhere between the Arid and Temperate regions. In this study, spatial changes in climate types of the U.S. megaregions were projected using shifts in the Budyko space. The economic and population growths of U.S. megaregions can be highly influenced by climate change, especially in regions that are likely to experience new climate regime in the future. Rapid population and economic growth combined with considerable shifts in climate and water resources in the megaregions may beget irrecoverable consequences at national scale. Planners, policy makers and politicians may improve preparedness by providing an insight to future changes in advance and implementing adaptation and mitigation strategies.

3.3. Results

This section summarizes changes in regional hydroclimatic conditions from the past period (1986-2015) to future period (2070-2099) for groups of NFs and NGs in eight National Forest service regions. Changes in hydroclimatic conditions of NFs and NGs were assessed by characterizing the direction and magnitude of shifts in the Budyko space. Finally, Fu's equation was applied to determine hotspot regions with the highest change in their basin characteristics. The results for NFs and NGs reported below are precisely for HUC8 watersheds containing all or part of NFs and NGs.

In addition, the hydroclimatology of U.S. megaregions may respond differently to future climate change. While some regions such as Houston are more likely to experience long-term drying periods in the future, some regions such as Los Angeles, San Diego, and San Francisco are more likely to experience long-term wetting periods in the future. Besides, the megaregions like Phoenix may have significant changes in their integrative basin characteristics. The climate types of basins in Seattle and Houston have respectively the lowest and highest shifts in response to climate change. This section is aimed to provide an improved understanding of the effects of climate change on hydroclimatic conditions and basin characteristics of fourteen U.S. megaregions.

3.3.1. Changes in Hydroclimatic Conditions of U.S. NFs and NGs

Table 3.2 summarizes average precipitation (PCP), water yield (YIELD), and potential evapotranspiration (PET) for NFs and NGs and the entire CONUS for the current (1986-2015) period from the combination of DAYMET and PRISM dataset. Values for HUC8s that include any proportion of NFs and NGs lands are area-weighted by fractional HUC area to make a comparison. The 30-year average of precipitation and water yield of NFs are above the CONUS average. However, the amounts of precipitation and water yield in NGs are considerably lower than the CONUS average. Although most NGs are in areas with low precipitation and water yield compared to the NFs, the 30-year averages of potential evapotranspiration of NFs and NGs are relatively close (Table 3.2). A higher proportion of precipitation was converted to water yield in the NFs than in the CONUS as a whole, confirming that NFs tend to be an important source of water yield.

Table 3.2. 30-year average of hydroclimatic variables under current conditions.

Type	PCP (mm)	YIELD (mm)	PET (mm)
NFs	909	400	1533
NGs	426	25	1523
CONUS	876	301	1617

Table 3.3 shows percentage changes in hydroclimatic variables of NFs and NGs from current conditions (1986-2015) to future conditions (2070-2099) under the MIDDLE, DRY, and WET scenarios. The 30-yr average precipitation of NFs increases under all three scenarios, and of NGs increases under the WET and MIDDLE scenarios. In contrast, average precipitation decreases for NGs under the DRY scenario, as it does for CONUS.

Projected changes in water yield among the three scenarios largely reflect the changes precipitation, with increases projected for the MIDDLE and WET scenarios in the CONUS as well as in NFs and NGs, and decreases projected for the DRY scenario for CONUS and NGs. The exception is NFs under the DRY scenario, where average water yield decreases despite a small average increase in precipitation.

Table 3.3. Changes in hydroclimatic variables of NFs, NGs, and CONUS from current conditions to future conditions (in percent).

Climate models	Type	PCP (%)	YIELD (%)	PET (%)
MIDDLE	NFs	13.51	8.05	0.80
	NGs	11.41	12.47	2.19
	CONUS	9.11	12.26	2.41
DRY	NFs	1.98	-8.76	3.34
	NGs	-2.81	-12.20	3.62
	CONUS	-6.63	-12.46	5.01
WET	NFs	18.22	21.38	-0.92
	NGs	10.63	18.99	-0.30
	CONUS	15.86	36.87	-0.48

The percentage change in average potential evapotranspiration is small compared to changes in the other hydroclimatic variables. While potential evapotranspiration increases under the MIDDLE and DRY scenarios for all NFs and NGs, it consistently decreases under the WET scenario. Although NGs have higher changes in the average potential evapotranspiration and water yield under MIDDLE and DRY scenarios, NFs see greater changes in potential evapotranspiration and water yield under the WET scenario.

Figures 3.4 and 3.5 illustrate spatial changes from the current to future time period in precipitation, potential evapotranspiration, and water yield of USFS land (NFs and NGs) of the eight USF regions of the CONUS. As shown in Figure 3.4, the direction and magnitude of changes in all three variables of most regions highly depends on the selected future climate model. Regarding the direction in average precipitation, for instance, in the Southwestern, Rocky Mountain, and Southern regions precipitation increases for the WET scenario and decreases under the DRY scenario, but consistently increases in the Northern, Intermountain, Pacific Southwest, Pacific Northwest, and Eastern regions.

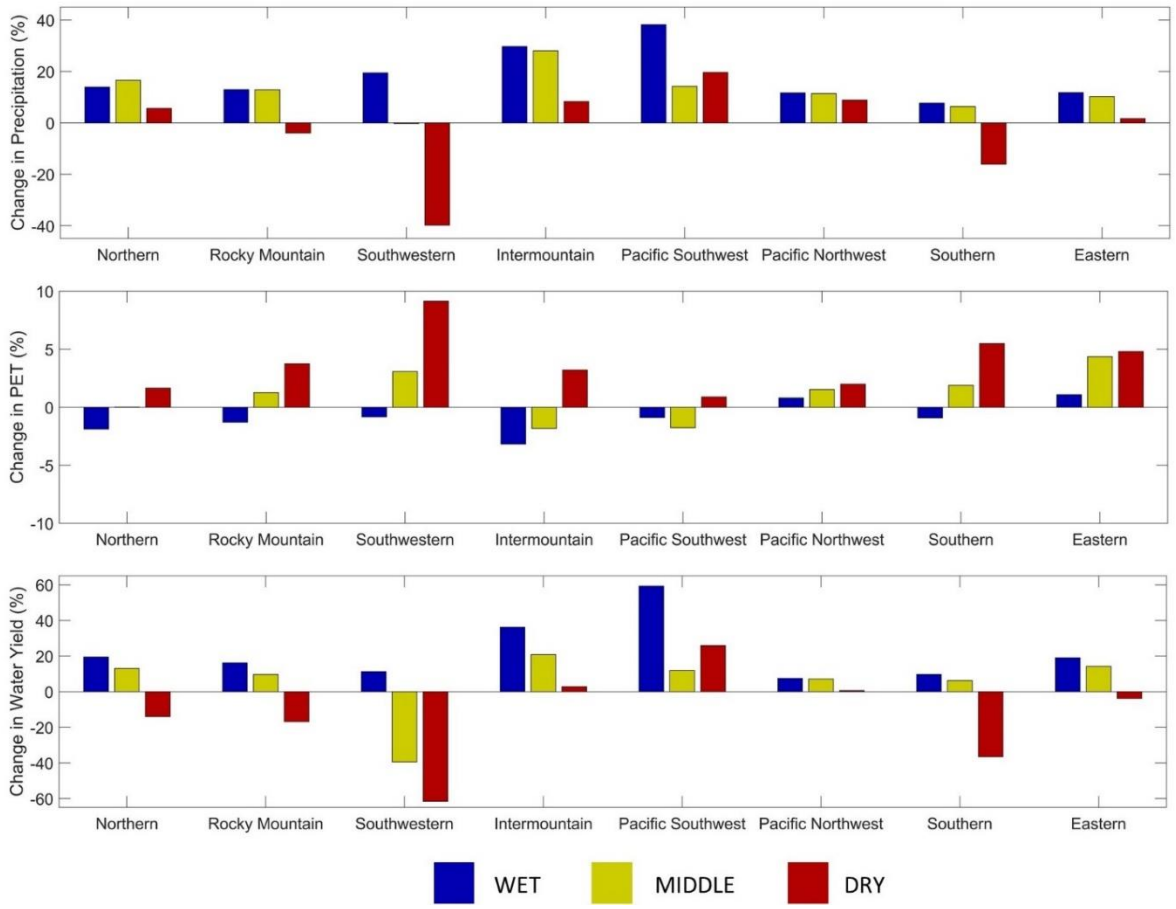

Figure 3.4. Changes in precipitation, PET, and water yield of NFs and NGs within USFS regions from current conditions to future conditions.

Despite the variability across future scenario, at least two findings stand out. First, precipitation is projected to increase in most regions under all three scenarios but decrease substantially in two regions (Southwestern and Southern) under the DRY scenario. Second, water yield is projected to increase under the WET and MIDDLE scenarios in all but one case (Southwestern under the MIDDLE scenario) and to decrease in five regions under the DRY scenario, with large percentage decreases in the Southwestern and Southern regions. Note, the DRY, MIDDLE, and WET climate models reflect conditions in general, not necessarily in every region.

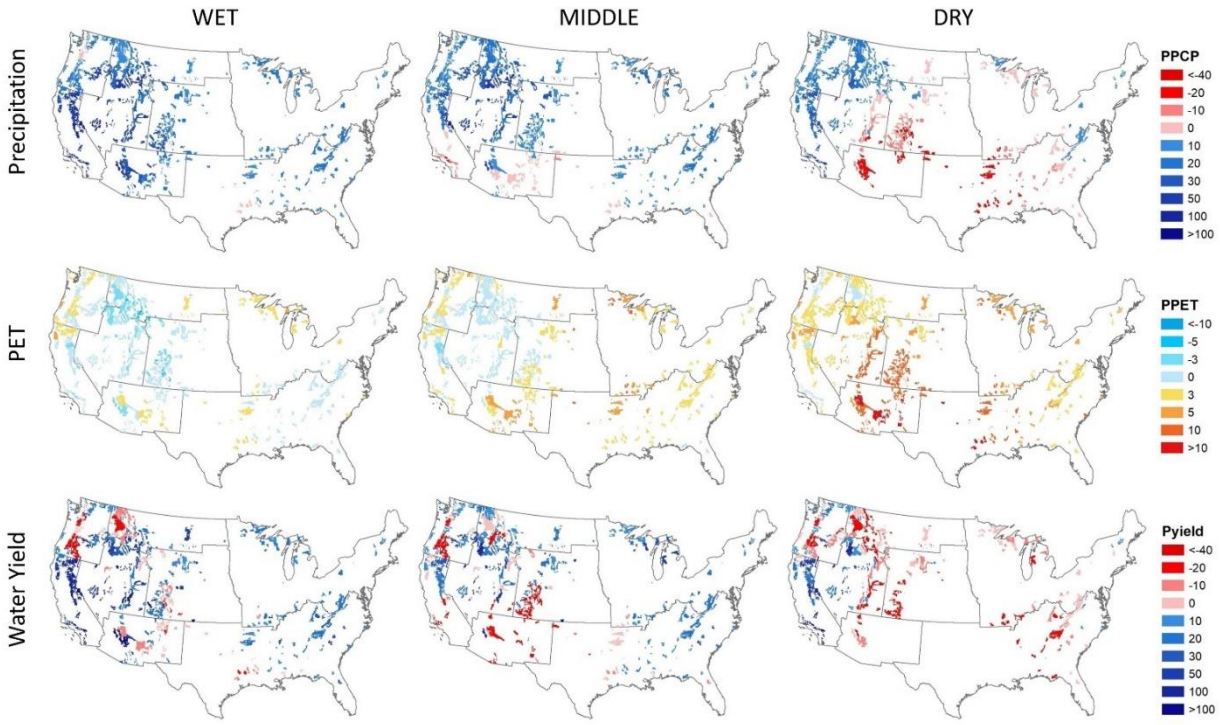

Figure 3.5. Maps of percent changes in precipitation, PET, and water yield of NFs and NGs regions from current conditions to future conditions under the DRY, MIDDLE and WET scenarios.

The NFs in high mountainous regions will experience higher changes in hydroclimatic variables than NGs and NFs at lower elevations (Figure 3.5). However, the direction of change varies based on the selected future climate model. Precipitation, PET, and water yield for the high mountainous NFs are likely to experience the largest changes in response to climate change. Table B-1 provides percentage changes in precipitation, potential evapotranspiration, and water yield of U.S. national forests and grasslands under WET, MID, and DRY climate scenarios in details.

The Wilcoxon signed-ranked test was used to assess the significance of the future changes in PCP, PET, and Yield under DRY, MIDDLE, and WET scenarios at the 5% significance level (Table B-2). Under the WET scenario, change in PCP is significant in most NFs and NGs within the Pacific Southwest, Intermountain, Southwestern, Eastern, and Southern regions. Change in PET is statistically significant for most NFs and NGs located in the Rocky Mountain and Northern

regions. Changes in Yield is significant in most regions within the Pacific Southwest and Pacific Northwest. Under the MIDDLE scenario, change in PCP is statistically significant in most NFs and NGs within the Northern and Intermountain regions. Change in PET is significant for most NFs and NGs located in the Southwestern, Southern, and Eastern regions. Changes in Yield is significant in most regions within the Southwestern and Pacific Northwest regions. Under the DRY scenario, change in PCP is significant in most NFs and NGs within the Southern, Rocky Mountain, and Southwestern regions. Change in PET is statistically significant for most NFs and NGs located in the Eastern, Southern, Rocky Mountain, Southern, and Intermountain regions. Changes in Yield is significant in most regions within the Southern, Southwestern, and Pacific Northwest regions.

Figures 3.6 shows the current aridity and evaporative indices of the NGs and NFs, and Figure 3.7 presents the averages of the current aridity and evaporative indices of the eight USFS regions. The NFs and NGs within the Southwestern, Rocky Mountain, and Intermountain regions currently have the most arid conditions along with the highest evaporative index. In contrast, the Southern, Eastern, and Pacific Northwest regions have the lowest aridity index and, along with the Pacific Southwest region, the lowest evaporative index, meaning that USFS and in these regions currently have generally a less arid climate with higher freshwater availability.

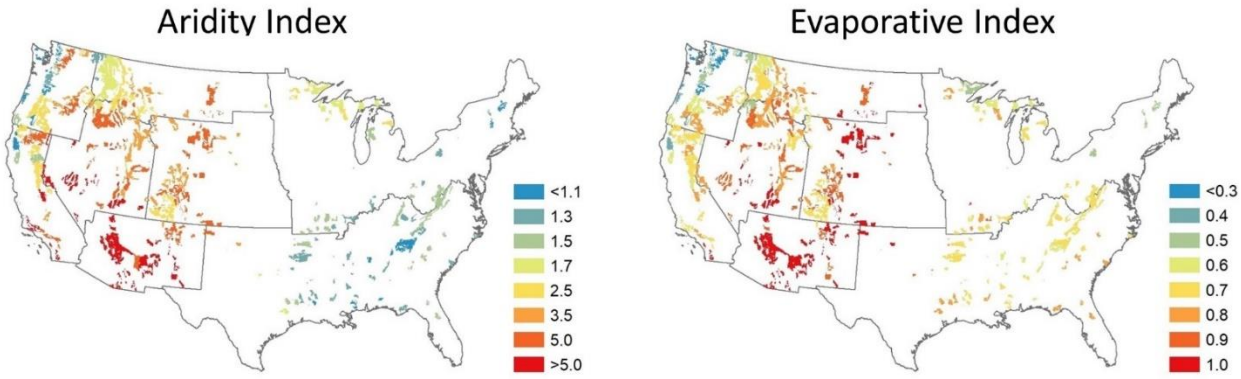

Figure 3.6. Current aridity and evaporative indices of NFs and NGs.

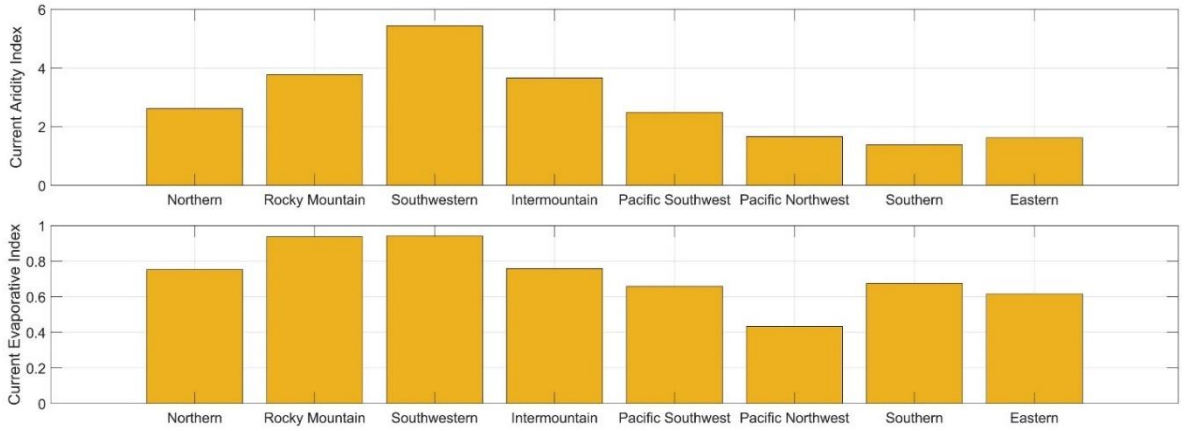

Figure 3.7. Current aridity and evaporative indices of NFs and NGs within USFS regions.

Figures 3.8 provides changes in the aridity and evaporative indices of NGs and NFs, and Figure 3.9 (right panel) shows changes in the average aridity and evaporative indices of those areas within the eight USFS regions. The Eastern, Southern, and Pacific Northwest regions, which are less arid under current conditions, are more likely to experience small changes in the aridity index under the future conditions.

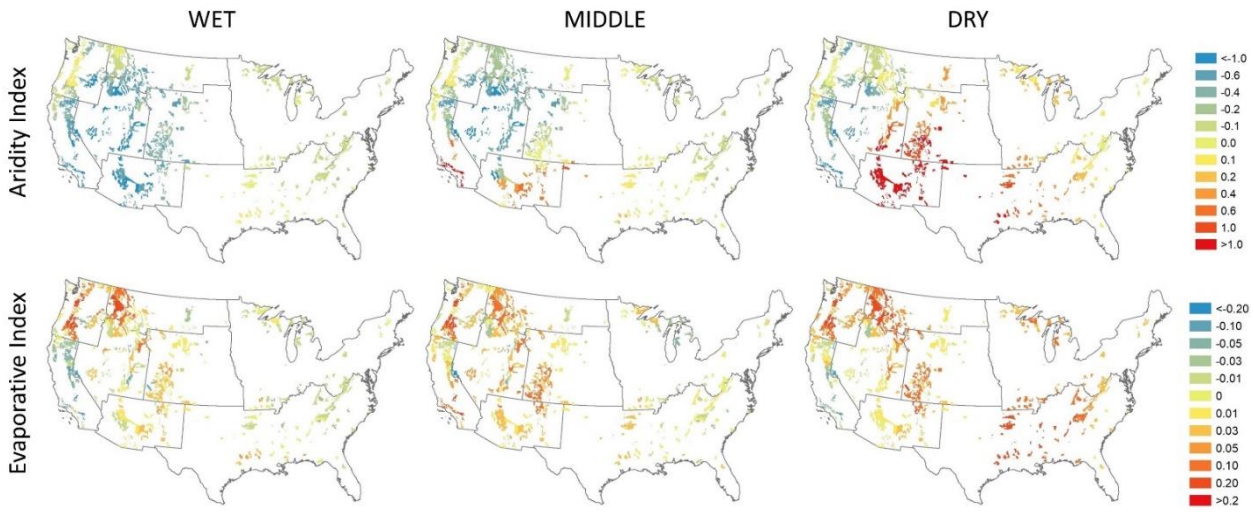

Figure 3.8. Changes in aridity and evaporative indices of NGs and NFs from current to future conditions.

Although the USFS lands of the Northern, Pacific Northwest, Southern, and Eastern regions, which are least arid under current conditions, are projected to incur only minor changes in aridity index under all three scenarios, the Southwestern, Intermountain, and Pacific Southwest regions are more likely to experience higher change in aridity index, especially under selected scenarios. The Intermountain, Pacific Southwest, and Pacific Northwest regions consistently are projected to experience a decrease in aridity index, meaning that they are likely to be less arid in the future. However, the Southwestern region under the DRY climate scenario shows the highest increase in aridity index, of approximately 5% meaning that this USFS region is vulnerable to a more highly arid condition in the future.

An increase in the evaporative index indicates that more of the available precipitation is evaporated than under current conditions. The generally increasing evaporative index among the regions and scenarios reflects the overall increase in projected temperature and thus energy for evaporation (plus in some cases the decrease in precipitation).

The significance of the future changes in the aridity and evaporative indices was assessed using the Wilcoxon signed-ranked test at the 5% significance level under DRY, MIDDLE, and WET scenarios (Table B-3). Under the WET scenario, change in aridity index is significant in most NFs and NGs within the Rocky Mountain, Intermountain, Pacific Southwest, and Northern regions. Change in evaporative index is statistically significant for most NFs and NGs located in the Pacific Southwest, Pacific Northwest, and Northern regions. Under the MIDDLE scenario, change in aridity index is statistically significant in most NFs and NGs within the Northern, Intermountain, and Pacific Southwest regions. Change in evaporative index is significant for most NFs and NGs located in Rocky Mountain, Southwestern, and Northern regions. Under the DRY scenario, change in aridity index is statistically significant in most NFs and NGs within the

Southwestern, Southern, Rocky Mountain regions. Change in evaporative index is statistically significant for most NFs and NGs located in the Southern, Eastern, Rocky Mountain, Northern, Southwestern, and Pacific Northwest regions.

Figure 3.9 (left panel) shows in the Budyko space the changes depicted in Figure 3.9 (right panel) using the Forest Service region numbers. The hydroclimatology of the Northern, Intermountain, Pacific Southwest, and Pacific Northwest regions show the most consistency across the three climate scenarios. While the Northern, Intermountain, and Pacific Northwest regions are projected to experience less arid condition but with lower freshwater availability, the Pacific Southwest region is projected (under the WET and DRY scenarios) to move to the lower-left, meaning less arid conditions and higher freshwater availability. Long-term changes in the hydroclimatology of the Rocky Mountain, Southwestern, Southern, and Eastern regions vary in aridity index across the three scenarios, with aridity consistently decreasing under the WET scenario and increasing under the DRY scenario, with variable results under the MIDDLE scenario.

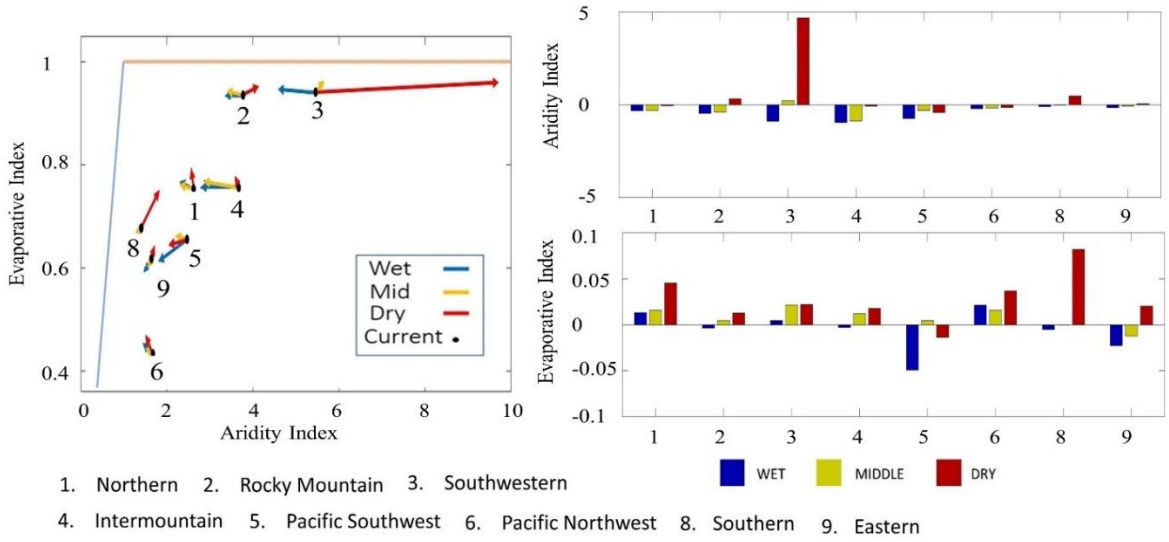

Figure 3.9. Changes in aridity index, evaporative index, and Budyko space of NFs and NGs within USFS regions from current to future conditions.

Under the WET scenario, all forest service regions move to the left meaning less arid conditions in the future. However, the USFS regions located in the Central and Western United States have a higher magnitude of changes indicating that these regions are more sensitive to climate change.

Under the MIDDLE scenario, similar to the WET scenario, most USFS regions move to the left. However, the magnitude of movements is smaller than in the WET scenario. Besides, the NFs and NGs within the Southwestern region behave differently under the MIDDLE scenario. Movements within the Southwestern region are more likely to the right indicating that this region may experience drier hydroclimatic conditions in the future.

Under the DRY scenario, the Eastern, Southern, Rocky Mountain, Southwestern regions consistently show drier conditions with less water yield with the highest magnitude in the Southwestern and Southern regions, respectively. NFs and NGs within the Northern, Pacific Northwest and Intermountain regions behave differently under the DRY scenario. However, movements within the Pacific Southwest region are to the left indicating that this region is more likely to experience less arid hydroclimatic conditions in the future.

Our findings are sensitive to the choice of climate model. The results presented in this study under DRY, MIDDLE and WET climate models are indicative of the effect the uncertainty associated with future climate change impacts on the hydroclimatology of U.S. NFs and NGs. Under all three scenarios, the Southwestern region has a high magnitude of change meaning that its hydroclimatic conditions have high sensitivity to future climate change. While the Southwestern region is getting warmer and drier with a high magnitude of change under the DRY and MIDDLE

scenarios, it is more likely to experience wetter and less arid hydroclimate conditions with high magnitude under the WET scenario.

In addition to the average magnitude and direction of each USFS region, we assessed the distribution of changes in frequency, magnitude, and direction of each region using the wind rose diagram (Figures B-4 to B-6). The wind rose diagram visualizes the summary of movements in the Budyko space for the 8-digit hydrologic unit (HUC8) river basins within NFs and NGs. This type of diagram has been used in global hydroclimatic change assessments (Destouni et al., 2013). Figures B-4 to B-6 provide wind rose diagrams of movements in the Budyko space under WET, MIDDLE, and DRY scenarios, respectively.

Figure B-7 compares changes in hydroclimatic conditions of NFs with NGs under the WET, MIDDLE, and DRY scenarios. Based on the wind rose diagrams under the DRY climate model, movements of river basins within US NGs are more likely to occur in the directions represented by the right quadrants of the rose diagram. The results indicate that most river basins in the NGs have a low magnitude of changes. However, under the MIDDLE and WET scenarios, river basin movements within both NGs and NFs are likely to occur in the directions represented by the left quadrant of the rose diagram. Although NFs are more likely to experience a higher magnitude of change under the WET scenario, NGs have a higher magnitude of change under the MIDDLE scenario. Table B-4 provides changes in the direction and magnitude of each U.S. NFs and NGs in the Budyko space under the WET, MID, and DRY scenarios.

3.3.2. Changes in Basin Characteristics of U.S. NFs and NGs

Changes in integrative properties of basins in response to hydroclimatic shifts can be represented by changes in ω of Fu's equation (Equation 3.5). Change over time in ω of a HUC8 could demonstrate changes in integrative properties of NFs and NGs such as differences in land

cover, vegetation cover, and climate Table 3.4 represents current and future average ω of NFs and NGs across the CONUS. The change in ω from the current to the future period is small under all three climate scenarios. Under all three climate scenarios, NFs have larger changes in ω than NGs, meaning that NFs are more likely to experience higher changes in their basin characteristics compared to NGs assuming that a specific amount of change in omega has the same effect on likelihood of shift in characteristics in all USFS regions and both forests and grasslands. Additionally, under the WET and MIDDLE climate scenarios, an increase in ω for NFs and NGs is above the CONUS average, indicating that they may experience higher shifts in their properties compared to other regions. Under the DRY scenario, although NFs have higher changes in ω, change in ω of NGs is below the CONUS average. NFs under all three climate scenarios and NGs under the WET, and MIDDLE climate scenarios experience increasing ω while NGs and CONUS average have minor decrease in the ω under the DRY climate scenario.

Table 3.4. Current and future ω of Fu's equation for the NGs and NFs.

Types	Current	WET	MID	DRY
Forest	1.82	1.924	1.939	1.927
Grassland	2.95	3.049	3.061	2.949
CONUS	2.135	2.162	2.159	2.133

Table 3.5 provides current and future ω of Fu's equation for the eight USFS regions under the WET, MIDDLE, DRY scenarios. The ω for eight regions is nearly always increasing under three climate scenarios, the main exception being the decrease in ω of the Southwestern region under the DRY climate scenario. The ω in the Eastern, Southern, Pacific Northwest, and Pacific Southwest regions changes only slightly, indicating that these regions are more likely to experience only minor shifts in the basin characteristics. However, the Southwestern, Northern,

Intermountain, and Rocky Mountain regions are more likely to experience higher shifts in their physiographic and ecological characteristics.

Table 3.5. Changes in ω of Fu's equation for the Forest Service regions.

Forest Service region	Current	WET	MIDDLE	DRY
Northern	1.80	1.91	1.92	1.95
Rocky Mountain	2.41	2.49	2.56	2.48
Southwestern	2.21	2.36	2.40	2.11
Intermountain	1.68	1.79	1.82	1.73
Pacific Southwest	1.61	1.66	1.67	1.65
Pacific Northwest	1.38	1.44	1.43	1.45
Southern	2.00	2.05	2.01	2.04
Eastern	1.71	1.71	1.71	1.74

In this study, we assessed changes in ω from current conditions to future conditions to find which NFs and NGs are more prone to be affected by long-term hydroclimatic changes. The NFs and NGs with larger changes in ω are likely to experience higher moving in the direction of a shift in integrative properties of basin. Thus, we figured out which US Forest Service regions have the highest sensitivity to experience considerable shifts in the structure and composition of forests and grasslands.

3.3.3. Changes in Hydroclimatic Conditions of U.S. Megaregions

The historic hydroclimatic conditions including the 30-year average of precipitation, evaporation, water yield, evapotranspiration, and temperature of the fourteen U.S. megaregions are shown in Figure B-8. Overall, Seattle has the highest amount of precipitation and water yield. Los Angeles, San Diego (LOS-SAN), Phoenix, and Denver have the lowest amount of historic precipitation, water yield, and evaporation. Miami, Houston, and Atlanta have the highest amount of evaporation and temperature. The variation in 30-year potential evapotranspiration of U.S.

megaregions is comparatively small compared to other hydroclimatic variables. Seattle has the lowest amount of potential evapotranspiration among all U.S. megaregions.

Changes in hydroclimatic conditions of U.S. megaregions from current (1986-2015) to future (2070-2099) periods are provided in Figure B-9 using DRY, MIDDLE, and WET climate models. Los Angeles, San Diego (LOS-SAN), San Francisco, and Phoenix have respectively the highest changes in precipitation. The precipitation and water yield in Los Angeles, San Diego (LOS-SAN), San Francisco, Washington D.C, Philadelphia, New York, Boston (WPHNB), and Seattle are more likely to consistently increase under all three climate models. Houston is more likely to experience a consistent decrease in precipitation and water yield under the three climate models. However, change in 30-year average precipitation and water yield of Phoenix, Denver, Miami, and Atlanta highly depends on the future climate model.

The potential evapotranspiration in Houston, Washington D.C, Philadelphia, New York, Boston (WPHNB), and Seattle is more likely to increase from current to future conditions. Although San Francisco is more likely to experience small changes in potential evapotranspiration, Phoenix, Denver, Miami, Atlanta, Los Angeles, San Diego, and Chicago shows various responses in potential evapotranspiration based on the future different climate model.

The current aridity and evaporative indices of U.S. megaregions are illustrated in Figure B-10. Los Angeles, San Diego (LOS-SAN), Phoenix, Denver, and San Francisco have a high aridity index indicating that these regions are more limited by water availability. Additionally, these regions have a high evaporative index meaning that a considerable amount of precipitation is likely to evaporate from these regions.

Other U.S. megaregions including Chicago, Miami, Houston, Atlanta, Washington D.C, Philadelphia, New York, Boston (WPHNB), and Seattle have around the same aridity index under the current climate conditions. However, Chicago, Miami, Houston, and Atlanta have a higher evaporative index compared to Washington D.C, Philadelphia, New York, Boston (WPHNB), and Seattle. The finding indicates that while these regions have the same ratio of potential evapotranspiration to precipitation under current conditions, water yield (or streamflow) is lower in Washington D.C, Philadelphia, New York, Boston (WPHNB), and Seattle.

Figure 3.10 shows changes in aridity and evaporative indices of U.S. megaregions in response to future climate change. Although variability in the projection of future hydroclimatic shifts is dominated by variability in climate change scenarios, projected changes in future hydroclimatology of U.S. megaregions showed some consistency across climate change models in terms of the direction and magnitude of changes.

Changes of aridity index are projected to be small in Seattle, Chicago, Miami, Washington D.C, Philadelphia, New York, Boston (WPHNB), and Atlanta, indicating that climate change may have relatively small impacts on regional climatology in these regions. However, the aridity index of Los Angeles, San Diego, and San Francisco are projected to increase consistently across DRY, WET, and MIDDLE climate models. This finding indicates that these regions are more likely to experience less arid climate conditions in the future.

The aridity index of Denver and Phoenix is highly dependent on climate models. While the aridity index may increase under the DRY climate model, it may remain constant under the MIDDLE climate model and decrease under the WET climate model. However, Houston is the only megaregion that consistently have an increasing aridity index under the three climate models,

indicating that Houston is more likely to have more arid climatic conditions by the end of the century.

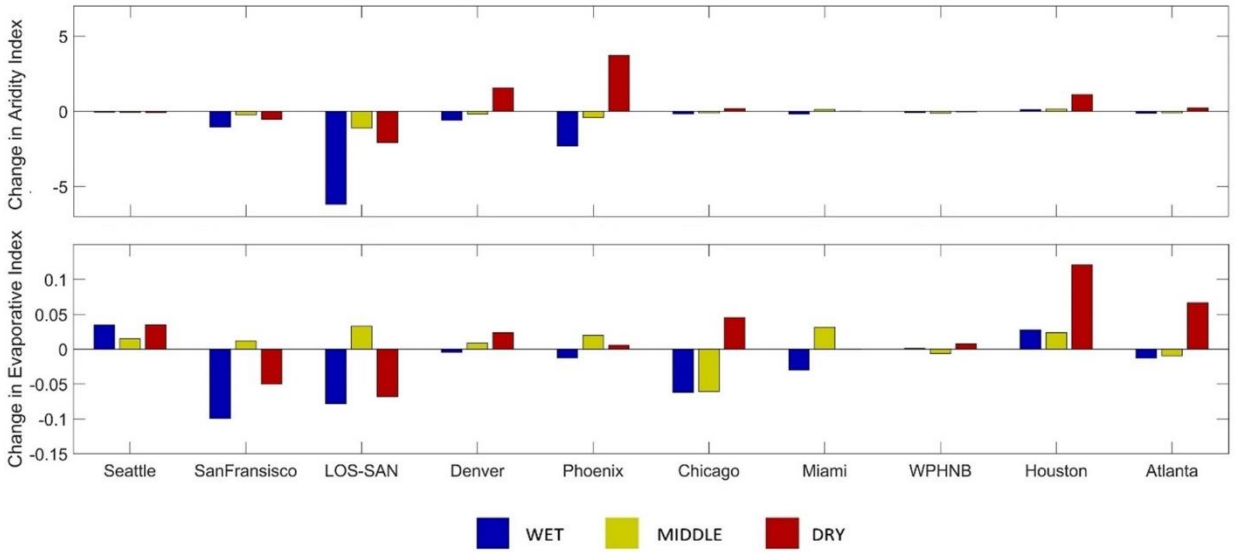

Figure 3.10. Change in 30-year average of hydroclimatic indices of the U.S. megaregions from current to future conditions.

Houston and Seattle are the only megaregions that show consistently increasing evaporative index, indicating that river discharge is more likely to decrease in these regions in the future. The evaporative index of other regions highly depends on the future climate model. While Denver, Washington D.C, Philadelphia, New York, Boston (WPHNB), and Phoenix show the lowest change in evaporative index in response to climate change under all three climate models, the evaporative index of San Francisco, Los Angeles, San Diego, Chicago, Atlanta, and Miami is highly variable in the future according to the selected climate model.

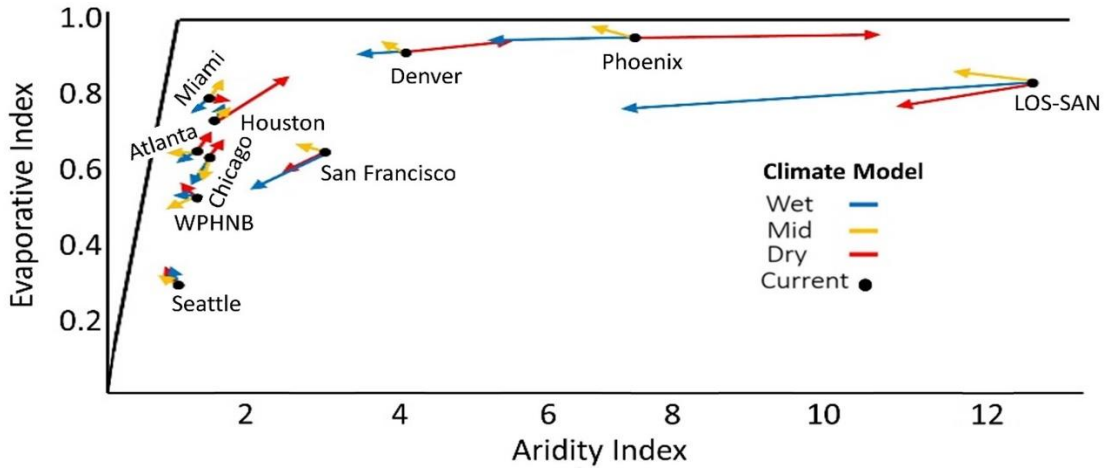

Figure 3.11. The average movements of U.S. Megaregions from current to future climate conditions.

Figure 3.11 shows the movement of each megaregion in the Budyko space under the DRY, MIDDLE, and WET climate models as the representation of changes in hydroclimatic conditions of each region. Houston is moving to the upper-right quadrant of the Budyko space under the three climate models meaning that Houston is more likely to get warmer and drier in the future. San Francisco, Los Angeles, San Diego (LOS-SAN), Washington D.C, Philadelphia, New York, Boston (WPHNB) are moving to the left quadrant of the Budyko space under the three climate models indicating that these regions are more likely to experience less arid climatic conditions in the future. Seattle is moving to the upper-left quadrant of the Budyko space under the three climate models meaning that the evaporative index is increasing while the aridity index is decreasing.

3.3.4. Changes in Basin Characteristics of U.S. Megaregions

In this section, we used the Fu's equation to characterize the effect of hydroclimatic change on basin characteristics of U.S. megaregion using the DRY, MIDDLE, and WET climate model. The basin characteristics of megaregions with a higher percentage of changes in ω are more sensitive to future estimated hydroclimatic change. Table 3.6 provides current and future ω under

the DRY, MIDDLE, and WET climate model for the fourteen U.S. megaregions. Changes in ω can be a sign for shifts in ecology, land cover, and vegetation cover (Coe et al., 2011; Zhang and Wei, 2012; Zhao et al., 2009; Zhou et al., 2015).

Table 3.6. Current and future ω of U.S. megaregion.

Mega region	Current	WET	MIDDLE	DRY
Seattle	1.31	1.38 (+5%)	1.35 (3%)	1.39 (6%)
San Francisco	1.53	1.50 (-2%)	1.57 (3%)	1.50 (-2%)
LOS-SAN	1.53	1.52 (-1%)	1.62 (6%)	1.45 (-5%)
Denver	2.18	2.25 (3%)	2.27 (4%)	2.16 (-1%)
Phoenix	2.15	2.25 (5%)	2.40 (12%)	2.03 (-6%)
Chicago	1.82	1.74 (-4%)	1.71 (-6%)	1.88 (3%)
Miami	2.46	2.49 (1%)	2.52 (2%)	2.44 (-1%)
WPHNB	1.69	1.74 (3%)	1.74 (3%)	1.73 (2%)
Houston	2.14	2.19 (2%)	2.14 (0%)	2.17 (1%)
Atlanta	1.98	2.06 (4%)	2.04(3%)	2.07 (5%)

Phoenix has the highest change in ω under all climate models, indicating that the basin characteristics of Phoenix are likely to experience higher shifts in response to the future hydroclimatic changes. Houston, San Francisco, Miami, Washington D.C, Philadelphia, New York, Boston (WPHNB) has comparatively lower changes in ω meaning that the basin characteristics of these regions are less sensitive to future hydroclimatic changes.

In this study, we focused on applying Fu's equation to characterize the U.S. megaregions that have the highest change in their basin characteristics in response to future hydroclimatic changes. Finding a statistical correlation between ω and various basin characteristics such as slope, physiography, ecology, landcover is more complicated and beyond the scope of this study.

3.3.5. Spatial Changes in the Climate Types of U.S. Megaregions

Changes in the spatial extent of climate types were also characterized by changes in the areas occupied by the Koppen climate types (Figure 3.12). The light-yellow color shows the

regions with no changes in their climate types. Under the WET and MIDDLE scenarios few HUC8 basins show change in climate classification. Under all three climate scenarios, some basins in the Washington D.C, Philadelphia, New York, and Boston (WPHNB) are projected to change from Continental to Temperate climate type. Under the WET scenario, some basins in Denver, Los Angeles, San Diego, Phoenix, and San Francisco megaregions are likely to change from Arid to Continental climate type. However, under the MIDDLE scenario, some basins in Los Angeles, San Diego, Phoenix, and Denver may experience shift from Continental to Arid.

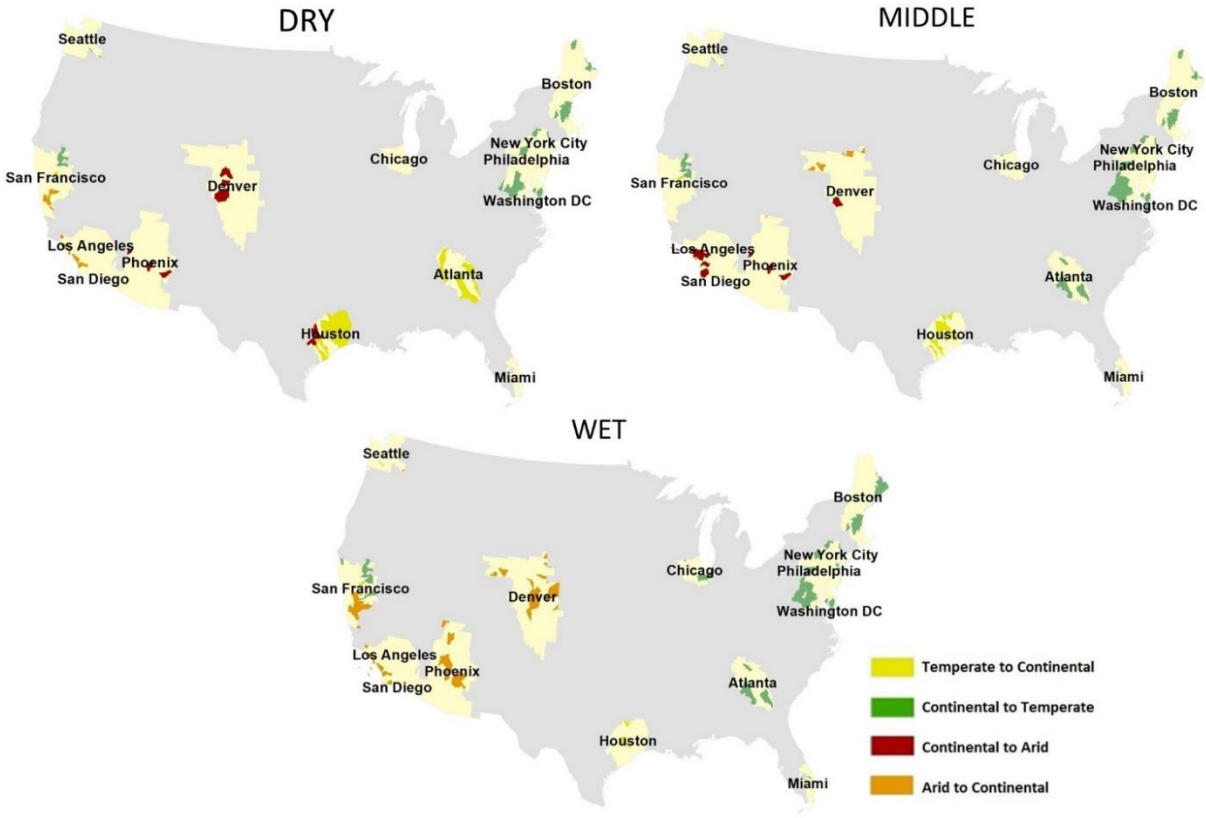

Figure 3.12. Shift in the U.S climate zones under three climate change scenarios (The light-yellow color shows the regions with no changes in their climate types).

Under the DRY climate scenario, most basins in Houston are likely to experience shifts in their climate type from Continental to Arid, or from Temperate to Continental. Additionally, most

basins in Atlanta are projected to change from Temperate to Continental. Some basins in Denver megaregion are likely to change from Continental to Arid climate type.

3.4. Discussion

Although the results of this study provide some possible insights about the potential hydroclimate changes in the U.S. NFs, NGs, and megaregions, a variety of uncertainties associated with climate models, emission scenarios, downscaling methods, hydroclimatic projections, and hydrological models are not considered in the current study. Thus, although the finding of this study provides an improved understanding of future hydroclimatology and basin characteristics of U.S. megaregions, NFs, and NGs, it is not an exact prediction of future conditions.

The results are subject to several sources of uncertainty, including those introduced by the choice of the climate models and the hydrological models we used. Climate models are uncertain because they highly depend on future anthropogenic and natural forcing scenarios. Besides, the future climate projections can be affected by the existence of internal climate variability and incomplete understanding and imprecise climate models (Wyard et al., 2020; Collins et al., 2020). Using ensemble simulation rather than specific climate scenarios can be a prospect for this study to assess decrease in climate model variability.

We focused on a range of possible future climate conditions, from driest to wettest, to account for current uncertainty about long-term future climatic conditions. Although variability in the projection of future climate conditions can be affected by some sources of uncertainty and variability in climate change scenarios, projected shifts in hydroclimatic conditions of some NFs, NGs, megaregions showed some consistency across climate change models in terms of the direction and magnitude of changes.

In addition to the uncertainty in the choice of climate models, some uncertainties remain, related to the hydrological model. The VIC model may not capture all physical basin characteristics, water management regulations, landcover changes (Naz et al., 2016). Besides, there are some uncertainties associated with parameters of the VIC model and structural deficiencies of the model simulation (Gharari et al., 2019, 2020; Melsen et al., 2016). Using multiple hydrologic models can be a prospect for this study to evaluate the modeling uncertainty associated with the role of hydrological models in hydroclimatic changes assessment (Oubeidillah et al., 2014). Furthermore, estimated changes in ω can originate from the assumptions associated to Fu's equation.

The hydroclimatology of U.S. megaregions can be influenced by anthropogenic factors such as rapid population growth. In the absence of any adaptive urban adaptation strategies, such as green, cool roof, and hybrid approaches, the temperature is expected to raise in response to the greenhouse gas-induced forcing (Benson-Lira et al., 2016; Georgescu et al., 2014). Increasing temperature itself can lead to shifts in hydroclimatic conditions of U.S. megaregions. Additionally, reservoir regulation and interbasin water transferred to support each megaregion was also not specifically addressed.

We only focused on the state watershed as the major source that the megaregions derive their water supply. However, water supply to some megaregions can be from watersheds /reservoirs outside of the regions or groundwater resources. Note, we assessed shifts in future hydroclimatology of megaregions and evaluating anthropogenic factors and socioeconomic consequences are out of the scope of this paper.

Additionally, future hydroclimatic changes may have various consequences for forests. For example, while a temperature rise is likely to decrease growth in lower elevations, it might increase

growth in higher elevations (Littell et al., 2012). Thus, future studies are needed to determine the relationships between hydroclimatology of US river basins and the composition, distribution, and growth of various types of forests and grasslands.

Despite these limitations, comparisons of differences in long-term hydroclimatic variables from the current period (1986-2015) to the future period (2070-2099) are more likely to be accurately estimated than are the absolute amounts from which the differences are computed. The structural deficiencies and assumptions in the VIC model can be addressed by aggregating outputs over longer time periods such as 30-yr average (Gharari et al., 2019). The results suggest a need for flexible and regionalized forest management strategies under these scenario-sensitive, spatially-heterogeneous projections of future hydroclimatic conditions.

3.5. Summary and Conclusions

Understanding change in hydroclimatic conditions of NFs, NGs, and megaregions and how those changes will impact natural and water resources, have risen in importance as our understanding of climate change has improved (Fekety et al., 2020). This study first focuses on shifts in long-term regional climate and hydrologic trends of two important sources of natural resources in the United States, National Forests (NFs) and National Grasslands (NGs). This study second evaluates changes in hydroclimatology and basin characteristics of fourteen U.S. megaregions in response to climate change using the Budyko framework.

Changes in current climatic conditions (1986-2015) were first derived from a combination of Daymet and PRISM with wind speed data from the NARR dataset at the 4km-by-4km spatial scale. Changes in future climatic variables (2070-2099) were obtained from the MACA climate dataset at 4km-by-4km spatial scale for three climate models, yielding projections for three quite different climate scenarios. The forcing parameters from that data were then used as inputs to the

VIC hydrological model to obtain hydrological estimates at a daily timestep. The output hydroclimatic variables were aggregated at the HUC8 river basin scale and annual timestep. The aggregated hydroclimatic variables were then used to estimate current and future hydroclimatic conditions of NFs, NGs, and megaregions across the CONUS. Long-term changes in those conditions were depicted as movement in the Budyko space. Finally, the Fu's equation was implemented to assess shifts in integrative basin characteristics.

The response of basins to climate change varies from NFs to NGs and from one climate scenario to another. However, there was some significant consistency in regional long-term hydroclimatic changes on NFs and NGs. Both NFs and NGs are projected to experience less arid hydroclimatic conditions under both the WET and MIDDLE climate scenarios, in contrast to generally more arid conditions under the DRY scenario. Under the DRY climate scenario, the Northern, Eastern, Southern, Rocky Mountain, and Southwestern regions all show drier conditions with less water yield. Under all three climate scenarios, NFs are likely to experience larger changes in the basin characteristics than are NGs. The hydroclimatology of the Southwestern Forest Service region is found to have the highest sensitivity to climate changes across the CONUS, with especially high aridity under the DRY climate scenario. The dramatic differences in results between the WET and DRY scenarios demonstrates current uncertainty about the future impacts of climate change.

Long-term hydroclimatic shifts may fundamentally change conditions of US forests and grasslands. This finding highlights the need to incorporate climate change impacts into forest and grassland resource management and planning. This study can be used as a roadmap for land and water managers to develop options for adapting to future climate change, such as increasing landscape diversity and facilitating biological diversity (Littell et al., 2012). This study can help

environmental scientists and water managers to mitigate the negative economic, social, and environmental consequences of climate change on US NFs and NGs.

Furthermore, the findings indicate that the hydroclimatic responses of U.S. megaregions may vary under WET, DRY, and MIDDLE climate models. There are some clear consistencies in regional shifts in long-term hydroclimatology and basin characteristics. The findings point out that Los Angeles, San Diego, and San Francisco may experience a decrease in aridity under all three climate models indicating that these regions may become less arid by the end of the 21st century. Additionally, Houston may experience more arid climatic conditions in the future by increasing aridity index under all three climate models. Besides, the evaporative indices of Houston and Seattle are projected to increase by the end of the century under all three climate models indicating that the evaporative loss of freshwater resources in Houston and Seattle are likely to increase in the future. The population of Houston and Seattle megaregions is projected to increase significantly over the 21st century (Ross 2008; Nelson 2017). Thus, these metropolitan regions are likely to face more severe challenges in water resource planning and management in the future.

Phoenix is also the megaregion with the highest change in ω consistently across all three climate models, suggesting that the basin characteristics of Phoenix may experience significant changes in the future. Under all three climate models, basins in Houston are likely to experience shifts in their climate type from Temperate to Continental. Besides, some basins in Washington D.C, Philadelphia, New York, Boston (WPHNB) are projected to change from Continental to Temperate climate type.

These findings highlight the need for developing a national development strategy that addresses climate change policies to improve robust economic growth and protect vulnerable natural, water, and food resources in the U.S. megaregions and hence reduce negative

consequences on the economy, society, and environment. Hydroclimatic change accompanied with rapid population growth, urbanization and land use change in U.S. megaregions can accelerate future challenges in the megaregions, particularly, water-scarce regions that may do not have the water and natural resources to overcome significant shifts in their hydroclimatology. This study can help decision-makers, planners, policy makers and politicians to improve the understanding, planning, and preparedness for the future hydroclimatic changes through the sustainable growth to protect.

CHAPTER 4.

A PROBABILISTIC APPROACH FOR CHARACTERIZATION OF SUB-ANNUAL SOCIOECONOMIC DROUGHT INTENSITY-DURATION-FREQUENCY (IDF) RELATIONSHIPS IN A CHANGING ENVIRONMENT

Changes in climate, land use, and population can alter the frequency and intensity of annual and interannual socioeconomic droughts in water-scarce regions. This study develops a probabilistic approach to improve characterization of sub-annual to decadal socioeconomic drought intensity-duration-frequency (IDF) relationships over a range of water supply and demand conditions. A mixture Gamma-Generalized Pareto (Gamma-GPD) probability model is developed to coherently characterize the probabilistic properties of both non-extreme and extreme socioeconomic droughts. Subsequently, the mixture model is used to determine sub-annual socioeconomic drought intensity-duration-frequency (IDF) relationships, return period, amplification factor, and drought risk. A global sensitivity analysis was performed to understand the influence and importance of the model parameters individually and in combinations on drought return periods. The application of the framework is demonstrated for the City of Fort Collins (Colorado, USA) water supply system. The water demand and supply time series for the 1985–2065 are estimated using the Integrated Urban water Model (IUWM) and the Soil and Water Assessment Tool (SWAT), respectively, with climate forcing from statistically downscaled CMIP5 projections. The results from the case study indicate that the mixture model leads to enhanced estimation of sub-annual socioeconomic drought frequencies, particularly for extreme events. The probabilistic approach presented in this study provides a procedure to update sub-annual socioeconomic drought IDF curves while taking into account changes in water supply and demand conditions.

4.1. Introduction

Climate change and rapid population growth can significantly beget shifts in water supply and demand at various spatial and temporal scales (Brown et al., 2019; Mahat et al., 2017; Naz et al., 2016; Wang et al., 2016). As the balance between water supply and demand becomes more unequal, socioeconomic drought becomes a major concern (Mehran et al., 2015; Rajsekhar et al., 2015). Socioeconomic drought refers to the condition when water demand exceeds water supply (Foti et al., 2014a; Hao et al., 2018; Mehran et al., 2015). Enhanced probabilistic characterization of socioeconomic drought properties in a changing environment plays an important role in water resource planning and management (Mishra & Singh, 2010; Rajsekhar et al., 2015; Salas et al., 2005). This study develops a probabilistic approach to characterize sub-annual socioeconomic drought intensity-duration-frequency (IDF) relationships, return periods, amplification factors, and drought risk under shifts in water supply and demand conditions.

Previous studies have used a wide range of methods to assess socioeconomic drought hazard (Brown et al., 2019; Foti et al., 2014a; Guo et al., 2019; Huang et al., 2016; Mehran et al., 2015; Rajsekhar et al., 2015; Warziniack & Brown, 2019; Zhao et al., 2019). However, studies that discuss methods for assessing changes in intensity, duration, and frequency relationships of sub-annual socioeconomic droughts under nonstationary conditions are limited. Drought IDF curves are commonly applied to the design of water resource systems such as municipal storm-water drainage systems. Three important considerations must be addressed to improve characterization of droughts IDF relationships in a changing environment:

First, changes in future socioeconomic drought IDF relationships should be assessed by assuming the nonstationary conditions in both water supply and demand time series. Previous studies often describe socioeconomic droughts in terms of deficiencies in water supply systems,

in which water demand is defined as a constant threshold of water supply (Guo et al., 2019; Tu et al., 2018). However, climate change and anthropogenic drivers such as population growth can lead to a significant change in water demand and patterns. In such cases, socioeconomic drought IDFs are anticipated to increase due to increasing differences between water supply and demand (Salas et al., 2018). Thus, an improved socioeconomic drought definition and characterization is essential to account for a changing environment to evaluate and update drought IDF curves under shifts in both water supply and demand conditions.

Second, a complete characterization of socioeconomic droughts may not be sufficiently obtained by comparing only annual water demand to annual water supply. Foti et al., (2014) proposed a probabilistic framework to assess vulnerability of water supply systems to shortage as the probability that annual water demand exceeds annual water supply (Foti et al., 2014a). However, interannual changes in weather and water consumption can lead to an increase in the variability of water supply and demand within a year (Gutzler & Nims, 2006; Yu et al., 2014). Even in regions where water is abundant overall, water scarcity during brief time periods within the year may be on the rise due to climate change and socioeconomic drivers (Jaeger et al., 2017). Characterizations of socioeconomic drought at sub-annual scale influences planning and management of water supply systems (Evans & Sadler, 2008; Wang et al., 2019).

Third, nonstationary conditions in climate, land use, and population are expected to considerably alter the distribution of socioeconomic drought over time with the increasing occurrence of extreme drought events (i.e., drought with high intensity and long duration) (Furrer & Katz, 2008; Salas et al., 2018; Zhao et al., 2018). Fitting one of the classic families of distributions to sub-annual socioeconomic drought might lead to inappropriate characterization of likelihood, as it either fits well to the bulk density or to the tail (A. MacDonald et al., 2011; Solari

& Losada, 2012). Thus, the commonly used continuous probability distributions may fail to simultaneously capture both the non-extreme and extreme socioeconomic droughts. Mixture probability models have been developed to simultaneously characterize the bulk and tail of random phenomena (Ghanbari et al., 2019, 2020; A. MacDonald et al., 2011; Stephens et al., 2018). However, their application has not been investigated for characterizations of sub-annual socioeconomic droughts.

Thus, this study develops a coherent probabilistic approach to address the aforementioned considerations by improving characterization of sub-annual socioeconomic drought IDF relationships under considerable shifts in water supply and demand conditions. Specifically, the objectives are to: (1) improve projection of future droughts by defining and characterizing sub-annual socioeconomic drought under nonstationary conditions in both water supply and demand conditions; (2) enhance characterization of both minor and major socioeconomic droughts using the mixture Gamma-Generalized Pareto Distribution (Gamma-GPD); (3) investigate intensity-duration-frequency relationships of socioeconomic droughts under nonstationary conditions; (4) evaluate the frequency amplification of sub-annual socioeconomic droughts; and (5) assess drought risk to update the accepted design drought event for water supply systems. The findings allow better characterization of sub-annual socioeconomic drought hazard in basins undergoing climate and socioeconomic changes. Improved assessment of sub-annual socioeconomic drought is critical for effective adaptation and mitigation strategies to reduce the impact of droughts on communities.

4.2. Materials and Methods

A probabilistic approach was developed to assess changes in IDF relationships of defined sub-annual socioeconomic drought under nonstationary shifts in both water supply and

demand conditions. A mixture Gamma-GPD distribution was proposed to simultaneously model both extreme and non-extreme socioeconomic drought events. The parameter estimation and goodness-of-fit (GOF) of the mixture model were discussed compared to the classic families of probabilistic distributions. Then, sub-annual socioeconomic drought IDF relationships, return period, frequency amplification factor and drought risk were characterized under nonstationary conditions. A global sensitivity analysis was performed to understand the influence and importance of the model parameters individually and in combinations on drought return periods.

4.2.1. Definition and Characterization of Sub-annual Socioeconomic Drought

Drought has been generally categorized into four types: meteorological, agricultural, hydrological, and socioeconomic drought. Meteorological drought implies a precipitation deficit. Agricultural drought refers a deficit in soil moisture. Hydrologic drought can be caused by a reduction in surface water (Bayissa et al., 2018; Otkin et al., 2018). Socioeconomic drought is defined in terms of deficiencies in water supply systems (Mehran et al., 2015; Rajsekhar et al., 2015; Zhao et al., 2019). However, the characterization of water supply, water demand and water deficit in this study differs from most definitions of socioeconomic drought indicators. The water deficit (d_t) at a time interval *t* is defined as:

$$d_t = Demand_t - Supply_t \quad d_t > 0 \tag{4.1}$$

where $Supply_t$ denotes the potential quantity of water allocated to a given or multiple sectors at a time interval t and $Demand_t$ denotes the potential quantity of water requested by users at a time interval t for a given or multiple sectors (Brown et al., 2019; Foti et al., 2014a; Warziniack & Brown, 2019).

Subsequently, drought events can be obtained from the time series of water deficits using the theory of runs (Yevjevich, 1967). Yevjevich, (1967) defined a drought event as a succession of consecutive periods in which water demand exceeds water supply. A drought event can be characterized by its duration (D), magnitude (M), intensity (I) and frequency (F) (Salas et al., 2005; Yevjevich, 1967) (Figure 4.1).

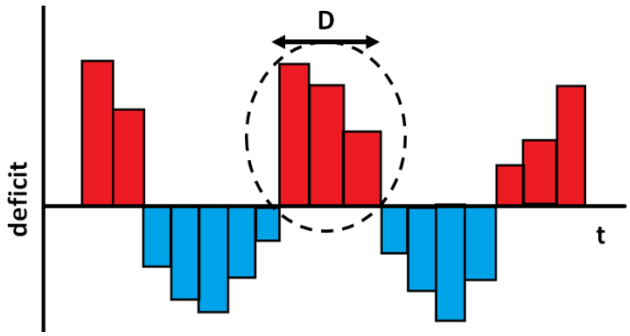

Figure 4.1. Schematic of drought properties.

Duration is defined as the number of consecutive months where the amount of water demanded exceeds the amount of water supplied to a given sector. Magnitude or severity is the cumulative deficit over the duration of the drought event defined as:

$$M = \sum_{j=t}^{t+D-1} (d_j) \tag{4.2}$$

Intensity of drought is the magnitude of a drought event divided by its duration given by:

$$I = \frac{M}{D} \tag{4.3}$$

and frequency can be defined as the number of times that a specific drought event occurs in a given period. Frequency can be predicted based on the theoretical probability distribution. The designs of water supply systems are based on historical drought IDF relationships. However, these

relationships may need to be modified under the impact of climate change by developing the sub-annual socioeconomic drought IDF curves (Cheng et al., 2014; Salas et al., 2018).

4.2.2. Gamma-GPD Mixture Model

Drought events have been modeled by many probabilistic distributions such as Gamma (Salas et al., 2005; Shiau, 2006; Zhao et al., 2017), Exponential (Shiau, 2006; Zhao et al., 2017), Normal (Foti et al., 2014a), Log-Normal and Weibull (Zhao et al., 2017). Gamma distribution is among the most commonly used probability distributions for characterizing drought properties (Andrade et al., 2017; Guo, et al., 2019; Mishra & Singh, 2010; Salas et al., 2005; Shiau, 2006). The Gamma distribution has a density function (De Andrade et al., 2017) as follows:

$$G(x; r, a) = \frac{1}{a\Gamma(r)} \left(\frac{x}{a}\right)^{r-1} exp\ \left(-\frac{x}{a}\right) \tag{4.4}$$

where x denotes drought properties (duration or intensity), and r and a are the shape and scale parameters, respectively.

Several characteristics motivate the use of the Gamma distribution for describing drought events. First, the distribution is bounded on the left at zero. Thus, it excludes negative values, which is important for drought applications because negative deficit, duration and intensity are impossible. Second, the Gamma distribution is positively skewed with an extended tail to the right. This property is well suited for characterization of droughts with frequent minor and infrequent extreme events. Third, the versatility of the Gamma distribution in taking exponential decay to nearly normal forms lends itself to modeling a range of drought intensity and duration combinations with reasonable accuracy (Husak et al., 2007).

However, extreme drought events especially under nonstationary conditions may not be adequately characterized by the upper tail of the Gamma distribution. The distribution of drought

events will become less positively skewed over time with the increasing occurrence of extreme drought events (Farahmand & AghaKouchak, 2015; Furrer & Katz, 2008). As the Gamma distribution becomes less positively skewed, the upper tail of the distribution will be insufficient to capture the increasing extreme drought events (Husak et al., 2007). Thus, the Gamma distribution may fail to adequately characterize the upper tail of drought events with higher intensities and durations under nonstationary shifts in water supply and demand conditions.

Extreme value analysis (EVA) is increasingly used for robust estimation of extreme events (Coles, 2001). The Generalized Extreme Value (GEV) approach of Block Maxima (BM) and Generalized Pareto Distribution (GPD) approach of Peak Over Threshold (POT) are two commonly used EVA methods for fitting the extremes of hydrological variables such as those used to characterize drought events (Engeland et al., 2005). However, the applicability of the GEV distribution by the method of BM is limited for assessment of drought events at sub-annual steps since only one extreme value per year is modeled. Thus, we use the GPD to fit the extreme of sub-annual drought events by applying the POT method (Engeland et al., 2005; Ganguli, 2014). The cumulative distribution function (CDF) of the GPD is given by:

$$g_{u,\xi,\beta}(x) = \Pr\,(X \le x | X > u) = \begin{cases} 1 - \left(1 + \xi \dfrac{x-u}{\beta}\right)^{-\frac{1}{\xi}} & for \;\; \xi \neq 0 \\ 1 - exp\left(-\dfrac{x-u}{\beta}\right) & for \;\; \xi = 0 \end{cases} \tag{4.5}$$

where u, ξ and β are the location (threshold), shape and scale parameters, respectively (Coles, 2001). The distribution is heavy-tailed when $\xi > 0$, medium-tailed when $\xi = 0$, and short-tailed with finite upper end point $u - \frac{\beta}{\xi}$ when $\xi < 0$ (De Andrade et al., 2017). The threshold should be

selected as the GPD location parameter to model statistical properties of events that exceed the threshold.

Here, the Gamma distribution was reconciled with the GPD in a mixture model to simultaneously model the bulk and upper tail of drought events. In this model, values below the GPD threshold (i.e., location parameter) were fitted by the Gamma distribution while values above the threshold were fitted by the GPD (Figure C-1). The mixture Gamma-GPD cumulative function (F) is given by:

$$F(x|r,a,\xi,\beta,u,\phi_u) = \begin{cases} (1-\phi_u)\dfrac{G(x|r,a)}{G(u|r,a)} & x < u \\ (1-\phi_u) + \phi_u\, g(x|\,\xi,\beta,u) & x \geq u \end{cases} \quad (4.6)$$

where $g(x|\,\xi,\beta,u)$ is the unconditional GPD function, $G(x|r,a)$ is the Gamma distribution function, u is the GPD location parameter (threshold), and ϕ_u is the probability of x being above the threshold (Behrens et al., 2004; A. MacDonald et al., 2011). Hence, the mixture model $F(x|r,a,\xi,\beta,u,\phi_u)$ can be used to model the distribution of both non-extreme and extreme droughts intensity and duration by inserting equations 4.4 and 4.5 into equation 4.6.

It should be noted that some previous studies have applied mixture distribution models to combine different distributions to simultaneously model both central and tail. However, the fit of mixture models has not been investigated in terms of sub-annual socioeconomic drought properties. It can be suggested that mixture models lead to better estimation of return periods of both minor and extreme drought events.

4.2.3. Joint Probability Distribution of Drought Intensity and Duration

The mixture Gamma-GPD model is used in this study to determine sub-annual socioeconomic drought IDF relationships. Drought intensity, duration, and frequency properties are correlated random variables. The joint probability distribution of drought events for intensity $I > I_0$ and duration $D > D_0$ can be constructed by the product of the conditional distribution of drought intensity for a given duration and the marginal distribution of drought duration as follows:

$$P\ (I > I_0\ \cap D > D_0) = P\ (I > I_0 \mid D > D_0)\ .P\ (D > D_0) \tag{4.7}$$

where D_0 and I_0 denote any given values of duration and intensity, respectively. The term $P\ (I > I_0| D > D_0)$ is the conditional probability of $I > I_0$ given $D > D_0$, and $P\ (D > D_0)$ is the marginal probability of drought with $D > D_0$. The marginal probability of $D > D_0$ from the mixture Gamma-GPD is given by:

$$P\ (D > D_0) = F(D > D_0)\ = \begin{cases} (1 - \phi_u)\dfrac{G(D > D_0|r,a)}{G(u|r,a)} & x < u \\ (1 - \phi_u) + \phi_u\ g(D > D_0|\ \xi,\beta,u) & x \geq u \end{cases} \tag{4.8}$$

The conditional probability of $P\ (I > I_0| D > D_0)$ can be determined in the same way considering that the mixture model should be fitted to just drought events with $D > D_0$ as follows:

$$P\ (I > I_0| D > D_0) = F(I > I_0|D > D_0) \tag{4.9}$$

Finally, the joint probability distribution of drought intensity and duration can be computed by inserting Equations (4.8) and (4.9) into Equation (4.7) and assuming drought events follow the mixture Gamma-GPD model. Thus, Equation (4.7) can be used to improve estimation of drought

intensity, duration, and frequency relationships by assuming that both marginal and conditional probabilities are Gamma-GPD distributed.

4.2.4. Parameter Estimation and Goodness-of-fit Tests

The proposed mixture Gamma-GPD distribution was linked with population and climate change models in this study as an effective way to address shifts in drought properties under a changing environment. Then, the applicability of the proposed mixture Gamma-GPD distribution was investigated compared to classic families of probabilistic distributions, especially under considerable shifts in water supply and demand conditions. Nonstationary conditions arising from sub-annual changes in supply and demand are represented by time-varying parameters. Mixture Gamma-GPD model parameters were re-estimated as a function of time using 30-year overlapping moving windows on the nonstationary time series of drought events.

In this study, the nonstationary climate data were obtained from the CMIP5 projections, and subsequently downscaled for meteorological stations in the region using a quantile-based empirical-statistical error correction method and a subsequent temporal (i.e., monthly to daily) downscaling procedure (Themeßl et al., 2012). Then, the nonstationary water demand and supply time series for the 1985–2065 were estimated using the Integrated Urban Water Model (IUWM) and the Soil and Water Assessment Tool (SWAT), respectively. The proposed mixture model holds the versatility to account for these changes in drought properties over time.

The location parameter of the GPD should be estimated to define the threshold between the bulk and tail distributions. The appropriate threshold is the location at which the mean residual life plot is approximately linear (A. MacDonald et al., 2011; Solari & Losada, 2012). It should be high enough to follow a GPD. In addition, the sample size should be large enough for inference.

The other parameters of Gamma-GPD mixture model were estimated using the maximum likelihood estimator (MLE) in MATLAB (MathWorks, Natick, MA, USA).

Several goodness-of-fit tests were applied to assess how well the proposed mixture Gamma-GPD model fits a set of drought intensities and durations. Here, the performance of the mixture model was evaluated using the chi-square goodness-of-fit test, root-mean-square error (RMSE), and the coefficient of determination. The performance of the model was compared with the performance of other standard distributions. Goodness-of-fit tests are frequently used as a measure of the differences between values predicted by a model or an estimator and the observed values (Alam et al., 2018; Chen et al., 2017). The smallest RMSE and Chi-square and largest R-squared indicate the model with the best performance.

4.2.5. Return Period

Return periods of drought events are often used to design the capacity of water supply systems (Salas et al., 2005). The return period of droughts with intensity greater than or equal to a target ($\mathrm{I} > \mathrm{I}_0$) was derived as a function of the expected drought interarrival time and cumulative drought intensity distribution function, expressed as:

$$T_{\mathrm{I}>\mathrm{I}_0|\ \mathrm{D}>\mathrm{D}_0} = \frac{E(\mathrm{D} > \mathrm{D}_0)}{P\ (\mathrm{I} > \mathrm{I}_0|\ \mathrm{D} > \mathrm{D}_0)} \times \frac{1}{P(\mathrm{D} > \mathrm{D}_0)} = \frac{E(\mathrm{D} > \mathrm{D}_0)}{P\ (\mathrm{I} > \mathrm{I}_0 \cap\ \mathrm{D} > \mathrm{D}_0)} \qquad (4.10)$$

where $E(\mathrm{D} > \mathrm{D}_0)$ is the expected drought interarrival time with $\mathrm{D} > \mathrm{D}_0$, which can be estimated from observed droughts, and $P\ (\mathrm{I} > \mathrm{I}_0 \cap\ \mathrm{D} > \mathrm{D}_0)$ can be obtained from Equation (4.7). The expected value of the interarrival time between two successive drought events with a certain duration or greater is given by (Shiau & Shen, 2001; Zhao et al., 2017):

$$E(\mathrm{D} > \mathrm{D}_0) = E(\sum_{i=1}^{N} \mathrm{DI}_\mathrm{i}) \tag{4.11}$$

where DI_i is drought interarrival time between two successive drought events with a certain duration or greater, and N is the number of drought events equal to or greater than a certain duration.

4.2.6. Drought Risk and Amplification Factor

The risk of failure over an *n*-year design or assessment period may be written as (Read & Vogel, 2015; Salas et al., 2018):

$$Risk\ (\mathrm{I} > \mathrm{I}_0 |\ \mathrm{D} > \mathrm{D}_0) = 1 - (1 - \frac{1}{T_{\mathrm{I}>\mathrm{I}_0|\ \mathrm{D}>\mathrm{D}_0}})^n \tag{4.12}$$

where $T_{\mathrm{I}>\mathrm{I}_0|\ \mathrm{D}>\mathrm{D}_0}$ is the return period of droughts with intensity and duration greater than or equal to a certain threshold ($\mathrm{I} > \mathrm{I}_0, D > D_0$) and *n* is the project life in years. Nonstationarity in drought risk projection can be accounted for by estimating changes in the exceedance probability of the mixture model using time-varying parameters.

In addition, the change in drought frequencies under nonstationary conditions can be quantified by dividing the exceedance probability of a given drought event in the future to the current condition as:

$$Amplification\ Factor\ (AF) = \frac{P_t(I > I_0)}{P_C(I > I_0)} \tag{4.13}$$

where AF is the frequency amplification factor of drought with $I > I_0$, and $P_C(I > I_0)$ and $P_t(I > I_0)$ are the exceedance probability of drought events with $I > I_0$ for current and future

conditions, respectively. The drought events with higher frequency amplification factor are more sensitive to nonstationary conditions.

4.2.7. Global Sensitivity Analysis

A global sensitivity analysis was performed to simultaneously assess both relative contributions and interactions between each of the individual mixture model parameters. Several techniques have been commonly used to execute global sensitivity analysis. In this study, the method of Sobol (Sobol, 1993) was applied using the SIMLAB software package (Giglioli & Saltelli, 2008). Sobol decomposes the variance of the output into fractions, which can be allocated to individual inputs. Both relative contributions and interactions of individual inputs were calculated using the first-order and total-order sensitivity indices. Sensitivity indices are defined to measure the importance of variables. The distribution of the mixture model parameters was assumed to be uniform. The selected ranges of mixture model parameters are shown in Table D-1 based on the observed data and their intervals.

First-order sensitivity indices were used to assess the contribution of an individual parameter to the output variance. Parameters with the greater first-order sensitivity indices are more critical for the model. Figure 4.2 (left-panel) and Table D-2 illustrate the first order sensitivity indices of model parameters to return period of drought with duration equal or greater than one month. Below the threshold (non-extreme drought events), the mixture model is governed by Gamma parameters. The drought return period is more sensitive to the Gamma shape parameter than the Gamma scale parameter. Above the threshold (extreme drought events), the mixture model is governed by GPD parameters. The drought return period is respectively sensitive to the location, scale, and shape parameters of the GPD.

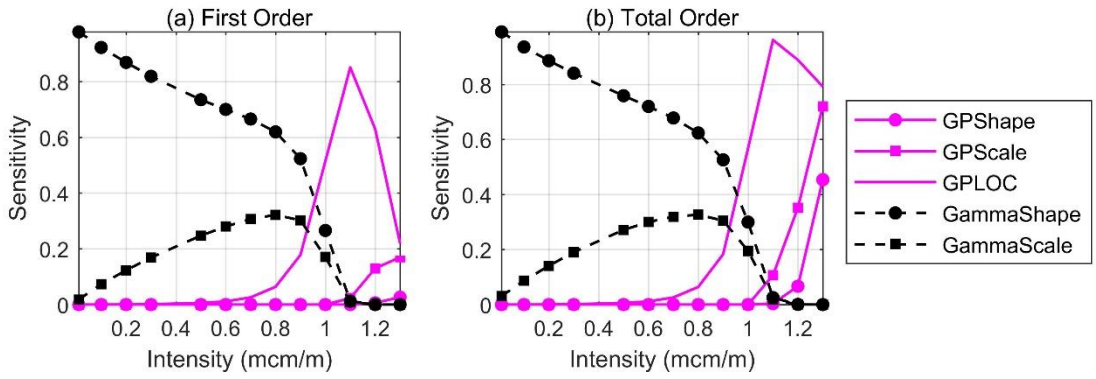

Figure 4.2. (a) The first order and (b) the total order sensitivity indices of Mixture Gamma-GPD model for drought return period.

Total-order sensitivity indices were used to assess the interaction between each of the input variables. Changes in the total order sensitivity indices are presented in Table D-3 and Figure 4.2 (right-panel). GPD scale and GPD shape parameters are more critical when the total-order sensitivity indices were considered. This indicates that shape and scale parameters of GPD have significant interactions with other parameters.

Figure 4.3 illustrates the interaction between the GPD shape and Gamma shape parameters with GPD location (threshold) parameter. Below the threshold (Figure 4.3 left-panel), as Gamma shape parameter increases, sensitivity of drought return period to change in GPD location parameter increases. Conversely, as GPD location parameter increases, the sensitivity of drought return period to change in the Gamma shape parameter increases. Above the threshold (Figure 4.3 right-panel), the sensitivity of drought return period to change in the GPD location parameter decreases. Conversely, as the GPD location parameter increases, the sensitivity of drought return period to the change in Gamma shape parameter decreases.

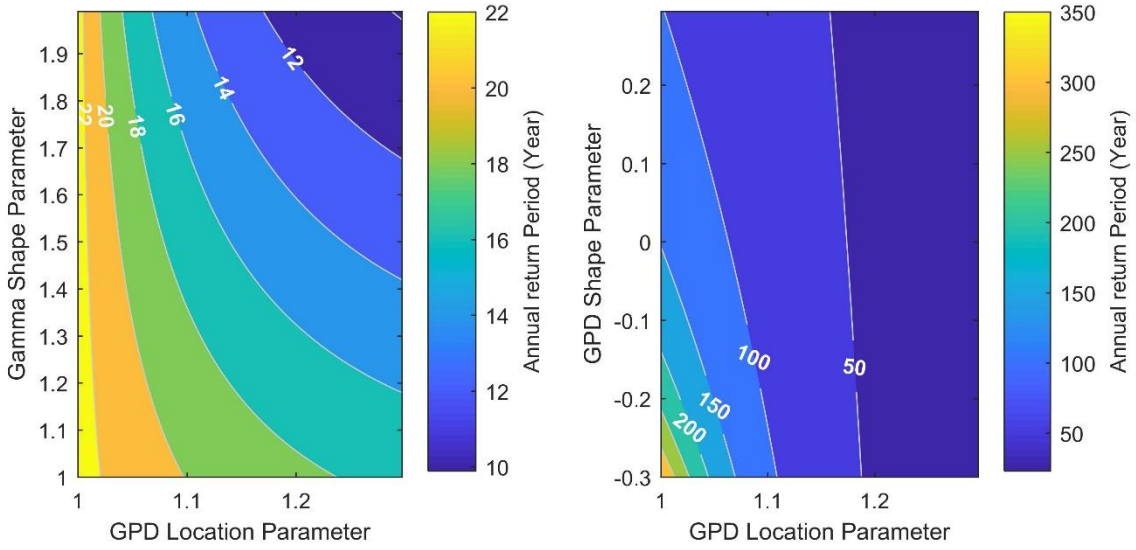

Figure 4.3. Sensitivity of drought return period to Gamma shape parameter and GPD location parameter below the threshold (left-panel) and GPD shape and GPD location parameters over the threshold (right-panel).

4.3. Application and Discussion

The proposed probabilistic approach was demonstrated for the City of Fort Collins (Colorado, USA) water supply system (Figure C-2) as a test case to investigate the applicability of the framework under considerable shifts in water supply and water demand conditions. Climate, water supply, and water demand for Fort Collins were projected out to 2065 under the hot-dry scenario to assess the capacity to improve characterization of sub-annual socioeconomic drought IDF relationships under significant shifts in water supply and demand conditions. The 1986–2015 period was used to represent "current" conditions and the 2035–2065 period represented the "mid-century" conditions. It should be emphasized that assessing various aspects of future drought impacts on the City of Fort Collins is not the purpose of this study. In fact, this study used the City of Fort Collins as a test case to demonstrate the application of the proposed approach under nonstationary conditions.

Fort Collins is in the semi-arid American West, which is prone to extended droughts. It lies within the Cache la Poudre (CLP) watershed in Northcentral Colorado. Currently, a drought event

is defined as one or more years of below average annual runoff in the CLP River (AMEC Environment & Infrastructure, 2014). An exceptionally severe drought was reported in Fort Collins from September 2001 to August 2002. Over the last decades, CLP River discharge has been below average in most years, and the city has been experiencing water shortage conditions since 2000. In addition, high levels of population growth are projected within the CLP watershed, compounding the water shortage problems (AMEC Environment & Infrastructure, 2014).

4.3.1. Future Climate Scenarios

Changes in precipitation and temperature for the CLP watershed were estimated under the representative concentration pathway (RCP) 8.5 and a hot-dry scenario described below. This combination was chosen to represent a worst-case condition for the region. Observed daily temperature and precipitation data were collected from the Global Historical Climatology Network (GHCN), the Colorado Agricultural Meteorological Network (CoAgMet), and Northern Colorado Water Conservancy District (NCWCD). Missing data were filled using auxiliary information obtained from nearby stations based on the probability of rainy days, R-Squared and Jaccard index between the two nearest stations.

Future monthly climate data were obtained from CMIP5 projections (U.S. Bureau of Reclamation, 2013). Subsequently, data were statistically downscaled for meteorological stations in the region using a quantile-based empirical-statistical error correction method (Themeßl et al., 2012). A downscaling procedure was performed to obtain daily climate information from downscaled monthly data. Two hundred and thirty downscaled climate models were classified into hot-dry, hot-wet, warm-dry, warm-wet, and median categories based on the difference in current and future temperature and precipitation (Figure C-3).

Changes in precipitation and minimum temperature in Fort Collins under the median of 230 climate models are shown in Figures 4.4(a) and 4.4(b), respectively. The average changes in minimum temperature for RCP 2.6, 4.5, 6.0 and 8.5 are also shown in Figure 4.4(c). Climate anomalies represent differences between the mid-century and current conditions. The kriging method in ArcGIS was applied to the spatial interpolation of precipitation and temperature anomaly records in the CLP watershed.

For the median of 230 climate models (Figure 4.4), temperature consistently is expected to increase across the watershed. In addition, the rate of warming tends to increase with elevation, indicating that high-mountain environments of the Colorado Rocky Mountains will experience rapid changes in temperature. However, a relatively small increase in precipitation was projected, particularly in higher elevation areas.

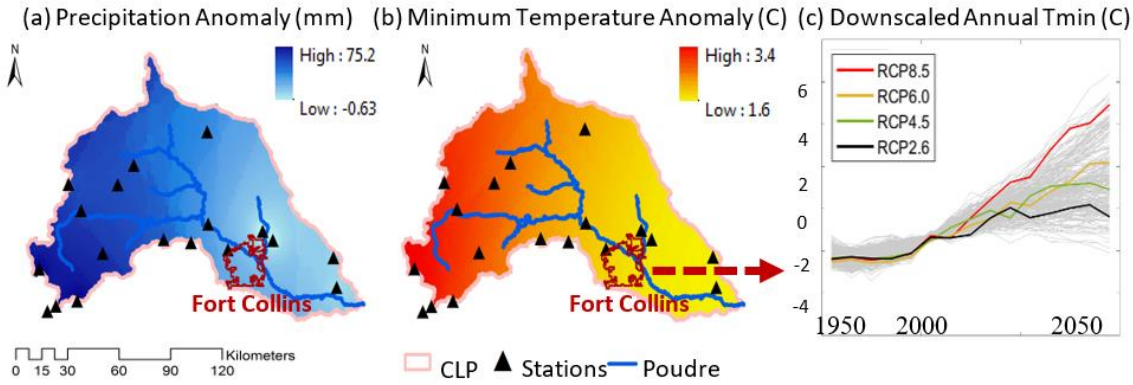

Figure 4.4. Mid-century (2035–2065) (a) precipitation anomaly for the CLP watershed; (b) minimum temperature anomaly for the CLP watershed; and (c) average annual minimum temperature time series for the City of Fort Collins meteorological station corresponding to the 230 climates.

In this study, the statistically downscaled 'ipsl-cm5a-mr' scenario was selected from the hot-dry category with RCP 8.5 to represent the worst-case scenario for the mid-century conditions. This scenario was selected in order to assess significance and applicability of the proposed

framework under considerable shifts in water supply and demand conditions. Figure C-4 and Figure C-5 show changes in precipitation and temperature for the hot-dry scenario from current conditions to mid-century conditions.

4.3.2. Water Supply Assessment

The City of Fort Collins receives native water from the Cache la Poudre (CLP) River and imported water from Horsetooth Reservoir as part of the Colorado Big Thomson (CBT) project. According to the Fort Collins Water Supply and Demand Management Policy Revision Report (AMEC Environment & Infrastructure, 2014), the amount of usable water from the Poudre River depends on factors such as water demand, dry-year yields and exchange potential. In addition, water deliveries from the Colorado Big Thompson system to the city of Fort Collins depend on an annual quota set by Northern Water each year ranging from 50% to 100% of annual yields (AMEC Environment & Infrastructure, 2014). In this study, the potential amount of water supplied to the City of Fort Collins in the future was calculated assuming that the historical coefficients of water deliveries from the CLP River will be preserved and the City owns the potential amount of water from the Horsetooth Reservoir as the most flexible source to fill gaps from other sources.

Changes in water yield in the CLP River at the Mouth of Canyon Station (National Water Information System (NWIS), 2019) was evaluated using the Soil and Water Assessment Tool (SWAT) (Arnold et al., 1998). SWAT is a comprehensive, distributed-parameter, process-based hydrologic model that has been used extensively to assess the hydrologic response to changes in climate and land use at a variety of scales (Chien et al., 2013; Ficklin et al., 2013; Gassman et al., 2014; Records et al., 2014). The model was calibrated to historic naturalized flow data at multiple locations within the watershed (Havel et al., 2018). The calibrated model was driven by projected

alternative future climates for the region to obtain monthly discharge at the City of Fort Collins water intake facilities on the CLP River.

4.3.3. Water Demand Assessment

Municipal water demand under climate, population, and water demand management scenarios was estimated using the Integrated Urban Water Demand Model (IUWM). IUWM is a mass balance model that simulates water demand and wastewater production associated with urban water demand management strategies. The model simulates municipal water demand through use of population, household, land cover and climate data. The model was calibrated and tested for the City of Fort Collins with options for assessing demand management scenarios based on the projected population, temperature and precipitation (Sharvelle et al., 2017). The parameters of the IUWM models were calibrated to historical conditions and were assumed to be preserved under future conditions. The model was driven with future climate scenarios to obtain monthly total water use for the City of Fort Collins under nonstationary conditions. Population and household information were obtained from the U.S. Census Bureau (Bureau, 2011). Population growth projections were based on those reported in AMEC Environment and Infrastructure (AMEC Environment & Infrastructure, 2014) with a projected population of 165,000 by the middle of century.

Figure 4.5 provides 12-month average of projected water supply and water demand for the City of Fort Collins under the hot-dry scenario. The balance between water supply and water demand becomes more unequal by the middle of the century under rapid climate changes and population growth. This situation can lead to considerable shifts in socioeconomic drought distributions. Thus, applicability of classic families of probabilistic distributions can be assessed compared to the mixture Gamma-GPD distribution in rapidly changing environment. Note that

changes in water resources management and strategies such as climate adaptation and mitigation strategies and water conservation were not assumed in the projection of water supply and water demand.

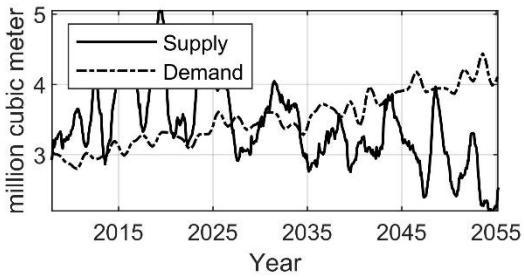

Figure 4.5. 12-month average of projected water supply and water demand under hot-dry scenario.

4.3.4. Water Deficit Record Extension

Extreme drought events are usually infrequent and insufficient for fitting to a GPD model (Link et al., 2020; Salas et al., 2005). To create a statistically large monthly water deficit sample, the autoregressive (AR) time series model was used. The AR model of order p, AR (p), is a time series defined by (Salas et al., 2005):

$$y_t = c + \sum_{i=1}^{p} \phi_i (y_{t-i}) + \varepsilon_t \quad (5.14)$$

with lagged values of y_t as predictors where ε_t is an uncorrelated normal random variable with mean zero and variance σ_ε^2, and ϕ_i, and c are the parameters of the model. The fourth-order autoregressive model was found to be effective for simulating a synthetic 67200-month deficits sample for the city of Fort Collins. This extended sample was used to determine intensity, duration, and frequency of drought events for the study system. The relative frequency distribution of

positive drought deficits ($d > 0$) from the historical record and the generated sample are shown in Figure 4.6. Furthermore, the synthetic sample was tested by comparing statistical properties of original data versus generated data using AR model for all deficits (Table 4.1).

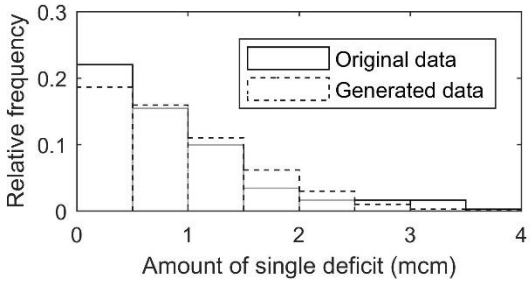

Figure 4.6. Relative frequency distribution of the deficit water.

Table 4.1. Statistical properties of original data versus generated data for city of Fort Collins.

Statistics	Original Data	Generated Data
Single Deficit		
Min (million cubic meter)	−3.851	−3.772
Max (million cubic meter)	4.214	4.170
Mean (million cubic meter)	0.173	0.173
Standard deviation	1.114	1.054
Coefficient of variation	6.422	6.070
Severity		
Mean (million cubic meter)	8.823	7.644
Standard deviation	22.380	22.323
Coefficient of variation	2.536	2.920
Intensity		
Mean (million cubic meter per month)	0.545	0.582
Standard deviation	0.379	0.335
Coefficient of variation	0.695	0.576
Duration		
Mean (month)	9.974	8.373
Standard deviation	18.576	17.456
Coefficient of variation	1.862	2.084

4.3.5. Importance of Nonstationarity Assumptions in Both Water Supply and Demand Conditions

While all types of droughts originate from a deficiency in water supplies, drought properties would not depend on only water supply conditions. Climate changes and population growth can lead to nonstationary conditions in both water supply and water demand conditions. Thus, definition and characterization of drought events that consider shifts in both water supply and demand are essential to account for a changing environment. However, most previous studies have defined socioeconomic drought only in terms of deficiencies in water supply systems (Guo et al., 2019; Tu et al., 2018).

Table 4.2 shows the impact of nonstationary assumptions in both water supply and demand conditions on drought properties compared to shifts in only water supply or water demand conditions. The average drought magnitude, duration, intensity, and maximum monthly water deficit are determined under shifts in (1) only demand conditions; (2) only supply conditions; and (3) both supply and demand conditions. While the average magnitude and duration of drought events considerably increase by assuming shifts in both water supply and demand conditions, the average drought intensity increases slightly. Based on the drought intensity definition (magnitude/duration), minor changes in drought intensity can be justified considering that intensity is a normalized value (water deficit per month). However, maximum monthly deficit will increase to 1.04 (mcm/month).

Table 4.2. Impacts of shifts in both water supply and water demand on drought properties.

Drought Properties	Shifts in Demand	Shifts in Supply	Shifts in Supply and Demand
Magnitude (mcm)	1.03	1.74	8.20
Duration (month)	4	3.30	9.38
Intensity (mcm/m)	0.22	0.40	0.53
Maximum water deficit (mcm)	0.32	0.68	1.04

Table 4.2 provides a general understanding of how shifts in water supply and water demand contribute to affect drought properties in the selected case-study. Under constant water demand assumption, the average magnitude, intensity, and maximum monthly water deficit are higher than the constant water supply assumption. Table 4.2 highlights that change in water supply may have higher impacts on drought magnitude and intensity compared to changes in water demand. It should be noted that these results are case-study specific and depend on the selected scenario.

4.3.6. Importance of Socioeconomic Drought Assessment at a Sub-annual Scale

Drought is traditionally defined as a climate phenomenon that takes many years. Most studies have characterized drought at annual scale. However, population growth and climate change can lead to higher interannual variability of water supply and water demand. Thus, characterization of socioeconomic drought properties at a sub-annual scale is needed in a changing environment. Figure 4.7 shows changes in drought intensity for D < 12 months from current conditions to future conditions. Intensity of within-year drought may increase significantly due to increases in interannual variability of water supply and demand conditions.

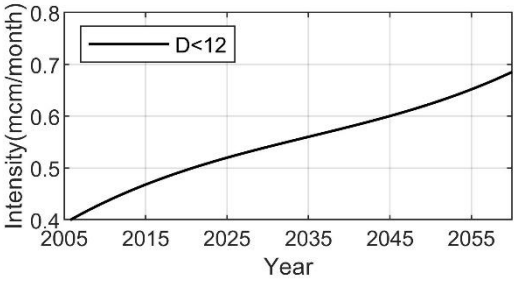

Figure 4.7. Change in intensities of droughts with duration less than 12 months (D < 12).

In addition, characterization of socioeconomic drought at a sub-annual scale makes a significant difference in the definition of drought duration. For example, droughts with duration

equal to 24 months (D = 24 months) are not equivalent to droughts with durations equal to 2 years (D = 2 years). In fact, droughts with D = 24 months mean that there are 24 consecutive months in which monthly water demand is greater than monthly water supply. However, droughts with D = 2 years mean that there are two consecutive years in which total annual water demand is greater than total annual water supply. Thus, even during a two-year drought, there may be months with water surplus. As a result, characterization of drought events at a sub-annual scale can help to identify months with water surplus that can lead to enhanced decision-making in water resource planning and management.

4.3.7. Importance of Applying Mixture Gamma-GPD Distribution under Nonstationary Conditions

The Mixture Gamma-GPD distribution was used to estimate the frequency of socioeconomic drought intensity and duration at a sub-annual scale for the City of Fort Collins. In this study, the threshold related to the 95th sample percentile (Behrens et al., 2004; Engeland et al., 2005; Ganguli, 2014) was chosen, which was supported by using the mean excess plots (Figures C-6 and C-7) as a graphical diagnostics method.

The model evaluation criteria including Chi-square, RMSE, and R-squared are summarized in Tables 4.3 to 4.6 for Exponential, Normal, Log-Normal, Weibull, Gamma and Gamma-GPD distributions under current and future conditions. Most classic families of distributions have better fit under current conditions compared to mid-century conditions. This finding indicates that the most standard probabilistic distributions will be insufficient to capture both bulk and tail of droughts distribution under shifts in drought properties by the mid-century. In addition, goodness of fit tests quantitively demonstrate that the standard Gamma distribution better fits to sub-annual socioeconomic drought durations and intensities compared to other probabilistic distributions for

both current and mid-century conditions. However, the mixture Gamma-GPD distribution leads to improved estimation of drought frequency compared to Gamma and other probabilistic distributions for both drought duration and intensity under current and future conditions. The approach improves the capacity to simultaneously characterize within-year and multi-year socioeconomics droughts.

Table 4.3. The goodness of fit of various models under current conditions (drought intensity).

Distribution	R-squared	RMSE	Chi-Square
Exponential	0.7104	0.14	86.1532
Normal	−16.8745	0.5912	333.0102
Log-Normal	0.6728	0.1414	42.3706
Weibull	0.6147	0.1749	186.4215
Gamma	0.9447	0.0652	10.9257
Gamma-GPD	0.9746	0.046	10.8214

Table 4.4. The goodness of fit of various models under mid-century conditions (drought intensity).

Distribution	R-squared	RMSE	Chi-Square
Exponential	0.2735	0.273	274.5355
Normal	−5.5551	0.6131	303.6521
Log-Normal	0.5086	0.2233	71.4617
Weibull	0.511	0.2145	321.0255
Gamma	0.8736	0.1207	24.9927
Gamma-GPD	0.945	0.0808	22.6967

Table 4.5. The goodness of fit of various models under current conditions (drought duration).

Distribution	R-squared	RMSE	Chi-Square
Exponential	0.701	7.2617	97.2247
Normal	−1.0406	19.7033	2393.4
Log-Normal	0.6563	10.6014	213.2408
Weibull	0.6739	7.5839	107.309
Gamma	0.6476	4.2436	35.82
Gamma-GPD	0.9488	1.6173	7.46

Table 4.6. The goodness of fit of various models under mid-century conditions (drought duration).

Distribution	R-squared	RMSE	Chi-Square
Exponential	0.5314	14.9834	440.1007
Normal	−1.0788	37.6708	9787.0
Log-Normal	0.3578	25.6947	1271.9
Weibull	0.7345	10.6867	201.576
Gamma	0.7705	5.01	47.09
Gamma-GPD	0.957	2.147	13.20

Figure 4.8 shows the quantile-quantile (QQ) plots of both Gamma-GPD and Gamma distributions for the current (1986–2015) and future (2035–2065) conditions. The Gamma-GPD model substantially improves characterization of socioeconomic drought intensity-duration relationships, particularly under nonstationary conditions. The proposed mixture model consistently provides a better fit to data compared to the standard Gamma distribution as QQ plots indicate.

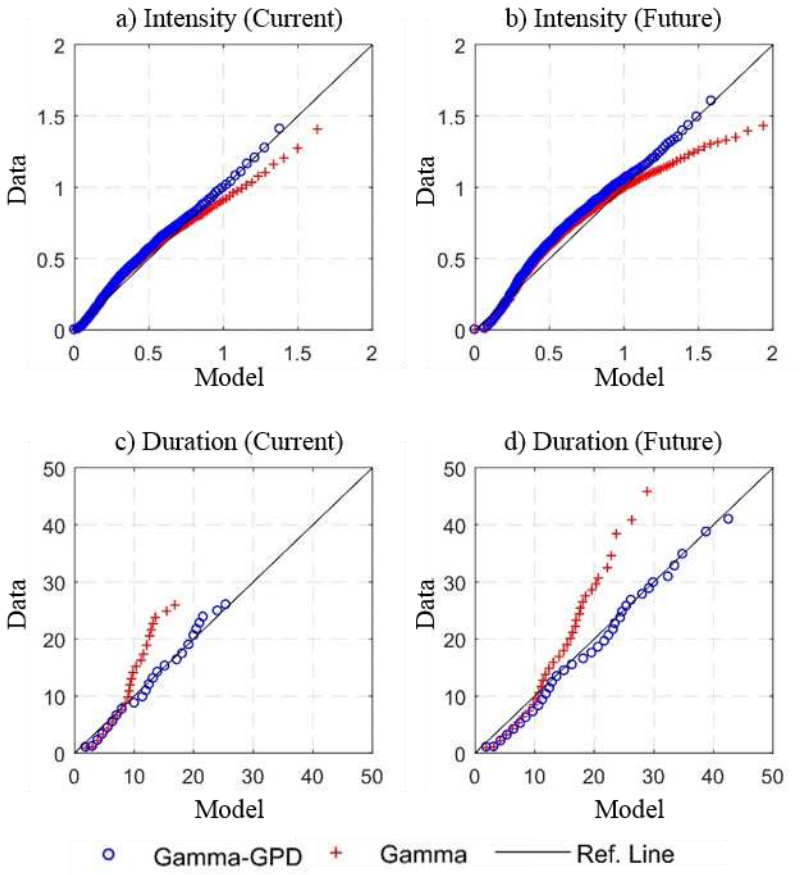

Figure 4.8. QQ plot of (a) the current and (b) future drought intensity (in million cubic meter), and (c) the current and (d) future drought duration (in month) for the mixture model versus gamma.

While the Gamma distribution (red plus sign) seems to be adequate for drought events with smaller duration and intensities (non-extreme droughts), it tends to be inadequate for droughts with larger duration and higher intensity (extreme droughts) by deviating from the reference line.

However, the Gamma –GPD distribution (blue circle sign) enhances the characterization of extreme drought events by converging to the reference line. Thus, characterizations of sub-annual socioeconomic drought intensity and duration by fitting to only Gamma distribution may lead to inadequate estimation of socioeconomic drought properties, particularly for extreme events. Application of Gamma distribution without nonstationary assumption in water supply and demand conditions can affect decisions or other water planning consideration.

Changes in the probability distribution functions of drought durations with intensity greater than zero (all drought events) are shown in Figure 4.9 left-panel. The GPD of drought durations is short-tailed ($\xi < 0$) under the current condition but becomes heavy-tailed ($\xi > 0$) during the mid-century period, meaning that the duration of drought events will increase by the middle of century. The scale parameter of the Gamma distribution for drought duration is increasing, which means that the variability of drought durations will increase in the middle of century.

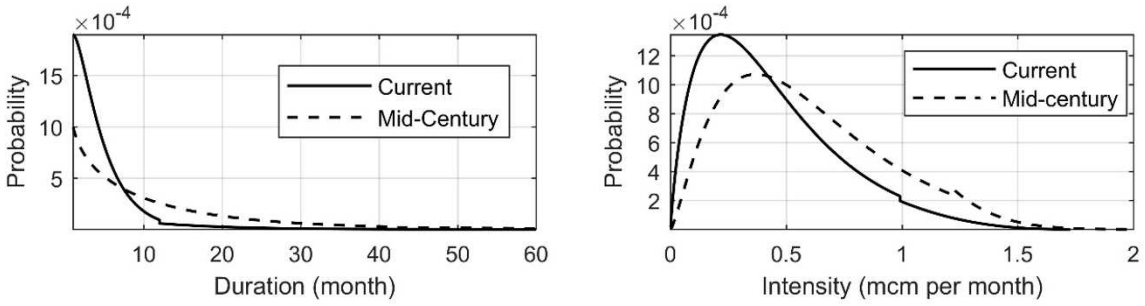

Figure 4.9. (left-panel) Probability distribution functions of drought durations; and (right-panel) probability distribution functions of drought intensities.

Drought intensities with duration greater than one month (all drought events) are depicted in the right panel of Figure 4.9. The GPD location parameter was increased over time from 1.0 to 1.22 mcm (million cubic meter) per month, meaning that drought events that are currently

characterized as extreme events become non-extreme events in the middle of century. The scale parameter of the Gamma distribution for drought intensity also increases, indicating that the variability of drought intensity will increase. Changes in climate and population alter the distribution of both drought durations and intensities over time. There may be a discontinuity in the density at the threshold; however, the mixture probability distribution will be continuous.

4.3.8. Application of Sub-annual Socioeconomic Drought IDF Relationships in a Changing Environment

How socioeconomic drought properties will change in the future is one of the key research questions in water resource management and planning. This section discusses the practicality of the proposed approach to update drought IDF curves and designed drought event for water supply systems. These critical factors can affect water supply and demand management policies and practices. First, we assess changes in sub-annual socioeconomic drought IDF curves for the City of Fort Collins under significant shifts in water supply and demand. Improving the estimation of socioeconomic drought IDF curves under nonstationary conditions can play an important role in the design of water supply systems. Second, we assess changes in the designed drought event for the City of Fort Collins water supply systems under nonstationary conditions.

IDF curves are commonly applied for the design of water resource systems such as municipal storm-water drainage systems. However, studies that discuss methods for assessing changes in IDF relationships of drought events are limited (Cheng et al., 2014; Salas et al., 2018). IDF curves were obtained through frequency analysis of drought events. Drought Intensity and duration time series were computed for overlapping 30-year moving windows to calculate changes in drought properties due to nonstationary water supply and demand. Changes in the parameters of the mixture model were estimated using overlapping 30-year moving windows and assuming

the parameters are time-varying. Figure 4.10 illustrates changes in the projected drought durations (left panel) and drought intensities (right panel) for the Fort Collins water supply system under the hot-dry scenario. Drought events with higher intensity have longer duration. Similarly, drought events with longer duration have higher intensities. The results also indicate that drought events with longer durations and higher intensities will be more frequent under the projected scenario.

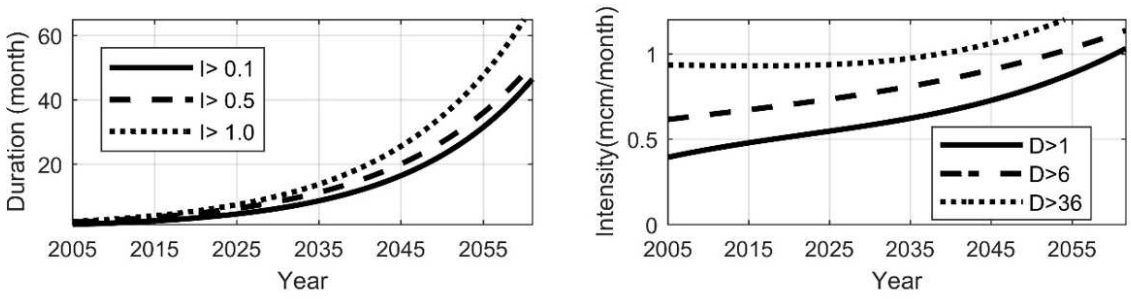

Figure 4.10. Change in drought durations (left) and intensities (right) (intensity is in mcm/month).

The expected value of interarrival time between two successive drought events is shown in Figure 4.11. The occurrence probability of drought events is expected to change significantly over time under the hot-dry scenario. Drought events with longer duration have higher changes in the expected interarrival time. As an example, Figure 4.11 indicates that under mid-century 20 month droughts are going to be roughly as common as the mean duration now (10 months).

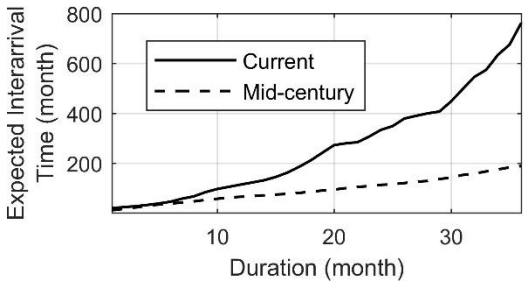

Figure 4.11. Expected interarrival time (month).

The amplification factor was also calculated for different drought durations and intensities. Multi-year and higher intensity droughts (extreme droughts) tend to be more sensitive to nonstationary conditions than droughts with duration less than a year (Figure 4.12). The results point to a substantial increase in the occurrence of extreme events from 2005 to 2060 (i.e., drought events with higher intensities and longer durations). Socioeconomic droughts with longer duration will have higher likelihood of occurrence in the mid-century compared to current conditions.

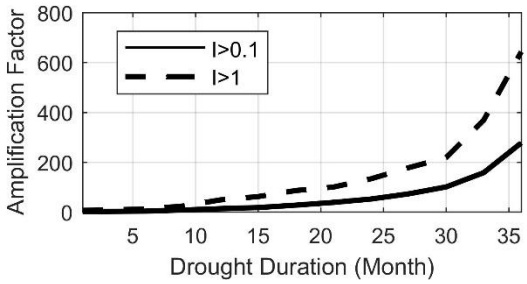

Figure 4.12. Amplification factor curves for frequency of drought events (intensity is in mcm/month).

Then, the marginal and conditional probabilities of drought events as well as the joint probability distribution of drought events for intensity and duration greater than or equal to a target ($I > I_0, D > D_0$) were computed. Drought frequency analysis was performed for each set of drought duration to determine the exceedance probability of drought intensity

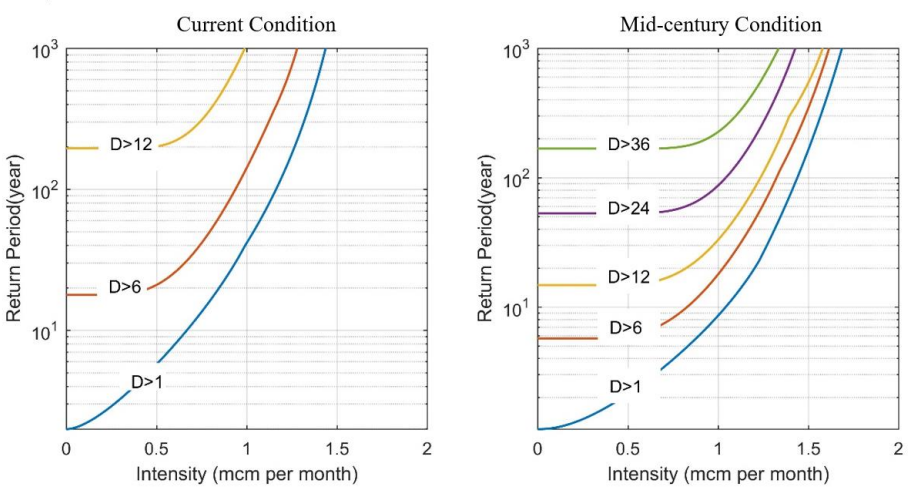

Figure 4.13. Intensity-duration-frequency curves for current (left-panel) and future conditions (right-panel).

Figure 4.13 depicts the drought IDF curves with durations greater than 1, 6, 12, 24 and 36 months under nonstationary conditions for both current and future conditions. The results indicate that current IDF curves substantially underestimate extreme drought events. For example, the return periods of drought events with durations greater than 24 and 36 months decrease to less than 1000 years in the future. In addition, the IDF curves for both current and future conditions indicate that the drought events with shorter durations tend to have higher intensities. Thus, current drought IDF curves seem inadequate for the design and management of water supply infrastructure under considerable shifts in water supply and demand conditions. The proposed probabilistic approach should be applied for improved characterization of future IDF relationships, particularly for extreme socioeconomic droughts.

Based on the Fort Collins Water Supply and Demand Management Policy Revision Report (AMEC Environment & Infrastructure, 2014), the City's water utility tries to maintain water supplies sufficient to meet demands during at least a 1-in-50 year drought. A 1-in-50 year drought is a drought event that occurs once every 50 years, on average (AMEC Environment &

Infrastructure, 2014). However, characterizing the intensity, duration, and frequency of sub-annual socioeconomic droughts may lead to the enhanced design of water supply systems and appropriate implementation of mitigation and adaptation strategies. Figure 4.14 shows the risk of 1-in-50 year drought events with different durations for current and mid-century conditions. 1-in-50 year drought risk decreases as drought intensity increases. The model used here shows that drought events with longer durations are more likely in the middle of the century compared to current conditions. Therefore, the design drought event for the City's water supply system should be updated according to the accepted risk for the middle of the century.

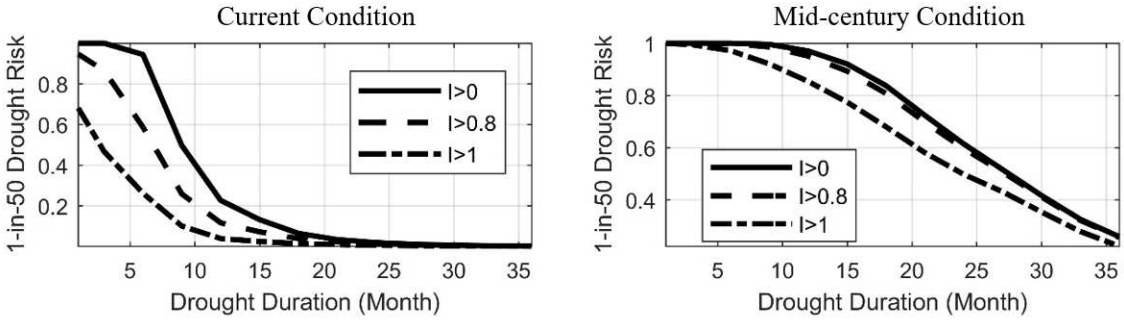

Figure 4.14. 1-in-50 year drought risk for current condition (left) and middle of century (right) (intensity is in mcm/month).

The proposed mixture model thus leads to enhanced assessment of sub-annual socioeconomic drought IDF relationships by simultaneously capturing non-extreme and extreme droughts under annual and interannual shifts in water supply and demand trends. Design of water supply systems by using the proposed probabilistic approach can improve the capacity of city water managers to adequately implement drought adaptation strategies such as water supply development, water demand management, and conservation (Brown et al., 2019; Ganguli, 2014; Gutzler & Nims, 2006; Warziniack & Brown, 2019). Updating drought IDF curves and designed drought events help decision makers and system designers to understand uncertainties under

climate change and population growth and develop climate adaptation strategies to increase resilience and flexibility of water supply systems (Buurman & Babovic, 2016).

Note that changes in the relationships between water supply and water demand conditions, and the implementation of future water resuorce management and adaptation strategies were not assumed in this study. Besides, the water supply from the Poudre river and the Horsetooth reservoir in the city of Fort Collins may change since the city has senior priority.

4.4. Conclusions

In rapidly urbanizing areas, population growth along with changes in climate can lead to nonstationary drought conditions where water demand exceeds water supply. Three important considerations were addressed in this study under growing unequal balance between water supply and water demand. First, an improved socioeconomic drought assessment can be characterized by assuming shifts in both water supply and demand conditions. Second, assessing the drought properties at a sub-annual scale is essential toward improved water resource management. Third, a mixture distribution is needed to account for considerable shifts in both water supply and water demand conditions. These considerations are addressed in this study to update drought IDF relationships using defined sub-annual socioeconomic drought terminology.

We outlined a statistically coherent probabilistic approach for assessing sub-annual socioeconomic drought IDF properties in a changing environment, while considering shifts in both water supply and water demand regimes to cope with climate changes and population growth. A mixture Gamma-GPD probability model was proposed to simultaneously represent the bulk and tail of drought events. The standard probabilistic distributions were found to be insufficient for modeling extreme socioeconomic droughts with longer duration and higher intensity especially in a rapidly changing environment. The proposed mixture model improved characterization of

socioeconomic drought intensity, duration, and frequency relationships at sub-annual time scales, particularly under significant shifts in water supply and demand trends. Under nonstationary water supply and demand conditions, current extreme and infrequent drought events may become more frequent. Thus, more attention should be given to the enhanced characterization of extreme socioeconomic droughts. The model can enhance the capacity to address challenges with interannual variability of water supply and demands under nonstationary conditions.

Application of the framework was demonstrated for the City of Fort Collins, Colorado, water supply system. Climate changes were derived from GCM projections, and supply and growing demand were calculated using SWAT and IUWM models respectively by considering population growth and future climate scenarios. The hot-dry scenario was selected to represent the worst-case conditions for nonstationary water supply and demand. Assessments of sub-annual drought frequency for City of Fort Collins indicate that climate change and population growth will significantly affect the vulnerability of municipal water supply systems to shortage. The proposed mixture model improved the projection of sub-annual socioeconomic drought intensities and durations, particularly for extreme drought events. In the case of the City of Fort Collins, the 1-in-50-year drought risk increases from current conditions by the mid-century, indicating that the City will experience socioeconomic droughts with higher intensity and longer duration. Moreover, drought events with longer duration have higher risk in the middle of century compared to current conditions. Drought events with longer duration are more sensitive to non-stationary conditions.

This study provides a framework to statistically assess impacts of large shifts in water supply and demand on sub-annual socioeconomic droughts. However, global assessment of sub-annual socioeconomic drought propagation under various anthropogenic water demand scenarios, climate change projections, and water supply infrastructure designed is needed.

The findings of this study can be applied to update socioeconomic drought IDF properties that are used to assess water storage, to plan water supply systems under nonstationary conditions, and to optimize water institutions and management including water rights in the American West. Finally, the methodology developed in this study can be applied for other sectors such as agriculture to evaluate the impacts of climate change, land-use change, and socioeconomic drivers on water shortage.

CHAPTER 5.

EFFECTS OF URBAN DEVELOPMENT PATTERNS ON MUNICIPAL WATER SHORTAGE

While urban areas are being threatened by water shortage due to climate change and rapid population growth, effects of urban development patterns on future municipal water shortage are rarely investigated. We address this aspect of urbanization by assessing the impacts of sprawl versus high-density patterns on future changes in the sub-annual socioeconomic drought intensity-duration-frequency (IDF) relationships. The City of Fort Collins, Colorado, water supply system is chosen as a representative region that is rapidly developing over the last decades. The future water supply is estimated using the Soil and Water Assessment Tool (SWAT) driven with a hot-dry climate model from the statistically downscaled Coupled Model Intercomparison Project, phase 5 (CMIP5) projections. Future water demand is projected using the Integrated Urban Water Model (IUWM) under both sprawl and high-density development patterns. The demonstration study reveals that urban areas under the sprawl development pattern are likely to experience socioeconomic drought events with higher intensity, duration, and frequency compared to the high-density pattern. Characterizing impacts of urban development patterns on future drought properties is required for sustainable water management and smart urban growth and can help urban planners and water managers to develop an adaptive path to meet future water demand and decrease the vulnerability of municipal water supply systems to socioeconomic drought.

5.1. Introduction

Municipal water shortage is a crucial problem around the world due to the integrated impacts of climate change and rapid urbanization (Liang et al., 2020; Mukherjee et al., 2018). Municipal water shortage can be defined as the lack of sufficient water supply to meet demand in

urban areas (Foti et al., 2014a; Heidari et al., 2020a; Zhao et al., 2019). Although water supply may be significantly affected in the future by climate change as a result of varying precipitation and increasing temperature, water demand may increase over time due to rapid urbanization (Liu et al., 2020).

Rapid urbanization can be a consequence of either population growth or urban development (Bhatta et al., 2010; Leyk et al., 2020; Xu et al., 2020). Previous studies have mostly assessed the impacts of climate change or population growth on municipal water shortage (Foti et al., 2014a; Hao et al., 2018; Rajsekhar et al., 2015; Sanchez et al., 2020; Warziniack & Brown, 2019), while the pattern of urban development itself can considerably affect the regional hydrological cycles through changing the geology of the river basins (e.g., slope, permeability, etc.) (Hemmati et al., 2020; McDonald et al., 2011; McGrane, 2016; Mukherjee et al., 2018; O'Donnell & Thorne, 2020).

In the spread of urban expansion, two patterns of urban development are frequently observed: Sprawl and high-density development patterns. Sprawl pattern refers to low-density urban areas with segregated land uses and homogenous populations, whereas a high-density pattern refers to urban areas with inhomogeneous populations accompanied by small areas of open or green space to accommodate large numbers of residential and commercial buildings (Western Resource Advocates, 2003). Pattern of urban development is one of the main drivers of rising municipal water demand (Bouziotas et al., 2015; House-peters, 2010). Sprawl development patterns can lead to increases in per capita rates of outdoor water use while the high-density development pattern can lead to lower outdoor water use (Sanchez et al., 2020; Western Resource Advocates, 2003).

The importance of urban development patterns for future water shortage has received less attention compared to climate change as a source of increasing drought hazard (Hemmati et al., 2020). Rapid urbanization compounded by climate change may pose significant pressures on municipal water supply systems in the future (Brown et al., 2019; Heidari et al., 2020a; Hemmati et al., 2020; McDonald et al., 2011). Understanding the important role of urban development patterns on municipal water resources in the future is required for smart urban development and sustainable water management (Bounoua et al., 2020; Forrest et al., 2020; Saraswat et al., 2017).

In the United States, the urban population has grown from 6% to 81% over the past 200 years (Leyk et al., 2020), and urban areas have increasingly expanded (Barrington-Leigh & Millard-Ball, 2015; Wheeler, 2008). The process of urban sprawl on the west and southwest of the United States has been exacerbated at tremendous rates (Hummel, 2020). While rapid urbanization seems inevitable in the United States, understanding a sustainable way to mitigate potential negative consequences on urban water resources in the future is an important challenge (Butler et al., 2017; Forrest et al., 2020; Saraswat et al., 2017).

Although previous studies have described the impacts of land use changes on water use, characterizing the combined effects of changes in both water supply and water demand is vital to effectively manage and plan for future urban water resources. Increasing water use along with climate change may lead to more frequent imbalance between municipal water demand and supply. In this case, to the impacts of urban development patterns on municipal water shortage can be represented by changes in socioeconomic drought properties, where socioeconomic drought is defined as the condition in which the quantities of water demand exceeds the quantities of water supply (Brown et al., 2019; Foti et al., 2014a; Heidari et al., 2020a; Warziniack & Brown, 2019).

Improved understanding of the role of urban growth patterns on municipal water shortage not only helps decision-makers to save municipal water supply by decreasing potential water demand, but also can mitigate the negative consequences of future socioeconomic droughts on water supply systems (Butler et al., 2017). This study highlights the importance of urban growth patterns, i.e. sprawl versus high-density, to future municipal water shortage for the city of Fort Collins as a required task for sustainable water management and smart urban development. The objectives are to: 1) assess how urban development patterns can affect municipal water demand; 2) evaluate the combined impacts of climate change and rapid urbanization on future water shortage; and 3) investigate the role of urban growth patterns on future socioeconomic drought IDF properties.

The city of Fort Collins, Colorado was selected as a drought-prone area to provide an insight into the importance of urban patterns on future water shortage. The city is experiencing substantial population growth and urban development in recent decades (Forrest et al., 2020; Heidari et al., 2020a; Sharvelle et al., 2017). A statistical approach proposed by Heidari et al., (2020a) was applied to assess the integrated effects of shifts in water supply and water demand on sub-annual socioeconomic drought intensity-duration-frequency (IDF) relationships under climate change and population growth. The probabilistic approach uses a mixture Gamma-GPD distribution model at sub-annual scale that leads to improved assessment of socioeconomic drought under considerable changes in both water supply and water demand. In this study, the same probabilistic approach was applied to compare future drought IDF characteristics under sprawl versus high-density development patterns.

5.2. Material and Methods

Based on the definition of socioeconomic drought, climate change, future water supply, and water demand projections are needed for the estimation of future socioeconomic drought properties. The Soil and Water Assessment Tool (SWAT) and the Integrated Urban Water Model (IUWM) were respectively used to estimate future water supply and water demand for the city of Fort Collins under a hot-dry climate model from the statistically downscaled Coupled Model Intercomparison Project, phase 5 (CMIP5) projections. Then, a probabilistic approach was used under sprawl and high-density patterns to assess the impacts of urban development patterns on socioeconomic drought intensity, duration, and frequency.

5.2.1. Study Region and Data

Fort Collins in northern Colorado as a growing small city characterized by mostly low to medium density development (AMEC Environment & Infrastructure, 2014) was selected as an appropriate case study to characterize the role of future urban growth patterns on municipal water shortage. The population of Fort Collins has increased by 14 percent from 2010 to 2017 (Bureau, 2011), forcing urban planners to develop a plan to support the growth.

The observed climate data were obtained from the Global Historical Climatology Network (GHCN), the Colorado Agricultural Meteorological Network (CoAgMet), and Northern Colorado Water Conservancy District (NCWCD). Future Climate changes were projected under the hot-dry climate model (ipsl-cm5a-mr) with the representative concentration pathway (RCP) 8.5 obtained from the CMIP5 dataset (U.S. Bureau of Reclamation, 2013) which represents the worst-case conditions in the future. Readers are also referred to Heidari, et al., (2020b) for the detailed descriptions of future climate model selection.

5.2.2. Future Water Supply

The selected hot-dry climate model was used to estimate water supply for the city of Fort Collins from 1986 to 2065. Horsetooth Reservoir and the Cache la Poudre (CLP) river are the two main water sources for the city of Fort Collins (AMEC Environment & Infrastructure, 2014). Water deliveries to the city of Fort Collins are based on the annual quota set by Northern Water (AMEC Environment & Infrastructure, 2014). Here, we assumed that the historical coefficients of water deliveries to the city of Fort Collins will be maintained as current conditions.

Future water yield in the CLP river basin at the Mouth of Canyon Station (National Water Information System (NWIS), 2019) was estimated using the Soil and Water Assessment Tool (SWAT) model (Arnold et al., 1998) driven with the hot-dry climate model. The SWAT model is a hydrological model that has been widely used to simulate streamflow in response to climate change (Chien et al., 2013; Ficklin et al., 2013; Gassman et al., 2014). Readers are referred to Havel et al. (2014) (Havel et al., 2018) for the details about the SWAT model set up, calibration, and evaluation for the CLP river basin. The monthly streamflow of the CLP river for the city of Fort Collins was simulated using the calibrated SWAT model driven with the hot-dry climate model.

5.2.3. Future Water Demand

The Integrated Urban Water Management (IUWM) model was applied to estimate future water demand for the city of Fort Collins. The IUWM is a process-based water balance model that has been used to project urban water demand (Sharvelle et al., 2017). The model was calibrated and evaluated for the city of Fort Collins (Sharvelle et al., 2017). In this study, the IUWM model was driven with the hot-dry climate model and the population growth scenario obtained from the U.S. Census Bureau with an estimated population of 165,000 for the middle of the century. Readers

are referred to Sharvelle et al., (2017) for the details about the IUWM model set up, calibration, and evaluation for the city of Fort Collins.

Housing density development has been identified as one of the factors that influence water use in urban areas (Western Resource Advocates, 2003). Thus, the future water demand for the city of Fort Collins was estimated under two high-density and sprawl development patterns using the IUWM model. Sprawl pattern refers to conditions when cities continue to grow horizontally that leads to higher occupied space and inefficient natural resource utilization (Bhatta et al., 2010; Rosni et al., 2016). Conversely, high-density development pattern refers to conditions that cities tend to grow vertically resulting in less occupied space and more efficient use of resources (Bhatta et al., 2010; Rosni et al., 2016).

Table 5.1 provides changes in population and population density (people per sq. mile) for the city of Fort Collins from 2010 to 2050. Population was estimated to increase by 165000 under both sprawl and high-density scenarios. This assumption helps to consider only the effects of different urban development patterns on socioeconomic drought IDF relationships in response to rapid urbanization. Population density was assumed to increase over time under high-density development by 4263 (people per sq. mile) while it was assumed to decrease by 2762 (people per sq. mile) under sprawl development.

Table 5.1. Estimated population and population density of the city of Fort Collins.

Scenario	Year	Population	Density (people/sq.m)
Baseline	2010	130000	3358
Sprawl	2020	150000	3709
	2030	158000	3576
	2040	161000	3192
	2050	165000	2762
High Density	2020	150000	3875
	2030	158000	4082
	2040	161000	4159
	2050	165000	4263

Figure 5.1 represents shifts in developed area including open, low, medium, and high intensities under sprawl and high-density growth patterns, respectively. Under current conditions, it was assumed that there is 38.7 (sq. miles) developed area for the city of Fort Collins including open (9.2 sq. miles), low (18.3 sq. miles), medium (8.8 sq. miles) and high (2.4 sq. miles) intensities. Under sprawl scenario, total developed area will increase from 38.7 (sq. miles) to 59.7 (sq. miles) by the middle of century with the highest growth in low intensity area (14.3 sq. miles), and no change in high intensity area. Open and medium intensity area were assumed to increase by 4 (sq. miles), and 2.7 (sq. miles), respectively.

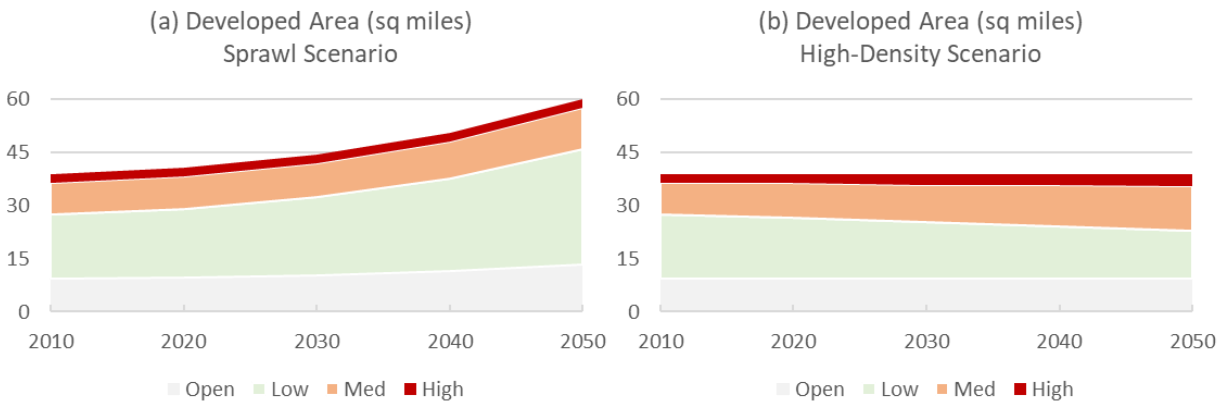

	2010	2020	2030	2040	2050
Open	9.2	9.6	10.3	11.5	13.2
Low	18.3	19.4	21.9	26.1	32.6
Med	8.8	9.1	9.5	10.5	11.5
High	2.4	2.4	2.4	2.4	2.4
Total	38.7	40.4	44.2	50.4	59.7

	2010	2020	2030	2040	2050
Open	9.2	9.2	9.2	9.2	9.2
Low	18.3	17.2	15.9	14.8	13.7
Med	8.8	9.7	10.7	11.6	12.5
High	2.4	2.6	2.9	3.1	3.3
Total	38.7	38.7	38.7	38.7	38.7

Figure 5.1. Estimation of population density (in sq. miles) for each developed area under high-density development.

Under high-density development, total developed area was assumed to remain constant; however, the proportion of intensity will change with the highest decrease in low intensity area (-4.6 sq. miles), and no change in open area by the middle of century. Medium and high intensity areas were assumed to increase by 3.7 (sq. miles), and 0.9 (sq. miles), respectively.

5.2.4. Socioeconomic Drought IDF Projection

Heidari et al. (2020a) showed that the average magnitude and duration of socioeconomic droughts significantly increase assuming changes in both future water supply and water demand conditions (Heidari et al., 2020a). The probabilistic approach developed by Heidari et al., (2020a) was applied for the city of Fort Collins to evaluate the important role of urban development patterns on municipal water shortage induced by changes in future socioeconomic drought characteristics.

A sub-annual socioeconomic drought event can be defined as a succession of consecutive months with water demand greater than water supply (Heidari et al., 2020a; Yevjevich, 1967).

Drought events can be identified by duration, magnitude, intensity and frequency (Heidari et al., 2020a; Salas et al., 2005; Yevjevich, 1967). Duration is the number of consecutive months in which water demand is greater than water supply. Magnitude is summation of monthly water deficit over the drought duration period. Intensity is the ratio of drought magnitude to duration and frequency is the number of times that an event occurs over a specific period. Drought intensity, duration and frequency (IDF) curves have been commonly used for design of municipal water supply systems (Heidari et al., 2020a).

Heidari et al., (2020a) showed that characterization of drought IDF can be improved by applying a mixture Gamma-GPD distribution model at a sub-annual scale. The mixture probability models have been widely used to simultaneously capture bulk and tail of distribution (Ghanbari et al., 2019, 2020; A. MacDonald et al., 2011; Stephens et al., 2018). Heidari et al. (2020a) proposed the cumulative distribution function of mixture Gamma-GPD model as below:

$$F(x|r,a,\xi,\beta,u,\phi_u) = \begin{cases} (1-\phi_u)\dfrac{G(x|r,a)}{G(u|r,a)} & x < u \\ (1-\phi_u) + \phi_u\, g(x|\,\xi,\beta,u) & x \geq u \end{cases} \quad (5.1)$$

where $G(x|r,a)$ is the Gamma distribution function (equation 5.2), $g(x|\,\xi,\beta,u)$ is the unconditional GPD function (equation 5.3), u is the threshold, and ϕ_u is the probability of x being above the threshold (Behrens et al., 2004; A. MacDonald et al., 2011).

$$G(x;r,a) = \frac{1}{a\Gamma(r)}\left(\frac{x}{a}\right)^{r-1} exp\left(-\frac{x}{a}\right) \quad (5.2)$$

$$g_{u,\xi,\beta}(x) = Pr\,(X \le x | X > u) = \begin{cases} 1 - \left(1 + \xi \dfrac{x-u}{\beta}\right)^{-\frac{1}{\xi}} & for \;\; \xi \neq 0 \\ 1 - exp\left(-\dfrac{x-u}{\beta}\right) & for \;\; \xi = 0 \end{cases} \tag{5.3}$$

Consequently, the joint probability distribution can be described as follows:

$$P\,(\mathrm{I} > \mathrm{I}_0 \cap \mathrm{D} > \mathrm{D}_0) = P\,(\mathrm{I} > \mathrm{I}_0 \mid \mathrm{D} > \mathrm{D}_0)\,.P\,(\mathrm{D} > \mathrm{D}_0) \tag{5.4}$$

where D_0 and I_0 are respectively given values of drought duration and intensity. The term $P\,(\mathrm{I} > \mathrm{I}_0|\,\mathrm{D} > \mathrm{D}_0)$ and $P\,(\mathrm{D} > \mathrm{D}_0)$ can be obtained from equation 5.1 using $F(\mathrm{I} > \mathrm{I}_0|\mathrm{D} > \mathrm{D}_0)$ and $F(\mathrm{D} > \mathrm{D}_0)$, respectively.

Moreover, drought return period and frequency amplification factor can be respectively defined as equations 5.5 and 5.6:

$$T_{\mathrm{I}>\mathrm{I}_0|\,\mathrm{D}>\mathrm{D}_0} = \frac{E(\mathrm{D} > \mathrm{D}_0)}{P\,(\mathrm{I} > \mathrm{I}_0|\,\mathrm{D} > \mathrm{D}_0)} * \frac{1}{P(\mathrm{D} > \mathrm{D}_0)} = \frac{E(\mathrm{D} > \mathrm{D}_0)}{P\,(\mathrm{I} > \mathrm{I}_0 \cap\, \mathrm{D} > \mathrm{D}_0)} \tag{5.5}$$

$$Amplification\ Factor\ (AF) = \frac{P_t(I > I_0)}{P_C(I > I_0)} \tag{5.6}$$

where $E(\mathrm{D} > \mathrm{D}_0)$ is the expected drought interarrival time for drought event with $\mathrm{D} > \mathrm{D}_0$, and $P_C(I > I_0)$ and $P_t(I > I_0)$ are the exceedance events probability with $I > I_0$ for current and future conditions, respectively.

Future assessment of municipal water shortage using the proposed sub-annual socioeconomic drought approach not only enhances understanding the effects of future urban patterns on urban water demand, but also provides an insight into how urban growth patterns and

to what extent leads to changes in future drought properties by considering sub-annual shifts in both water supply and water demand conditions (Heidari et al., 2020a)

5.3. Results and Discussion

How urban growth patterns can lead to shifts in socioeconomic drought characteristics is a fundamental question for improved understanding of sustainable water resource management and planning. This section aims to provide a general understanding of how urban growth patterns can affect municipal water shortage in the city of Fort Collins to help decision makers to properly supply water and mange demand in the future. The drought event properties were assessed under two different urban development patterns (high-density and sprawl). The results indicate that urban areas under sprawl patterns are likely to have drought with higher intensity, duration, and frequency compared to the high-density pattern. In fact, sprawl development plays an important role in increasing vulnerability of cities to socioeconomic drought. The 1986-2015 and 2035-2065 periods were used to respectively represent the current and mid-century conditions.

5.3.1. Future Water Supply and Demand Assessment

While water supply decreases due to climate change, water demand increases in the future by the growing population and water use. Figure 5.2 presents 12-month average of projected monthly water supply and water demand for the City of Fort Collins under both sprawl and high-density development and the hot-dry climate model by the middle of the century. We characterized the potential amount of available water supply and water demand for the city of Fort Collins and did not account for problems such as water deliveries or water conservation and storage in the future.

The effects of urban development patterns, in particular, on future water supply and water demand has been evident over time (Figure 5.2). Although water demand for the city of Fort

Collins increases over time due to population growth, sprawl development results in higher total water demand compared to the high-density development pattern. This would be due to rising in per capita water use for keeping landscapes green and irrigation purposes.

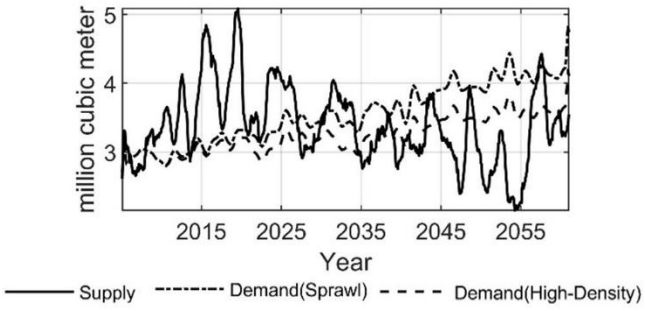

Figure 5.2. 12-month average of estimated water supply and water demand under the hot-dry climate model.

Therefore, sprawl development leads to a higher gap between water supply and water demand by the middle of the century. By the middle of the century, sprawl development is likely to approximately double monthly water deficits for the city of Fort Collins, water supply system compared to the high-density development pattern (Figure 5.3).

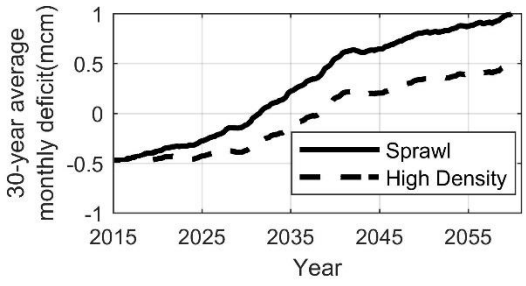

Figure 5.3. 30-year average of monthly water deficit in million cubic meters (mcm) under the hot-dry climate model.

Figure 5.3 indicates that developing cities under the high-density pattern can lead to saving a significant amount of water demanded and decreases pressure on municipal water supply systems in the future under climate changes and rapid population growth.

Integrating climate models, hydrological models, and urban growth models may lead to high uncertainties in future drought hazard assessment and the future projections should not be considered definitive for the city of Fort Collins. The main purpose of this study was to identify the role of urban development patterns on municipal water shortage through two urban growth scenarios as a comparative study. A comprehensive assessment of future water supply and demand conditions in response to climate change is beyond the scope of this study.

5.3.2. Changes in Sub-annual Socioeconomic Drought IDF Properties under Sprawl and High-Density

Sub-annual socioeconomic drought events can be characterized by the estimated monthly water deficit according to definitions and the applied probabilistic framework (Heidari et al., 2020aa). While the expected interarrival time is forecasted to change significantly from the current conditions (1986-2015) to future conditions (2036-2035) under both sprawl and high-density patterns, sprawl development can lead to higher decreases in the expected interarrival than high-density development (Figure 5.4). However, socioeconomic drought events with longer durations are more sensitive to urban growth patterns than droughts with a duration of less than a year. In fact, within-year drought events ($D<12$) would be less influenced by changing urban development patterns.

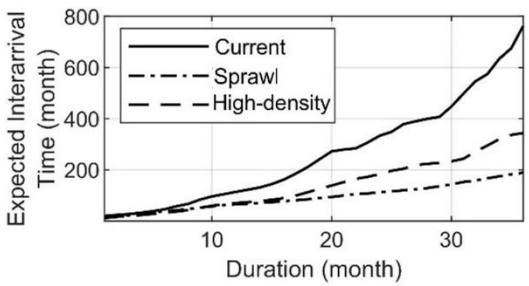

Figure 5.4. Expected interarrival time (in month).

Figure 5.5 shows changes in frequency amplification factors under sprawl and high-density development patterns with various drought durations. Although the frequencies of sub-annual socioeconomic drought are estimated to increase as a result of climate change and population growth, changes in their frequencies are not the same under sprawl and high-density development patterns. The results indicate that the drought frequency for the study system was substantially higher for a sprawl urban growth compared to development under high-density patterns.

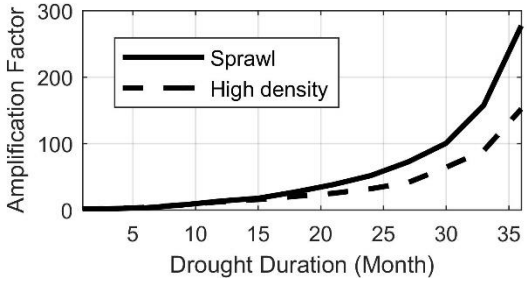

Figure 5.5. Frequency amplification factor curves for drought events (intensity in mcm/month).

Changes in IDF curves of sub-annual socioeconomic droughts were obtained using the developed approach by Heidari et al (2020a). Future drought IDF curves were generated with a duration greater than 1, 6, 12, 24, and 36 months for sprawl and high-density patterns (Figure 5.6). The comparison of the IDF curves for sprawl and high-density development patterns highlights

the importance of the pattern of urban growth on increasing sub-annual socioeconomic drought events.

The return period of socioeconomic drought events under sprawl development is smaller than high-density development consistently under all varying drought durations (Figure 5.6). For a given return period, drought events with higher intensity and longer duration were estimated under the sprawl pattern compared to the high-density pattern for the middle of the century. The results indicate that urban development patterns can substantially affect future drought IDF curves. Drought IDF curves are widely applied for the design of municipal water supply systems. Thus, the choice of future urban development patterns can directly affect design of water supply systems in the future.

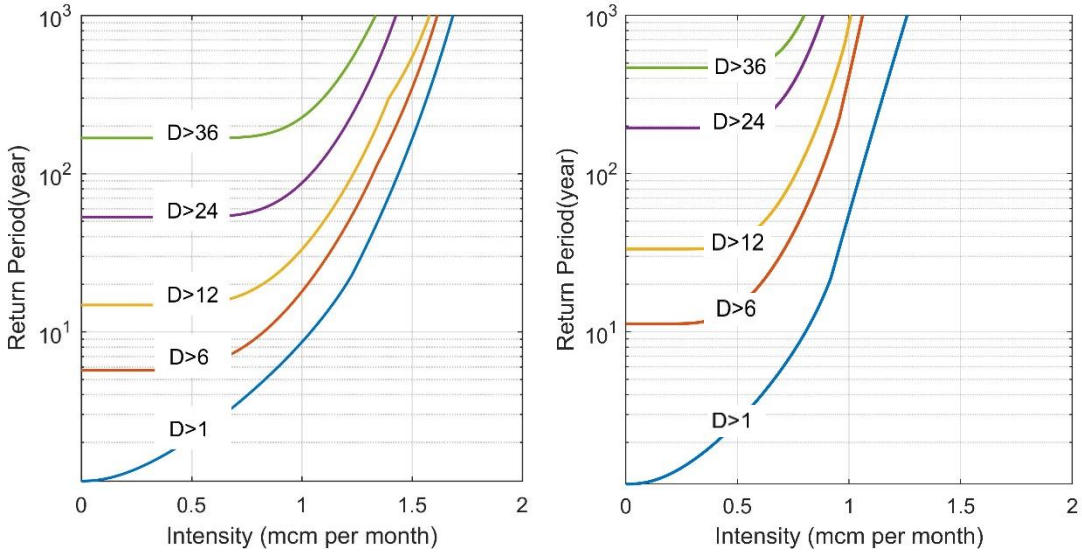

Figure 5.6. Drought intensity-duration-frequency (IDF) curves for future conditions under sprawl patterns (left-panel) and high-density pattern (right-panel) for duration (D) greater than 1, 6, 12, 24, and 36 months.

Quantitative parameters were estimated to demonstrate effects of urban growth patterns on drought properties (Table 5.2). The average drought magnitude, duration, intensity, and maximum water deficit were calculated under both sprawl and high-density development patterns. The socioeconomic drought magnitude, duration, and intensity substantially increase under the sprawl pattern with a higher rate in duration and magnitude. These results highlight that the choice of urban growth patterns may substantially affect future municipal water shortage. The choice of urban patterns plays a key role in sustainable development and water use.

Table 5.2. Impacts of urban growth patterns (sprawl vs high-density) on sub-annual socioeconomic drought properties.

Drought Properties	Sprawl	High-Density
Magnitude (mcm)	8.2	3.62
Duration (month)	9.38	5.4
Intensity (mcm/m)	0.53	0.45
Maximum water deficit (mcm)	1.04	0.87

Although climate change and rapid urbanization are two major causes of water shortage in urban areas, the results of this study in overall identified that the choice of the urban sprawl pattern, in particular, is as a fundamental factor contributing to raising drought intensity, duration, and frequency by growing future water consumption. Sprawl development itself can also lead to increases in pollutant emissions such as carbon monoxide over the long-term (Stone et al., 2007; Zhang et al., 2020), and hence exacerbating climate change.

While urbanization under the high-density development pattern can lead to lower socioeconomic drought hazard in the future, it may have negative consequences on other aspects of urban water cycle such as an increase in stormwater due to more impervious areas. Thus, an integrated water resources and land management strategy is required to mitigate negative

consequences on society, economy, and environment. Rapid urbanization can change the behavior of river basins through changing their topology, geology, and hydrology and have some significant negative consequences on air, energy, land, and water noted in various studies (Wilson & Chakraborty, 2013). High density development typically results in high impervious area, and increased stormwater runoff with detrimental impacts for receiving water bodies and combined sewer overflow events (Bouziotas et al., 2015). Innovative stormwater management techniques such as low impact development (LID), and green infrastructure (GI) can reduce these negative impacts in high density development areas (Seo et al., 2017; Zhang et al., 2017).

Decisions on land management should seek to balance impacts of water use and environmental impacts of urbanization. The importance of water shortage between sprawl and high-density development patterns may be different so that shortage for the sprawl pattern may mean not irrigating lawns while for the high-density pattern may mean no showers.

Thus. this study aims to highlight the importance of urban growth patterns on drought hazard assessment rather than policy implementation or planning strategies. Comprehensive planning regulation and strategies for sustainable urban development in the future needs an interdisciplinary collaborative work between hydrologist, geologist, policymakers, economist, and social scientist that is beyond the scope of this paper.

5.4. Summary and Conclusions

As population and urban areas continue to grow, enhanced urban planning and sustainable water resource management become more crucial. This study aimed to draw attention to the role of urban growth patterns in future drought hazard to provide insights for decision makers, water, and land managers. Improved understanding of factors that reduce future water shortage conditions

can help local and regional planners to identify policy solutions that result in more efficiency of future water use.

Results indicated that sprawl development can result in more water consumption due to higher quantities of water used for outdoor activities such as landscape irrigation. The high-density pattern not only can save municipal water supply by decreasing future water use, but also can lead to decreasing drought impacts on municipal water supply systems by decreasing drought intensity, duration, and frequency.

The findings of this study recommended that modification to development densities can reduce vulnerability to socioeconomic drought. However, decisions on future urban development patterns must balance considerations of drought with possible negative impacts of urbanization and include innovative strategies for stormwater management to mitigate those impacts.

CHAPTER 6.

VULNERABILITY TO WATER SHORTAGE UNDER CURRENT AND FUTURE WATER SUPPLY-DEMAND CONDITIONS ACROSS U.S. RIVER BASINS

Climate change, population growth, urbanization, and interactions thereof may alter the water supply-demand balance and lead to shifts in water shortage characteristics at different timescales. This study assesses the vulnerability of water supply systems to the interannual to the decadal water shortage across the contiguous United States (CONUS) by characterizing shifts in intensity, duration, and frequency (IDF) of events from current (1986-2015) to future (2070-2099) periods. The monthly water yield was estimated using the Variable Infiltration Capacity (VIC) hydrological model driven with the Multivariate Adaptive Constructed Analogs (MACA) climate model with RCP 4.5 and 8.5 emission scenarios. The monthly water demand was projected under the A1B population growth scenario. The Water Evaluation and Planning (WEAP) model was applied to determine water shortage conditions in which water demand exceeds water supply. Changes in characteristics of water shortage conditions were assessed using the Mixture Gamma-GPD probability model. The results indicate that the frequency and intensity of over-year (D>12 months) events at the monthly scale and decadal (D>10 years) events at the annual scale tend to increase in the Southwest, Southern, middle Great Plain, and Great Lakes regions. Conversely, the frequency of interannual (D<12 months) events at the monthly scale and annual (D>1 year) and multi-year (D>3 years) events at the annual scale are likely to increase in the West Coast regions. River basins with a higher rate of aridification are likely to experience more frequent over-year (D>12 months) events while river basins with a decrease in aridification were projected to undergo more frequent interannual (D<12 months) events due to an increase in the variability of extreme

weather anomalies within a year under future climate conditions. The findings of this study provide new insights in understanding current and future water shortage conditions and can inform the development of effective mitigation and/or adaptation strategies for river basins across the CONUS.

6.1. Introduction

Water availability plays a critical role in a wide range of environmental, agricultural, industrial, and recreational activities. However, urbanization, population growth, and climate change may lead to shifts in water supply-demand conditions in river basins and culminate in short-term or chronic water shortages (Brown et al., 2019; Engström et al., 2020; Heidari et al., 2020a; Heidari, et al., 2020b; Mahat et al., 2017; Naz et al., 2016; Warziniack & Brown, 2019; Xing et al., 2018). Water shortage occurs when water demand exceeds water supply and can be assessed on various spatial and temporal scales (Foti et al., 2012; Jose D. Salas et al., 2005; Yevjevich, 1967). Enhanced characterization of shifts in water shortage conditions is increasingly discussed in response to climate change and rapid population growth (Cheng et al., 2014; Heidari, et al., 2020a; Salas et al., 2018).

Water shortage events have recently increased across multiple U.S. river basins with longer duration, higher intensity, and greater spatial extent than has occurred over the last decades (Martin et al., 2020). Although diverse methods have been used in previous studies for the assessment of future water shortage conditions across the United States, a few studies discussed the effects of shifts in both water supply and water demand on the intensity, duration, and frequency (IDF) relationships of water shortage events across the United States at various spatial and temporal

scales (Guo et al., 2019; Heidari et al., 2020a; Salas et al., 2018; Tu et al., 2018) and more research is needed to support actionable managements to mitigate negative impacts.

Recent assessments of future water supply and demand across the conterminous United States (CONUS) have shown an increase in the frequency of water shortage in western basins (Brown et al., 2013, 2019; Foti et al., 2012, 2014b; Mahat et al., 2017; Mehran et al., 2017; Warziniack & Brown, 2019). While these studies examine frequency of long-term water shortage conditions, the effects of changes must be assessed in intensity, duration, and frequency (IDF) relationships of events at interannual to decadal timescales (Cayan et al., 2010; Gober & Kirkwood, 2010; Jaeger et al., 2017; G. M. MacDonald, 2010; Mann & Gleick, 2015; McDonald et al., 2011; Rosegrant & Cai, 2002; Sun et al., 2008; Yigzaw & Hossain, 2016).

Previous studies have mainly focused on the frequency of water shortage occurrence. Foti et al., (2014b) assessed the vulnerability of the U.S. water supply system to the shortage as the probability that annual water supply is less than annual water demand. Brown et al., (2019) and Warziniack & Brown, (2019) quantified the frequency of water shortage as the number of months over a given multiyear time period when shortages occur. Engström et al., (2020) assessed the drought exposure of each state within the CONUS using drought frequency, population density, and protected waters indicators. They represented the drought frequency to show how often a state is in drought.

However, few studies discussed the effects of shifts in both water supply and water demand on intensity, duration, and frequency (IDF) relationships of water shortage events at various temporal scales from interannual to decadal (Heidari et al., 2020a). Although IDF curves have been commonly used for the characterization of the designed event for water supply systems, these relationships may need to be modified in a changing environment under nonstationary conditions.

The improved estimation of future IDF relationships can enhance the management and planning of future water resources (Buurman & Babovic, 2016; Heidari et al., 2020a).

Furthermore, interannual changes in the variability of weather and water consumption in the future may cause unequal supply-demand balance within a year (Gutzler & Nims, 2006; Yu et al., 2014). The assessments of water shortage conditions at various timescales allow characterizing of both prolonged and short-term events (Maliva & Missimer, 2013). Many regions that are prone to prolonged water shortage conditions may not have the food, water, and economic resources to overcome multi-year water shortage conditions (Maliva & Missimer, 2013). Besides, even in regions where water is abundant, water scarcity during short time periods within the year may be on the rise due to climate change and rapid population growth (Jaeger et al., 2017). Interannual water shortage conditions can lead to significant impacts, especially on agricultural regions during the growing seasons (Otkin et al., 2018).

Recently, Heidari et al., (2020a) developed a probabilistic approach for enhanced characterization of intensity, duration, and frequency (IDF) relationships of water shortage events at a sub-annual scale under considerable shifts in water supply and demand conditions. The approach uses the mixture Gamma-Generalized Pareto (Gamma-GPD) model to simultaneously improve the characterization of both non-extreme and extreme events. The application of the developed probabilistic approach was demonstrated in this study for the CONUS at a 4-digit hydrologic unit code (HUC4) basin scale under the IPSL-CM5A-MR model obtained from the Multivariate Adaptive Constructed Analogs (MACA) dataset as the driest climate model with the highest projected decrease in average precipitation (Joyce & Coulson, 2020).

This study assesses future shifts in intensity, duration, and frequency (IDF) of water shortage conditions at interannual, annual, multi-year, and decadal scales across the CONUS in

response to shifts in water supply and water demand conditions. Specifically, the objectives are to: (1) assess shifts in IDF properties of water shortage events across U.S. river basins from current to future conditions; (2) evaluate the frequency amplification factors of water shortage events; and (3) identify factors that govern changes in water shortage frequency (or intensity) across regions in CONUS. The findings of this study can help decision-makers to assess and improve the ability of various water supply systems to shortage and address the considerations in water resource planning and management under considerable shifts in water supply and demand conditions.

6.2. Material and Methods

The characterization of future water shortage conditions at various timescales and understanding mechanisms behind that is required for the enhanced water resource management and planning (Andreadis & Lettenmaier, 2006; Hagenlocher et al., 2019; Svoboda et al., 2002; Tu et al., 2018). Figure 6.1 illustrates the roadmap of this study. Current climate conditions (1986-2015) of U.S. river basins were projected using the combination of the Daymet (Thornton et al., 1997b) and the Parameter-elevation Regressions on Independent Slopes Model (PRISM) (Daly et al., 2008) datasets. Future climate conditions (2016-2099) were estimated using the driest MACAclimate model with RCPs 4.5 and 8.5 emission scenarios from the downscaled Multivariate Adaptive Constructed Analogs (MACA) datasets (Abatzoglou & Brown, 2012). The forcing climate variables were used as inputs to the variable infiltration capacity (VIC version 4.1) model to project the monthly water yields across the CONUS at the HUC4 river basin scale (Figure D-1).

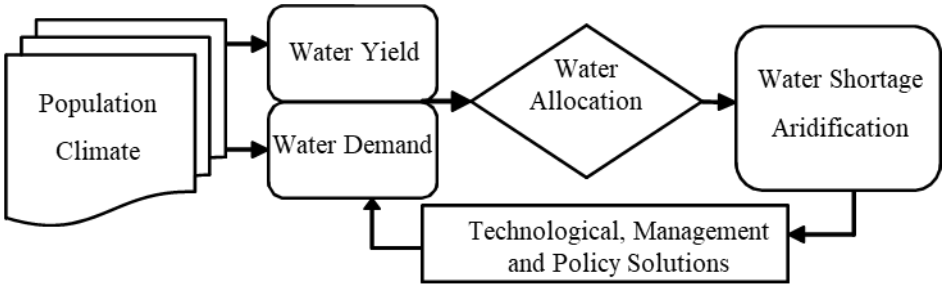

Figure 6.1. The proposed framework of water shortage analysis

The monthly water demand of each basin was estimated in light of population growth and climate change. Then, the water supply of each basin was obtained using the Water Evaluation and Planning (WEAP) model. The estimated water supply and water demand were used to characterize changes in characteristics of water shortage events from current (1986-2015) to future (2070-2099) conditions. Additionally, the statistical relationships between the sub-annual water shortage conditions and aridification were assessed. Finally, regions with a level of shortage in the future were categorized into supply-based, demand-based, and supply/demand-based regions. Changes in the average duration, intensity, and frequency of water shortage events were characterized under shifts in only water demand conditions (demand-based), only water yield conditions (supply-based) and both supply and demand conditions (supply/demand-based). We applied the term baseline to denote the historical period (1986-2015) as a basis for comparison with the future climate conditions.

6.2.1. Hydroclimatic Projection

The daily precipitation and temperature of U.S. river basins for the current conditions (1986-2015) were obtained from the Daymet dataset (Thornton et al., 1997b) and then biased corrected using the Parameter-elevation Regressions on Independent Slopes Model (PRISM) climate dataset (Daly et al., 2008) at the monthly scale. The daily wind speed of U.S. river basins

for the current conditions was also calculated from the North American Regional Reanalysis (NARR) dataset (Mesinger et al., 2006). Readers are referred to Oubeidillah et al. (2014) and Naz et al. (2016) for more detailed information about the historical climate projection.

The future precipitation, minimum and maximum temperature, and wind speed of U.S. river basins were obtained from the downscaled Multivariate Adaptive Constructed Analogs (MACA) datasets (Abatzoglou & Brown, 2012). The MACA climate dataset includes twenty downscaled climate models at the grid size of ~4 km (1/24 degree) with the RCP 4.5 and RCP 8.5 emission scenarios. In this study, we selected the IPSL-CM5A-MR model for future climate projection over the CONUS where RCP 4.5 and RCP 8.5 were used as bounding scenarios. Note that the selected MACA climate model has on average the driest projection at the conterminous scale (Joyce & Coulson, 2020).

A good representation of current climate conditions is a vital need required to realistically simulate future climate conditions. Figure D-2 compares the 30-year average of annual projected precipitation and temperature of the IPSL-CM5A-MR climate model and the baseline climate model (the combination of PRISM and Daymet) over the historical period (1986-2015) at the HUC4 basin scale. The 30-year average of precipitation and temperature for the climate model has a high correlation with the baseline historical model under both RCP 4.5 and 8.5 emission scenarios. The IPSL-CM5A-MRclimate model with RCPs 4.5 and 8.5 shows a strong linear correlation (from 0.9928 to 0.9985) for both annual precipitation and temperature. Readers are referred to Heidari, et al., (2020b), and Joyce & Coulson, (2020) for more detailed information about the future climate projections.

The current and future climate projections were then inputted to the semi-distributed macroscale Variable Infiltration Capacity (VIC) version 4.1.1 hydrologic model (Liang et al.,

1994; Cherkauer et al., 2003) at a daily time step to simulate the water yield of U.S. river basins at the grid size of ~4 km (1/24 degree). The VIC model has been commonly applied to project streamflow over different large river basins in North America (Andreadis & Lettenmaier, 2006). Topography, soil characteristics, vegetation, and land surface classification are other key hydrological inputs to the VIC model.

The aggregated monthly runoff obtained from the USGS National Water Information System gauge observations (WaterWatch dataset) (Brakebill et al., 2011) was used to calibrate the VIC model for each HUC4 basin. Organized and calibrated VIC input data for the US Geological Survey (USGS) eight-digit hydrologic subbasins (HUC8) across the entire CONUS were obtained from Oubeidillah et al., (2014). The daily water yield outputs from the VIC model were then aggregated to monthly values or each HUC4 river basin.

Figure D-3 compares the observed versus simulated annual water yield for each HUC4 river basin within the CONUS over the 1986-2015 period. The VIC model shows a strong linear correlation (0.9894) between observed and simulated mean annual water yield. Readers are referred to Oubeidillah et al. (2014), Naz et al. (2016), and Heidari et al., (2020b) for the detailed description of the VIC model set up, calibration, evaluation, and simulation.

6.2.2. Water Demand Projection

The method used in this study to estimate water demand follows that described by Brown et al., (2013, 2019). The monthly water demand of each HUC4 river basin was estimated by summing projections for six water use sectors including domestic and public, agricultural irrigation, thermoelectric, industrial, commercial, and mining, livestock, and aquaculture. The current water use data were obtained from the USGS water use circulars and for thermoelectric power water use from Diehl and Harris (Diehl & Harris, 2014). The future water withdrawal for

each sector was estimated as the product of a water use driver such as population and irrigated area; and a water withdrawal rate such as domestic withdrawals per capita and irrigation withdrawal per unit area.

The A1B scenario from the Intergovernmental Panel on Climate Change (IPCC) Fourth Assessment set of global socioeconomic scenarios was chosen to project future changes in population and income levels using the AIM global emissions model (Brown et al., 2013; Nakicenovic, 2000). The A1B scenario closely extends the current trends in population and economic growth and simulates a high level of technological change and rapid spread of efficient technologies by assuming a balanced emphasis on all energy sources. The population of the United States has been estimated to approximately increase of 67% from current to future conditions with an annual growth rate that gradually declines by about 62% (Brown et al., 2013).

Irrigated area has been estimated to rise in the East and decrease in the West (Brown et al., 2013); and per capita total electricity consumption has been projected to increase about 7% from current to future conditions with an annual growth rate that gradually declines by 100%. Impacts of climate change on water demand were included in domestic, public, irrigation, and thermoelectric demand (Brown et al., 2013). Projected changes under the driest climate model can affect water use in several sectors (Brown et al., 2019; Georgakakos et al., 2014), as rising potential evapotranspiration rates, plus decreasing precipitation can lead to a significant increase in agriculture and landscape irrigation demands.

6.2.3. Water Supply Assessment

The Water Evaluation and Planning (WEAP) model (Yates et al., 2005) was applied in this study to estimate the water supply allocated to each HUC4 river basin. The WEAP model applies linear programming to allocate water in order to maximize demand satisfaction that is subject to

allocation priorities, mass balances, water availability, and other constraints (Brown et al., 2019). The approach of the WEAP model is to satisfy demands and maintain reservoir storage levels. The water demand is satisfied from the current water yield before the utilization of reservoir storage.

The WEAP model used in this study was set up by Brown et al., (2019) at HUC04 watersheds spatial scale. The WEAP model runs at the monthly time step for the period of 1985 to 2099 to calculate the past and future water supply of each HUC4 river basin. The monthly water yield, water demand, trans-basin diversion capacity, instream flow constraint; reservoir storage capacity, evaporation rate, and volume-elevation curve; and priorities of the different water uses are the key inputs to the WEAP model.

The water supply of a basin was defined as the amount of water available to meet demands for a given month and obtained from the sum of water yield, net trans-basin diversions, reservoir storage from the prior month, and inflow from upstream minus the sum of required instream flow release, reservoir evaporation, and any required release to satisfy downstream demands. Note, the net trans-basin diversion is positive if the basin imports water and negative if the basin exports water. The surplus water supply will be stored in the reservoir when water supply exceeds consumptive use demands.

This order of priority of different water uses was assumed so that a minimal amount of water for environmental and ecosystem needs will be maintained and major water diversion agreements will be satisfied. The highest priority was given to the instream flow requirement and trans-basin diversions and then the next two lower priorities were assigned to within basin consumptive demands, and the lowest propriety was given to the reservoir storage. Readers are referred to Brown et al., (2019) and Warziniack & Brown, (2019) for the detailed description of the WEAP model set up, calibration and evaluation.

6.2.4. Characterization of Water Shortage IDF Relationships

The probabilistic approach developed by Heidari et al., (2020a) was used in this study to assess shifts in intensity, duration, and frequency (IDF) of water shortage events across the CONUS at the monthly and annual scales. The projected water demand and water supply from sections 2.3 and 2.4 were used as inputs to identify changes from current to future conditions.

The duration (D), intensity (I), and frequency (F) of a water shortage event were respectively defined as the number of consecutive months/years where water demand exceeds water supply, the cumulative water deficit divided by its duration and the number of times that a specific event occurs (Figure D-4).

The water shortage events were modeled using the mixture Gamma-GPD distribution to simultaneously capture bulk and tails of events. In this model, values below the GPD threshold (i.e., location parameter) were modeled by the Gamma distribution while values above the threshold were modeled by the GPD. The mixture Gamma-GPD cumulative function (F) is given by:

$$F(x|r,a,\xi,\beta,u,\phi_u) = \begin{cases} (1-\phi_u)\dfrac{G(x|r,a)}{G(u|r,a)} & x < u \\ (1-\phi_u) + \phi_u\, g(x|\,\xi,\beta,u) & x \geq u \end{cases} \tag{6.1}$$

where $g(x|\,\xi,\beta,u)$ is the unconditional GPD function, $G(x|r,a)$ is Gamma distribution function, u is the GPD location parameter (threshold), and ϕ_u is the probability of x being above the threshold.

The joint probability distribution of events for intensity $I > I_0$ and duration $D > D_0$ can be obtained by the product of the conditional distribution of intensity for a given duration and the marginal distribution of duration as:

$$P\ (\mathrm{I} > \mathrm{I}_0\ \cap \mathrm{D} > \mathrm{D}_0) = P\ (\mathrm{I} > \mathrm{I}_0 \mid \mathrm{D} > \mathrm{D}_0)\ .P\ (\mathrm{D} > \mathrm{D}_0) \tag{6.2}$$

where D_0 and I_0 denote any given values of duration and intensity, respectively. $P\ (\mathrm{D} > \mathrm{D}_0)$ is the marginal probability of events with $\mathrm{D} > \mathrm{D}_0$ and the term $P\ (\mathrm{I} > \mathrm{I}_0 | \mathrm{D} > \mathrm{D}_0)$ is the conditional probability of $\mathrm{I} > \mathrm{I}_0$ given $\mathrm{D} > \mathrm{D}_0$. The marginal probability of $\mathrm{D} > \mathrm{D}_0$ from the mixture Gamma-GPD is given by:

$$P\ (\mathrm{D} > \mathrm{D}_0) = F(\mathrm{D} > \mathrm{D}_0)\ = \begin{cases} (1-\phi_u)\dfrac{G(\mathrm{D} > \mathrm{D}_0|r,a)}{G(\mathrm{u}|r,a)} & x < u \\ (1-\phi_u) + \phi_u\ g(\mathrm{D} > \mathrm{D}_0|\ \xi,\beta,u) & x \geq u \end{cases} \tag{6.3}$$

The conditional probability of $P\ (\mathrm{I} > \mathrm{I}_0 | \mathrm{D} > \mathrm{D}_0)$ can be determined in the same way considering that the mixture model should be fitted to just water shortage events with $\mathrm{D} > \mathrm{D}_0$ as follows:

$$P\ (\mathrm{I} > \mathrm{I}_0 | \mathrm{D} > \mathrm{D}_0) = F(\mathrm{I} > \mathrm{I}_0 | \mathrm{D} > \mathrm{D}_0 | r, a, \xi, \beta, u, \phi_u) \tag{6.4}$$

The annual return period of events under nonstationary conditions with intensity greater than or equal to a target ($\mathrm{I} > \mathrm{I}_0$) were calculated as a function of the expected interarrival time and cumulative intensity distribution function, expressed as:

$$T_{\mathrm{I}>\mathrm{I}_0|\ \mathrm{D}>\mathrm{D}_0} = \frac{E(\mathrm{D} > \mathrm{D}_0)}{P\ (\mathrm{I} > \mathrm{I}_0 | \mathrm{D} > \mathrm{D}_0)} * \frac{1}{P(\mathrm{D} > \mathrm{D}_0)} = \frac{E(\mathrm{D} > \mathrm{D}_0)}{P\ (\mathrm{I} > \mathrm{I}_0 \cap\ \mathrm{D} > \mathrm{D}_0)} \tag{6.5}$$

where $E(\mathrm{D} > \mathrm{D}_0)$ is the expected interarrival time with $\mathrm{D} > \mathrm{D}_0$. The expected value of interarrival time between two successive socioeconomic events with $\mathrm{D} > \mathrm{D}_0$ is given by (Shiau & Shen, 2001; Zhao et al., 2017):

$$E(\mathrm{D} > \mathrm{D}_0) = E(\sum_{i=1}^{N} \mathrm{DI}_\mathrm{i}) \tag{6.6}$$

where DI_i is interarrival time between two successive events with $\mathrm{D} > \mathrm{D}_0$, and N is the number of events equal to or greater than a certain duration.

The change in frequencies under nonstationary conditions can be also quantified by dividing the exceedance probability of a given water shortage event in the future to the current condition as follows:

$$Amplification\ Factor\ (AF) = \frac{P_t(I > I_0)}{P_C(I > I_0)} \tag{6.7}$$

where AF is the frequency amplification factor of events with $I > I_0$, and $P_C(I > I_0)$ and $P_t(I > I_0)$ are respectively the exceedance probability of events with $I > I_0$ for current and future conditions.

The applied probabilistic approach allows enhanced assessments of vulnerability to water shortage at the both interannual and annual time steps in basins undergoing climate and socioeconomic changes (Heidari et al., 2020a). Improved characterization of IDF relationships is critical in the design of water supply systems under nonstationary conditions (Guo et al., 2019; Heidari et al., 2020a; Mehran et al., 2015; Salas et al., 2018).

6.2.5. Characterization of Changes in the Aridity Index

long-term changes in the relationship between climate and water budgets of river basins may lead to aridification or desertification (Maliva & Missimer, 2013). Aridification can be defined as the long-term severe lack of freshwater availability in a region. Recent water shortage events across the conterminous United States (CONUS) have shown that severe events can develop

very rapidly if climate change leads to aridification in a region (Andreadis & Lettenmaier, 2006; Piemontese et al., 2019).

The aridity (or dryness) index is commonly used in previous studies to characterize regions that are more prone to aridification in response to long-term climate change (Yang et al., 2006; Q. Zhang et al., 2017). The aridity index is defined as the ratio of annual potential evapotranspiration (PET) to annual precipitation (P). The river basins with increases in the long-term average aridity index are more likely to face aridification in the future.

The annual precipitation of HUC4 river basins was obtained from the IPSL-CM5A-MR(driest) climate model of the MACA dataset. The potential evapotranspiration of HUC4 river basins was calculated using the VIC hydrological model. The Penman-Monteith equation was implemented in the VIC model for the estimation of the PET. The VIC model assumes that PET is from open water meaning that there are sufficient open water supplies. Thus, the PET values are the maximum (potential) evapotranspiration capacity.

In this study, the statistical correlation between changes in aridity index, and changes in the intensity and duration of sub-annual water shortage events were calculated at the HUC4 river basin scale to figure out how long-term anomalies such as aridification can be related to short-term anomalies such as sub-annual water shortage events. The hypothesis defined as there is no correlation. Thus, the *p*-values less than the significance level (0.05) indicate rejection of the hypothesis meaning that changes in aridity index water shortage characteristics are statistically correlated.

6.3. Results and Discussion

The study reveals that shifts in IDF relationships of water shortage conditions in response to climate change and population growth vary from one HUC4 river basin to another. The majority of HUC4 river basins within the Southwest, Southern, and the middle Great Plain regions were projected to undergo a significant increase in intensities and frequencies of over-year (D>12 months) events at the monthly scale, and decadal (D>1-0 years) events at the annual scale. However, most river basins within the West Coast regions were estimated to experience a decrease in the intensity of water shortage conditions. However, the frequency of interannual (D<12 months) events at the monthly scale and annual (D>1 year) and multi-year (D>3 years) events at the annual scale were projected to increase in the West Coast regions under the driest climate projection for the CONUS.

Note that the characterization of water shortage at the monthly and annual scales makes a significant difference in the definition of water shortage events. The events with duration (D) = n months mean that there are n consecutive months in which monthly water demand is greater than monthly water supply. However, events with duration (D) = n years mean that there are n consecutive years in which total annual water demand is greater than total annual water supply. For example, events with duration equal to 24 months (D = 24 months) are not equivalent to events with duration equal to two years (D = 2 years). Thus, even during a two-year event, there may be months with water surplus. As a result, characterization of water shortage events at both monthly and annual scale can help to identify interannual to decadal events that can lead to enhanced decision-making in water resource planning and management.

6.3.1. Changes in Water Yield and Demand

Figure 6.2 shows changes in monthly water yield and water demand of HUC4 river basins under climate change with RCPs 4.5 and 8.5 emission scenarios. The current water yield and water demand vary substantially across the HUC4 basins with higher water yield in the wetter regions (e.g., Southeast and Northwest US) and the higher water demand in drier regions (e.g., the West, Southwest, and Midwest US) (Figure 6.2.a). Note that higher water demand is likely to occur in basins with lower water yield. The unit of deficit in this study is million cubic meters (MCM) and the unit of water yield is cubic meters per second (CMS).

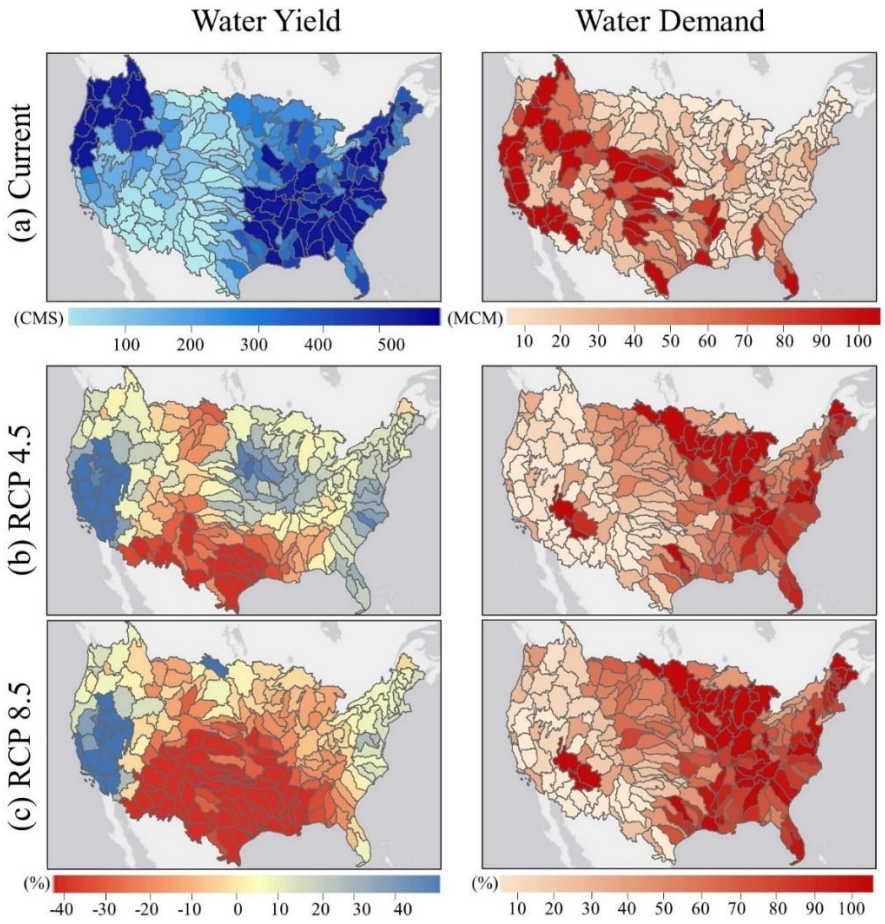

Figure 6.2. (a) Current monthly water yield and water demand by basin; and projected changes from current (1986-2015) to future (2070-2099) conditions under the driest MACA climate model with (b) RCP 4.5 and (c) RCP 8.5.

Changes in water yield from current (1986-2015) to future (2070-2099) conditions are highly variable from a 30% decrease in the southern United States to more than 50% increase in the western United States under RCP 4.5 (Figure 6.2.b). While the pattern of changes in water yield under the RCP 8.5 scenario is like the RCP 8.5 scenario, a decrease in water yield tends to be extended to some river basins in the Southwest, middle Great Plains, and Southeast United States (Figure 6.2.c).

Estimated changes in water demand from current to future conditions are highly variable across the CONUS, that is positive in most HUC4 basins but slightly changes in basins located in the West, Southwest and Northwest United States under both RCPs 4.5 and 8.5 emission scenarios (Figures 6.2.b and 6.2.c) due to the effect of the projected decrease in the irrigated area (Brown et al., 2013). The highest increase in future water demand is likely to occur in the Ohio Valley and Upper Midwest United States. Decreasing water yield, increasing water demand, or especially their combination can lead to potential conditions for water shortage.

6.3.2. Changes in IDF Relationships of water shortage conditions at the monthly scale

Under the driest climate model and RCP 4.5 and 8.5 emission scenarios, 64 and 73 HUC4 river basins were respectively projected to experience some level of monthly water shortage in the future (Figure 6.3.a). Thus, in this study, we assessed shifts in intensity, duration, and frequency (IDF) of water shortage events across these basins. Although the majority of basins located in the Southwest region were projected to experience a higher increase in the number of months with water shortage in the future, the HUC4 river basins in the West Coast region were estimated to have decrease in the number of months with water shortage.

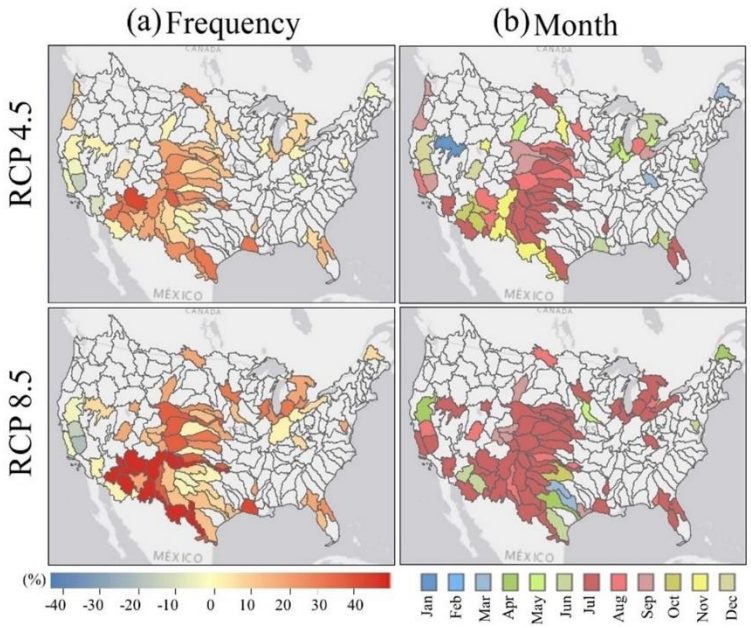

Figure 6.3. Changes in the frequency of months with water shortage by basin from current (1986-2015) to future (2070-2099) conditions and (b) the months with the highest occurrence of water shortage under RCP 4.5 and RCP 8.5.

Furthermore, Figure 6.3.b shows the months with the highest occurrence of water shortage conditions in each HUC4 river basin. The majority of water shortage conditions were projected to occur over the summer months (July, Aug, and Sep).

We then assessed the IDF relationships of current (1986-2015) and future (2070-2099) water shortage conditions at the monthly scale to estimate shifts in characteristics of interannual and over-year (D>12 months) water shortage events. Figure 6.4.a shows the current IDF relationships of HUC4 river basins across the United States. Under the current conditions and for a given return period (e.g., T=10 years), the intensity decreases as the duration becomes longer.

Additionally, for a given duration (e.g., D>1 month), the intensity was projected to slightly change as the return period increases (e.g., from T=10 years to T=100 years). Overall, the West Coast and the middle Great Plain river basins were projected to currently have more intense water shortage conditions (~ 400 mcm/months) at the sub-annual scale.

However, under the future conditions (Figure 6.4.b), the intensity of water shortage events was projected to mostly increase from current to future conditions with a higher rate of increase in events with longer duration and higher return period. Water shortage events with a duration greater than one month (D>1 month) and a return period of 10 years (T=10 years) have the lowest increase in intensity. Conversely, events with a duration greater than twelve months (D>12 months) and a return period of 100 years (T=100 years) were projected to have the highest increase in intensity.

For T=10 years, the intensity was projected to significantly increases from D>1 month to D>6 months while for T=100 years, the highest increase in intensity was projected from D>6 months D>12 months. The result means that at the sub-annual scale, the intensity of water shortage events with a duration greater than 12 months (12 consecutive months with water deficit) is more vulnerable to climate change and population growth compared to the intensity of interannual water shortage events, especially for longer return periods.

For water shortage events with D>1 month, there are minor differences in the intensity of current and future water shortage events. Additionally, the intensity of future events with D>1 month was projected to slightly change as the return period increases (e.g., from T=10 years to T=100 years). The finding indicates that sub-annual events that occur every 10 years are likely to experience the same magnitude of increase in intensity compared to sub-annual events that occur every 100 years.

For water shortage events with D>6 months, the majority of river basins are more likely to experience higher increases in the intensity of more frequent events (T=10 years) compared to the less frequent events (T=100 years). Thus, this reveals that events that occur every 10 years are likely to experience a higher magnitude of changes in the intensity compared to events that occur every 100 years.

Conversely, for water shortage events with D>12 months (12 consecutive months with water deficit), river basins are more likely to experience higher changes in the intensity of less frequent events (T=100 years) compared to the more frequent events (T=10 years). This means that events with a duration greater than twelve months (D>12 months) that occur every 10 years are likely to experience a lower magnitude of changes in intensity than events with a duration greater than twelve months (D>12 months) that occur every 100 years.

The results indicate that less frequent (T=100 years) and longer (D>12 months) sub-annual events and more frequent (T=10 years) and shorter (D>6 months) sub-annual events are likely to experience the highest increase in intensity in the future. Overall, the majority of river basins in the Southwest, Southern, and the middle Great Plain regions were estimated to experience interannual water shortage conditions with higher intensity in the future. However, West Coast river basins are likely to experience a decrease in the intensity of interannual water shortage events up to more than -90%.

Figures D-5 to D-68 show intensity-duration-frequency (IDF) curves of each HUC4 river basin for current and future conditions. The unit of intensity in this study is the million cubic meters per month (MCM/month). In general, the assessment of water shortage at the monthly scale indicates that the interannual water shortage conditions are likely to become more intense in the

future. Note that the driest climate model under the RCP 8.5 emission scenario leads to a higher increase in the intensity of interannual events although the patterns are similar.

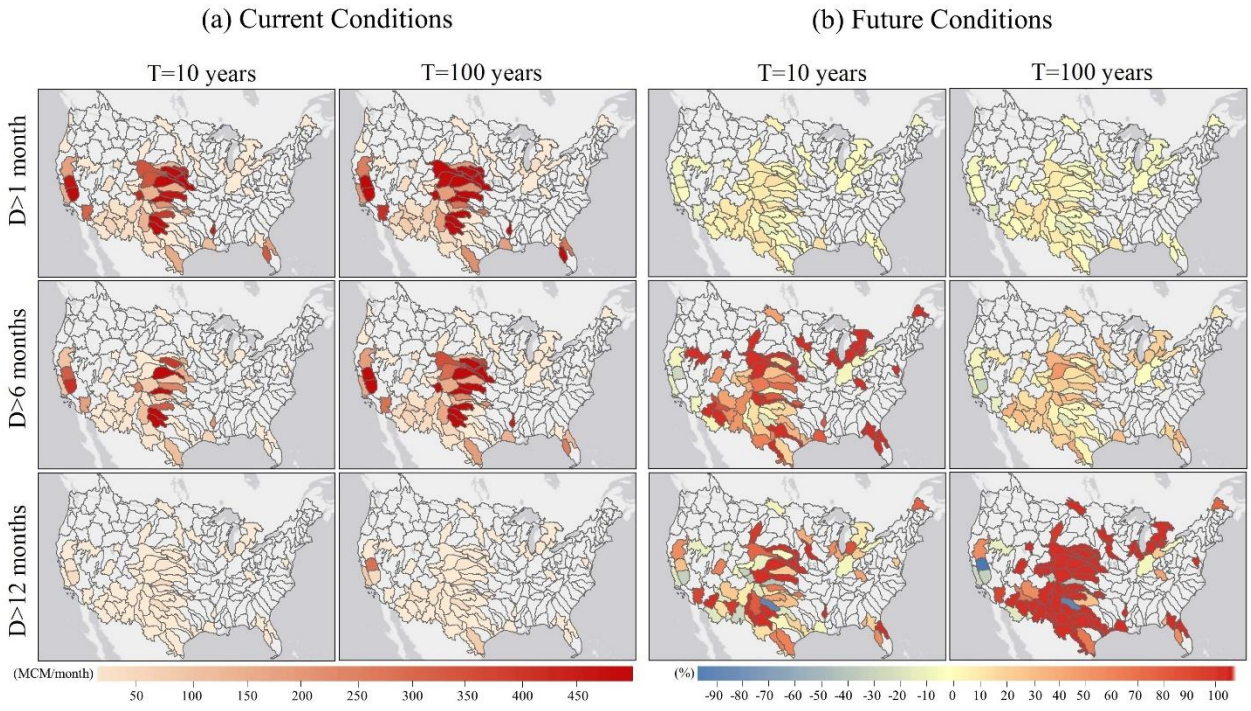

Figure 6.4. (a) Current intensity and (b) changes in the intensities of events from current (1986-2015) to future (2070-2099) conditions under RCP 8.5 at the monthly scale.

Then, we investigated the effects of shifts in future water supply and demand conditions on the frequency of sub-annual water shortage events using the frequency amplification factor (AF). Figure 6.5 compares the frequency amplification factors of water shortage events with the duration less than twelve months (D<12 months) with water shortage events with the duration greater than twelve months (D>12 months) across the united states for both RCP 4.5 and 8.5 emission scenarios.

Although both RCPs 4.5 and 8.5 show the same spatial pattern of amplification factors, the RCP 8.5 emission scenario projected a greater amplification factor meaning that water shortage events will become more frequent under the RCP 8.5 emission scenario. In the Southwest, Southern, and middle Great Plain river basins, while the frequency amplification factors of events with D<12 months (interannual events) have slightly decreased, the amplification factor of events with D>12 months (12 consecutive months that monthly water demand exceeds monthly water supply) was projected to increase.

The result reveals that the frequency of over-year events (D>12 months) is likely to increase in the future while interannual events are likely to be less frequent in the future. However, the river basins in the West Coast region are more likely to experience less frequent over-year (D>12 months) events and more frequent interannual (D<12 months) events.

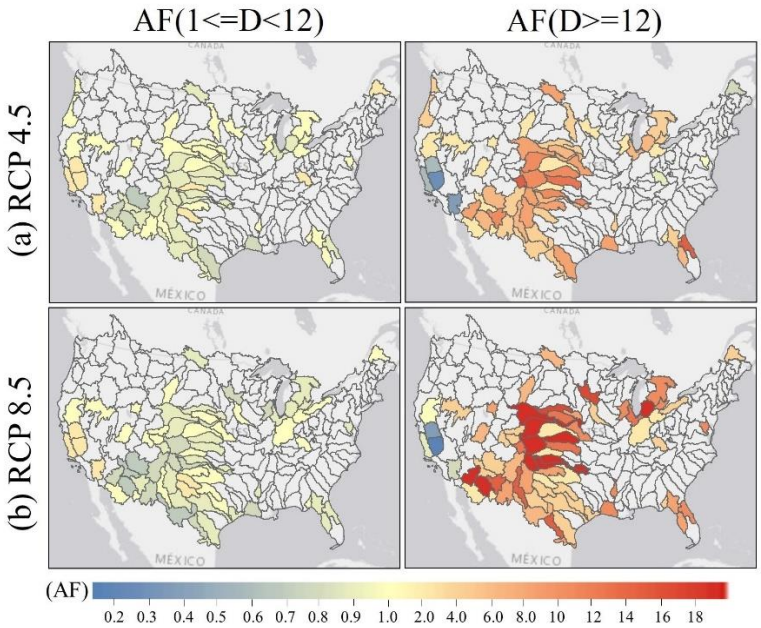

Figure 6.5. The frequency amplification factor (AF) under (a) RCP 4.5 and (b) RCP 8.5 at the monthly scale.

In general, the assessment of water shortage at the monthly scale indicates that the Southwest, Southern, and the middle Great Plain river basin are likely to experience more intense sub-annual water shortage conditions in the future with more frequent over-year events (D>12 months) and less frequent interannual events (D<12 months). Conversely, the West Coast river basins are likely to experience a decrease in the intensity of sub-annual water shortage events in the future with less frequent over-year (D>12 months) events and more frequent interannual (D<12 months) events.

6.3.3. Changes in IDF Relationships of water shortage conditions at the annual scale

We assessed the IDF relationships of current and future water shortage conditions in this section at the annual scale to estimate shifts in characteristics of annual (D>1 year), multi-year (D>3 years) and decadal (D>10 years) water shortage events. Figure 6.6.a shows the current IDF relationships of HUC4 river basins across the United States at an annual scale. In general, water shortage events at the annual scale tend to slightly have higher intensity compared to water shortage events at the sub-annual scale.

Under the current conditions and for a given return period (e.g., T=50 years), the intensity decreases as the duration becomes longer. Additionally, for a given duration (e.g., D>1 year), the intensity was projected to slightly change as the return period increases (e.g., from T=50 years to T=100 years). Overall, similar to the water shortage at the sub-annual scale, the West Coast and the middle Great Plain river basins were projected to currently have more intense water shortage conditions (~ 400 mcm/year) at the annual scale.

However, under the future conditions (Figure 6.6.b), the intensity of water shortage events was projected to mostly increase from current to future conditions, particularly for water shortage

events with longer duration (multi-year and decadal) and higher return period (T=100 years). Water shortage events with shorter duration and a lower return period were projected to experience smaller changes in intensity. Conversely, events with a longer duration (e.g., D>10 years) and a higher return period (e.g., T=100 years) were projected to experience a higher increase in the intensity of water shortage events.

For a given return period (e.g., T=50 years), the decadal events were projected to experience a higher increase in the intensity compared to the multi-year and annual water shortage events. The result means that at the annual scale, the intensity of decadal water shortage events (i.e., D>10 years) is more vulnerable to climate change and population growth compared to the intensity of annual and multi-year water shortage events. Subsequently, the intensity of multi-year water shortage events (i.e., D>3 years) can be more affected by climate change and population growth compared to the intensity of annual water shortage events.

For a given duration (e.g., D>10 years), the intensity of future events was projected to slightly alter as the return period increases from T=50 years to T=100 years. Additionally, for water shortage events with D>1 year, there are minor differences in the intensity of current and future water shortage events. The finding indicates that at an annual scale, events that occur every 50 years are likely to experience the same magnitude of increase in intensity compared to annual events that occur every 100 years. The results indicate that less frequent (T=100 years) and longer (D>10 years) water shortage events tend to experience a higher increase in the intensity in the future.

Overall, most river basins in the Southwest, Southern, and the middle Great Plain regions were estimated to experience more intense water shortage conditions in the future, particularly for decadal and multi-year events. However, West Coast river basins are likely to experience a

decrease in the intensity of decadal and multi-year water shortage events up to more than -90%. The unit of intensity is the million cubic meters per month (MCM/year). In general, the assessment of water shortage at the annual scale indicates that the multi-year and decadal water shortage events are likely to become more intense in the future.

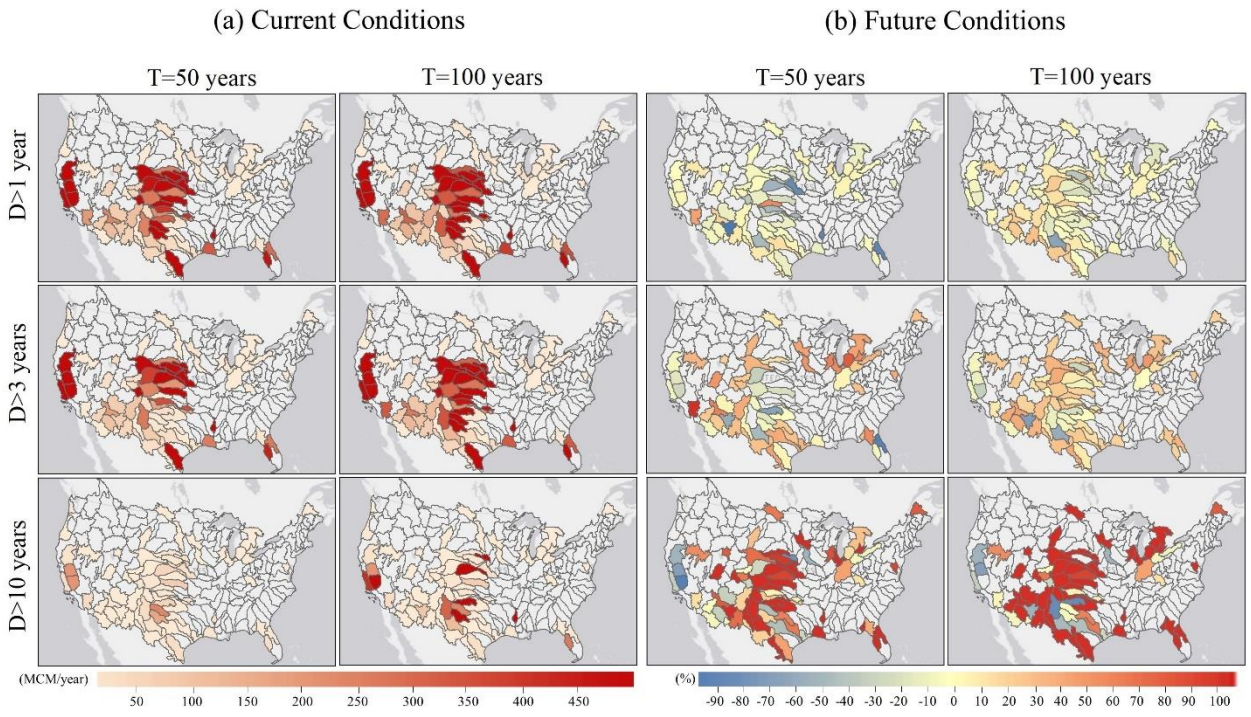

Figure 6.6. (a) Current intensity and (b) changes in the intensities of events from current (1986-2015) to future (2070-2099) conditions under RCP 8.5 at the annual scale.

Then, we investigated the effects of shifts in annual water supply and demand conditions on the frequency of annual, multi-year, and decadal water shortage events using the frequency amplification factor (AF). Figure 6.7 compares the frequency amplification factors of water shortage events with 1<D<3 years, 3<D<10 years, and D>10 years across CONUS for both RCP 4.5 and 8.5 emission scenarios. RCPs 4.5 and 8.5 emission scenarios approximately show the same spatial pattern of amplification factors.

For events with 1<=D<3 years, the frequency was projected to mostly decrease (AF ~ 0.2) in the Southwest, Southern, and middle Great Plain river basins. However, the West Coast river basins are more likely to experience more frequent water shortage events (AF ~ 0.2 to 0.4). For events with 3<=D<10 years, the frequency was projected to mostly decrease (AF ~ 0.2) in the middle Great Plain river basins with a lower rate (AF ~ 0.5) compared to events with 1<=D<3 years. However, the frequency was estimated to increase in the West Coast river basins with a lower rate compared to the events with 1<=D<3 years.

For events with D>10 years, unlike the events with 1<=D<3 years and 3<=D<10 years, the frequency is more likely to increase in most river basins located in the Southwest, Southern, and middle Great Plain regions. Additionally, the decadal events were projected to decrease in the West Coast region. Note that the highest increase in the frequency of decadal events was projected to occur in Great Lakes regions.

Overall, the result indicates that the frequency of decadal events (D>10 years) is likely to increase in the future while annual and multi-year events are likely to be less frequent. Conversely, the West Coast river basins are more likely to experience less frequent decadal (D>10 years) events and more frequent annual and multi-year events in the future.

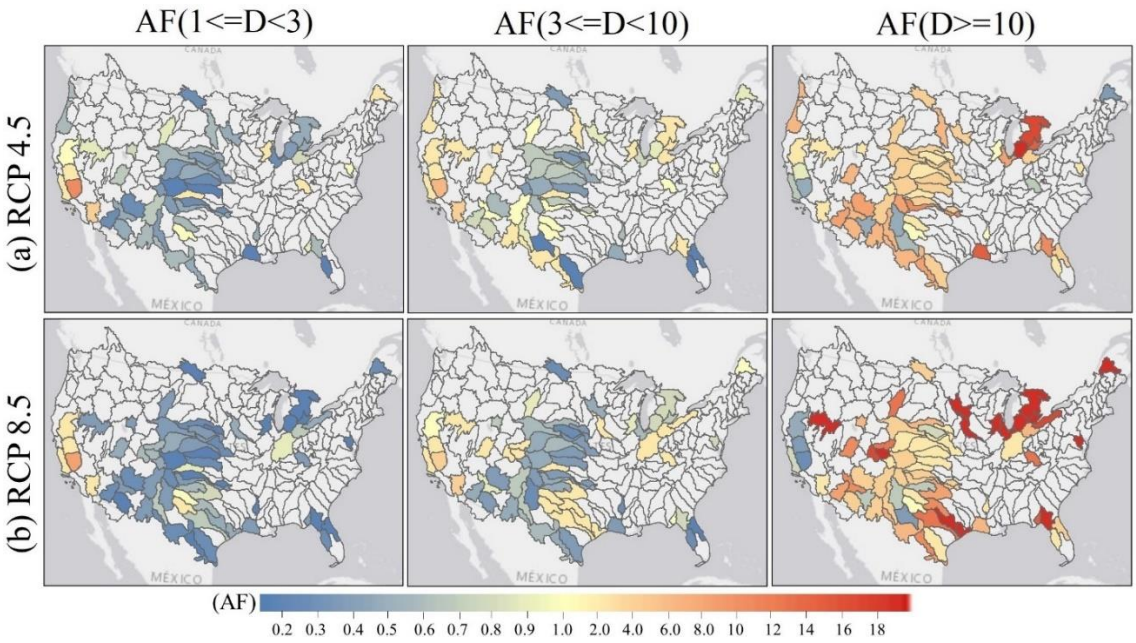

Figure 6.7. The frequency amplification factor (AF) under (a) RCP 4.5 and (b) RCP 8.5.

Additionally, the assessment of water shortage at the annual scale indicates that the Southwest and the middle Great Plain river basin are more likely to experience more intense multi-year and decadal water shortage events with more frequent decadal events (D>10 years) and less frequent annual and multi-year events. Conversely, the West Coast river basins are likely to experience a decrease in the intensity of multi-year and decadal water shortage events in the future with less frequent decadal (D>10 years) events and more frequent annual and multi-year events.

6.3.4. Relationship between water shortage characteristics and changes in water supply and demand conditions

In this section, we separately evaluated the effects of changes in water supply and water demand conditions on the water shortage properties to characterize change in which of them is more effective on shifts in water shortage IDF relationships for each HUC4 river basin. For this purpose, we considered two different scenarios: first, we assumed that demand would remain

constant from current to future conditions, and second, we assumed that water yield will not change from current to future conditions. Then, HUC4 river basins with higher changes in water shortage characteristics under the first scenario were considered demand-based basins (more vulnerable to changes in the demand), and HUC4 river basins with higher changes under the second scenario were considered supply-based basins (more vulnerable to changes in the supply).

Figure 6.8 shows demand-based, supply-based, and supply/demand-based river basins according to higher changes in intensity, duration, and frequency of water shortage conditions. According to changes in the intensity of water shortage events, the river basin within the middle Great Plain region is demand-based under both RCP 4.5 and 8.5 emission scenarios meaning that keeping the water demand constant in this region leads to a higher decrease in the intensity of water shortage conditions in the future. Thus, implementation of demand-based adaptation and mitigation strategies can be recommended in this region. Conversely, most river basins located in the Southwest region are supply-based under both RCP 4.5 and 8.5 emission scenarios indicating that keeping the water yield conditions constant in this region leads to more reduction in the intensity of water shortage events in the future. Therefore, the application of supply-based strategies can be more effective to attenuate the effects of climate change.

Besides, according to changes in the duration of water shortage events, the river basin within the middle Great Plain region is demand-based under RCP 4.5 and supply-based under RCP 8.5 emission scenarios meaning that the implementation of adaptation and mitigation strategies for decreasing the duration of water shortage events in this region can be sensitive to the future emission pathway scenario. However, the Southwest river basins are supply-based under both RCP 4.5 and 8.5 emission scenarios. This means that keeping the water yield conditions constant in this region leads to more reduction in both intensity and duration of water shortage events compared

to keeping the water demand constant. Therefore, the application of supply-based strategies can be recommended to reduce both the intensity and duration of water shortage events in this region.

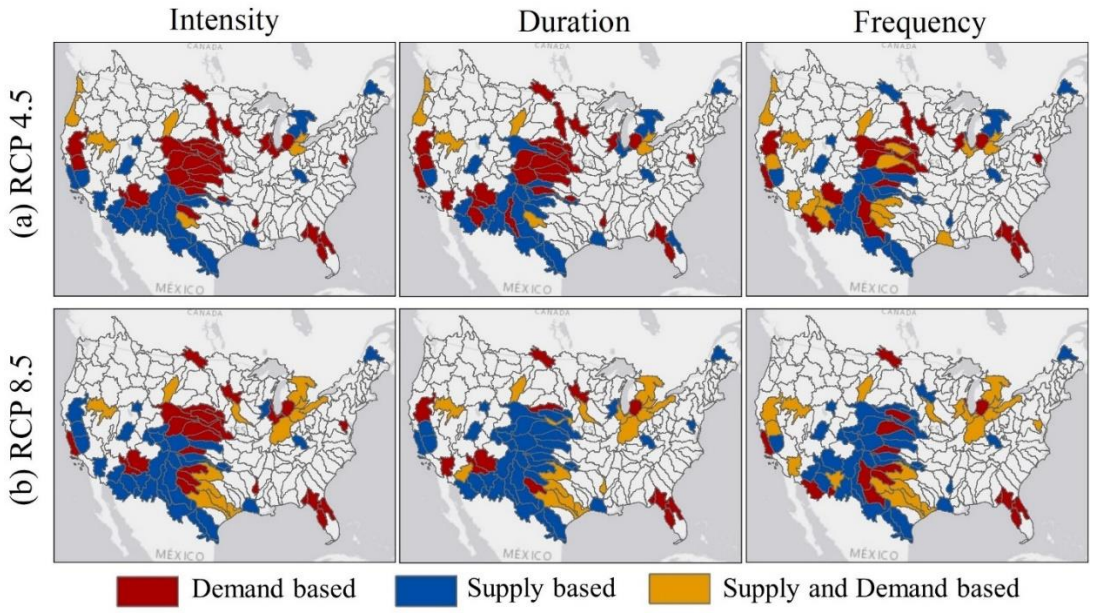

Figure 6.8. The characterization of river basins that are more vulnerable to changes in demand (demand-based), supply (supply-based), or both water demand and water supply (supply/demand-based) under (a) RCP 4.5 and (b) RCP 8.5.

Finally, we compared the two aforementioned scenarios in terms of decreases in the frequency of water shortage events in the future. Under this assumption, there are more river basins (e.g., Great Lakes region) that both supply-based and demand-based strategies can be recommended meaning that keeping water supply and water demand constant have similar effects on decreases in the frequency of water shortage events.

Additionally, we statistically assessed the relationships between the intensity, duration, and frequency of water shortage events and aridity index (the ratio of the potential evapotranspiration to the precipitation) in the supply-based regions. Figure D-69 shows changes in the aridity index

of river basins from current to future conditions. We aimed to figure out how the long-term anomalies such as changes in aridity index can affect the short-term anomalies such as sub-annual water shortage events. Table 6.1 provides the coefficient and the P-value of correlation between aridity index with the frequency amplification factor (AF) and intensity of sub-annual water shortage events.

The p-value under all correlations is less than 0.05 indicating that there is a significant correlation between the aridity index with all sub-annual water shortage characteristics. Although the frequency amplification factor of events with D>12 months is directly correlated with the aridity index, the frequency amplification factor of events with 1<=D<12 months is inversely correlated with the aridity index. This indicates that the increase in the aridity index is likely to increase the frequency of over-year (D>12 months) water shortage events while decrease the frequency of interannual (D<12 months) events.

Overall, the South, Southwest, middle Great Plain, and Great Lakes regions are likely to experience aridification under long-term changes in climate and freshwater availability. This situation may also lead to water shortage events with more frequency, higher intensity, and longer duration. The findings highlight that long-term increases in the aridity index of river basins can lead to the initiation of prolonged events, particularly in more arid regions where natural, water, and economic resources even during normal years may be inadequate to meet water needs. Besides, the intensity of water shortage events is significantly correlated to the aridity index, meaning that an increase in aridity index can lead to an increase in the intensity of sub-annual water shortage events.

Conversely, the West Coast region is likely to experience wetter hydroclimatic conditions. Although this condition can lead to higher freshwater availability, this region is likely to

experience more frequent water shortage events within the year due to an increase in extreme weather anomalies over the basin. The findings highlight that while the long-term hydroclimatology of a river basin can tend to wetter conditions, the frequency of interannual events may increase very rapidly if extreme weather anomalies rise over the basin. Interannual water shortage events are likely to occur during the growing seasons that may exacerbate the negative consequences on agriculture and crop productions.

Table 6.1. Statistical correlation between changes in the aridity index and water shortage events

Aridity index correlation with	Coefficient	P-value
AF (D>12)	0.40	0.0059
AF (1<=D<12)	-0.54	0.0002
Intensity (T=100 years)	0.66	0.0000

The results of this study were subject to several sources of uncertainty in the climate model and population growth projections, water demand, water yield and water allocation simulations, and characterization of water shortage IDF relationships. In this study, we only used the IPSL-CM5A-MR (driest) climate model under RCP 4.5 and 8.5 emission scenarios as the worst-case projection on average for the CONUS to compare the various responses of HUC4 river basins to shifts in water shortage properties under the worst-case future climate projection. Note that the IPSL-CM5A-MR climate model is not always the driest in all river basins across the CONUS. The driest climate model indicates the model that is on average the driest MACA models at the conterminous scale. Using ensemble climate simulation or more different climate models can be a prospect for this study to assess the vulnerability of the U.S. water supply to water shortage under a wider range of future climate possibilities.

In addition to the uncertainties in the climate projections, some uncertainties remain associated with the population growth and water demand estimation, VIC model, and WEAP model. Using multiple socioeconomic scenarios and different hydrologic and network analysis models at a finer resolution with accurate legal arrangements can be also a prospect for this study to assess the uncertainty in future water shortage IDF characterization. Despite these limitations and uncertainties in our methods, the important role of water shortage IDF characterization from the interannual to decadal scales can be highlighted in the future water resource planning and management. The approach improves the capacity to simultaneously characterize extreme and non-extreme events over a range of temporal scales.

6.4. Summary and Conclusions

Climate change and rapid population growth may exacerbate the decrease in freshwater availability and increase in water demand. This situation increases the vulnerability of water supply systems to water shortage at various spatial and temporal scales. The evolution, propagation, and spread of water shortage conditions at the various temporal scales from interannual to multi-year and decadal are crucial considerations to be appropriately characterized across the Unites States over the 21st century. Enhanced assessments of water shortage characteristics under climate, population growth, and socioeconomic changes can be applied to improve the design of water supply systems, and optimize water institutions and management, particularly in the American West. The characterization of water shortage events at various timescales allows determining short-term dry periods during a long-term wet period. The more frequent interannual water shortage events can lead to significant impacts, especially on agricultural regions during the growing seasons.

The monthly water demand and water supply at the HUC4 watershed level were projected under the A1B population growth scenario and the driest climate model with RCP 4.5 and 8.5 emission scenarios for current (1986-2015) and future (2070-2099) conditions. The water demand data was also obtained from the product of a water use driver and a water withdrawal rate for six water use sectors including domestic and public, agricultural irrigation, thermoelectric, industrial, commercial, and mining, livestock, and aquaculture. The WEAP model was used to project the water supply allocated to each HUC4 river basin.

A consistent spatial pattern of changes in the IDF relationships of water shortage events was found across the RCP 4.5 and RCP 8.5 emission scenarios. However, the RCP 8.5 emission scenario also leads to a higher increase in the intensity of events. Besides, the water shortage events will become more frequent under the RCP 8.5 emission scenario.

Changes in intensity, duration, and frequency of water shortage conditions at monthly and annual scales were assessed using the Mixture Gamma-GPD model. The projected shifts in water shortage characteristics of river basins across the CONUS vary from one region to another. The current patterns of water yield and water demand indicate that higher water demand occurs in basins with lower water yield.

Overall, the characterization of water shortage conditions at various temporal scales from interannual to decadal events indicates that the river basins located in the Southwest, Southern, and the middle Great Plain regions may experience more intense water shortage conditions. Besides, the Southwest, Southern, and the middle Great Plain river basin are likely to experience less frequent interannual (D<12 months), annual (D>1 year), and multi-year (D>3 years) events in the future. However, the frequency of over-year (D>12 months) events at the sub-annual scale and

decadal (D>10 years) events at the annual scale were projected to increase in the future in these regions.

Conversely, the river basins located in the West Coast region are likely to experience a decrease in the intensity of water shortage conditions. Although the frequency of over-year (D>12 months), and decadal (D>10 years) events were estimated to decrease in the West Coast regions, the interannual (D<12 months) events at the monthly scale and annual (D>1 year) and multi-year (D>3 years) events at the annual scale were projected to increase in the future in the West Coast regions. The intensity of water shortage events with longer duration and higher return periods is likely to be more affected in the future in response to climate changes and population growth.

Then, we characterized the statistical relationships between the aridity index as the long-term anomalies and sub-annual water shortage events as the short-term anomalies. The results indicate that river basins with a higher increase in aridity index from current to future conditions are more prone to experience more intense water shortage conditions in the future. We found that increase in the aridity index of river basins in the future tends to increase the frequency of over-year (D>12 months) events and decrease the frequency of interannual (D<12 months) events. Subsequently, we figured out that river basins with the projected decrease in aridity index are likely to experience more frequent interannual (D<12 months) water shortage conditions due to the increase in extreme weather anomalies under future climate conditions. Besides, the results illustrated that most river basins located in the Southwest, middle Great Plain, and Great Lakes regions are respectively supply-based, demand-based, and supply/demand-based.

Rising CO2 concentrations, increasing temperatures, rapid population growth, and precipitation changes will combine to cause shifts in IDF relationships of water shortage events at various spatial and temporal scales leading to prolonged events in drier regions and interannual

events in wetter regions. The results recommend that more attention should be gain to prolonged water shortage conditions in drier regions and interannual events in wetter regions of the United States at the end of the 21st century. This study highlights the importance of water shortage IDF assessments at both sub-annual and annual scales and findings are the crucial considerations to be characterized sufficiently on a national scale in the United States for enhanced water resource managements in the future in response to climate change and population growth.

CHAPTER 7.

SUMMARY AND CONCLUSIONS

Water shortage events have recently increased across multiple U.S. river basins with longer duration, higher intensity, and greater spatial extent that are unprecedented over the last decades (Martin et al., 2020). Climate change and rapid population growth may exacerbate the decrease in freshwater availability and increase in water demand (Mehran et al., 2017). This situation increases the vulnerability of water supply systems to water shortage at various spatial and temporal scales. The main goal of this dissertation was to enhance the characterization of shifts in both hydroclimatic conditions and water shortage IDF relationships across the conterminous United States (CONUS) over the 21st century.

First, hydroclimatic variables were projected over the 21st century using VIC hydrological model driven by downscaled MACA climate dataset. Hydroclimatic shifts of U.S. river basins at the HUC8 basin scale in response to climate change were evaluated by movements in the Budyko space. HUC8 river basins were clustered into seven unique hydroclimatic groups associated with the regional climate, landform, and ecosystem. The results challenge the stationary assumption of long-term water and energy cycles indicating that climate change may cause shifts in long-term water and energy balances and changes in hydroclimatic conditions. South and Southwest U.S. are the hotspots regions of shifts in long-term hydroclimatic conditions.

Then, we focused on the characterization of future hydroclimatic changes in U.S. national forests and national grasslands that provide a wide range of hydrological, ecological, social, economic, recreational, and aesthetic services. The Pacific Northwest, Intermountain, and Northern regions may have a less arid climate with lower freshwater availability. The

hydroclimatic conditions of the Southwestern Forest Service region are likely to have the highest sensitivity to future climate changes with especially high aridity under the DRY climate scenario. We then focused on the characterization of shifts in hydroclimatic conditions of U.S. megaregions as the clustered metropolitan regions where climate change may amplify negative impacts on water and natural resources. We found that Houston is likely to experience the highest changes in hydroclimatic conditions with some shifts from Temperate to Continental climate type.

Furthermore, we developed a probabilistic approach to improve the characterization of socioeconomic drought (or water shortage) intensity, duration, and frequency (IDF) characteristics under climate change and population growth. The application of the probabilistic approach was first demonstrated for the city of Fort Collins, Colorado. The results indicate that the proposed approach enhances the estimation of sub-annual drought IDF relationships, particularly for extreme events. Then, we assessed shifts in future drought IDF relationships for the City of Fort Collins, Colorado under two different urban development patterns, sprawl versus high density. The findings recommended that high-density development is likely to reduce vulnerability to socioeconomic drought due to lower water consumption used for outdoor activities.

Finally, the developed probabilistic approach was applied to assess changes in future IDF relationships of sub-annual and annual water shortage conditions across the CONUS at the HUC4 basin scale. The WEAP model was used to project the water supply allocated to each HUC4 river basin. The water demand data was also obtained from the product of a water use driver and a water withdrawal rate for six water use sectors including domestic and public, agricultural irrigation, thermoelectric, industrial, commercial, and mining, livestock, and aquaculture. The findings show that although the frequency of interannual events in the West Coast region is likely to rise in the future, the frequency of prolonged events is likely to increase in the Southwest, South, and the

middle Great Plain region. The results recommend that more attention should be gain to prolonged water shortage conditions in drier regions and interannual events in wetter regions of the United States at the end of the 21st century.

Overall, the South and Southwest US are likely to experience aridification under long-term changes in climate and freshwater availability. This situation may also lead to water shortage events with more frequency, higher intensity, and longer duration. The findings highlight that long-term changes in hydroclimatic conditions of river basins can lead to the initiation of prolonged events, particularly in more arid regions where natural, water, and economic resources even during normal years may be inadequate to meet local needs.

Conversely, the West US is likely to experience wetter hydroclimatic conditions. Although this condition can lead to higher freshwater availability, this region is likely to experience more frequent water shortage events within the year in response to climate change and rapid population growth. The findings highlight that while the long-term hydroclimatology of a river basin can tend to wetter conditions, interannual events may develop very rapidly if extreme weather anomalies rise over the basin. Interannual water shortage events are likely to occur during the growing seasons that may exacerbate the negative impacts of interannual events on agriculture.

The findings of this dissertation can be used as an input into a comprehensive plan to determine the most appropriate preparedness actions that can be implemented for drought-related disasters in response to future changes in climate and population of the United States. The developed steps in this dissertation can help decision-makers to assess the efficiency of various adaptation and mitigation strategies at a regional and national scale to attenuate the negative consequences of water shortage conditions. The adequacy of adaptation and mitigation strategies such as the reduced irrigation, instream flow reductions, groundwater mining, municipal water

demand management strategies, and additional reservoir storage capacity can be examined to accommodate the projected increase in intensity, duration, and frequency of water shortage conditions across the U.S. river basins.

Furthermore, the primary impacts of future changes in hydroclimatology, decadal, and interannual water shortage events in agricultural regions and crop yield projections can be investigated as another prospect for this dissertation. Agriculture is by far one of the largest water users in many regions of the United States. Long-term hydroclimatic changes may force farmers to change their crops based on the new regional climate conditions.

Improvements in the characterization of water shortage conditions from interannual to decadal events by incorporating shifts in long-term hydroclimatic conditions across the CONUS over the 21st century can result in enhanced infrastructure operation and water allocation, particularly during increasingly severe future events. Although the results of the study are directly beneficial to water planners and policymakers in the United States, the developed approach can be applied to any other regions of the world.

REFERENCES

Abatzoglou, J. T., & Brown, T. J. (2012). A comparison of statistical downscaling methods suited for wildfire applications. *International Journal of Climatology*, *32*(5), 772–780. https://doi.org/10.1002/joc.2312

Abatzoglou, J. T., & Ficklin, D. L. (2017). Climatic and physiographic controls of spatial variability in surface water balance over the contiguous United States using the Budyko relationship. *Water Resources Research*, *53*(9), 7630–7643. https://doi.org/10.1002/2017WR020843

Alam, M., Emura, K., Farnham, C., & Yuan, J. (2018). Best-Fit Probability Distributions and Return Periods for Maximum Monthly Rainfall in Bangladesh. *Climate*, *6*(1), 9. https://doi.org/10.3390/cli6010009

Allen, C. D., Macalady, A. K., Chenchouni, H., Bachelet, D., McDowell, N., Vennetier, M., et al. (2010). A global overview of drought and heat-induced tree mortality reveals emerging climate change risks for forests. *Forest Ecology and Management*, *259*(4), 660–684. https://doi.org/10.1016/j.foreco.2009.09.001

AMEC Environment & Infrastructure. (2014). *Fort Collins Water Supply and Demand Management Policy Revision Report*.

America 2050. (2006). A Prospectus. Regional Planning Association, New York, 1–4. https://doi.org/10.1016/b978-0-444-88480-0.50006-x

De Andrade, T. A. N., Fernandez, L. M. Z., Gomes-Silva, F., & Cordeiro, G. M. (2017). The Gamma Generalized Pareto Distribution with Applications in Survival Analysis. *International Journal of Statistics and Probability*, *6*(3), 141.

https://doi.org/10.5539/ijsp.v6n3p141

Andreadis, K. M., & Lettenmaier, D. P. (2006). Trends in 20th century drought over the continental United States. *Geophysical Research Letters*, *33*(10), 1–4. https://doi.org/10.1029/2006GL025711

Arnold, J. G., Srinivasan, R., Muttiah, R. S., & Williams, J. R. (1998). LARGE AREA HYDROLOGIC MODELING AND ASSESSMENT PART I: MODEL DEVELOPMENT. *JOURNAL OF THE AMERICANWATERRESOURCES ASSOCIATION AMERICAN WATER RESOURCES ASSOCIATION FEBRUARY*, *34*(1), 73–89. https://doi.org/10.1016/S0899-9007(00)00483-4

Ashfaq, M., Ghosh, S., Kao, S. C., Bowling, L. C., Mote, P., Touma, D., et al. (2013). Near-term acceleration of hydroclimatic change in the western U.S. *Journal of Geophysical Research Atmospheres*, *118*(19), 10676–10693. https://doi.org/10.1002/jgrd.50816

Astigarraga, J., Andivia, E., Zavala, M. A., Gazol, A., Cruz-Alonso, V., Vicente-Serrano, S. M., & Ruiz-Benito, P. (2020). Evidence of non-stationary relationships between climate and forest responses: increased sensitivity to climate change in Iberian forests. *Global Change Biology*, (May), 1–14. https://doi.org/10.1111/gcb.15198

Barrington-Leigh, C., & Millard-Ball, A. (2015). A century of sprawl in the United States. *Proceedings of the National Academy of Sciences of the United States of America*, *112*(27), 8244–8249. https://doi.org/10.1073/pnas.1504033112

Bayissa, Y., Maskey, S., Tadesse, T., van Andel, S. J., Moges, S., van Griensven, A., & Solomatine, D. (2018). Comparison of the performance of six drought indices in characterizing historical drought for the upper Blue Nile Basin, Ethiopia. *Geosciences (Switzerland)*, *8*(3). https://doi.org/10.3390/geosciences8030081

Behrens, C. N., Lopes, H. F., & Gamerman, D. (2004). Bayesian analysis of extreme events with threshold estimation. *Statistical Modeling*, *4*(3), 227–244. https://doi.org/10.1191/1471082X04st075oa

Benson-Lira, V., Georgescu, M., Kaplan, S., & Vivoni, E. R. (2016). Loss of a lake system in a megacity: The impact of urban expansion on seasonal meteorology in Mexico City. *Journal of Geophysical Research: Atmospheres*, *121*(7), 3079–3099. https://doi.org/10.1002/2015JD024102

Bhatta, B., Saraswati, S., & Bandyopadhyay, D. (2010). Quantifying the degree-of-freedom, degree-of-sprawl, and degree-of-goodness of urban growth from remote sensing data. *Applied Geography*, *30*(1), 96–111. https://doi.org/10.1016/j.apgeog.2009.08.001

Bonan, G. B. (2008). Forests and climate change: Forcings, feedbacks, and the climate benefits of forests. *Science*, *320*(5882), 1444–1449. https://doi.org/10.1126/science.1155121

Bounoua, L., Fathi, N., El Berkaoui, M., El Ghazouani, L., & Messouli, M. (2020). Assessment of Sustainability Development in Urban Areas of Morocco. *Urban Science*, *4*(2), 18. https://doi.org/10.3390/urbansci4020018

Bouziotas, D., Rozos, E., & Makropoulos, C. (2015). Water and the city: Exploring links between urban growth and water demand management. *Journal of Hydroinformatics*, *17*(2), 176–192. https://doi.org/10.2166/hydro.2014.053

Brakebill, J. W., Wolock, D. M., & Terziotti, S. E. (2011). Digital Hydrologic Networks Supporting Applications Related to Spatially Referenced Regression Modeling1. *JAWRA Journal of the American Water Resources Association*, *47*(5), 916–932. https://doi.org/10.1111/j.1752-1688.2011.00578.x

Brown, T. C., Foti, R., & Ramirez, J. A. (2013). Projected freshwater withdrawals in the United

States under a changing climate. *Water Resources Research*, *49*(3), 1259–1276. https://doi.org/10.1002/wrcr.20076

Brown, T. C., Mahat, V., & Ramirez, J. A. (2019). Adaptation to Future Water Shortages in the United States Caused by Population Growth and Climate Change. *Earth's Future*, *7*(3), 219–234. https://doi.org/10.1029/2018EF001091

Budyko, M. I. (1974). Climate and life,International geophysical series. *New York: Academic Press*, *18*.

Budyko, M. I. (1982). The earth's climate: Past and future. *International Geophysics Series: Academic Press*, *29*.

Bureau, U. S. C. (2011). *2010 Census of Population and Housing (Demographic Profile Summary File: Technical Documentation)*.

Butler, D., Ward, S., Sweetapple, C., Astaraie-Imani, M., Diao, K., Farmani, R., & Fu, G. (2017). Reliable, resilient and sustainable water management: the Safe & SuRe approach. *Global Challenges*, *1*(1), 63–77. https://doi.org/10.1002/gch2.1010

Buurman, J., & Babovic, V. (2016). Adaptation Pathways and Real Options Analysis: An approach to deep uncertainty in climate change adaptation policies. *Policy and Society*, *35*(2), 137–150. https://doi.org/10.1016/j.polsoc.2016.05.002

Cayan, D. R., Das, T., Pierce, D. W., Barnett, T. P., Tyree, M., & Gershunova, A. (2010). Future dryness in the Southwest US and the hydrology of the early 21st century drought. *Proceedings of the National Academy of Sciences of the United States of America*, *107*(50), 21271–21276. https://doi.org/10.1073/pnas.0912391107

Chen, D., & Chen, H. W. (2013). Using the Köppen classification to quantify climate variation and change: An example for 1901-2010. *Environmental Development*, *6*(1), 69–79.

https://doi.org/10.1016/j.envdev.2013.03.007

Chen, L., Singh, V. P., & Xiong, F. (2017). An entropy-based generalized gamma distribution for flood frequency analysis. *Entropy*, *19*(6). https://doi.org/10.3390/e19060239

Cheng, L., AghaKouchak, A., Gilleland, E., & Katz, R. W. (2014). Non-stationary extreme value analysis in a changing climate. *Climatic Change*, *127*(2), 353–369. https://doi.org/10.1007/s10584-014-1254-5

Cherkauer, K. A., & Lettenmaier, D. P. (2003). Simulation of spatial variability in snow and frozen soil. *Journal of Geophysical Research D: Atmospheres*, *108*(22), 1–14. https://doi.org/10.1029/2003jd003575

Chien, H., Yeh, P. J. F., & Knouft, J. H. (2013). Modeling the potential impacts of climate change on streamflow in agricultural watersheds of the Midwestern United States. *Journal of Hydrology*, *491*(1), 73–88. https://doi.org/10.1016/j.jhydrol.2013.03.026

Coe, M. T., Latrubesse, E. M., Ferreira, M. E., & Amsler, M. L. (2011). The effects of deforestation and climate variability on the streamflow of the Araguaia River, Brazil. *Biogeochemistry*, *105*(1), 119–131. https://doi.org/10.1007/s10533-011-9582-2

Coles, S. (2001). An Introduction to Modelling of Extremes. Retrieved from https://pdfs.semanticscholar.org/f56e/f9a1dd7fa38b93e9454300f55694c9b78791.pdf

Collins, M., R. Knutti, J. Arblaster, J.-L. Dufresne, T. Fichefet, P. Friedlingstein, X. Gao, W.J. Gutowski, T. Johns, G. Krinner, M. Shongwe, C. Tebaldi, A. J. W. and M. W. (2013). Long-term climate change: Projections, commitments and irreversibility. In: Climate Change 2013: The Physical Science Basis. Contribution. *Contribution of Working Group I to the Fifth Assessment Report of the Intergovernmental Panel on Climate Change [Stocker, T.F., D. Qin, G.-K. Plattner, M. Tignor, S.K. Allen, J. Boschung, A. Nauels, Y. Xia, V. Bex and P.M.*

Midgley (Eds.)]. Cambridge Unive, *9781107057*. https://doi.org/10.1017/CBO9781107415324.024

Cook, B. I., Ault, T. R., & Smerdon, J. E. (2015). Unprecedented 21st century drought risk in the American Southwest and Central Plains. *Science Advances*, *1*(1), e1400082. https://doi.org/10.1126/sciadv.1400082

Cristianini, N., & Shawe-Taylor, J. (2000). *An Introduction to Support Vector Machines and Other Kernel-based Learning Methods*. Cambridge University Press. https://doi.org/10.1017/CBO9780511801389

Daly, C., Halbleib, M., Smith, J. I., Gibson, W. P., Doggett, M. K., Taylor, G. H., et al. (2008). Physiographically sensitive mapping of climatological temperature and precipitation across the conterminous United States. *International Journal of Climatology*, *28*(15), 2031–2064. https://doi.org/10.1002/joc.1688

Demaria, E. M., Nijssen, B., & Wagener, T. (2007). Monte Carlo sensitivity analysis of land surface parameters using the Variable Infiltration Capacity model. *Journal of Geophysical Research Atmospheres*, *112*(11). https://doi.org/10.1029/2006JD007534

Deng, W., Song, J., Bai, H., He, Y., Yu, M., Wang, H., & Cheng, D. (2018). Analyzing the impacts of climate variability and land surface changes on the annual water-energy balance in the Weihe River Basin of China. *Water (Switzerland)*, *10*(12), 1–15. https://doi.org/10.3390/w10121792

Deser, C., Knutti, R., Solomon, S., & Phillips, A. S. (2012). Communication of the role of natural variability in future North American climate. *Nature Climate Change*, *2*(11), 775–779. https://doi.org/10.1038/nclimate1562

Deser, C., Hurrell, J. W., & Phillips, A. S. (2017). The role of the North Atlantic Oscillation in

European climate projections. *Climate Dynamics*, *49*(9–10), 3141–3157. https://doi.org/10.1007/s00382-016-3502-z

Destouni, G., Jaramillo, F., & Prieto, C. (2013). Hydroclimatic shifts driven by human water use for food and energy production. *Nature Climate Change*, *3*(3), 213–217. https://doi.org/10.1038/nclimate1719

Dewar, M., & Epstein, D. (2007). Planning for "Megaregions" in the United States. *Journal of Planning Literature*, *22*(2), 108–124. https://doi.org/10.1177/0885412207306615

Diehl, T. H., & Harris, M. A. (2014). *Withdrawal and Consumption of Water by Thermoelectric Power Plants in the United States , 2010*.

Duan, K., Sun, G., Sun, S., Caldwell, P. V., Cohen, E. C., McNulty, S. G., et al. (2016). Divergence of ecosystem services in U.S. National Forests and Grasslands under a changing climate. *Scientific Reports*, *6*(April), 2–11. https://doi.org/10.1038/srep24441

Engeland, K., Hisdal, H., & Frigessi, A. (2005). Practical extreme value modelling of hydrological floods and droughts: A case study. *Extremes*, *7*(1), 5–30. https://doi.org/10.1007/s10687-004-4727-5

Engström, J., Jafarzadegan, K., & Moradkhani, H. (2020). Drought vulnerability in the United States: An integrated assessment. *Water (Switzerland)*, *12*(7). https://doi.org/10.3390/w12072033

Esquivel-Muelbert, A., Baker, T. R., Dexter, K. G., Lewis, S. L., Brienen, R. J. W., Feldpausch, T. R., et al. (2019). Compositional response of Amazon forests to climate change. *Global Change Biology*, *25*(1), 39–56. https://doi.org/10.1111/gcb.14413

Evans, R. G., & Sadler, E. J. (2008). Methods and technologies to improve efficiency of water use. *Water Resources Research*, *44*(7), 1–15. https://doi.org/10.1029/2007WR006200

Farahmand, A., & AghaKouchak, A. (2015). A generalized framework for deriving nonparametric standardized drought indicators. *Advances in Water Resources*, *76*, 140–145. https://doi.org/10.1016/j.advwatres.2014.11.012

Fekety, P. A., Crookston, N. L., Hudak, A. T., Filippelli, S. K., Vogeler, J. C., & Falkowski, M. J. (2020). Hundred year projected carbon loads and species compositions for four National Forests in the northwestern USA. *Carbon Balance and Management*, *15*(1), 1–14. https://doi.org/10.1186/s13021-020-00140-9

Ficklin, D. L., Luo, Y., & Zhang, M. (2013). Climate change sensitivity assessment of streamflow and agricultural pollutant transport in California's Central Valley using Latin hypercube sampling. *Hydrological Processes*, *27*(18), 2666–2675. https://doi.org/10.1002/hyp.9386

Forrest, N., Stein, Z., & Wiek, A. (2020). Transferability and scalability of sustainable urban water solutions–A case study from the Colorado River Basin. *Resources, Conservation and Recycling*, *157*(June 2019), 104790. https://doi.org/10.1016/j.resconrec.2020.104790

Foti, R., Ramirez, J. A., & Brown, T. C. (2012). Vulnerability of U.S. water supply to shortage: a technical document supporting the Forest Service 2010 RPA Assessment, *295*. Retrieved from http://www.treesearch.fs.fed.us/pubs/42363

Foti, R., Ramirez, J. A., & Brown, T. C. (2014a). A probabilistic framework for assessing vulnerability to climate variability and change: The case of the US water supply system. *Climatic Change*, *125*(3–4), 413–427. https://doi.org/10.1007/s10584-014-1111-6

Foti, R., Ramirez, J. A., & Brown, T. C. (2014b). A probabilistic framework for assessing vulnerability to climate variability and change: The case of the US water supply system. *Climatic Change*, *125*(3–4), 413–427. https://doi.org/10.1007/s10584-014-1111-6

Furrer, E. M., & Katz, R. W. (2008). Improving the simulation of extreme precipitation events by

stochastic weather generators. *Water Resources Research*, *44*(12), 1–13. https://doi.org/10.1029/2008WR007316

Ganguli, P. (2014). Probabilistic analysis of extreme droughts in Southern Maharashtra using bivariate copulas. *ISH Journal of Hydraulic Engineering*, *20*(1), 90–101. https://doi.org/10.1080/09715010.2013.843279

Gassman, P. W., Sadeghi, A. M., & Srinivasan, R. (2014). Applications of the SWAT Model Special Section: Overview and Insights. *Journal of Environmental Quality*, *43*(1), 1–8. https://doi.org/10.2134/jeq2013.11.0466

Georgakakos, A., Fleming, P., Dettinger, M., Peters-Lidard, C., Richmond, T. (T. C. ., Reckhow, K., et al. (2014). *Ch. 3: Water Resources. Climate Change Impacts in the United States: The Third National Climate Assessment*. Washington, DC. https://doi.org/10.7930/J0G44N6T

Georgescu, M., Morefield, P. E., Bierwagen, B. G., & Weaver, C. P. (2014). Urban adaptation can roll back warming of emerging megapolitan regions. *Proceedings of the National Academy of Sciences of the United States of America*, *111*(8), 2909–2914. https://doi.org/10.1073/pnas.1322280111

Ghanbari, M., Arabi, M., Obeysekera, J., & Sweet, W. (2019). A Coherent Statistical Model for Coastal Flood Frequency Analysis Under Nonstationary Sea Level Conditions. *Earth's Future*, *7*(2), 162–177. https://doi.org/10.1029/2018EF001089

Ghanbari, M., Arabi, M., & Obeysekera, J. (2020). Chronic and Acute Coastal Flood Risks to Assets and Communities in Southeast Florida, *146*(7), 1–10. https://doi.org/10.1061/(ASCE)WR.1943-5452.0001245

Gharari, S., Clark, M. P., Mizukami, N., Wong, J. S., Pietroniro, A., & Wheater, H. S. (2019). Improving the Representation of Subsurface Water Movement in Land Models. *Journal of*

Hydrometeorology, *20*(12), 2401–2418. https://doi.org/10.1175/JHM-D-19-0108.1

Gharari, S., Clark, M. P., Mizukami, N., Knoben, W. J. M., Wong, J. S., & Pietroniro, A. (2020). Flexible vector-based spatial configurations in land models. *Hydrology and Earth System Sciences*, *24*(12), 5953–5971. https://doi.org/10.5194/hess-24-5953-2020

Giglioli, N., & Saltelli, A. (2008). Simlab 2.2 Reference Manual. *Ispra, Italy: Institute for Systems Informatics and Safety (Joint Research Centre, European Commission)*.

Gober, P., & Kirkwood, C. W. (2010). Vulnerability assessment of climate-induced water shortage in Phoenix. *Proceedings of the National Academy of Sciences of the United States of America*, *107*(50), 21295–21299. https://doi.org/10.1073/pnas.0911113107

Goodman, L. A., & Kruskal, W. H. (1954). Measures of Association for Cross Classifications Author (s): Leo A . Goodman and William H . Kruskal Source : Journal of the American Statistical Association , Vol . 49 , No . 268 (Dec ., 1954), pp . 732- Published by : American Statistical Associati. *Journal of the American Statistical Association*, *49*(268), 732–764.

Greve, P., Gudmundsson, L., Orlowsky, B., & Seneviratne, S. I. (2015). Introducing a probabilistic Budyko framework. *Geophysical Research Letters*, *42*(7), 2261–2269. https://doi.org/10.1002/2015GL063449

Greve, Peter, Orlowsky, B., Mueller, B., Sheffield, J., Reichstein, M., & Seneviratne, S. I. (2014). Global assessment of trends in wetting and drying over land. *Nature Geoscience*, *7*(10), 716–721. https://doi.org/10.1038/NGEO2247

Guo, Y., Huang, S., Huang, Q., Wang, H., Fang, W., Yang, Y., & Wang, L. (2019). Assessing socioeconomic drought based on an improved Multivariate Standardized Reliability and Resilience Index. *Journal of Hydrology*, *568*(August 2018), 904–918. https://doi.org/10.1016/j.jhydrol.2018.11.055

Guo, Y., Huang, S., Huang, Q., Wang, H., Wang, L., & Fang, W. (2019). Copulas-based bivariate socioeconomic drought dynamic risk assessment in a changing environment. *Journal of Hydrology*, *575*(May), 1052–1064. https://doi.org/10.1016/j.jhydrol.2019.06.010

Gutzler, D. S., & Nims, J. S. (2006). Interannual Variability of Water Demand and Summer Climate in Albuquerque, New Mexico. *Journal of Applied Meteorology*, *44*(12), 1777–1787. https://doi.org/10.1175/jam2298.1

Hagenlocher, M., Meza, I., Anderson, C. C., Min, A., Renaud, F. G., Walz, Y., et al. (2019). Drought vulnerability and risk assessments: State of the art, persistent gaps, and research agenda. *Environmental Research Letters*, *14*(8). https://doi.org/10.1088/1748-9326/ab225d

Hagler, Y. (2009). Defining U.S. Megaregions. *Americ 2050*, (November), 1–8. Retrieved from http://library.rpa.org/pdf/2050-Paper-Defining-US-Megaregions.pdf

Hao, Z., Singh, V. P., & Xia, Y. (2018). Seasonal Drought Prediction: Advances, Challenges, and Future Prospects. *Reviews of Geophysics*, *56*(1), 108–141. https://doi.org/10.1002/2016RG000549

Havel, A., Tasdighi, A., & Arabi, M. (2018). Assessing the hydrologic response to wildfires in mountainous regions. *Hydrology and Earth System Sciences*, *22*(4), 2527–2550. https://doi.org/10.5194/hess-22-2527-2018

Hay, L. E., Markstrom, S. L., & Ward-Garrison, C. (2011). Watershed-scale response to climate change through the twenty-first century for selected basins across the United States. *Earth Interactions*, *15*(17), 1–37. https://doi.org/10.1175/2010EI370.1

Heidari, H., Arabi, M., Ghanbari, M., & Warziniack, T. (2020). A Probabilistic Approach for Characterization of Sub-Annual Socioeconomic Drought Intensity- Duration-Frequency (IDF) Relationships in a Changing Environment. https://doi.org/10.3390/w12061522

Heidari, H., Arabi, M., Warziniack, T., & Kao, S. C. (2020). Assessing Shifts in Regional Hydroclimatic Conditions of U.S. River Basins in Response to Climate Change over the 21st Century. *Earth's Future*, *8*(10), 1–14. https://doi.org/10.1029/2020EF001657

Heidari, H., Warziniack, T., Brown, T. C., & Arabi, M. (2021). Impacts of Climate Change on Hydroclimatic Conditions of U.S. National Forests and Grasslands. *Forests*, *12*(2), 139. https://doi.org/10.3390/f12020139

Hemmati, M., Ellingwood, B. R., & Mahmoud, H. N. (2020). The Role of Urban Growth in Resilience of Communities Under Flood Risk. *Earth's Future*, *8*(3), 1–14. https://doi.org/10.1029/2019EF001382

House-peters, L. (2010). PDXScholar Examining the Effects of Climate Change and Urban Development on Water Demand : A Multi-Scale Analysis of Future Water Demand in Hillsboro , Oregon.

Huang, S., Huang, Q., Leng, G., & Liu, S. (2016). A nonparametric multivariate standardized drought index for characterizing socioeconomic drought: A case study in the Heihe River Basin. *Journal of Hydrology*, *542*, 875–883. https://doi.org/10.1016/j.jhydrol.2016.09.059

Hummel, D. (2020). The effects of population and housing density in urban areas on income in the United States. *Local Economy*, *35*(1), 27–47. https://doi.org/10.1177/0269094220903265

Husak, G., Michaelsen, J., & Funk, C. (2007). Use of the gamma distribution to represent monthly rainfall in Africa for drought monitoring applications. *Int. J. Climatol*, *27*(December), 935–944. https://doi.org/10.1002/joc.1441

Jaeger, W. K., Amos, A., Bigelow, D. P., Chang, H., Conklin, D. R., Haggerty, R., et al. (2017). Finding water scarcity amid abundance using human–natural system models. *Proceedings of the National Academy of Sciences*, *114*(45), 11884–11889.

https://doi.org/10.1073/pnas.1706847114

Jaramillo, F., Cory, N., Arheimer, B., Laudon, H., Van Der Velde, Y., Hasper, T. B., et al. (2018). Dominant effect of increasing forest biomass on evapotranspiration: Interpretations of movement in Budyko space. *Hydrology and Earth System Sciences*, *22*(1), 567–580. https://doi.org/10.5194/hess-22-567-2018

Jeong, J. H., Resop, J. P., Mueller, N. D., Fleisher, D. H., Yun, K., Butler, E. E., et al. (2016). Random forests for global and regional crop yield predictions. *PLoS ONE*, *11*(6), 1–15. https://doi.org/10.1371/journal.pone.0156571

Joyce, L., & Coulson, D. (2020). Climate scenarios and projections, a technical document supporting the USDA Forest Service 2020 RPA assessment, *Tech. Rep.*

Joyce, L. A., Blate, G. M., Littell, J. S., McNulty, S. G., Millar, C. I., Moser, S. C., et al. (2008). Adaptation Options for Climate-Sensitive Ecosystems and Resources. *National Service Center for Environmental Publications (NSCEP)*, *60*(2), 129.

Jump, A. S., Ruiz-Benito, P., Greenwood, S., Allen, C. D., Kitzberger, T., Fensham, R., et al. (2017). Structural overshoot of tree growth with climate variability and the global spectrum of drought-induced forest dieback. *Global Change Biology*, *23*(9), 3742–3757. https://doi.org/10.1111/gcb.13636

Kjellström, E., Thejll, P., Rummukainen, M., Christensen, J., Boberg, F., Christensen, O., & Fox Maule, C. (2013). Emerging regional climate change signals for Europe under varying large-scale circulation conditions. *Climate Research*, *56*(2), 103–119. https://doi.org/10.3354/cr01146

Kumar, S., Moglen, G. E., Godrej, A. N., Grizzard, T. J., & Post, H. E. (2018). Trends in water yield under climate change and urbanization in the US Mid-Atlantic region. *Journal of Water*

Resources Planning and Management, *144*(8), 1–12. https://doi.org/10.1061/(ASCE)WR.1943-5452.0000937

Leyk, S., Uhl, J. H., Connor, D. S., Braswell, A. E., Mietkiewicz, N., Balch, J. K., & Gutmann, M. (2020). Two centuries of settlement and urban development in the United States. *Science Advances*, *6*(23), eaba2937. https://doi.org/10.1126/sciadv.aba2937

Li, Y., Liu, C., Yu, W., Tian, D., & Bai, P. (2019). Response of streamflow to environmental changes: A Budyko-type analysis based on 144 river basins over China. *Science of the Total Environment*, *664*, 824–833. https://doi.org/10.1016/j.scitotenv.2019.02.011

Liang, X., Lettenmaier, D. P., Wood, E. F., & Burges, S. J. (1994). A simple hydrologically based model of land surface water and energy fluxes for general circulation models. *Journal of Geophysical Research*, *99*(D7). https://doi.org/10.1029/94jd00483

Liang, Z., Wu, S., Wang, Y., Wei, F., Huang, J., Shen, J., & Li, S. (2020). The relationship between urban form and heat island intensity along the urban development gradients. *Science of the Total Environment*, *708*, 135011. https://doi.org/10.1016/j.scitotenv.2019.135011

Link, R., Wild, T. B., Snyder, A. C., Hejazi, M. I., & Vernon, C. R. (2020). 100 Years of Data Is Not Enough To Establish Reliable Drought Thresholds. *Journal of Hydrology X*, *7*(January), 100052. https://doi.org/10.1016/j.hydroa.2020.100052

Littell, J. S., Peterson, D. L., Millar, C. I., & O'Halloran, K. A. (2012). U.S. National Forests adapt to climate change through Science-Management partnerships. *Climatic Change*, *110*(1–2), 269–296. https://doi.org/10.1007/s10584-011-0066-0

Liu, X., Huang, Y., Xu, X., Li, X., Li, X., Ciais, P., et al. (2020). High-spatiotemporal-resolution mapping of global urban change from 1985 to 2015. *Nature Sustainability*. https://doi.org/10.1038/s41893-020-0521-x

MacDonald, A., Scarrott, C. J., Lee, D., Darlow, B., Reale, M., & Russell, G. (2011). A flexible extreme value mixture model. *Computational Statistics and Data Analysis*, *55*(6), 2137–2157. https://doi.org/10.1016/j.csda.2011.01.005

MacDonald, G. M. (2010). Water, climate change, and sustainability in the Southwest. *Proceedings of the National Academy of Sciences of the United States of America*, *107*(50), 21256–21262. https://doi.org/10.1073/pnas.0909651107

Mahat, V., Ramírez, J. A., & Brown, T. C. (2017). Twenty-First-Century Climate in CMIP5 Simulations: Implications for Snow and Water Yield across the Contiguous United States. *Journal of Hydrometeorology*, *18*(8), 2079–2099. https://doi.org/10.1175/jhm-d-16-0098.1

Maliva, R., & Missimer, T. (2013). *Arid lands water evaluation and management*. *Environmental Science and Engineering*. https://doi.org/10.5860/choice.50-4453

Mann, M. E., & Gleick, P. H. (2015). Climate change and California drought in the 21st century. *Proceedings of the National Academy of Sciences of the United States of America*, *112*(13), 3858–3859. https://doi.org/10.1073/pnas.1503667112

Martin, J. T., Pederson, G. T., Woodhouse, C. A., Cook, E. R., McCabe, G. J., Anchukaitis, K. J., et al. (2020). Increased drought severity tracks warming in the United States' largest river basin. *Proceedings of the National Academy of Sciences of the United States of America*, *117*(21). https://doi.org/10.1073/pnas.1916208117

McDonald, R. I., Green, P., Balk, D., Fekete, B. M., Revenga, C., Todd, M., & Montgomery, M. (2011). Urban growth, climate change, and freshwater availability. *Proceedings of the National Academy of Sciences of the United States of America*, *108*(15), 6312–6317. https://doi.org/10.1073/pnas.1011615108

McGrane, S. J. (2016). Impacts of urbanisation on hydrological and water quality dynamics, and

urban water management: a review. *Hydrological Sciences Journal*, *61*(13), 2295–2311. https://doi.org/10.1080/02626667.2015.1128084

McIntyre, P. J., Thorne, J. H., Dolanc, C. R., Flint, A. L., Flint, L. E., Kelly, M., & Ackerly, D. D. (2015). Twentieth-century shifts in forest structure in California: Denser forests, smaller trees, and increased dominance of oaks. *Proceedings of the National Academy of Sciences of the United States of America*, *112*(5), 1458–1463. https://doi.org/10.1073/pnas.1410186112

Mehran, A., Mazdiyasni, O., & Aghakouchak, A. (2015). A hybrid framework for assessing socioeconomic drought: Linking. *Joiurnal of Geophysical Research: Atmospheres*, 1–14. https://doi.org/10.1002/2015JD023147.Received

Mehran, A., AghaKouchak, A., Nakhjiri, N., Stewardson, M. J., Peel, M. C., Phillips, T. J., et al. (2017). Compounding Impacts of Human-Induced Water Stress and Climate Change on Water Availability. *Scientific Reports*, *7*(1), 1–9. https://doi.org/10.1038/s41598-017-06765-0

Melsen, L., Teuling, A., Torfs, P., Zappa, M., Mizukami, N., Clark, M., & Uijlenhoet, R. (2016). Representation of spatial and temporal variability in large-domain hydrological models: case study for a mesoscale pre-Alpine basin. *Hydrology and Earth System Sciences*, *20*(6), 2207–2226. https://doi.org/10.5194/hess-20-2207-2016

Mesinger, F., DiMego, G., Kalnay, E., Mitchell, K., Shafran, P. C., Ebisuzaki, W., et al. (2006). North American regional reanalysis. *Bulletin of the American Meteorological Society*, *87*(3), 343–360. https://doi.org/10.1175/BAMS-87-3-343

Mishra, A. K., & Singh, V. P. (2010). A review of drought concepts. *Journal of Hydrology*, *391*(1–2), 202–216. https://doi.org/10.1016/j.jhydrol.2010.07.012

Mukherjee, S., Bebermeier, W., & Schütt, B. (2018). An overview of the impacts of land use land

cover changes (1980-2014) on urban water security of Kolkata. *Land*, *7*(3). https://doi.org/10.3390/land7030091

Nakicenovic, N. et al. (2000). Emissions Scenarios: A Special Report of Working Group III ofthe Intergovernmental Panel on Climate Change,. *Cambridge Univ. Press, Cambridge, U. K*, *599 pp.*

Naz, B. S., Kao, S. C., Ashfaq, M., Rastogi, D., Mei, R., & Bowling, L. C. (2016). Regional hydrologic response to climate change in the conterminous United States using high-resolution hydroclimate simulations. *Global and Planetary Change*, *143*, 100–117. https://doi.org/10.1016/j.gloplacha.2016.06.003

Nelson, A. C. (2017). Megaregion Projections 2015 to 2045 with Transportation Policy Implications. *Transportation Research Record*, *2654*, 11–19. https://doi.org/10.3141/2654-02

Nelson, G. D., & Rae, A. (2016). An economic geography of the United States: From commutes to megaregions. *PLoS ONE*, *11*(11), 1–23. https://doi.org/10.1371/journal.pone.0166083

O'Donnell, E. C., & Thorne, C. R. (2020). Drivers of future urban flood risk. *Philosophical Transactions of the Royal Society A: Mathematical, Physical and Engineering Sciences*, *378*(2168). https://doi.org/10.1098/rsta.2019.0216

Omernik, J. M., & Griffith, G. E. (2014). Ecoregions of the Conterminous United States: Evolution of a Hierarchical Spatial Framework. *Environmental Management*, *54*(6), 1249–1266. https://doi.org/10.1007/s00267-014-0364-1

Otkin, J. A., Svoboda, M., Hunt, E. D., Ford, T. W., Anderson, M. C., Hain, C., & Basara, J. B. (2018). Flash droughts: A review and assessment of the challenges imposed by rapid-onset droughts in the United States. *Bulletin of the American Meteorological Society*, *99*(5), 911–

919. https://doi.org/10.1175/BAMS-D-17-0149.1

Oubeidillah, A. A., Kao, S. C., Ashfaq, M., Naz, B. S., & Tootle, G. (2014). A large-scale, high-resolution hydrological model parameter data set for climate change impact assessment for the conterminous US. *Hydrology and Earth System Sciences*, *18*(1), 67–84. https://doi.org/10.5194/hess-18-67-2014

Peterson, D. L., Millar, C. I., Joyce, L. A., Furniss, M. J., Halofsky, J. E., Neilson, R. P., & Morelli, T. L. (2011). Responding to climate change in national forests: A guidebook for developing adaptation options. *USDA Forest Service - General Technical Report PNW-GTR*, (855), 1–99. https://doi.org/10.2737/PNW-GTR-855

Piemontese, L., Fetzer, I., Rockström, J., & Jaramillo, F. (2019). Future Hydroclimatic Impacts on Africa: Beyond the Paris Agreement. *Earth's Future*, 748–761. https://doi.org/10.1029/2019EF001169

Ponce Campos, G. E., Moran, M. S., Huete, A., Zhang, Y., Bresloff, C., Huxman, T. E., et al. (2013). Ecosystem resilience despite large-scale altered hydroclimatic conditions. *Nature*, *494*(7437), 349–352. https://doi.org/10.1038/nature11836

Rajsekhar, D., Singh, V. P., & Mishra, A. K. (2015). Integrated drought causality, hazard, and vulnerability assessment for future socioeconomic scenarios: An information theory perspective. *Journal of Geophysical Research*, *120*(13), 6346–6378. https://doi.org/10.1002/2014JD022670

Read, L. K., & Vogel, R. M. (2015). Reliability, return periods, and risk under nonstationarity. *Water Resources Research*, *51*(3), 6381–6398. https://doi.org/10.1111/j.1752-1688.1969.tb04897.x

Records, R. M., Arabi, M., Fassnacht, S. R., Duffy, W. G., Ahmadi, M., & Hegewisch, K. C.

(2014). Climate change and wetland loss impacts on a western river's water quality. *Hydrology and Earth System Sciences*, *18*(11), 4509–4527. https://doi.org/10.5194/hess-18-4509-2014

Redmond, K. T. (2002). The depiction of drought: A commentary. *Bulletin of the American Meteorological Society*, *83*(8), 1143–1147. https://doi.org/10.1175/1520-0477(2002)083<1143:TDODAC>2.3.CO;2

Rehfeldt, G. E., Ferguson, D. E., & Crookston, N. L. (2009). Aspen, climate, and sudden decline in western USA. *Forest Ecology and Management*, *258*(11), 2353–2364. https://doi.org/10.1016/j.foreco.2009.06.005

Reis, D. S., Cerqueira, C. M., Vieira, R. F., & Martins, E. S. (2013). Budyko's framework and climate elasticity concept in the estimation of climate change impacts on the long-term mean annual streamflow. *World Environmental and Water Resources Congress 2013: Showcasing the Future - Proceedings of the 2013 Congress*, 1110–1120. https://doi.org/10.1061/9780784412947.107

Renner, M., Seppelt, R., & Bernhofer, C. (2012). Evaluation of water-energy balance frameworks to predict the sensitivity of streamflow to climate change. *Hydrology and Earth System Sciences*, *16*(5), 1419–1433. https://doi.org/10.5194/hess-16-1419-2012

Rosegrant, M. W., & Cai, X. (2002). Global Water Demand and Supply Projections: Part 2. Results and Prospects to 2025. *Water International*, *27*(2), 170–182. https://doi.org/10.1080/02508060208686990

Rosni, N. A., Noor, N. M., & Abdullah, A. (2016). Managing urbanisation and urban sprawl in Malaysia by using remote sensing and GIS applications. *Planning Malaysia*, *4*(Special Issue 4), 17–30. https://doi.org/10.21837/pmjournal.v14.i4.145

Ross, C. L. (2008). Megaregions: Literature Review of the Implications for US Infrastructure Investment and Transportation Planning, 1–103.

Rouholahnejad Freund, E., & Kirchner, J. W. (2017). A Budyko framework for estimating how spatial heterogeneity and lateral moisture redistribution affect average evapotranspiration rates as seen from the atmosphere. *Hydrology and Earth System Sciences*, *21*(1), 217–233. https://doi.org/10.5194/hess-21-217-2017

Salas, J. D., Obeysekera, J., & Vogel, R. M. (2018). Techniques for assessing water infrastructure for nonstationary extreme events: a review. *Hydrological Sciences Journal*, *63*(3), 325–352. https://doi.org/10.1080/02626667.2018.1426858

Salas, Jose D., Fu, C., Cancelliere, A., Dustin, D., Bode, D., Pineda, A., & Vincent, E. (2005). Characterizing the Severity and Risk of Drought in the Poudre River, Colorado. *Journal of Water Resources Planning and Management*, *131*(5), 383–393. https://doi.org/10.1061/(asce)0733-9496(2005)131:5(383)

Sanchez, G. M., Terando, A., Smith, J. W., García, A. M., Wagner, C. R., & Meentemeyer, R. K. (2020). Forecasting water demand across a rapidly urbanizing region. *The Science of the Total Environment*, *730*, 139050. https://doi.org/10.1016/j.scitotenv.2020.139050

Sanford, W. E., & Selnick, D. L. (2013). Estimation of Evapotranspiration Across the Conterminous United States Using a Regression With Climate and Land-Cover Data. *Journal of the American Water Resources Association*, *49*(1), 217–230. https://doi.org/10.1111/jawr.12010

Sankarasubramanian, A., & Vogel, R. M. (2003). Hydroclimatology of the continental United States. *Geophysical Research Letters*, *30*(7), 1–4. https://doi.org/10.1029/2002GL015937

Saraswat, C., Mishra, B. K., & Kumar, P. (2017). Integrated urban water management scenario

modeling for sustainable water governance in Kathmandu Valley, Nepal. *Sustainability Science*, *12*(6), 1037–1053. https://doi.org/10.1007/s11625-017-0471-z

Seo, M., Jaber, F., Srinivasan, R., & Jeong, J. (2017). Evaluating the impact of Low Impact Development (LID) practices on water quantity and quality under different development designs using SWAT. *Water (Switzerland)*, *9*(3). https://doi.org/10.3390/w9030193

Sharvelle, S., Dozier, A., Arabi, M., & Reichel, B. (2017). A geospatially-enabled web tool for urban water demand forecasting and assessment of alternative urban water management strategies. *Environmental Modelling and Software*, *97*, 213–228. https://doi.org/10.1016/j.envsoft.2017.08.009

Shiau, J.-T., & Shen, H. W. S. (2001). RECURRENCE ANALYSIS OF HYDROLOGIC DROUGHTS OF DIFFERING SEVERITY, *127*(February), 30–40.

Shiau, J. T. (2006). Fitting drought duration and severity with two-dimensional copulas. *Water Resources Management*, *20*(5), 795–815. https://doi.org/10.1007/s11269-005-9008-9

Sobol, I. . (1993). *Sensitivity analysis for non-linear mathematical models*. Mathematical Modeling Computational Experiment (English, Translation).

Solari, S., & Losada, M. A. (2012). A unified statistical model for hydrological variables including the selection of threshold for the peak over threshold method. *Water Resources Research*, *48*(10), 1–15. https://doi.org/10.1029/2011WR011475

Stephens, S. A., Bell, R. G., & Lawrence, J. (2018). Environmental Research Letters Developing signals to trigger adaptation to sea-level rise Developing signals to trigger adaptation to sea-level rise. *Environ. Res. Lett*, *13*, 104004. https://doi.org/10.1088/1748-9326/aadf96

Stone, B., Mednick, A. C., Holloway, T., & Spak, S. N. (2007). Is compact growth good for air quality? *Journal of the American Planning Association*, *73*(4), 404–418.

https://doi.org/10.1080/01944360708978521

Sun, G., McNulty, S. G., Moore Myers, J. A., & Cohen, E. C. (2008). Impacts of multiple stresses on water demand and supply across the southeastern United States. *Journal of the American Water Resources Association*, *44*(6), 1441–1457. https://doi.org/10.1111/j.1752-1688.2008.00250.x

Svoboda, M., LeComte, D., Hayes, M., Heim, R., Gleason, K., Angel, J., et al. (2002). The drought monitor. *Bulletin of the American Meteorological Society*, *83*(8), 1181–1190. https://doi.org/10.1175/1520-0477(2002)083<1181:TDM>2.3.CO;2

Themeßl, M. J., Gobiet, A., & Heinrich, G. (2012). Empirical-statistical downscaling and error correction of regional climate models and its impact on the climate change signal. *Climatic Change*, *112*(2), 449–468. https://doi.org/10.1007/s10584-011-0224-4

Thomas B. McKee, N. J. D. and J. K. (1993). Analysis of Standardized Precipitation Index (SPI) data for drought assessment. *Water (Switzerland)*, *26*(2), 1–72. https://doi.org/10.1088/1755-1315/5

Thornton, P. E., Running, S. W., & White, M. A. (1997a). Generating surfaces of daily meteorological variables over large regions of complex terrain. *Journal of Hydrology*, *190*(3–4), 214–251. https://doi.org/10.1016/S0022-1694(96)03128-9

Thornton, P. E., Running, S. W., & White, M. A. (1997b). Generating surfaces of daily meteorological variables over large regions of complex terrain. *Journal of Hydrology*, *190*(3–4), 214–251. https://doi.org/10.1016/S0022-1694(96)03128-9

Todorovich, P. (2009). America's emerging megaregions and implications for a national growth strategy. *International Journal of Public Sector Management*, *22*(3), 221–234. https://doi.org/10.1108/09513550910949208

Tu, X., Wu, H., Singh, V. P., Chen, X., Lin, K., & Xie, Y. (2018). Multivariate design of socioeconomic drought and impact of water reservoirs. *Journal of Hydrology*, *566*(August), 192–204. https://doi.org/10.1016/j.jhydrol.2018.09.012

U.S. Bureau of Reclamation. (2013). *Downscaled CMIP3 and CMIP5 climate and hydrology 795 projections: Release of downscaled CMIP5 climate projections, comparison with preceding 796 information, and summary of user needs*.

Van der Velde, Y., Vercauteren, N., Jaramillo, F., Dekker, S. C., Destouni, G., & Lyon, S. W. (2014). Exploring hydroclimatic change disparity via the Budyko framework. *Hydrological Processes*, *28*(13), 4110–4118. https://doi.org/10.1002/hyp.9949

Wang, D., & Hejazi, M. (2011). Quantifying the relative contribution of the climate and direct human impacts on mean annual streamflow in the contiguous United States. *Water Resources Research*, *47*(9). https://doi.org/10.1029/2010WR010283

Wang, H., Asefa, T., Bracciano, D., Adams, A., & Wanakule, N. (2019). Proactive water shortage mitigation integrating system optimization and input uncertainty. *Journal of Hydrology*, *571*(December 2018), 711–722. https://doi.org/10.1016/j.jhydrol.2019.01.071

Wang, X. jun, Zhang, J. yun, Shahid, S., Guan, E. hong, Wu, Y. xiang, Gao, J., & He, R. min. (2016). Adaptation to climate change impacts on water demand. *Mitigation and Adaptation Strategies for Global Change*, *21*(1), 81–99. https://doi.org/10.1007/s11027-014-9571-6

Warziniack, T., & Brown, T. C. (2019). The importance of municipal and agricultural demands in future water shortages in the United States. *Environmental Research Letters*, *14*(8), 084036. https://doi.org/10.1088/1748-9326/ab2b76

Weed, A. S., Ayres, M. P., & Hicke, J. A. (2013). Consequences of climate change for biotic disturbances in North American forests. *Ecological Monographs*, *83*(4), 441–470.

https://doi.org/10.1890/13-0160.1

Weiskel, P. K., Wolock, D. M., Zarriello, P. J., Vogel, R. M., Levin, S. B., & Lent, R. M. (2014). Hydroclimatic regimes: A distributed water-balance framework for hydrologic assessment, classification, and management. *Hydrology and Earth System Sciences*, *18*(10), 3855–3872. https://doi.org/10.5194/hess-18-3855-2014

Westerling, A. L., Hidalgo, H. G., Cayan, D. R., & Swetnam, T. W. (2006). Warming and earlier spring increase Western U.S. forest wildfire activity. *Science*, *313*(5789), 940–943. https://doi.org/10.1126/science.1128834

Western Resource Advocates. (2003). Smart Water: A Comparative Study of Urban Water Use Efficiency Across the Southwest, 178. Retrieved from http://www.westernresourceadvocates.org/water/smartwater.php

Wheeler, S. M. (2008). The evolution of built landscapes in Metropolitan Regions. *Journal of Planning Education and Research*, *27*(4), 400–416. https://doi.org/10.1177/0739456X08315889

Wilson, B., & Chakraborty, A. (2013). The environmental impacts of sprawl: Emergent themes from the past decade of planning research. *Sustainability (Switzerland)*, *5*(8), 3302–3327. https://doi.org/10.3390/su5083302

Wyard, C., Scholzen, C., Doutreloup, S., Hallot, É., & Fettweis, X. (2020). Future evolution of the hydroclimatic conditions favouring floods in the south-east of Belgium by 2100 using a regional climate model. *International Journal of Climatology*, (March 1988), 1–16. https://doi.org/10.1002/joc.6642

Xing, W., Wang, W., Shao, Q., Yong, B., Liu, C., Feng, X., & Dong, Q. (2018). Estimating monthly evapotranspiration by assimilating remotely sensed water storage data into the

extended Budyko framework across different climatic regions. *Journal of Hydrology*, *567*(October), 684–695. https://doi.org/10.1016/j.jhydrol.2018.10.014

Xing, W., Wang, W., Zou, S., & Deng, C. (2018). Projection of future runoff change using climate elasticity method derived from Budyko framework in major basins across China. *Global and Planetary Change*, *162*(November 2017), 120–135. https://doi.org/10.1016/j.gloplacha.2018.01.006

Xu, F., Wang, Z., Chi, G., & Zhang, Z. (2020). The impacts of population and agglomeration development on land use intensity: New evidence behind urbanization in China. *Land Use Policy*, *95*(December 2019), 104639. https://doi.org/10.1016/j.landusepol.2020.104639

Yang, D., Sun, F., Liu, Z., Cong, Z., & Lei, Z. (2006). Interpreting the complementary relationship in non-humid environments based on the Budyko and Penman hypotheses. *Geophysical Research Letters*, *33*(18), 1–5. https://doi.org/10.1029/2006GL027657

Yates, D., Sieber, J., Purkey, D., & Huber-Lee, A. (2005). WEAP2—A demand-, priority-, and preference-driven water planning model part 1: Model characteristics. Water International, 30(4), 487–500. *Water International*, *30(4)*, 487–500.

Yevjevich, V. (1967). An objective approach to definitions and investigations of continental hydrologic droughts. *Journal of Hydrology*, (August). https://doi.org/10.1016/0022-1694(69)90110-3

Yigzaw, W., & Hossain, F. (2016). Water sustainability of large cities in the United States from the perspectives of population increase, anthropogenic activities, and climate change. *Earth's Future*, *4*(12), 603–617. https://doi.org/10.1002/2016EF000393

Yu, P. S., Yang, T. C., Kuo, C. M., & Wang, Y. T. (2014). A stochastic approach for seasonal water-shortage probability forecasting based on seasonal weather outlook. *Water Resources*

Management, *28*(12), 3905–3920. https://doi.org/10.1007/s11269-014-0717-9

Yu Yannian. (1990). Hydrological effects of forests. *The Hydrological Basis for Water Resources Management. Proc., Symposium, Beijing, 1990*, (197), 413–423.

Yue, X., Mickley, L. J., Logan, J. A., & Kaplan, J. O. (2013). Ensemble projections of wildfire activity and carbonaceous aerosol concentrations over the western United States in the mid-21st century. *Atmospheric Environment*, *77*, 767–780. https://doi.org/10.1016/j.atmosenv.2013.06.003

Zaninelli, P. G., Menéndez, C. G., Falco, M., López-Franca, N., & Carril, A. F. (2019). Future hydroclimatological changes in South America based on an ensemble of regional climate models. *Climate Dynamics*, *52*(1–2), 819–830. https://doi.org/10.1007/s00382-018-4225-0

Zhang, D., Gersberg, R. M., Ng, W. J., & Tan, S. K. (2017). Conventional and decentralized urban stormwater management: A comparison through case studies of Singapore and Berlin, Germany. *Urban Water Journal*, *14*(2), 113–124. https://doi.org/10.1080/1573062X.2015.1076488

Zhang, L., Hickel, K., Dawes, W. R., Chiew, F. H. S., Western, A. W., & Briggs, P. R. (2004). A rational function approach for estimating mean annual evapotranspiration. *Water Resources Research*, *40*(2), 1–14. https://doi.org/10.1029/2003WR002710

Zhang, M., & Wei, X. (2012). The effects of cumulative forest disturbance on streamflow in a large watershed in the central interior of British Columbia, Canada. *Hydrology and Earth System Sciences*, *16*(7), 2021–2034. https://doi.org/10.5194/hess-16-2021-2012

Zhang, Q., Liu, J., Singh, V. P., Shi, P., & Sun, P. (2017). Hydrological responses to climatic changes in the Yellow River basin, China: Climatic elasticity and streamflow prediction. *Journal of Hydrology*, *554*, 635–645. https://doi.org/10.1016/j.jhydrol.2017.09.040

Zhang, W., Li, Y., Li, Z., Wei, X., Ren, T., Liu, J., & Zhu, Y. (2020). Impacts of climate change, population growth, and urbanization on future population exposure to long-term temperature change during the warm season in China. *Environmental Science and Pollution Research*, *27*(8), 8481–8491. https://doi.org/10.1007/s11356-019-07238-9

Zhao, F., Xu, Z., Zhang, L., & Zuo, D. (2009). Streamflow response to climate variability and human activities in the upper catchment of the Yellow River Basin. *Science in China, Series E: Technological Sciences*, *52*(11), 3249–3256. https://doi.org/10.1007/s11431-009-0354-3

Zhao, G., Gao, H., Kao, S. C., Voisin, N., & Naz, B. S. (2018). A modeling framework for evaluating the drought resilience of a surface water supply system under non-stationarity. *Journal of Hydrology*, *563*(April), 22–32. https://doi.org/10.1016/j.jhydrol.2018.05.037

Zhao, M., Huang, S., Huang, Q., Wang, H., Leng, G., & Xie, Y. (2019). Assessing socio-economic drought evolution characteristics and their possible meteorological driving force. *Geomatics, Natural Hazards and Risk*, *10*(1), 1084–1101. https://doi.org/10.1080/19475705.2018.1564706

Zhao, P., Lü, H., Fu, G., Zhu, Y., Su, J., & Wang, J. (2017). Uncertainty of hydrological drought characteristics with copula functions and probability distributions: A case study of Weihe River, China. *Water (Switzerland)*, *9*(5). https://doi.org/10.3390/w9050334

Zhou, G., Wei, X., Chen, X., Zhou, P., Liu, X., Xiao, Y., et al. (2015). Global pattern for the effect of climate and land cover on water yield. *Nature Communications*, *6*, 1–9. https://doi.org/10.1038/ncomms6918

Zhou, S., Yu, B., Huang, Y., & Wang, G. (2015). The complementary relationship and generation of the Budyko functions. *Geophysical Research Letters*, *42*(6), 1781–1790. https://doi.org/10.1002/2015GL063511

APPENDIX A

SUPPORTING INFORMATION FOR CHAPTER 2:

ASSESSING SHIFTS IN REGIONAL HYDROCLIMATIC CONDITIONS OF U.S. RIVER BASINS IN RESPONSE TO CLIMATE CHANGE OVER THE 21ST CENTURY

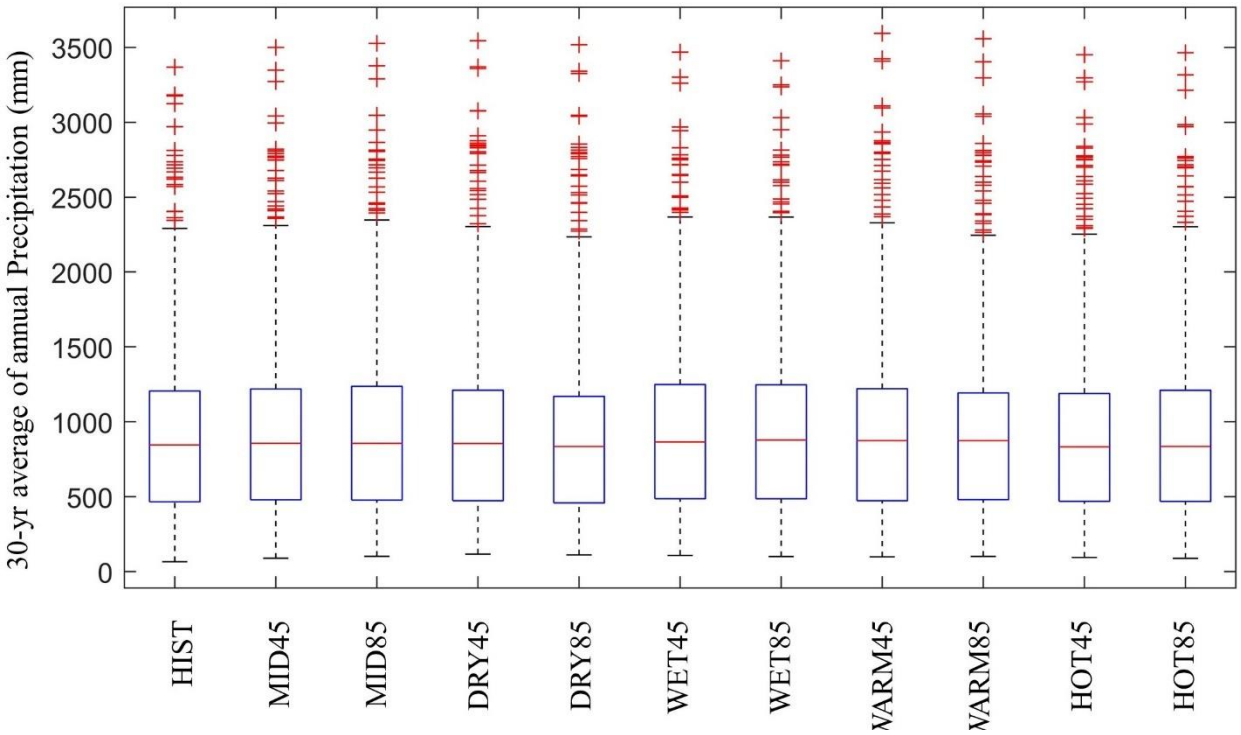

Figure A-1. Comparing 30-yr average annual precipitation of the baseline model and MACA climate models over the historical period

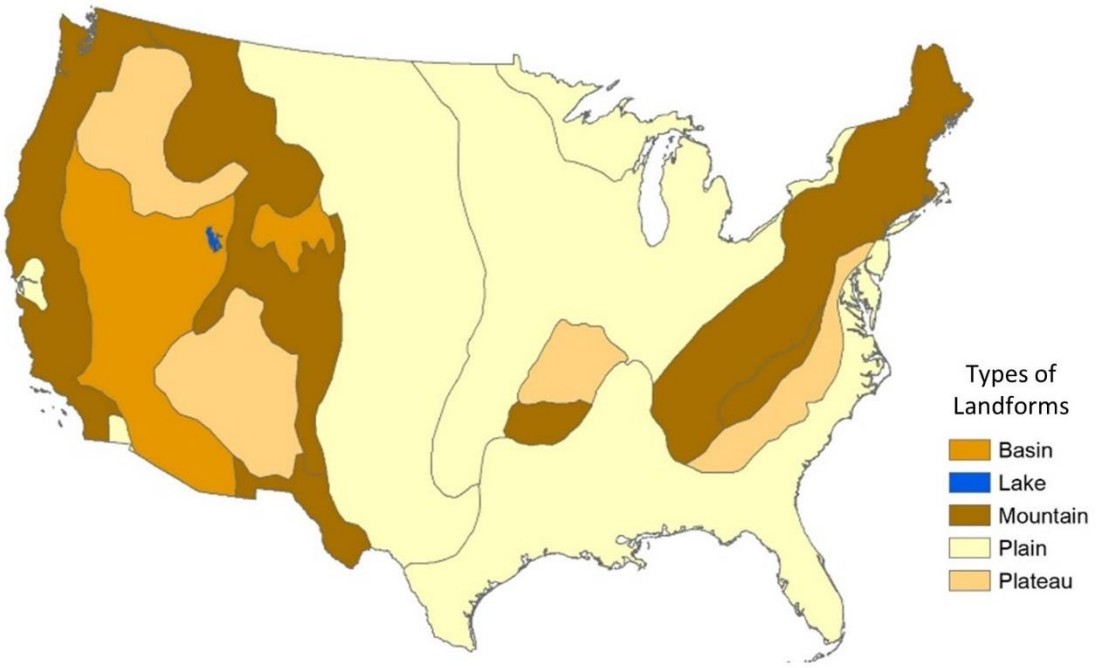

Figure A-2. Map of the types of landforms for the United States

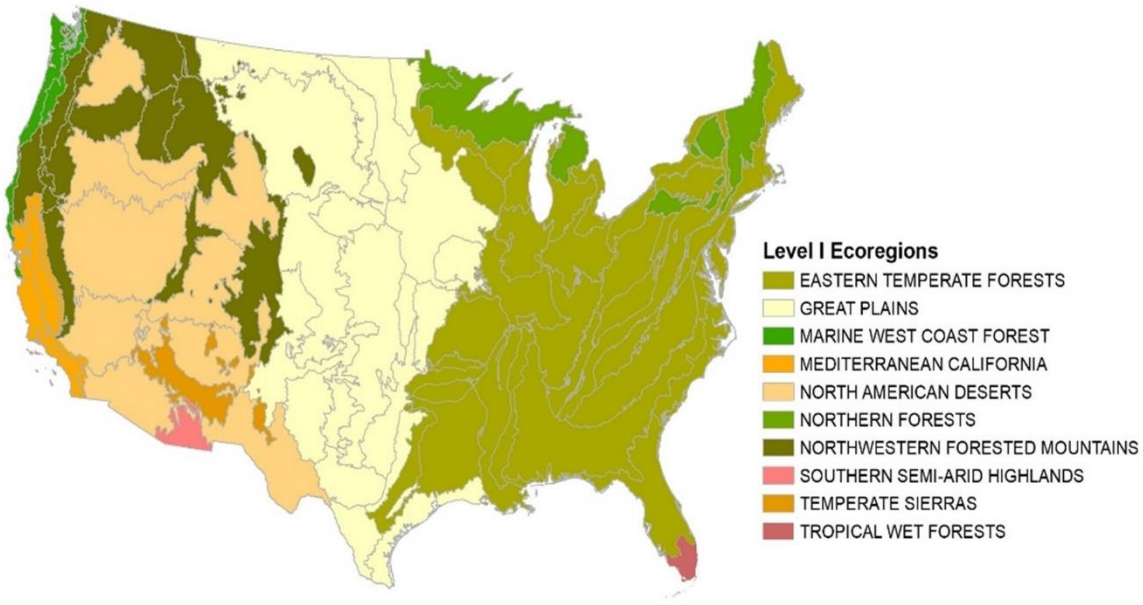

Figure A-3. Map of the ecoregions Level I for the United States

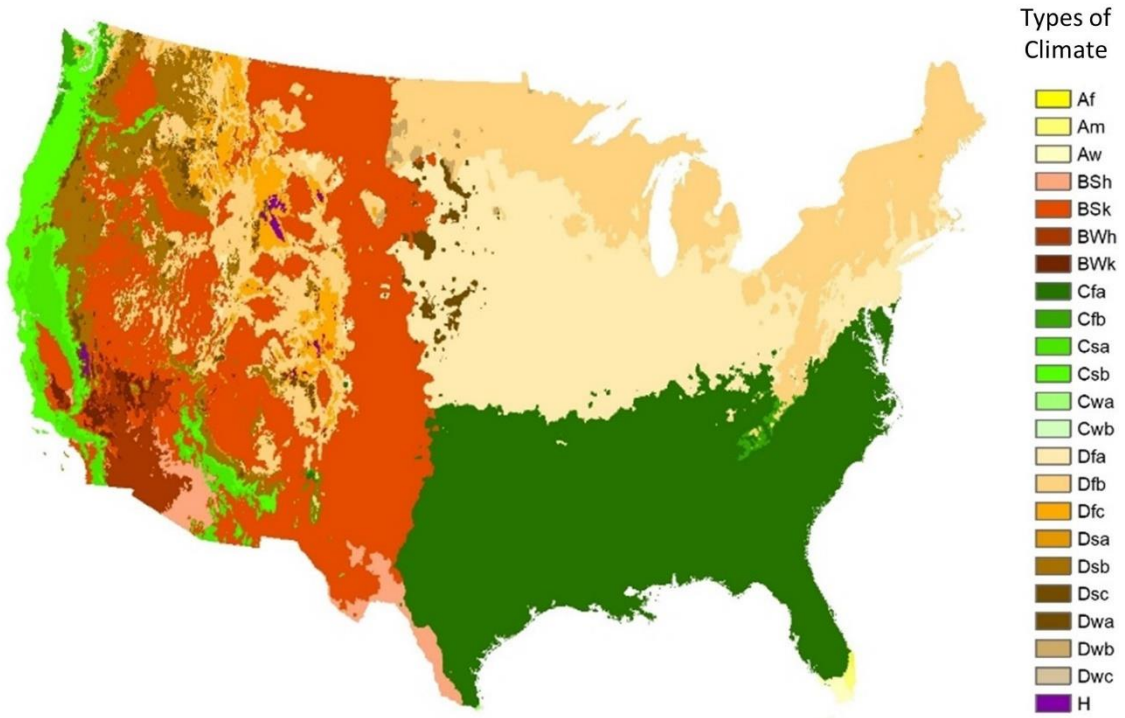

Figure A-4. Map of the Koppen climate classification of the United States

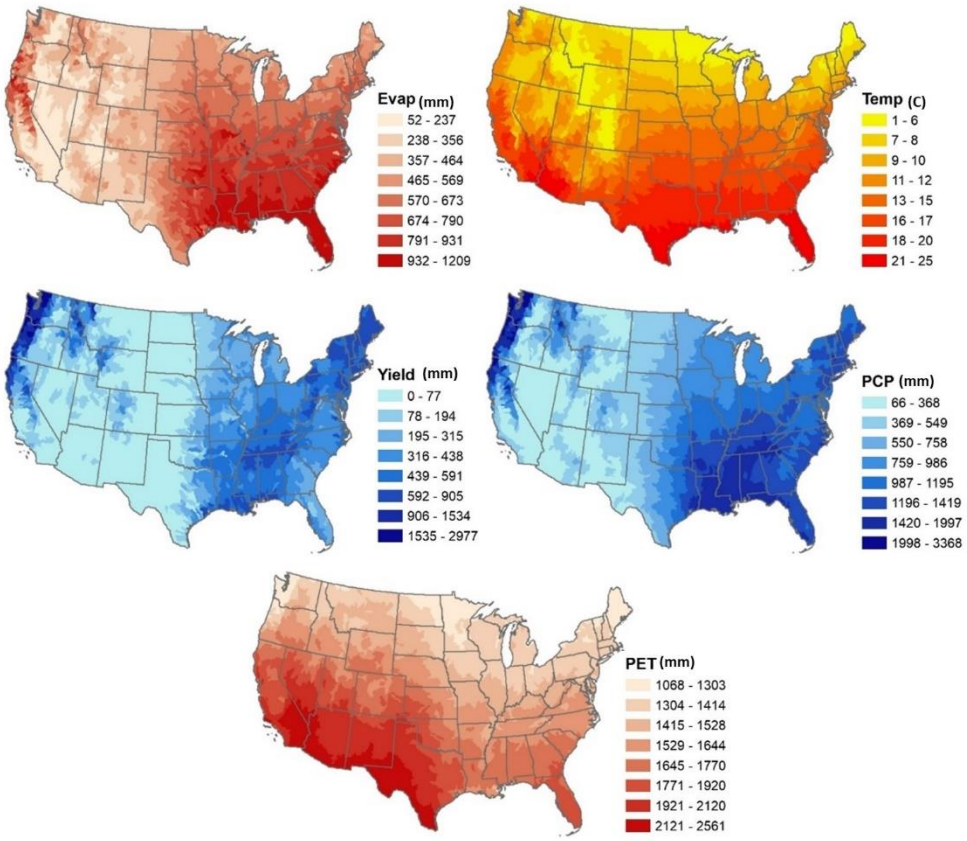

Figure A-5. Maps of 30-yr average of annual U.S. hydroclimatic parameters for the baseline period (1986-2015)

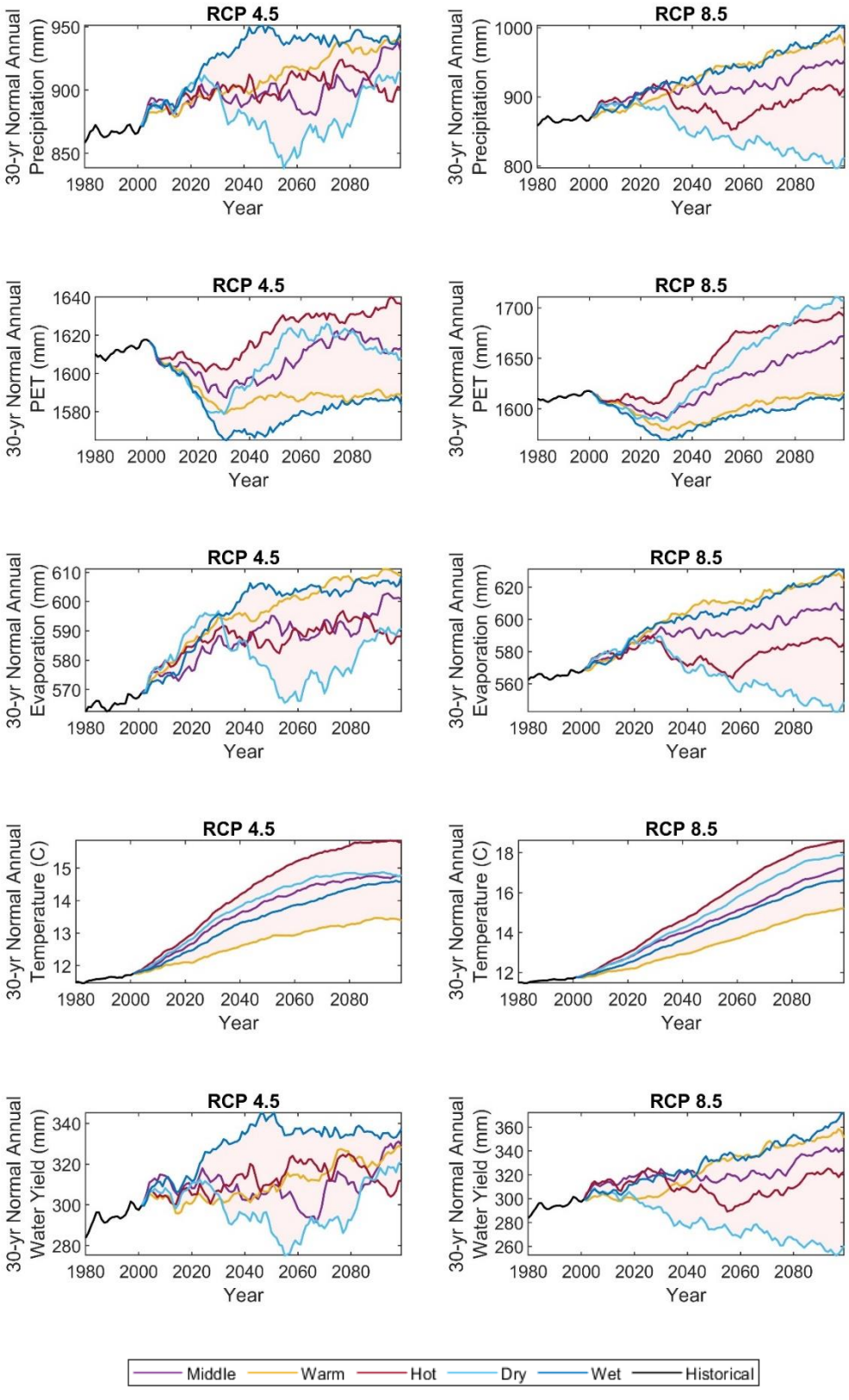

Figure A-6. Temporal changes in 30-yr normal annual hydroclimatic variables of all HUC8 U.S river basins

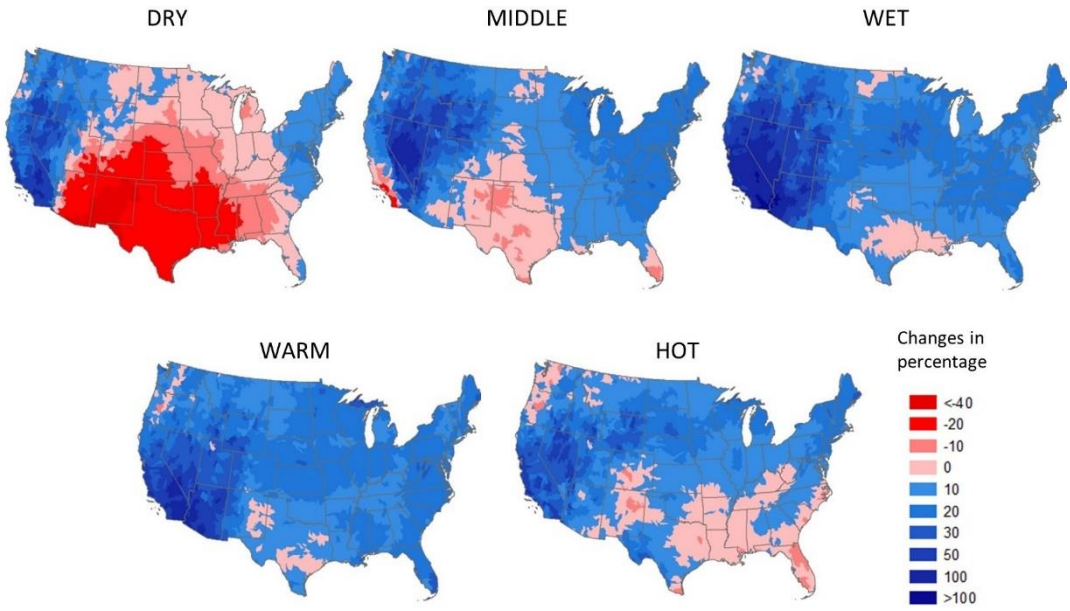

Figure A-7. Spatial changes in normal precipitation from current condition to future condition

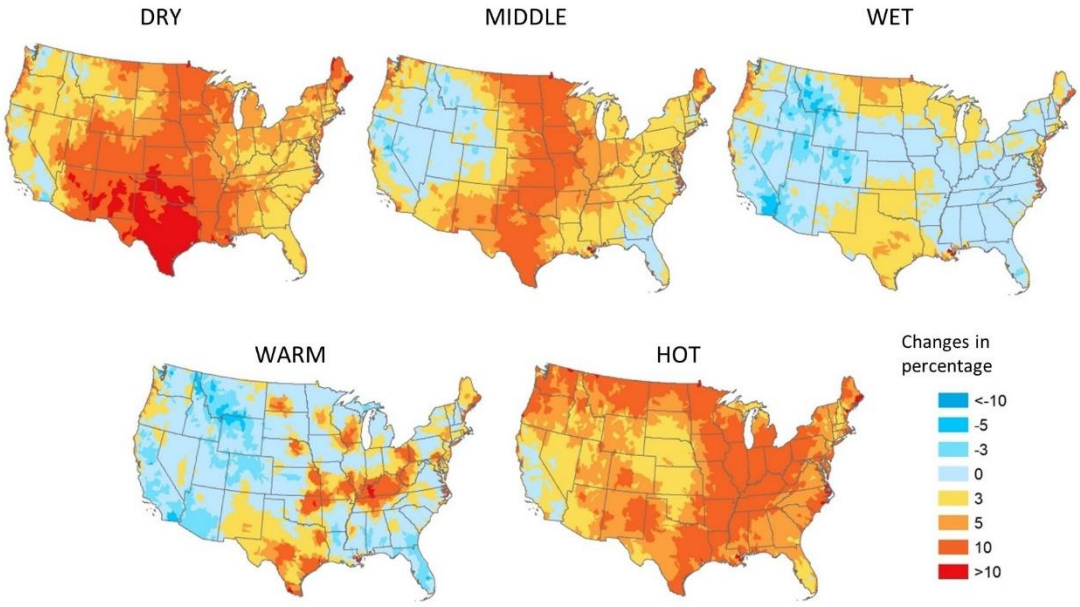

Figure A-8. Changes in normal PET from current condition to future condition

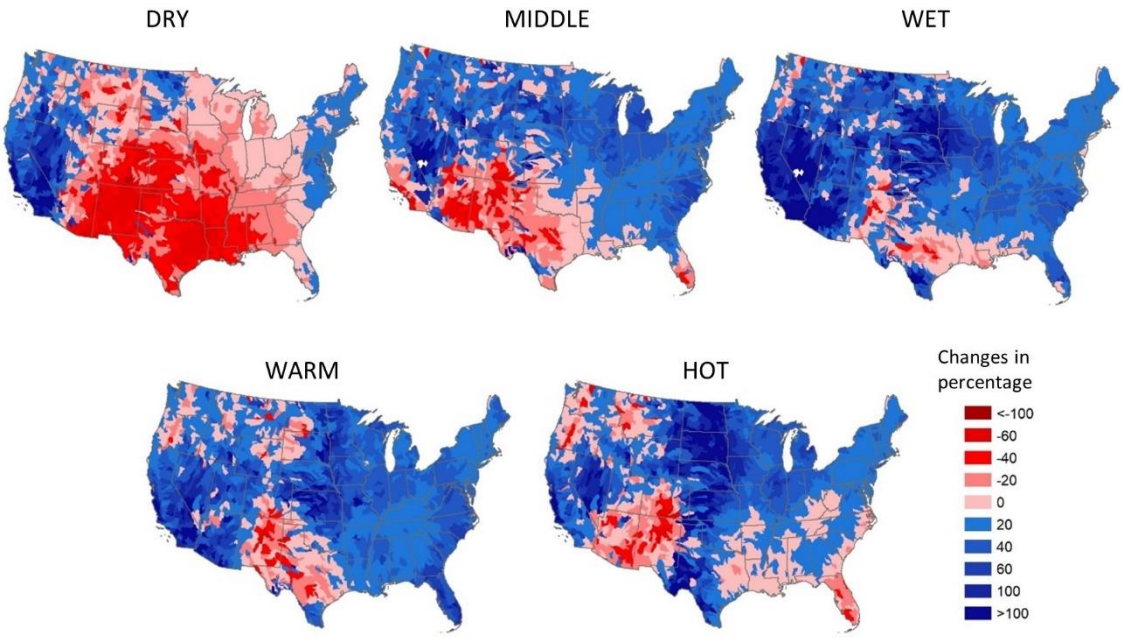

Figure A-9. Changes in normal water yield from current condition to future condition

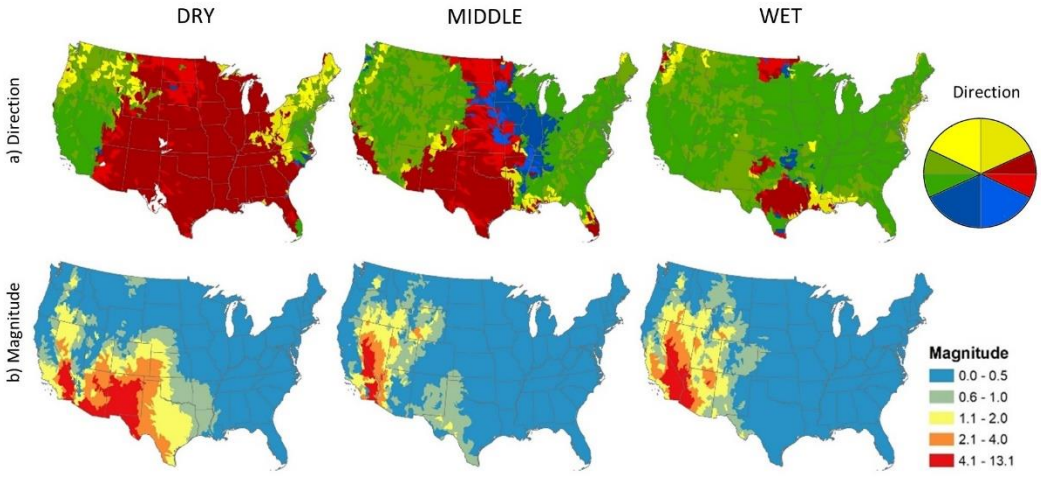

Figure A-10. Movements in the Budyko space under all three climate projections

Table A-1. Koppen climate classification groups

1st	2nd	3rd
A (Tropical)	f (Rainforest)	
	m (Monsoon)	
	w (Savanna, Wet)	
	s (Savanna, Dry)	
B (Arid)	W (Desert)	
	S (Steppe)	
		h (Hot)
		k (Cold)
C (Temperate)	s (Dry summer)	
	w (Dry winter)	
	f (Without dry season)	
		a (Hot summer)
		b (Warm summer)
		c (Cold summer)
D (Continental)	s (Dry summer)	
	w (Dry winter)	
	f (Without dry season)	
		a (Hot summer)
		b (Warm summer)
		c (Cold summer)
		d (Very cold winter)
E (Polar)	T (Tundra)	
	F (Eternal winter (ice cap))	

APPENDIX B

SUPPORTING INFORMATION FOR CHAPTER 3:

IMPACTS OF CLIMATE CHANGE ON HYDROCLIMATIC CONDITIONS OF U.S. MEGAREGIONS, NATIONAL FORESTS, AND NATIONAL GRASSLANDS

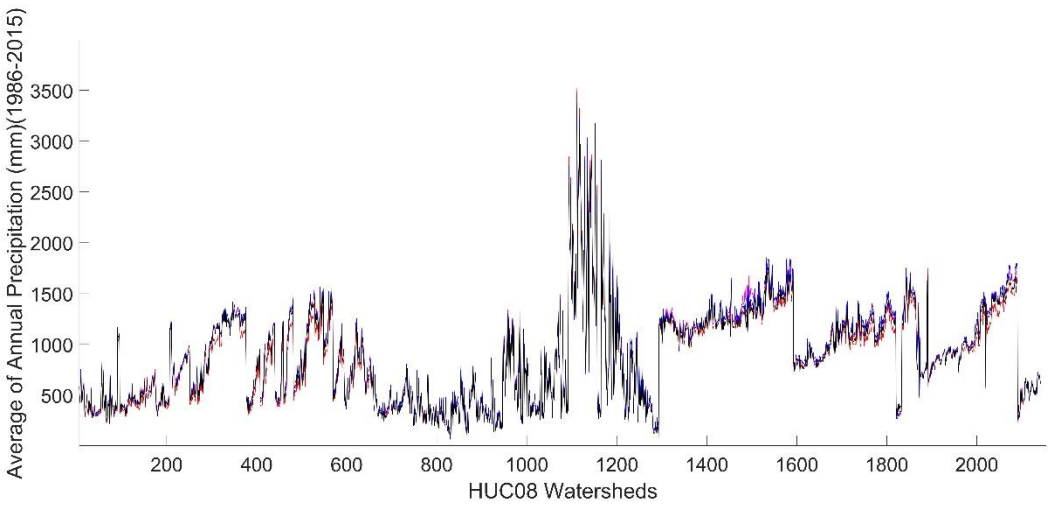

Figure B-1. 30-yr average of precipitation (1986-2015) for HUC08 watersheds

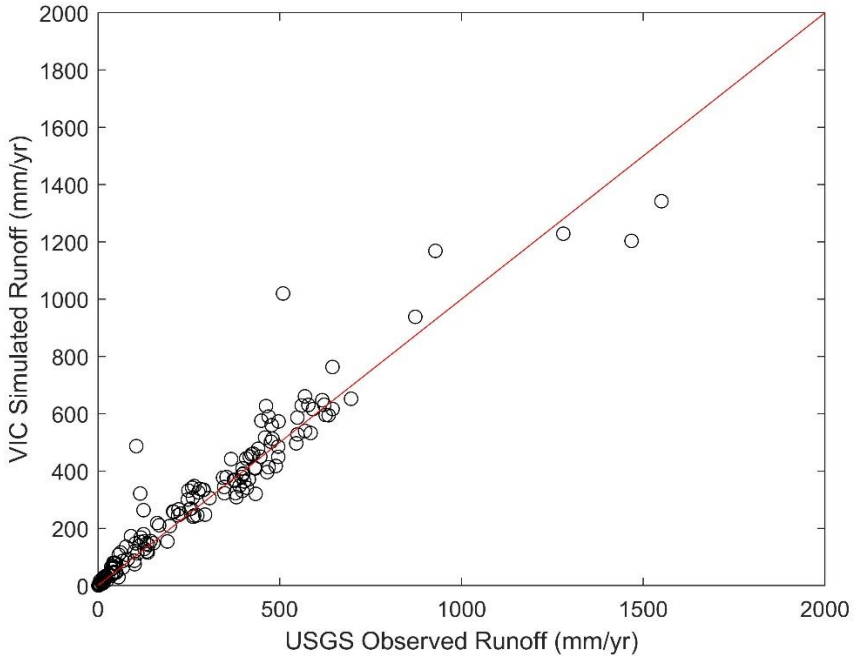

Figure B-2. Comparison of simulated and observed annual water yield for 1986–2015 period for each NFs and NGs

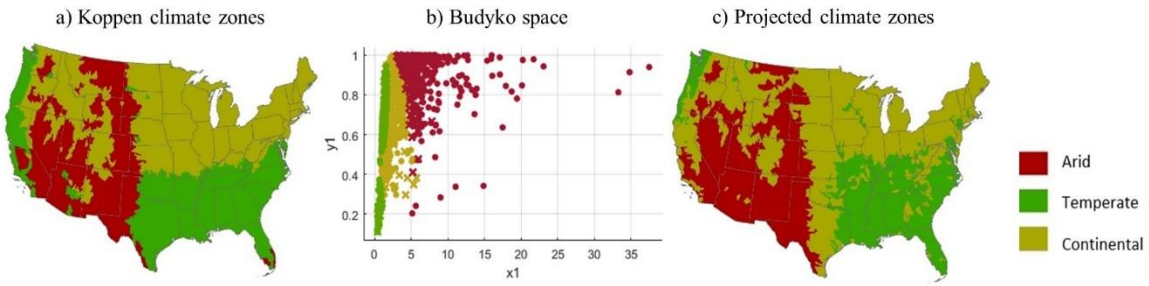

Figure B-3. a) U.S Koppen climate zones, b) Clustering Budyko space based on Koppen climate classification, C) Projected U.S Climate zones based on the Budyko space classification

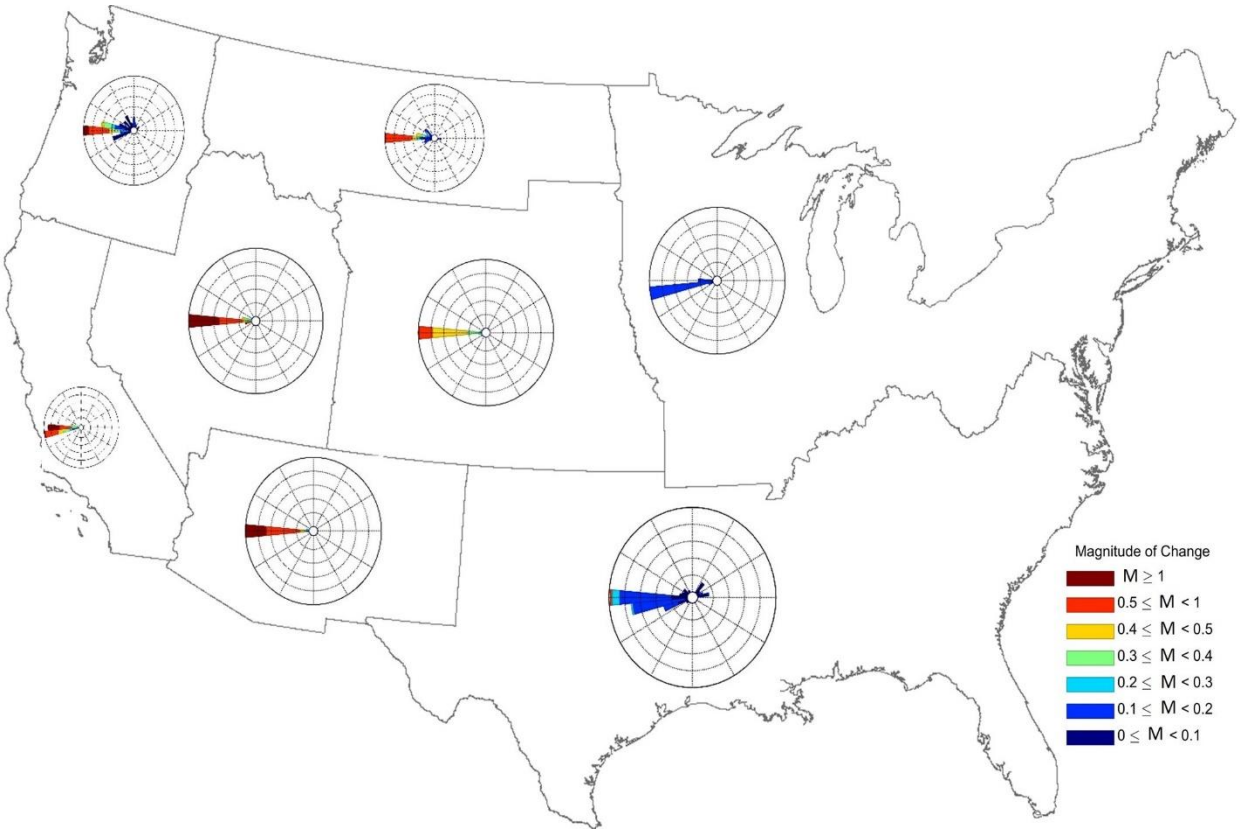

Figure B-4. Wind rose diagrams of movements in the Budyko under the WET climate model

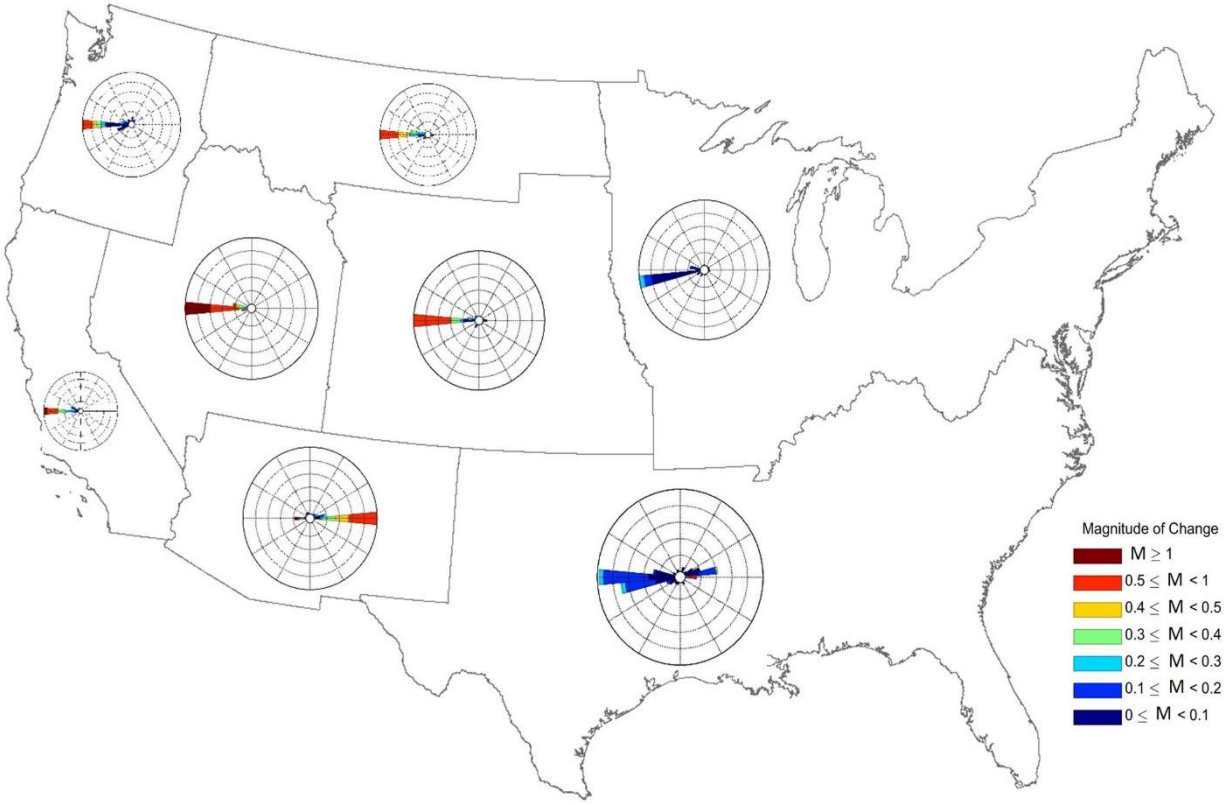

Figure B-5. Wind rose diagrams of movements in the Budyko under the MIDDLE climate model

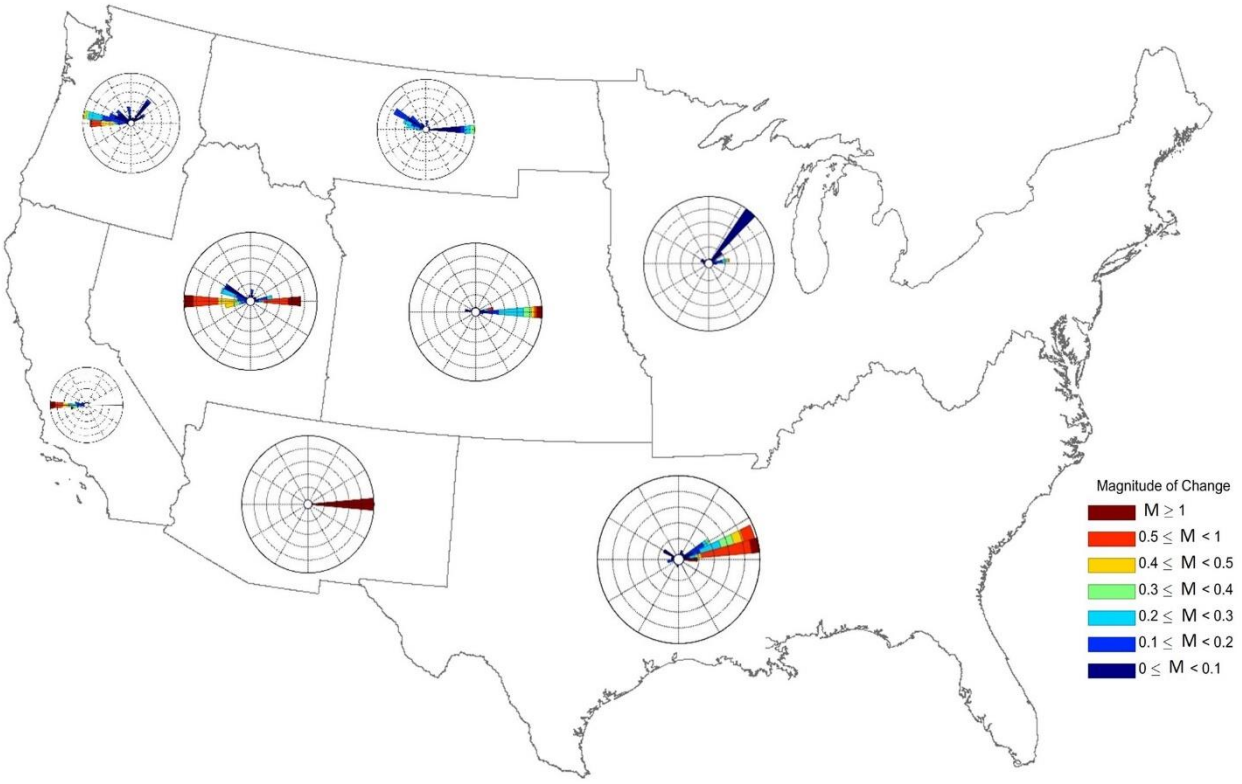

Figure B-6. Wind rose diagrams of movements in the Budyko under the DRY climate model

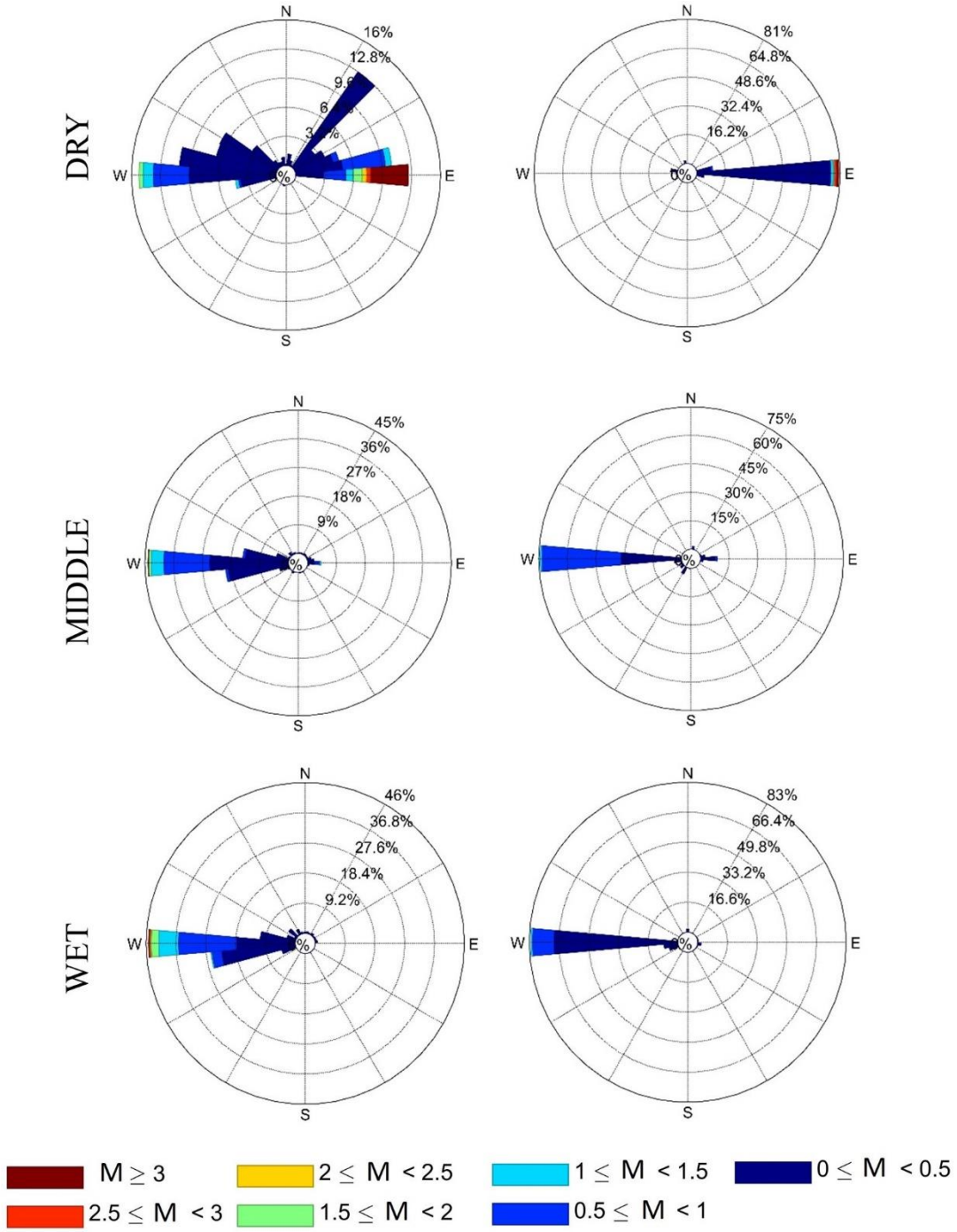

Figure B-7. Wind rose diagrams of movements in the Budyko for NFs and NGs under DRY, MIDDLE and WET climate models

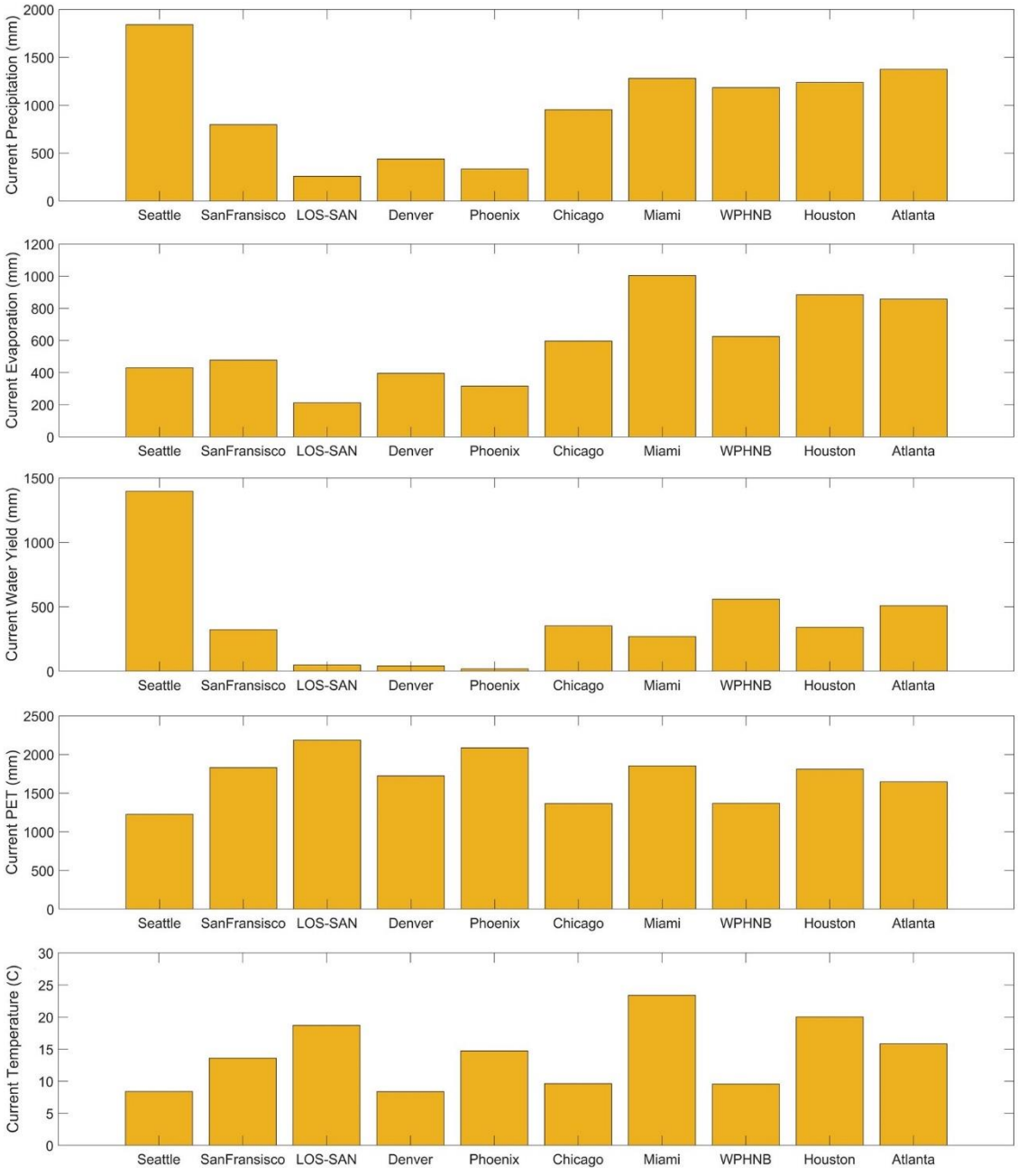

Figure B-8. 30-year average of current hydroclimatic variables in the U.S. Megaregions

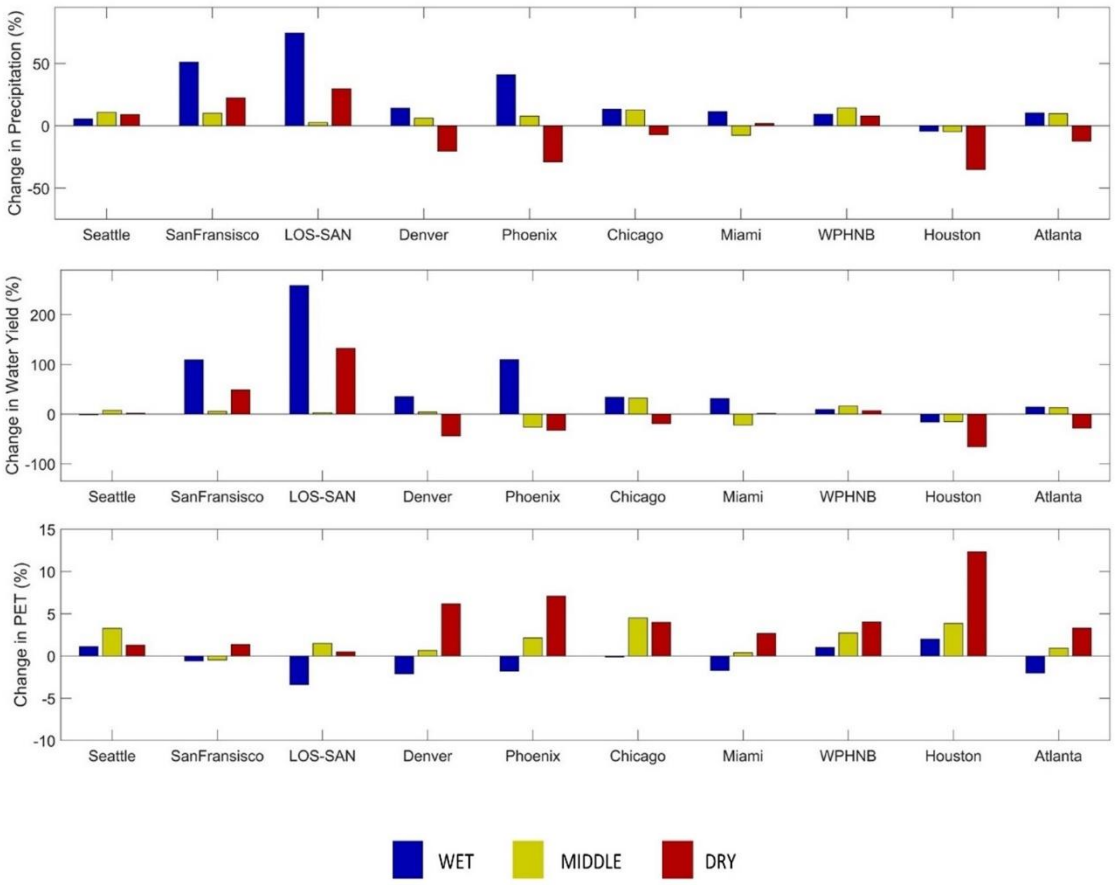

Figure B-9. Change in 30-year average of hydroclimatic variables from current conditions to future conditions in the U.S. Megaregions

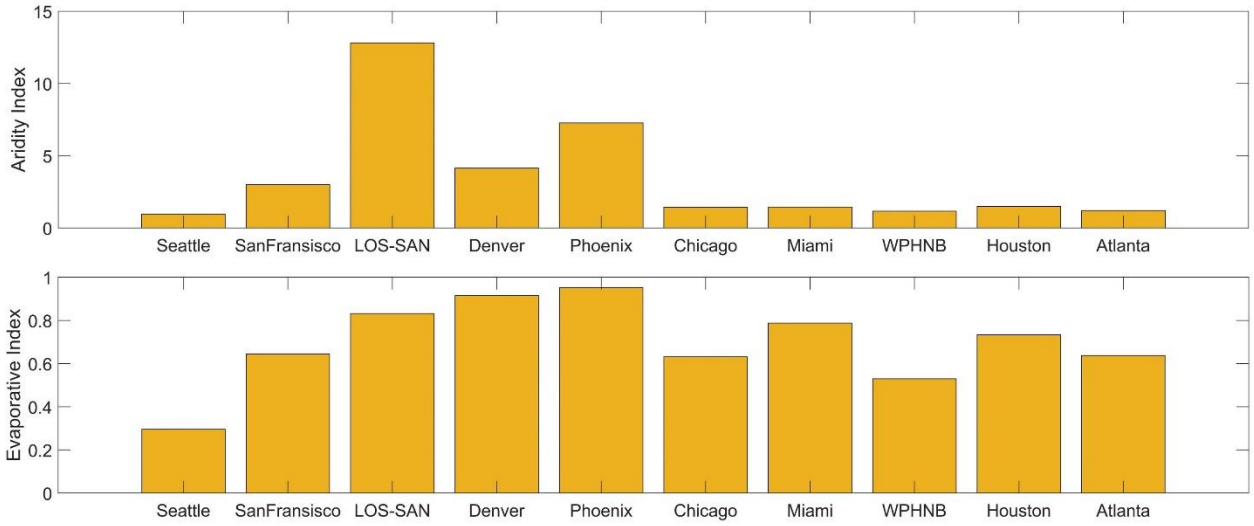

Figure B-10. 30-year average of current hydroclimatic indices in the U.S. Megaregions

Table B-1. Changes in precipitation, PET and water yield of U.S. national forests and grasslands

Name	Current (mm)			Future (WET) - Change (%)			Future (MID) - Change (%)			Future (DRY) - Change (%)		
	PCP	Yield	PET	PCP	Yield	PET	PCP	Yield	PET	PCP	Yield	PET
Tonto National Forest	414.9	23.4	2091.6	47.8	113.6	-3.4	-1.8	-47	2.8	-24.9	-16.7	6.8
Sitgreaves National Forest	307.4	1.9	1999.8	37.3	48.9	-0.9	5	-39.1	3.3	-34.8	-56.4	8.5
Coconino National Forest	394.5	12.9	1996.8	20.7	-14	1.7	9.7	-36.6	3.3	-37.2	-51.8	10.7
Kaibab National Forest	340.3	19.4	1982.6	26	1.4	-0.3	11.8	-36.7	1	-25.6	-37.6	7.9
Prescott National Forest	353.2	19.5	2085	54.8	107.4	-2	32.1	25	0.3	-22.3	-20.3	6.4
Coronado National Forest	377.4	12	2141.6	21.4	37.2	-1.3	-0.2	-39	4.2	-44.9	-60.4	9.1
Saint Francis National Forest	1363.5	575.7	1598.7	9.8	22.2	-1.5	3.3	10	2.6	-23.4	-45.1	5.7
Ouachita National Forest	1439.7	554.4	1692.6	5.6	5.5	0.8	0.1	-7.4	4.3	-29.9	-56.7	9.8
Ozark National Forest	1260.6	401.5	1623.2	6.9	10.8	-0.1	1	-3.4	4.8	-23.9	-55.1	7.7
Tuskegee National Forest	1353.8	443.7	1677.3	6	2.1	-2	3.9	1.6	0.1	-16.7	-38.6	2.8
Conecuh National Forest	1626.5	672.7	1729.3	2	-5.5	-1	1	-2.5	0.5	-16.7	-34.7	3.2
William B. Bankhead National Forest	1507.9	616.1	1657.8	8.3	10.6	-2.6	6.3	8	1	-18.6	-41.1	3.4
Talladega National Forest	1393.6	521.6	1655.2	8.2	9.2	-2	5.6	6.3	0.7	-17	-36.5	3.2
Roosevelt National Forest	635.5	142.4	1632.3	7.9	-10.2	-4	4.8	-24	-1.8	-15.8	-60.9	5.3
Grand Mesa National Forest	395.3	121.3	1733.9	29.7	53.6	-2.1	17.1	18.8	0.1	-13.1	-30.9	7.1
Arapaho National Forest	605	131	1668.8	13.6	8.1	-4.3	8.1	-15	-1.8	-15.1	-48.1	5.4
White River National Forest	607.7	178.6	1651.3	16.3	9.8	-3.9	12	-4.1	-1.6	-12.6	-33.8	6.3
San Juan National Forest	738.3	245.6	1711.2	22.8	19.1	-2.6	4	-22.2	1	-19.4	-38	8.9
Pike National Forest	502.7	69	1699.6	16.3	5.4	-3.2	6.7	-26.1	-0.4	-20.3	-49.7	7
Uncompahgre National Forest	539.7	112.2	1758.1	29.4	52.7	-3.6	10	-12.1	-0.9	-18.5	-54	7.2
Gunnison National Forest	738.3	245.6	1711.2	22.8	19.1	-2.6	4	-22.2	1	-19.4	-38	8.9
Rio Grande National Forest	644.4	166.4	1725.2	20.1	0.1	-3.4	3	-43.4	0.3	-22.2	-57.9	7.8
San Isabel National Forest	456.5	8	1753.3	14.8	-37.7	-5.1	0.9	-85.8	-1	-27.9	-97.9	5.6
Comanche National Grassland	411.7	8.2	1843.4	12.4	-50	-2.6	-1	-69.3	0.9	-34.3	-81.8	7.6
Routt National Forest	650.6	185.9	1639.7	13.2	6	-4.3	10.8	-4.8	-2.2	-11.3	-39.7	5.5
Tahoe National Forest	829.9	321.3	1811.3	44.9	54.9	-1.9	21.2	14.9	-3.8	21.4	17.8	1.1
Stanislaus National Forest	862.9	347.8	1861.6	59.2	97.5	-2.5	11.9	3.7	-2.9	22.9	38.3	0.7

Six Rivers National Forest	2000.9	1166.5	1630.9	26.7	35.9	1.6	9.2	8	-0.5	10.9	7.8	1.8
Sierra National Forest	258.3	67.9	1895.9	50.9	86.8	-0.7	-6.2	-22.4	1.2	12.3	19.6	2
Shasta National Forest	1330.6	606.8	1667	41.7	67.2	-1	19.9	26.9	-2.1	23.3	30.1	0.5
Sequoia National Forest	567.9	222.1	1859.8	65.2	117.1	-1.9	-2.9	-20.8	-0.4	33.7	66.9	1.4
Plumas National Forest	1336.4	487	1775.8	44.7	80.3	-3.4	15.8	16.1	-4.7	18.6	17.8	-1.6
Modoc National Forest	397.7	131.7	1642.4	38.8	60.1	0.7	25.3	29.4	-0.1	26.2	39.8	3.2
Mendocino National Forest	1170.7	522.3	1731.2	31.2	46.9	-0.6	3.7	-4.9	-1.5	9.6	9.8	0.6
Lassen National Forest	898.2	310.5	1783.6	46.9	80.1	-1.2	20.5	25	-2.3	22.6	32.3	0.6
Cleveland National Forest	379.3	29	2037.5	62.9	138.3	-1.8	-21.1	-57.7	3.4	35.9	134.5	3
Yurok Redwood Experimental Forest	2619.9	2215.9	1576.9	23.9	26	0.1	10.3	9.5	-1.9	8.6	7	-0.3
Ocala National Forest	1259.7	331.7	1714.9	10.5	19.8	-2.4	7.1	9.7	-0.1	-9.1	-22.6	2.6
Apalachicola National Forest	1473.7	396.2	1778.9	8.1	8.6	-2.6	8.6	14.4	-1.4	-6.8	-24.7	1.3
Osceola National Forest	1313.7	268.7	1812.6	8.1	12	-2.3	8.2	12.6	-1.4	-1	-2.5	1.4
Chattahoochee National Forest	1514.8	628.2	1608.4	11.5	15.6	-1.4	11	13.9	1.9	-12.7	-30.2	4.2
Rich Mountain Wilderness	1486.1	586.8	1623.6	10.9	10.3	-1.6	10.4	8.3	1.8	-14.9	-37.6	4.3
Clearwater National Forest	914.6	325.9	1376.8	6.3	-23.7	-3.6	15.3	-5.2	-2.7	10.1	-23.2	-1.1
Salmon National Forest	523.3	130.9	1440.3	26.7	20.7	-4.4	27.5	5	-2.1	5.5	-27	2.6
Challis National Forest	655.1	206.3	1526.1	24.4	9.8	-3.6	28.9	12.8	-2.2	16.2	-4.7	2
Coeur D	824.1	371.8	1355.4	9.4	-7.8	-2.4	19.3	10.3	-1.7	11.3	-10	-0.3
Curlew National Grassland	343.1	92.1	1631.9	40.1	28.7	-3.8	41.9	23.6	-2.2	12.2	0.1	2.5
Boise National Forest	729.1	266.1	1571.2	22.2	29.1	-4.3	24.9	38.6	-3.2	20.9	26.7	0.2
Saint Joe National Forest	1092.1	551.2	1385.1	8.6	-1.4	-4	17.4	14.2	-2.9	6.5	-8.2	-1.5
Poyette National Forest	750.6	382	1512.8	19.8	14	-3.2	21.8	18.8	-2.3	15.7	7.2	1.2
Nez Perce National Forest	743.1	263.4	1425.7	16.9	1	-2.4	20.8	10	-1.6	9.2	-14.9	1.8
Shawnee National Forest	1258.7	471	1520.1	7.9	14.9	-1.1	4.9	11.3	3.6	-11.5	-29	3.9
Hoosier National Forest	1230.7	511.9	1459	9.3	17.7	-1.2	8.9	18.9	3.1	-3.9	-13.1	2.5
Cimarron National GrassLand	439.4	0.4	1942.8	6.6	159.8	-0.3	-7.4	132.6	3.1	-36.7	-43.9	9.1
Daniel Boone National Forest	1190	429.9	1531.7	14.2	23.4	-2.2	11.8	13.3	1.7	-5	-20.4	2.8
Kisatchie National Forest	1507.7	483.7	1745.1	-0.7	-9	0.2	2	-0.3	1.4	-28.9	-61.4	8.1
Superior National Forest	732	285.6	1281.4	12.6	20.6	1.8	9.2	12.3	5.2	4.4	1.5	5.2
Chippewa National Forest	676.7	155.7	1289.5	7.9	17	1.1	4	6.7	6	-2.7	-9.2	6.3
Delta National Forest	1429.2	560.2	1643.8	8.4	16	-1.1	5.7	10.8	2.2	-24.5	-45.9	5.8
Tombigbee National Forest	1452.8	594	1624.1	9.7	14.9	-1.6	3.9	5	2.3	-21.1	-42.6	5.1

Holly Springs National Forest	1469.5	628.9	1627.3	12.9	24.3	-1.6	4.3	7.5	3.2	-18.3	-37.7	5.4
DeSoto National Forest	1586.4	526.1	1742.7	4	-1.3	-1	4.2	4.5	0.5	-20.4	-48.8	4.4
Homochitto National Forest	1493.3	408.9	1720.9	3.2	3.3	-0.6	5.5	13.1	1.1	-26.7	-59.2	6.5
Bienville National Forest	1477.3	502.4	1705	6.7	5	-0.8	6.1	8.6	1.8	-22.9	-50.3	5.7
Mark Twain National Forest	1182.5	334.8	1576.1	6.3	12.6	-0.3	3	2.4	4.7	-17.7	-43.1	5.7
Deerlodge National Forest	514.2	92.7	1435.8	23.4	14.9	-4.8	19.1	-8.4	-2	4.9	-37.1	1.3
Gallatin National Forest	668.1	237.2	1442.3	29.1	34.1	-5	26.5	17.8	-2.2	9.9	-9.2	1.8
Lewis and Clark National Forest	479.1	100.9	1413.2	22.3	19.4	-3	19.3	1.6	-0.3	7.5	-20.6	2
Beaverhead National Forest	535.6	118.2	1428.1	32	34.6	-4.8	31.3	14.8	-2.2	7.5	-23.5	2.5
Flathead National Forest	782	379.4	1351.1	10.8	0.8	-2.3	21	15.6	-1.4	11.6	-2.5	0.7
Helena National Forest	496.8	118.2	1432.7	25	25.2	-4.5	18.7	0.2	-1.4	6.8	-20.6	1.2
Lolo National Forest	741.2	294	1372.9	10.7	-6.4	-3.2	18.2	7.2	-2	11	-11.5	-0.3
Oglala National Grassland	428	9.6	1522.3	9.9	8.8	-1.5	9	5.6	0.8	-6.1	-19.6	2.9
Inyo National Forest	937.3	263.4	1792.9	55.5	95	-4.2	7.7	-17.9	-4.4	22.8	22	0.2
Humboldt National Forest	336.1	36.5	1684.8	41.6	63.5	-2.1	38.9	43.3	-0.9	25.8	50.9	3.3
Toiyabe National Forest	321.6	94	1992.4	55.9	96.1	-2.2	51.8	91	-2.7	22.2	48.8	1.8
Santa Fe National Forest	436.6	39.5	1931.3	12	-19.1	-1.2	-6.5	-57.5	2.3	-42.3	-80.3	9.7
Gila National Forest	341.6	21.1	2106.9	14.7	-8.7	0.4	-3.2	-48	4.8	-46.9	-77.1	9.9
Nantahala National Forest	1513.3	654.4	1621	13.2	19	-2.4	13	16.5	1.1	-9.6	-25.4	3.3
Uwharrie National Forest	1172.3	333.9	1597.6	17.3	33.3	-2.3	20.7	37.4	-0.1	4	0.5	1.7
Pisgah National Forest	1306.4	485.2	1601.7	14.4	21.5	-2.4	14.8	18.2	0.6	-3.9	-16.5	2.8
Croatan National Forest	1398.9	441.7	1568.9	12	22.6	1.3	13.6	19.4	2.9	5.1	11.1	4.7
Little Missouri National Grassland	416.4	29.1	1353.5	1.3	39.6	3.4	2.7	21.6	4.9	-2.4	3.3	4.2
Wayne National Forest	1088.9	393.7	1451.3	11.4	17.5	-1.3	13.8	19.4	1.9	-1.1	-12	2.9
Black Kettle National GrassLand	711.4	4.6	1859.8	1.9	-7.8	1.6	-3.2	-13.9	6.3	-27.9	-45	10.3
Umpqua National Forest	1017	410.7	1575.7	14.7	4.6	1	8.2	-3.7	0.3	8.8	-5.7	2.3
Wallowa-Whitman National Forest	630.1	248.7	1449.2	21.6	22.1	-2.4	21.3	23.8	-1.8	4.8	-11.4	1.7
Malheur National Forest	465.6	110.2	1573.5	30.7	52.9	-1.8	20.4	28.8	-1	19.2	26.4	2
Ochoco National Forest	430.5	93.7	1555	24.2	32.8	-0.7	16.5	16.8	-0.2	21.4	28.5	2.2
Rogue River National Forest	1108.2	613.5	1577.6	13.6	11	-0.6	5.8	1.4	-1.1	8.5	2.7	0.9
Deschutes National Forest	819.4	293.2	1564.5	5.8	-30.5	0.7	4.1	-27.6	0.6	8	-24.9	1.9
Mount Hood National Forest	1738.3	1290.1	1343.6	3.8	-0.9	0.5	9.3	7.3	1.1	9.4	4.2	0.9
Winema National Forest	1271.4	727.1	1526.6	11.2	-12	0.9	6.5	-16	0.6	9.6	-12	2.1

Fremont National Forest	567.4	160.6	1662.1	26.1	21	-0.9	16	3.1	-1.4	22	18.7	1.5
Oregon Dunes National Recreation Area	1884.9	1123.9	1368.1	8	6.1	4.4	5.6	2.5	3.1	-4.5	-16.8	5.1
Crooked River National Grassland	850.1	363.5	1544.8	0.6	-33.1	1.2	0.5	-28.4	1.2	3.4	-28.7	2.1
Allegheny National Forest	1152.9	594.8	1401	11.3	14.6	0.3	15.3	17.2	2.7	0.9	-4.4	4.1
Sumter National Forest	1298	434	1656.5	13.4	22.3	-2.7	13.8	22	-0.1	-5.7	-17.4	2.2
Black Hills National Forest	425.9	12.3	1515.1	10.9	17.8	-1.3	15.7	35.8	0.9	0	-15.8	2.7
Buffalo Gap National Grassland	474.6	20.5	1485.9	13.4	47.7	-0.3	6.1	9.3	3.5	-3.9	-2.6	3.3
Lyndon B Johnson National GrassLand	874.8	115.6	1887.4	-0.4	-14.8	2.3	-7.3	-29.5	6.4	-29.1	-48.2	12.1
Angelina National Forest	1323.2	306.8	1795.5	-5.2	-16.3	1.7	-5.5	-17.7	3	-36.6	-78.7	11
Sabine National Forest	1404.4	337.5	1766.7	-4.6	-12.1	1.5	-4.3	-12.6	2.8	-35	-72.3	10.3
Sam Houston National Forest	1200.3	258.9	1815.6	-4.3	-13.2	1.5	-3.4	-8.2	3	-35.9	-75.2	10.8
Davy Crockett National Forest	1315.8	266.4	1812.7	-5.3	-21.7	1.5	-4.7	-17.9	2.6	-37	-79.7	11.1
Cache National Forest	581.4	140	1551	25.7	35.6	-3	31.5	48.8	-1.2	3.2	-0.6	4.3
Wasatch National Forest	517.5	88.9	1627.4	28.6	30.5	-4.2	26.6	10.7	-2.1	-0.5	-19.2	3.5
Ashley National Forest	405.7	61.9	1662.1	30.2	38.7	-2.8	28.2	11.3	-1.8	-7.3	-25.4	5.6
Fishlake National Forest	432.8	55	1741.5	32.7	77.8	-2.1	24.2	13.5	-1.3	-3.7	-1.3	5.9
Caribou National Forest	464.7	111.1	1552.2	31	74.8	-3.3	37.6	93.4	-2	8.1	24.1	3.5
Dixie National Forest	375.6	25	1877.9	29.3	35	-0.9	16	-36.2	-0.5	-13.5	-15.5	6.7
Uinta National Forest	475.6	78.1	1638.5	28.2	24.3	-3.7	25	0.7	-1.6	-1.6	-15.9	4.4
Green Mountain National Forest	1229.8	657	1338.1	14.2	17.8	-0.8	18	21.8	1.2	7.8	5.2	3.7
Umatilla National Forest	512.4	163.4	1436.4	22.7	29.8	-1.7	19.8	23.7	-0.8	8.6	-5.6	2
Okanogan National Forest	1458.6	1164.1	1264.4	12.2	7.7	1.2	11.6	8.9	3.5	12.9	7.2	2.1
Wenatchee National Forest	773.8	475.4	1405.4	3.1	-8	-0.1	7.4	0.5	2.2	11.1	0.1	-0.3
Osceola National Forest	3367.5	2977.3	1171.8	7.8	6.8	1.4	14.2	14.1	2.8	8.5	7.1	2.1
Colville National Forest	721.2	405	1316.8	14.4	11.6	0.4	14.8	13.6	2.3	11.7	6.9	1.9
Gifford Pinchot National Forest	1151.9	626.8	1406.7	-6.6	-37.6	-2.4	2.7	-21.3	0	1.8	-25.7	-2.6
Mount Baker-Snoqualmie National Forest	2418.9	2008.8	1139.9	10.1	5.7	-0.7	12.7	9.2	3	10.4	4.9	0
Nicolet National Forest	775.6	234.5	1344.4	11.6	19.9	1	19.6	38.3	2.2	-1.8	-8	4.5
Teton National Forest	601.8	267.3	1544.8	12.4	0.8	-3.2	19.4	4.8	-1.5	1.1	-11.3	4.2
Medicine Bow National Forest	461	94.6	1695.6	17.1	9.4	-3	17.6	4.7	-1.2	-3.9	-25.2	4.9
Thunder Basin National Grassland	362	5.3	1537.7	11.4	-0.9	-0.9	16.9	12.5	1	-0.4	-13.8	3.4
Shoshone National Forest	454.8	165.1	1496.1	16.3	10.2	-4.1	21.1	12.4	-1.7	2.3	-16.2	2.5

Bighorn National Forest	422.3	46.7	1452.7	21.3	-5	-4.7	24.6	-11.2	-2.7	3.3	-53.2	0.1
Bridger National Forest	489.5	165.3	1589.8	16.4	3.5	-2.9	21.6	2.2	-1.6	2.9	-11.8	4
Manistee National Forest	937.9	374.2	1389.3	4	6	0.8	17.8	35.4	1.9	-9.7	-19.7	3.9
Ottawa National Forest	855.4	344.3	1309	10.9	9.2	1.4	13.6	10	3.3	-1.9	-16.5	4.5
Hiawatha National Forest	851.1	384.2	1307	11.8	15	2.3	17.8	27.7	2	-6.4	-14.7	4.1
Huron National Forest	771	243.8	1373.8	8.4	13	1	17.8	32.9	1.3	-7	-12.3	3.3
Siskiyou National Forest	1328	761	1527.4	15	19.9	2.3	7.8	8.5	1.1	3.3	-0.9	3.1
Siuslaw National Forest	2190.7	1520.6	1305.9	8.6	9.7	5.3	10.9	12.7	4.3	0.3	-4.8	5.8
Cherokee National Forest	1362.6	586.3	1592.5	13.8	16.6	-2	13.6	11.9	1.4	-6.9	-20.9	3.6
Los Padres National Forest	259.4	86.8	2031.5	54	83	-3	-11.4	-31.5	0.4	33.8	61	-0.1
Angeles National Forest	509.5	107.6	2033.9	44.3	57.1	-3.1	-22.6	-55.9	-0.1	33.1	55.9	-1.3
Nebraska National Forest	494.4	35.1	1540.8	10	3.7	-0.6	3.2	-3.7	3	-10.5	-25	3.7
Midewin National Tallgrass Prairie	996.1	378.3	1363.6	11	26	0	12.7	31.4	4.1	-5.3	-13.3	3.7
McClellan Creek National Grassland	587	28.6	1956	-0.2	-15.2	1.5	-12	-31.9	6.2	-34.5	-55.1	10.8
Kaniksu National Forest	958.8	481.7	1303	9.9	0.7	-0.8	21.5	19.3	0.3	13.1	0.8	0.9
Bitterroot National Forest	664.3	189.7	1457.8	14.5	-12.9	-4.6	14.2	-21.4	-2.3	2.1	-46.8	1.2
Samuel R McKelvie National Forest	570.3	63.1	1532.9	13.8	96.3	-0.8	-2.1	18	4.4	-14.6	-30.5	4.5
Kootenai National Forest	865.8	347.9	1345.7	6.1	-9.9	-1.3	18.7	14.7	-0.7	11.7	-6.1	0.3
Eldorado National Forest	854.3	330.7	1772.2	49.3	88.6	-1.8	12.3	14.8	-2	19.1	32.3	0.5
Apache National Forest	422.4	6.7	2009	26.7	-18.9	-0.1	-0.4	-56.1	4.3	-42.5	-72.5	10.7
Carson National Forest	480.6	78.6	1812.7	17.5	9.6	-2.3	-1.2	-39.7	0.9	-32	-69.7	8.3
Chequamegon National Forest	825.8	286.4	1318.4	10.7	18	1.1	12.8	19.6	3.9	-3	-13.4	5.4
Cibola National Forest	333.9	10.7	2017.7	17.3	-4.1	-0.1	-3.8	-43.7	3.8	-44	-69.5	9.6
George Washington National Forest	1061.7	341.4	1546.4	13.4	19.7	-1.3	16.8	21.7	0.9	10	11.4	2.4
Jefferson National Forest	1102.2	378.2	1554.7	12.2	14.7	-1.6	14.5	14.6	0.7	5.7	0.4	2.6
Klamath National Forest	713.6	173	1645.7	27.6	33.4	-0.8	12.4	4	-2.2	15.3	10.3	0.8
Lincoln National Forest	326	33.3	2184.4	10.8	-2.7	0.6	-3.5	-21.4	4.5	-43.8	-53.1	10.1
Monongahela National Forest	1086.8	371.3	1551.8	12.8	16.4	-1.6	14.9	16	0.7	5.3	-0.1	2.8
San Bernardino National Forest	428.4	92.6	2034.1	61.2	116.5	-2.7	-18.1	-47.3	2.1	42.3	114.5	0.7
Targhee National Forest	454.3	95.9	1433.6	31.2	27.5	-4.5	33.5	11.6	-2.2	6.2	-21.2	2.7
Trinity National Forest	1483.7	679.9	1673.3	30.3	45.2	0	10.1	7.2	-1.8	12.7	8	0.9
White Mountain National Forest	1293.4	717.6	1304.2	11.1	11.2	-1	12.1	10	0.8	5.8	0.3	3.4
Custer National Forest	464.4	87.2	1467.3	12.1	31.5	-0.7	14.7	24.1	1.1	1	-17.9	2.6

Francis Marion National Forest	1317.5	331.7	1660.8	9.6	14.6	1.1	13.1	16.7	2.9	-1.1	-7.9	5.2
Cedar River National Grassland	429.8	18.6	1434.3	1.2	19.3	1.9	2.7	22.8	4.1	-0.6	0.6	2.6
Fort Pierre National Grassland	570.1	19	1449.1	17.6	200.7	-0.6	5.3	83.5	5.1	-9.2	-0.6	5
Fort Pierre National Grassland	420.2	16.2	1460.5	3.7	42.2	1.7	5.7	22.4	3.7	0.4	-9.9	2.8
Kiowa National Grassland	431.9	5	1974.9	4.7	-7.8	-0.4	-9.6	-37.7	2.9	-41.1	-59.1	9.3
Pawnee National Grassland	389	34.1	1630	11.6	35.9	-2.6	9	0.5	-0.2	-17.6	-61.6	4.4
Rita Blanca National Grassland	427.1	3.9	1994.6	3	-4.4	-0.1	-11.3	-29.3	3.4	-39.2	-49.3	9.5
Sheyenne National Grassland	594	29.4	1264.5	4.7	17.5	2.1	0.1	8.6	7.2	-6.2	-5.8	6.6
Finger Lakes National Forest	972.9	411.5	1312.4	13.4	21.4	-1	13.3	18.8	2.4	5.9	3.5	3.5
Sawtooth National Forest	371	92.6	1608.3	33.7	36	-3.2	34.8	27.8	-1.7	13.4	8.8	2.8
Snoqualmie National Forest	2230.8	1817.9	1225.2	2.4	-1.7	-0.4	9.7	8.3	2.1	8.4	4.1	-0.8
Mount Baker National Forest	2344.2	1974.4	1207.4	4.4	-2.4	-1.4	8.8	3.1	1.7	7.8	0.4	-1.4
La Sal National Forest	448.7	63.1	1802.8	30.7	33.8	-3.8	11.1	-25.3	-1.1	-18.7	-38.2	6.3
Manti National Forest	350.7	79.9	1740.8	25	56.7	-2.1	20.8	35.4	-1.1	-11.6	-25.2	6.1
Caddo National GrassLand	1149.4	242.8	1738.5	2.6	6.7	1.5	-2.2	-12.2	4.5	-29.8	-66.6	10.5
Jefferson National Forest	1115.6	443.1	1536.7	13.6	16.6	-2.1	13.9	11.6	1	-2.2	-14.4	3

Table B-2. P-values of Wilcoxon signed-ranked test at the 5% level (PCP, PET, Yield)

Name	PCP			PET			Yield		
	MID	DRY	WET	MID	DRY	WET	MID	DRY	WET
Allegheny National Forest	0	0.8	0	0	0	0.81	0	0.44	0
Angeles National Forest	0.17	0.14	0	0.59	0.12	0	0.03	0.26	0.05
Angelina National Forest	0.23	0	0.44	0.02	0	0.24	0.15	0	0.12
Apache National Forest	0.89	0	0	0	0	0.81	0	0	0.25
Apalachicola National Forest	0.11	0.18	0.11	0.14	0.25	0.02	0.25	0.01	0.52
Arapaho National Forest	0.27	0	0.13	0.13	0	0	0	0	0.11
Ashley National Forest	0	0.45	0	0.12	0	0.01	0.04	0.02	0
Beaverhead National Forest	0	0.32	0	0.07	0.04	0	0.07	0	0
Bienville National Forest	0.18	0	0.14	0.04	0	0.44	0.43	0	0.93
Bighorn National Forest	0	0.59	0	0	0.96	0	0.14	0	0.53
Bitterroot National Forest	0	0.75	0	0.04	0.39	0	0	0	0.21
Black Hills National Forest	0.01	0.56	0.15	0.63	0.03	0.52	0.03	0.49	0.3
Black Kettle National GrassLand	0.49	0	0.98	0	0	0.33	0.09	0	0.27
Boise National Forest	0	0.01	0	0	0.39	0	0	0.04	0
Bridger National Forest	0	0.8	0.09	0.98	0	0.34	0.6	0.18	0.36
Buffalo Gap National Grassland	0.42	0.56	0.05	0.01	0.05	0.88	0.7	0.61	0.11
Cache National Forest	0	0.94	0	0.48	0	0.54	0.06	0.4	0.08
Caddo National GrassLand	0.8	0	0.77	0	0	0.21	0.7	0	0.99
Caribou National Forest	0	0.83	0.03	0.21	0	0.02	0.01	0.83	0.03
Carson National Forest	0.32	0	0.13	0.23	0	0.17	0	0	0.12
Cedar River National Grassland	0.69	0.91	0.57	0	0.21	0.35	0.64	0.91	0.33
Challis National Forest	0	0.05	0	0.49	0.01	0.04	0.25	0.81	0.08
Chattahoochee National Forest	0.05	0.01	0.05	0.05	0	0.1	0.01	0	0.09
Chequamegon National Forest	0.01	0.8	0.03	0	0	0.11	0.05	0.17	0.03
Cherokee National Forest	0	0.69	0.01	0.04	0	0.21	0.04	0.29	0.03
Chippewa National Forest	0.5	0.54	0.04	0	0	0.29	0.3	0.18	0.01
Cibola National Forest	0.26	0	0.08	0	0	0.6	0	0	0.72
Cimarron National GrassLand	0.15	0	0.54	0.02	0	0.59	0.69	0	0.43
Clearwater National Forest	0.01	0.04	0.12	0.03	0.2	0	0.26	0	0
Cleveland National Forest	0.04	0.14	0	0	0	0.19	0	0.04	0
Coconino National Forest	0.22	0	0.02	0	0	0.07	0	0	0.14
Coeur D'Alene National Forest	0.01	0.04	0.12	0.03	0.2	0	0.26	0	0
Colville National Forest	0	0.08	0.01	0.89	0.77	0.08	0.01	0.56	0.13
Comanche National Grassland	0.37	0	0.06	0.24	0	0.01	0	0	0
Conecuh National Forest	0.85	0	0.67	0.43	0	0.33	0.77	0	0.25
Coronado National Forest	0.64	0	0.08	0	0	0.44	0.01	0	0.98
Croatan National Forest	0.02	0.64	0.02	0	0	0.09	0.11	0.78	0.17
Crooked River National Grassland	0.69	0.8	0.86	0.13	0.12	0.21	0	0	0

Curlew National Grassland	0	0.2	0	0.14	0.1	0	0.01	0.94	0
Custer National Forest	0.16	0.73	0.4	0.06	0.04	0.44	0.29	0.2	0.89
Daniel Boone National Forest	0.01	0.48	0	0.03	0.02	0.03	0.09	0.07	0.01
Davy Crockett National Forest	0.34	0	0.38	0.05	0	0.19	0.24	0	0.07
Deerlodge National Forest	0	0.05	0	0.01	0.33	0	0.66	0	0.08
Delta National Forest	0.37	0	0.11	0.02	0	0.37	0.16	0	0.23
Deschutes National Forest	0.69	0.8	0.86	0.13	0.12	0.21	0	0	0
DeSoto National Forest	0.52	0	0.4	0.31	0	0.26	0.93	0	0.63
Dixie National Forest	0.03	0.1	0.01	0.48	0	0.56	0.02	0.05	0.69
Eldorado National Forest	0.09	0.15	0	0.1	0.96	0.06	0.34	0.3	0
Finger Lakes National Forest	0	0.08	0	0	0	0.49	0	0.61	0
Fishlake National Forest	0	0.43	0	0.05	0.03	0	0	0.94	0
Flathead National Forest	0	0.17	0.02	0.61	0.15	0.23	0.94	0	0.26
Fort Pierre National Grassland	0.42	0.81	0.47	0	0.09	0.26	0.93	0.67	0.61
Francis Marion National Forest	0.02	0.66	0.08	0	0	0.09	0.29	0.12	0.45
Fremont National Forest	0.04	0.07	0.01	0.85	0.25	0.91	0	0.04	0
Gallatin National Forest	0	0.11	0	0.31	0.59	0	0.44	0.08	0
George Washington National Forest	0	0.03	0	0.18	0.03	0.12	0.01	0.16	0.02
Gifford Pinchot National Forest	0.42	0.7	0.17	0.72	0.02	0.03	0	0	0
Gila National Forest	0.39	0	0.11	0	0	0.83	0.03	0	0.56
Grand Mesa National Forest	0.02	0.02	0	0.64	0	0.09	0.21	0	0
Green Mountain National Forest	0	0.2	0	0.86	0	0.12	0	0.93	0.03
Gunnison National Forest	0.8	0	0	0.34	0	0.01	0.01	0	0.59
Helena National Forest	0	0.25	0	0.3	0.39	0	0.17	0	0
Hiawatha National Forest	0	0.09	0.01	0.34	0.01	0.42	0	0.01	0.01
Holly Springs National Forest	0.23	0	0.02	0	0	0.19	0.44	0	0.02
Homochitto National Forest	0.19	0	0.57	0.19	0	0.43	0.42	0	0.96
Hoosier National Forest	0.01	0.78	0.02	0	0	0.52	0.01	0.25	0.01
Humboldt National Forest	0	0	0	0.33	0.05	0.02	0.07	0.22	0
Huron National Forest	0	0.12	0.02	0.27	0	0.48	0	0.01	0
Inyo National Forest	0.25	0.08	0	0	0.63	0	0.37	0.69	0
Jefferson National Forest	0	0.16	0	0.21	0.01	0.01	0.02	0.01	0.01
Kaibab National Forest	0.25	0.03	0	0.48	0	0.06	0	0.03	0.27
Kaniksu National Forest	0	0	0.01	0.25	0.17	0.01	0.01	0.73	0.67
Kiowa National Grassland	0.05	0	0.66	0.02	0	0.54	0	0	0.43
Kisatchie National Forest	0.6	0	0.49	0.07	0	0.49	0.99	0	0.19
Klamath National Forest	0.02	0.03	0	0.99	0.01	0.19	0.06	0.08	0
Kootenai National Forest	0	0.03	0.34	0.7	0.98	0.21	0.16	0.08	0.1
La Sal National Forest	0.05	0.02	0	0.17	0	0	0.12	0.04	0.54
Lassen National Forest	0.03	0.1	0	0.17	0.44	0.59	0.06	0.29	0
Lewis and Clark National Forest	0	0.17	0.02	0.61	0.15	0.23	0.94	0	0.26
Lincoln National Forest	0.66	0	0.22	0	0	0.85	0.03	0	0.52

Little Missouri National Grassland	0.93	0.78	0.96	0	0.02	0.03	0.06	0.49	0.02
Lolo National Forest	0	0.01	0.01	0.5	0.83	0.05	0	0.07	0.1
Los Padres National Forest	0.36	0.04	0	0.91	0.5	0	0.04	0.07	0
Lyndon B Johnson National GrassLand	0.29	0	0.75	0	0	0.1	0.01	0	0.13
Malheur National Forest	0	0.07	0	0.25	0.37	0.02	0.72	0.26	0.12
Manistee National Forest	0	0.04	0.12	0.02	0	0.24	0	0	0.08
Manti National Forest	0	0.06	0	0.39	0	0.07	0.01	0.13	0.02
Manti-La Sal National Forest - La Sal Division	0.3	0.01	0	0.35	0	0.02	0	0	0.01
Mark Twain National Forest	0.57	0	0.3	0	0	0.96	0.88	0	0.6
McClellan Creek National Grassland	0.1	0	0.96	0	0	0.44	0	0	0.05
Medicine Bow National Forest	0	0.5	0	0.32	0	0.01	0.56	0.03	0.24
Mendocino National Forest	0.91	0.63	0	0	0.09	0.01	0.4	0.77	0
Midewin National Tallgrass Prairie	0.01	0.12	0	0.01	0	0.61	0	0.08	0
Modoc National Forest	0.02	0.03	0	0.99	0.01	0.19	0.06	0.08	0
Monongahela National Forest	0	0.25	0.01	0.39	0.01	0.14	0.04	0.85	0.08
Mount Baker National Forest	0.78	0.16	0.5	0.01	0.88	0.66	0	0	0
Mount Baker-Snoqualmie National Forest	0	0	0	0	0.01	0.31	0	0.03	0.01
Mount Hood National Forest	0.08	0.14	0.94	0.18	0.73	0.78	0.15	0.47	0.53
Nantahala National Forest	0.06	0.08	0.09	0.57	0.01	0.01	0.02	0	0.14
Nebraska National Forest	0.81	0.01	0.07	0	0	0.99	0.13	0	0.29
Nez Perce National Forest	0	0.07	0	0.69	0.04	0.16	0.53	0.05	0.78
Nicolet National Forest	0	0.85	0.02	0.01	0	0.42	0	0.14	0.02
Ocala National Forest	0.48	0.81	0.04	0.31	0.02	0.01	0.05	0.15	0.18
Oconee National Forest	0.08	0.01	0.06	0.81	0.01	0.01	0.07	0	0.15
Oglala National Grassland	0.17	0.32	0.42	0.5	0.01	0.43	0.6	0.06	0.64
Okanogan National Forest	0.1	0.13	0	0	0	0.04	0.02	0.01	0
Olympic National Forest	0	0.05	0.01	0	0	0.01	0	0.1	0.04
Oregon Dunes National Recreation Area	0.19	0.69	0.15	0.01	0	0	0.27	0.37	0.19
Osceola National Forest	0	0.08	0.06	0.01	0.08	0.34	0.01	0.15	0.16
Ottawa National Forest	0	0.75	0.02	0	0	0.28	0.14	0.02	0.13
Ouachita National Forest	0.94	0	0.52	0	0	0.67	0.6	0	0.98
Ozark National Forest	0.99	0	0.2	0	0	0.48	0.66	0	0.52
Pawnee National Grassland	0.18	0	0.25	0.86	0	0.06	0.75	0	0.31
Pike National Forest	0.06	0	0	0.08	0	0	0.04	0	0.3
Pisgah National Forest	0	0.22	0.01	0.35	0	0.01	0.03	0.01	0.01
Plumas National Forest	0.06	0.15	0	0	0.12	0	0.11	0.38	0
Poyette National Forest	0	0.13	0	0.04	0.8	0	0.01	0.56	0.04
Prescott National Forest	0.01	0	0	0.36	0	0.35	0.63	0.01	0
Rich Mountain Wilderness	0.08	0.01	0.05	0.03	0	0.14	0.42	0	0.36
Rio Grande National Forest	0.44	0	0.01	0.5	0	0	0	0	0.04
Rita Blanca National Grassland	0.05	0	0.66	0.02	0	0.54	0	0	0.43

Rita Blanca National Grassland	0.05	0	0.66	0.02	0	0.54	0	0	0.43
Rogue River National Forest	0.94	0.81	0.05	0.83	0.08	0.26	0.7	0.53	0.18
Roosevelt National Forest	0.27	0	0.13	0.13	0	0	0	0	0.11
Routt National Forest	0.27	0	0.13	0.13	0	0	0	0	0.11
Sabine National Forest	0.22	0	0.52	0.02	0	0.36	0.34	0	0.22
Saint Francis National Forest	0.52	0	0.14	0.01	0	0.17	0.39	0	0.09
Saint Joe National Forest	0.01	0.04	0.12	0.03	0.2	0	0.26	0	0
Salmon National Forest	0	0.75	0	0.04	0.39	0	0	0	0.21
Sam Houston National Forest	0.56	0	0.42	0.03	0	0.24	0.28	0	0.07
Samuel R McKelvie National Forest	0.61	0.01	0.11	0	0	0.73	0.21	0.01	0
San Bernardino National Forest	0.31	0.13	0	0.04	0.07	0.01	0.03	0.1	0
San Isabel National Forest	0.44	0	0.01	0.5	0	0	0	0	0.04
San Juan National Forest	0.8	0	0	0.34	0	0.01	0.01	0	0.59
Santa Fe National Forest	0.12	0	0.02	0.57	0	0.02	0	0	0.44
Sawtooth National Forest	0	0.05	0	0.49	0.01	0.04	0.25	0.81	0.08
Sequoia National Forest	0.43	0.01	0	0.83	0.88	0.01	0.85	0.02	0
Shasta National Forest	0.02	0.05	0	0.36	0.49	0.96	0.03	0.12	0
Sheyenne National Grassland	0.78	0.38	0.4	0	0	0.06	0.53	0.53	0.17
Shoshone National Forest	0	0.61	0	0.01	0.54	0	0	0.15	0.01
Sierra National Forest	0.91	0.44	0	0.29	0.09	0.47	0.12	0.73	0
Siskiyou National Forest	0.2	0.64	0.01	0.38	0.08	0.13	0.27	0.81	0.03
Sitgreaves National Forest	0.54	0	0	0	0	0.31	0	0	0.05
Siuslaw National Forest	0.3	0.52	0.72	0	0	0	0.39	0.32	0.61
Six Rivers National Forest	0.2	0.31	0	0.07	0.88	0.99	0.27	0.88	0
Snoqualmie National Forest	0.07	0.13	0.78	0.31	0.44	0.39	0.12	0.27	0.42
Stanislaus National Forest	0.11	0.08	0	0.02	0.78	0.02	0.77	0.25	0
Sumter National Forest	0.01	0.15	0.02	0.89	0.02	0.01	0	0.02	0.01
Superior National Forest	0.01	0.44	0	0	0	0.15	0.04	0.81	0.01
Tahoe National Forest	0.01	0.08	0	0.01	0.42	0.11	0.15	0.52	0
Talladega National Forest	0.56	0	0.2	0.24	0	0.18	0.81	0	0.66
Targhee National Forest	0	0.32	0	0.07	0.04	0	0.07	0	0
Teton National Forest	0	0.7	0.02	0.08	0.02	0	0.63	0.23	0.98
Thunder Basin National Grassland	0	0.57	0.09	0.12	0	0.59	0.2	0.38	0.57
Toiyabe National Forest	0	0.03	0	0.02	0.01	0.48	0.26	0.18	0
Tombigbee National Forest	0.2	0	0.03	0.09	0	0.04	0.52	0	0.06
Tonto National Forest	0.83	0.01	0	0.01	0	0	0.04	0.15	0.01
Trinity National Forest	0.17	0.2	0	0.14	0.01	0	0.38	0.38	0
Tuskegee National Forest	0.42	0	0.18	0.98	0	0.04	0.86	0	0.77
Uinta National Forest	0	0.03	0	0.47	0	0.08	0.26	0.01	0.38
Umatilla National Forest	0	0.02	0	0.85	0.49	0.05	0	0.48	0
Umpqua National Forest	0.04	0.07	0.01	0.85	0.25	0.91	0	0.04	0
Uncompahgre National Forest	0.08	0.01	0	0.4	0	0	0.73	0	0

Uwharrie National Forest	0	0.48	0	0.94	0.05	0.02	0	0.83	0.01
Wallowa-Whitman National Forest	0	0.43	0	0.02	0.98	0	0	0.42	0
Wasatch National Forest	0	0.45	0	0.12	0	0.01	0.04	0.02	0
Wayne National Forest	0	0.7	0.01	0.02	0	0.11	0.04	0.1	0.01
Wenatchee National Forest	0.49	0.53	0.44	0.05	0.36	0.47	0	0	0
White Mountain National Forest	0	0.18	0	0.21	0	0.49	0.02	0.7	0.03
White River National Forest	0	0.34	0	0	0	0	0.25	0.04	0.11
William B. Bankhead National Forest	0.15	0	0.09	0.24	0	0.01	0.34	0	0.26
Winema National Forest	0.69	0.8	0.86	0.13	0.12	0.21	0	0	0
Yurok Redwood Experimental Forest	0.11	0.32	0	0.17	0.83	0.86	0.16	0.45	0

Table B-3. P-values of Wilcoxon signed-ranked test at the 5% level (Aridity, Evaporative)

Name	Aridity index			Evaporative index		
	MID	DRY	WET	MID	DRY	WET
Allegheny National Forest	0	0.34	0.01	0.12	0.04	0.07
Angeles National Forest	0.49	0.15	0	0	0.45	0.24
Angelina National Forest	0.23	0	0.3	0.21	0	0.05
Apache National Forest	0.31	0	0.02	0	0	0
Apalachicola National Forest	0.18	0.17	0.09	0.57	0	0.7
Arapaho National Forest	0.23	0	0.03	0	0	0.02
Ashley National Forest	0	0.17	0	0.1	0.01	0.19
Beaverhead National Forest	0	0.73	0	0.02	0	0.63
Bienville National Forest	0.5	0	0.38	0.88	0	0.37
Bighorn National Forest	0	0.73	0	0	0	0
Bitterroot National Forest	0.01	0.83	0	0	0	0
Black Hills National Forest	0.04	0.77	0.2	0.05	0.42	0.37
Black Kettle National GrassLand	0.17	0	0.54	0	0	0
Boise National Forest	0	0.06	0	0.02	0.17	0.02
Bridger National Forest	0	0.8	0	0.02	0.05	0.53
Buffalo Gap National Grassland	0.94	0.25	0.13	0.44	0.6	0.21
Cache National Forest	0	0.24	0	0.33	0.11	0.73
Caddo National GrassLand	0.47	0	0.85	0.43	0	0.98
Caribou National Forest	0	0.38	0.02	0.21	0.78	0.32
Carson National Forest	0.27	0	0.19	0	0	0.01
Cedar River National Grassland	0.66	0.73	0.67	0.66	0.93	0.36
Challis National Forest	0	0.34	0	0.2	0.21	0.52
Chattahoochee National Forest	0.12	0	0.08	0.1	0	0.21
Chequamegon National Forest	0.2	0.19	0.12	0.53	0.01	0.26
Cherokee National Forest	0.01	0.53	0.01	0.49	0.02	0.48
Chippewa National Forest	0.5	0.06	0.28	0.73	0.21	0.05
Cibola National Forest	0.09	0	0.02	0	0	0.01
Cimarron National GrassLand	0.09	0	0.99	0.61	0	0.99
Clearwater National Forest	0	0.08	0.04	0	0	0
Cleveland National Forest	0.03	0.49	0	0	0.02	0.02
Coconino National Forest	0.78	0	0.14	0	0	0
Coeur D'Alene National Forest	0	0.08	0.04	0	0	0
Colville National Forest	0	0.14	0.01	0.77	0.12	0.53
Comanche National Grassland	0.29	0	0.1	0	0	0
Conecuh National Forest	0.88	0	0.73	0.53	0	0.04
Coronado National Forest	0.21	0	0.15	0	0	0.47

Croatan National Forest	0.1	0.54	0.09	0.69	0.98	0.52
Crooked River National Grassland	0.83	0.75	0.69	0	0	0
Curlew National Grassland	0	0.57	0	0.02	0.06	0.14
Custer National Forest	0.3	0.59	0.93	0.39	0.14	0.88
Daniel Boone National Forest	0.03	0.2	0	0.85	0.01	0.05
Davy Crockett National Forest	0.23	0	0.3	0.21	0	0.05
Deerlodge National Forest	0	0.11	0	0.03	0	0.33
Delta National Forest	0.8	0	0.24	0.48	0	0.47
Deschutes National Forest	0.83	0.75	0.69	0	0	0
DeSoto National Forest	0.72	0	0.57	0.57	0	0.16
Dixie National Forest	0.04	0.03	0.01	0	0.15	0
Eldorado National Forest	0.06	0.39	0	0.99	0.47	0.04
Finger Lakes National Forest	0	0.59	0	0.04	0.38	0.02
Fishlake National Forest	0	0.72	0	0.1	0.81	0.02
Flathead National Forest	0	0.63	0.03	0	0	0
Fort Pierre National Grassland	0.96	0.88	0.75	0.54	0.17	0.83
Francis Marion National Forest	0.1	0.21	0.18	0.89	0.07	0.75
Fremont National Forest	0.03	0.18	0.01	0	0	0
Gallatin National Forest	0.01	0.47	0	0	0	0.61
George Washington National Forest	0	0.14	0.01	0.33	0.69	0.27
Gifford Pinchot National Forest	0.35	0.44	0.52	0	0	0
Gila National Forest	0.1	0	0.24	0	0	0.16
Grand Mesa National Forest	0.09	0.01	0.01	0.75	0	0.23
Green Mountain National Forest	0	0.81	0	0.36	0.09	0.91
Gunnison National Forest	0.88	0	0	0	0.02	0.54
Helena National Forest	0	0.8	0	0	0	0.98
Hiawatha National Forest	0	0.06	0.03	0.01	0.01	0.34
Holly Springs National Forest	0.8	0	0.08	0.53	0	0.05
Homochitto National Forest	0.57	0	0.66	0.67	0	0.67
Hoosier National Forest	0.09	0.39	0.03	0.02	0.05	0.09
Humboldt National Forest	0	0.02	0	0.47	0.88	0.24
Huron National Forest	0	0.05	0.08	0	0.02	0.04
Inyo National Forest	0.1	0.25	0	0.04	0.54	0.2
Jefferson National Forest	0.01	0.09	0	0.5	0	0.05
Kaibab National Forest	0.29	0.01	0	0	0.26	0.35
Kaniksu National Forest	0	0	0	0.59	0.07	0.2
Kiowa National Grassland	0.03	0	0.77	0	0	0.03
Kisatchie National Forest	0.98	0	0.63	0.61	0	0.14
Klamath National Forest	0.02	0.15	0	0.57	0.32	0.02
Kootenai National Forest	0	0.05	0.24	0.2	0	0
La Sal National Forest	0.08	0.01	0	0.01	0.15	0.59
Lassen National Forest	0.01	0.25	0	0.91	0.67	0.03
Lewis and Clark National Forest	0	0.63	0.03	0	0	0

Lincoln National Forest	0.56	0	0.3	0	0	0.24
Little Missouri National Grassland	0.53	0.32	0.38	0.01	0.54	0
Lolo National Forest	0	0.04	0.01	0.04	0.01	0
Los Padres National Forest	0.57	0.13	0	0.02	0.09	0.17
Lyndon B Johnson National GrassLand	0.1	0	0.56	0	0	0.02
Malheur National Forest	0	0.3	0	0.06	0	0.15
Manistee National Forest	0	0.01	0.33	0	0	0.35
Manti National Forest	0.01	0.01	0.01	0.14	0.25	0.11
Manti-La Sal National Forest - La Sal Division	0.54	0	0.01	0	0.18	0.75
Mark Twain National Forest	0.52	0	0.42	0.49	0.03	0.98
McClellan Creek National Grassland	0.03	0	0.48	0	0	0.02
Medicine Bow National Forest	0	0.14	0	0.04	0.01	0.49
Mendocino National Forest	0.42	0.66	0	0.02	0.15	0.31
Midewin National Tallgrass Prairie	0.12	0.06	0.02	0	0.12	0.01
Modoc National Forest	0.02	0.15	0	0.57	0.32	0.02
Monongahela National Forest	0.01	0.89	0.01	0.85	0.29	0.43
Mount Baker National Forest	0.73	0.33	0.42	0	0	0
Mount Baker-Snoqualmie National Forest	0.05	0.08	0.06	0.54	0.11	0.25
Mount Hood National Forest	0.09	0.32	0.78	0.04	0.01	0.01
Nantahala National Forest	0.07	0	0.01	0.49	0	0.23
Nantahala National Forest	0.01	0.01	0	0.33	0	0.07
Nebraska National Forest	0.99	0.13	0.52	0.08	0	0.11
Nez Perce National Forest	0	0.42	0.01	0.11	0	0.01
Nicolet National Forest	0	0.35	0.06	0	0.16	0.36
Ocala National Forest	0.59	0.59	0.05	0.03	0.05	0.48
Ochoco National Forest	0	0.09	0	0.21	0.36	0.01
Oconee National Forest	0.15	0	0.05	0.3	0.01	0.32
Oglala National Grassland	0.49	0.21	0.5	0.5	0.01	0.57
Okanogan National Forest	0.5	0.44	0.03	0.75	0.64	0.89
Olympic National Forest	0.04	0.1	0.15	0.85	0.14	0.23
Oregon Dunes National Recreation Area	0.27	0.26	0.49	0.6	0.01	0.35
Osceola National Forest	0.04	0.1	0.15	0.85	0.14	0.23
Ottawa National Forest	0.02	0.25	0.05	0.47	0	0.6
Ouachita National Forest	0.45	0	0.66	0.42	0	0.96
Ozark National Forest	0.21	0	0.25	0.24	0	0.86
Pawnee National Grassland	0.31	0	0.19	0.35	0	0.36
Pike National Forest	0.09	0	0	0	0	0.69
Pisgah National Forest	0.01	0.1	0.01	0.52	0	0.12
Plumas National Forest	0.01	0.22	0	0.91	0.94	0.01
Poyette National Forest	0	0.32	0	0.93	0.44	0.83
Prescott National Forest	0.01	0.05	0	0.88	0.2	0.04

Rich Mountain Wilderness	0.23	0	0.03	0.73	0	0.93
Rio Grande National Forest	0.64	0	0.01	0	0	0.01
Rita Blanca National Grassland	0.03	0	0.77	0	0	0.03
Rogue River National Forest	0.85	0.72	0.07	0.22	0.14	0.49
Roosevelt National Forest	0.23	0	0.03	0	0	0.02
Routt National Forest	0.23	0	0.03	0	0	0.02
Sabine National Forest	0.18	0	0.39	0.31	0	0.2
Saint Francis National Forest	0.77	0	0.25	0.24	0	0.11
Saint Joe National Forest	0	0.08	0.04	0	0	0
Salmon National Forest	0.01	0.83	0	0	0	0
Sam Houston National Forest	0.33	0	0.36	0.29	0	0.05
Samuel R McKelvie National Forest	0.25	0	0.23	0.09	0.01	0
San Bernardino National Forest	0.32	0.4	0	0	0.04	0.09
San Isabel National Forest	0.64	0	0.01	0	0	0.01
San Juan National Forest	0.88	0	0	0	0.02	0.54
Santa Fe National Forest	0.09	0	0.02	0	0	0.06
Sawtooth National Forest	0	0.34	0	0.2	0.21	0.52
Sequoia National Forest	0.49	0.08	0	0.45	0.04	0.04
Shasta National Forest	0.01	0.14	0	0.61	0.66	0.02
Shawnee National Forest	0.44	0.01	0.03	0.21	0.02	0.13
Sheyenne National Grassland	0.14	0.07	0.96	0.28	0.56	0.08
Shoshone National Forest	0	0.94	0	0.69	0	0.5
Sierra National Forest	0.88	0.77	0	0.03	0.94	0.19
Siskiyou National Forest	0.25	0.94	0.02	0.69	0.1	0.18
Sitgreaves National Forest	0.85	0	0	0	0	0.64
Siuslaw National Forest	0.54	0.19	0.33	0.86	0.04	0.47
Six Rivers National Forest	0.11	0.47	0	0.63	0.28	0.06
Snoqualmie National Forest	0.09	0.15	0.93	0.77	0.21	0.23
Stanislaus National Forest	0.05	0.29	0	0.47	0.4	0.15
Sumter National Forest	0.02	0.08	0.01	0.01	0	0.03
Superior National Forest	0.49	0.59	0.03	0.34	0.2	0.11
Tahoe National Forest	0.01	0.27	0	0.36	0.64	0.43
Talladega National Forest	0.19	0	0.03	0.94	0	0.96
Targhee National Forest	0	0.73	0	0.02	0	0.63
Teton National Forest	0	0.8	0.02	0.01	0.02	0.05
Thunder Basin National Grassland	0.03	0.98	0.24	0.8	0.09	0.61
Toiyabe National Forest	0	0.22	0	0.27	0.31	0.22
Tombigbee National Forest	0.6	0	0.06	0.85	0	0.33
Tonto National Forest	0.44	0	0	0	0.39	0.11
Trinity National Forest	0.23	0.59	0	0.48	0.36	0.02
Tuskegee National Forest	0.56	0	0.17	0.6	0	0.38
Uinta National Forest	0.01	0.01	0.01	0.01	0.02	0.63
Umatilla National Forest	0	0.08	0	0.06	0.09	0.01

Umpqua National Forest	0.03	0.18	0.01	0	0	0
Uncompahgre National Forest	0.18	0	0	0.2	0	0.17
Uwharrie National Forest	0	0.73	0	0.06	0.37	0.06
Wallowa-Whitman National Forest	0	0.7	0	0.21	0.1	0.17
Wasatch National Forest	0	0.53	0	0.43	0.01	0.67
Wayne National Forest	0.02	0.35	0.01	0.34	0.04	0.08
Wenatchee National Forest	0.37	0.53	0.77	0	0	0
White Mountain National Forest	0	0.53	0.01	0.57	0.17	0.85
White River National Forest	0	0.22	0	0.28	0.01	0.69
William B. Bankhead National Forest	0.49	0	0.08	0.75	0	0.8
Winema National Forest	0.83	0.75	0.69	0	0	0
Yurok Redwood Experimental Forest	0.05	0.49	0	0.45	0.16	0.43

Table B-4. Changes in the direction and magnitude of the Budyko space for the U.S. national forests and grasslands

	Current		Future (WET)		Future (MID)		Future (DRY)	
Name	x1	y1	Dir	Mag	Dir	Mag	Dir	Mag
Tonto National Forest	5	0.9	180.8	1.7	6.2	0.2	359.8	2.1
Sitgreaves National Forest	6.5	1	180	1.8	178.5	0.1	0	4.3
Coconino National Forest	5.1	1	179.3	0.8	177.3	0.3	0.1	3.9
Kaibab National Forest	5.9	0.9	179.5	1.2	176.5	0.6	0.2	2.7
Prescott National Forest	6	0.9	180.4	2.2	179.6	1.5	180	2.2
Coronado National Forest	5.7	1	180.2	1	3.5	0.3	0.1	5.8
Saint Francis National Forest	1.2	0.6	201.5	0.1	254	0	15	0.5
Ouachita National Forest	1.2	0.6	176.4	0.1	29.6	0.1	12.3	0.7
Ozark National Forest	1.3	0.7	187.2	0.1	15.9	0.1	13.5	0.6
Tuskegee National Forest	1.2	0.7	172.8	0.1	170.8	0	16.5	0.3
Conecuh National Forest	1.1	0.6	135.6	0	113	0	19.3	0.3
William B. Bankhead National Forest	1.1	0.6	184.5	0.1	187.1	0.1	20.8	0.3
Talladega National Forest	1.2	0.6	181.9	0.1	186.3	0.1	17.2	0.3
Roosevelt National Forest	2.6	0.8	172.7	0.3	155.8	0.2	10.4	0.7
Grand Mesa National Forest	4.6	0.7	182.9	1.1	180.6	0.7	2.4	1.1
Arapaho National Forest	2.8	0.8	178	0.4	170.7	0.3	7	0.7
White River National Forest	2.8	0.7	179.1	0.5	172.8	0.3	8.3	0.7
San Juan National Forest	2.3	0.7	178.8	0.5	128.6	0.1	5.4	0.8
Pike National Forest	3.4	0.9	178.8	0.6	168.4	0.2	2.7	1.2
Uncompahgre National Forest	3.3	0.8	183	0.8	173.6	0.3	5.1	1
Gunnison National Forest	2.3	0.7	178.8	0.5	128.6	0.1	5.4	0.8
Rio Grande National Forest	2.8	0.8	179	0.5	141.8	0.1	3.8	1.1
San Isabel National Forest	3.8	1	179.3	0.7	168.2	0.1	0.5	1.8
Comanche National Grassland	4.5	1	178.9	0.6	10.4	0.1	0.3	2.9
Routt National Forest	2.5	0.7	177.4	0.4	171.8	0.3	10	0.5
Tahoe National Forest	2.2	0.6	182.2	0.7	177.4	0.5	178.2	0.4
Stanislaus National Forest	2.2	0.6	186.6	0.8	174.1	0.3	187.4	0.4
Six Rivers National Forest	0.8	0.4	194.8	0.2	175	0.1	166.8	0.1
Sierra National Forest	7.3	0.7	181.4	2.5	4.5	0.6	181.5	0.7
Shasta National Forest	1.5	0.6	191	0.4	186.3	0.3	185.4	0.3
Sequoia National Forest	3.4	0.6	185.2	1.4	96.9	0.2	187.1	0.8
Plumas National Forest	1.3	0.6	191.5	0.5	180.2	0.2	179.4	0.2
Modoc National Forest	4.2	0.7	182.6	1.2	180.8	0.9	182.4	0.8
Mendocino National Forest	1.5	0.6	187.9	0.4	154.6	0.1	179	0.1
Lassen National Forest	2.3	0.6	187.3	0.8	181.8	0.5	184	0.5

Cleveland National Forest	5.4	0.9	181.1	2.2	1.2	1.7	182.8	1.3
Yurok Redwood Experimental Forest	0.6	0.2	186.9	0.1	174.9	0.1	165.6	0.1
Ocala National Forest	1.4	0.7	187.6	0.2	150.9	0.1	13.2	0.2
Apalachicola National Forest	1.2	0.7	180.6	0.1	187.3	0.1	26.3	0.1
Osceola National Forest	1.4	0.8	183.2	0.1	183.9	0.1	5.4	0
Chattahoochee National Forest	1.1	0.6	186.8	0.1	186.2	0.1	21.7	0.2
Rich Mountain Wilderness	1.1	0.6	179	0.1	175.1	0.1	23.1	0.3
Clearwater National Forest	1.5	0.6	144.5	0.2	164.9	0.2	144.8	0.2
Salmon National Forest	2.8	0.8	178.2	0.7	176	0.7	138.3	0.1
Challis National Forest	2.7	0.7	173.3	0.7	175	0.7	167.5	0.3
Coeur D	1.7	0.5	159.4	0.2	173.4	0.3	155.6	0.2
Curlew National Grassland	4.8	0.7	179.2	1.5	178.7	1.5	176	0.4
Boise National Forest	2.3	0.6	179.9	0.5	182.2	0.5	179.5	0.4
Saint Joe National Forest	1.3	0.5	163.9	0.2	177.2	0.2	145.8	0.1
Poyette National Forest	2.1	0.5	176	0.4	178.3	0.4	171.8	0.3
Nez Perce National Forest	2	0.7	170	0.3	174.1	0.4	149.9	0.2
Shawnee National Forest	1.2	0.6	194.1	0.1	244.6	0	19.5	0.2
Hoosier National Forest	1.2	0.6	195.7	0.1	212	0.1	27.4	0.1
Cimarron National GrassLand	4.4	1	180.3	0.3	359.8	0.5	0	3.2
Daniel Boone National Forest	1.3	0.6	188.4	0.2	181.7	0.1	29.1	0.1
Kisatchie National Forest	1.2	0.7	83.9	0	140.2	0	13.7	0.6
Superior National Forest	1.8	0.6	188.4	0.2	189.4	0.1	45.9	0
Chippewa National Forest	1.9	0.8	189.3	0.1	351	0	4.9	0.2
Delta National Forest	1.2	0.6	195.4	0.1	206.5	0	13.5	0.5
Tombigbee National Forest	1.1	0.6	189.8	0.1	174.1	0	16.7	0.4
Holly Springs National Forest	1.1	0.6	196.9	0.1	228	0	17.6	0.3
DeSoto National Forest	1.1	0.7	156.2	0.1	177.1	0	19.2	0.4
Homochitto National Forest	1.2	0.7	180.3	0	202.5	0.1	13.1	0.5
Bienville National Forest	1.2	0.7	176.3	0.1	189.4	0	15.8	0.4
Mark Twain National Forest	1.3	0.7	181	0.1	126.9	0	11.7	0.4
Deerlodge National Forest	2.8	0.8	178.2	0.7	174.7	0.5	135.7	0.1
Gallatin National Forest	2.2	0.7	181.1	0.6	177.1	0.5	157.1	0.2
Lewis and Clark National Forest	3	0.8	177.8	0.6	176.3	0.5	144.4	0.2
Beaverhead National Forest	2.8	0.8	180.3	0.8	177.9	0.7	149.8	0.1
Flathead National Forest	1.8	0.5	164.1	0.2	176.4	0.3	158.6	0.2
Helena National Forest	3	0.8	178.7	0.7	175.8	0.5	158.4	0.2
Lolo National Forest	1.9	0.6	162.5	0.3	172.3	0.3	154.8	0.2
Oglala National Grassland	3.6	1	180	0.4	179.9	0.3	0.5	0.3
Inyo National Forest	1.9	0.7	185.5	0.7	162.8	0.2	179.7	0.4
Humboldt National Forest	5.2	0.9	180.4	1.6	180.1	1.5	170	0.9
Toiyabe National Forest	8.2	0.8	181.4	3.1	179.7	3.1	182.4	1.2

Santa Fe National Forest	4.6	0.9	176.8	0.6	8.7	0.4	1	4.2
Gila National Forest	6.2	0.9	179.1	0.8	3.1	0.5	0.3	6.6
Nantahala National Forest	1.1	0.6	188.8	0.1	186.9	0.1	26.4	0.2
Uwharrie National Forest	1.4	0.7	189.6	0.2	189.6	0.2	162.6	0
Pisgah National Forest	1.2	0.6	187.2	0.2	184.4	0.2	30.8	0.1
Croatan National Forest	1.1	0.7	195.6	0.1	188.7	0.1	258.5	0
Little Missouri National Grassland	3.3	0.9	311.2	0.1	314.8	0.1	177.9	0.2
Wayne National Forest	1.3	0.6	187.4	0.2	187.4	0.1	37.8	0.1
Black Kettle National GrassLand	2.6	1	175.9	0	0.2	0.3	0.1	1.4
Umpqua National Forest	1.6	0.6	181.5	0.2	176.1	0.1	150.4	0.1
Wallowa-Whitman National Forest	2.4	0.6	180.4	0.5	181.1	0.5	123.4	0.1
Malheur National Forest	3.4	0.8	183.2	0.8	181.9	0.6	181.8	0.5
Ochoco National Forest	3.7	0.8	180.4	0.7	178.3	0.5	181.2	0.6
Rogue River National Forest	1.5	0.5	175.7	0.2	159	0.1	143.5	0.1
Deschutes National Forest	1.9	0.6	112.7	0.2	110.4	0.2	122.4	0.2
Mount Hood National Forest	0.9	0.3	128.4	0	168.7	0.1	153.1	0.1
Winema National Forest	1.5	0.6	138.6	0.2	137.5	0.1	138.9	0.2
Fremont National Forest	3.1	0.7	177	0.7	173.9	0.5	177.6	0.6
Oregon Dunes National Recreation Area	0.7	0.4	169.2	0	151.6	0	42	0.1
Crooked River National Grassland	1.8	0.6	85.8	0.1	84	0.1	99.5	0.1
Allegheny National Forest	1.2	0.5	187.1	0.1	183.5	0.1	35.2	0
Sumter National Forest	1.3	0.7	187.7	0.2	189.4	0.2	22	0.1
Black Hills National Forest	3.6	1	180.2	0.4	180.4	0.5	101.6	0.1
Buffalo Gap National Grassland	3.1	1	182.1	0.4	226.3	0.1	219.3	0.2
Lyndon B Johnson National GrassLand	2.2	0.9	17.7	0.1	5.7	0.3	1.6	1.3
Angelina National Forest	1.4	0.8	14.9	0.1	13.8	0.1	8.6	1
Sabine National Forest	1.3	0.8	13	0.1	12.2	0.1	8.9	0.9
Sam Houston National Forest	1.5	0.8	12.5	0.1	6	0.1	6.8	1.1
Davy Crockett National Forest	1.4	0.8	19.4	0.1	14.7	0.1	7.4	1.1
Cache National Forest	2.8	0.8	179.4	0.6	180.1	0.7	89.3	0.2
Wasatch National Forest	3.3	0.8	179.9	0.9	178.5	0.8	46	0.2
Ashley National Forest	4.2	0.9	180.1	1.1	178.3	1	2.8	0.6
Fishlake National Forest	4.1	0.9	182.5	1.1	179.9	0.9	224.2	0.5
Caribou National Forest	3.5	0.8	183.6	0.9	184.2	1	222.5	0.2
Dixie National Forest	5.1	0.9	180.4	1.2	177.3	0.7	143.9	1.3
Uinta National Forest	3.5	0.8	179.5	0.9	177.4	0.7	53.5	0.2
Green Mountain National Forest	1.1	0.5	186	0.1	186	0.2	157.3	0
Umatilla National Forest	2.8	0.7	179.3	0.6	179.4	0.5	131	0.3
Okanogan National Forest	1.9	0.3	164.8	0.2	170.5	0.1	163.9	0.2
Wenatchee National Forest	2.3	0.4	125	0.1	158.7	0.1	161.5	0.3

Osceola National Forest	0.3	0.1	157.9	0	179.1	0	151.7	0
Colville National Forest	2	0.4	176.4	0.2	178.7	0.2	171.1	0.2
Gifford Pinchot National Forest	1.2	0.5	73.2	0.2	104.1	0.1	109.7	0.2
Mount Baker-Snoqualmie National Forest	0.5	0.2	150.4	0.1	157.4	0.1	144.7	0.1
Nicolet National Forest	1.7	0.7	187.9	0.2	190.6	0.3	9.6	0.1
Teton National Forest	2.7	0.6	174.8	0.4	175.5	0.5	38.5	0.1
Medicine Bow National Forest	3.8	0.8	178.8	0.6	177.6	0.6	6.5	0.3
Thunder Basin National Grassland	4.3	1	179.8	0.5	179.9	0.6	14.1	0.2
Shoshone National Forest	3.4	0.6	178.3	0.6	177.9	0.6	85.9	0.1
Bighorn National Forest	3.4	0.9	178.1	0.7	177.6	0.8	150.5	0.1
Bridger National Forest	3.3	0.7	175.1	0.5	174.8	0.6	95.3	0.1
Manistee National Forest	1.5	0.6	187.1	0	196.5	0.2	11.5	0.2
Ottawa National Forest	1.5	0.6	177.3	0.1	174.7	0.1	31.2	0.1
Hiawatha National Forest	1.5	0.5	185.7	0.1	190.5	0.2	13	0.2
Huron National Forest	1.8	0.7	186.2	0.1	189.1	0.3	5.2	0.2
Siskiyou National Forest	1.2	0.4	190.3	0.1	182.9	0.1	109	0
Siuslaw National Forest	0.6	0.3	168	0	185.1	0	46.6	0
Cherokee National Forest	1.2	0.6	183.5	0.2	177.3	0.1	36.6	0.2
Los Padres National Forest	7.8	0.7	181.2	2.9	4.2	1	182	2
Angeles National Forest	4	0.8	180.8	1.3	4.5	1.2	182	1
Nebraska National Forest	3.1	0.9	179.4	0.3	122	0.1	1.1	0.5
Midewin National Tallgrass Prairie	1.4	0.6	201	0.1	211.4	0.1	13.9	0.1
McClellan Creek National Grassland	3.3	1	7.7	0.1	0.9	0.7	0.4	2.3
Kaniksu National Forest	1.4	0.5	162.9	0.1	177.7	0.2	160.9	0.2
Bitterroot National Forest	2.2	0.7	168.3	0.4	165.7	0.3	93.4	0.1
Samuel R McKelvie National Forest	2.7	0.9	193.1	0.4	352.7	0.2	2	0.6
Kootenai National Forest	1.6	0.6	149.2	0.1	174.7	0.3	155.9	0.2
Eldorado National Forest	2.1	0.6	188.2	0.7	181.9	0.3	187.5	0.3
Apache National Forest	4.8	1	179.7	1	2.2	0.2	0.1	4.4
Carson National Forest	3.8	0.8	180.3	0.6	40.2	0.1	2.5	2.4
Chequamegon National Forest	1.6	0.7	188.9	0.1	188.4	0.1	14.7	0.1
Cibola National Forest	6.1	1	179.5	0.9	1.6	0.5	0.2	5.8
George Washington National Forest	1.5	0.7	185.3	0.2	183.6	0.2	175.6	0.1
Jefferson National Forest	1.4	0.7	182.1	0.2	179.8	0.2	155.2	0
Klamath National Forest	2.4	0.8	180.2	0.5	170.4	0.3	168.5	0.3
Lincoln National Forest	6.7	0.9	178.5	0.6	1.9	0.6	0.2	6.4
Monongahela National Forest	1.4	0.7	183.5	0.2	181	0.2	152.6	0
San Bernardino National Forest	4.9	0.8	182.3	2	3.2	1.2	183.9	1.4
Targhee National Forest	3.2	0.8	179.3	0.9	177.6	0.9	152.6	0.1

Trinity National Forest	1.1	0.6	190.6	0.3	175	0.1	173	0.1
White Mountain National Forest	1	0.4	180.2	0.1	173.3	0.1	129.5	0
Custer National Forest	3.3	0.8	183.6	0.3	180.2	0.4	48.5	0.2
Francis Marion National Forest	1.3	0.7	186.7	0.1	184	0.1	12.3	0.1
Cedar River National Grassland	3.3	1	341.4	0	349.3	0	359.7	0.1
Fort Pierre National Grassland	2.5	1	187.5	0.4	259.7	0	359.5	0.4
Fort Pierre National Grassland	3.5	1	187.5	0.1	189.4	0.1	73.9	0.1
Kiowa National Grassland	4.6	1	179.6	0.2	0.5	0.6	0.1	3.9
Pawnee National Grassland	4.2	0.9	182	0.5	178.7	0.4	2.4	1.1
Rita Blanca National Grassland	4.7	1	179.7	0.1	0.1	0.8	0	3.7
Sheyenne National Grassland	2.1	1	186.3	0.1	358.4	0.2	360	0.3
Finger Lakes National Forest	1.3	0.6	189.9	0.2	188.8	0.1	163.1	0
Sawtooth National Forest	4.7	0.8	178.8	1.3	178.6	1.3	176.8	0.4
Snoqualmie National Forest	0.6	0.2	129.6	0	176.5	0	155.5	0.1
Mount Baker National Forest	0.6	0.2	150.5	0.1	161.8	0.1	153.1	0.1
La Sal National Forest	4.3	0.9	180.2	1.1	173	0.5	1.6	1.4
Manti National Forest	5	0.8	183.1	1.1	181.8	0.9	2	1
Caddo National GrassLand	1.5	0.8	207.2	0	9.6	0.1	6.8	0.9
Jefferson National Forest	1.4	0.6	183	0.2	177	0.2	39.2	0.1

APPENDIX C

SUPPORTING INFORMATION FOR CHAPTER 4:

A PROBABILISTIC APPROACH FOR CHARACTERIZATION OF SUB-ANNUAL SOCIOECONOMIC DROUGHT INTENSITY-DURATION-FREQUENCY (IDF) RELATIONSHIPS IN A CHANGING ENVIRONMENT

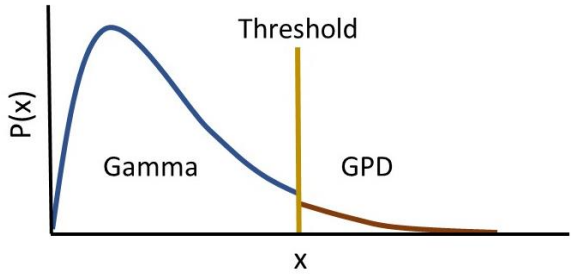

Figure C-1. Schematic of Gamma-GPD mixture model.

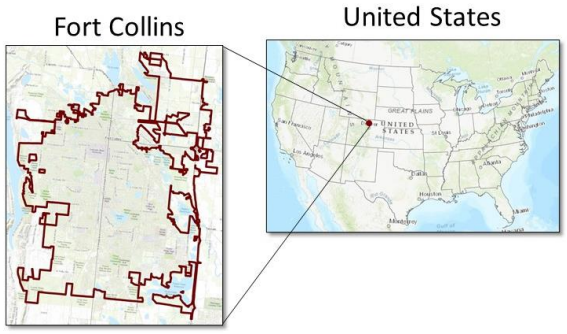

Figure C-2. City of Fort Collins, Colorado, USA.

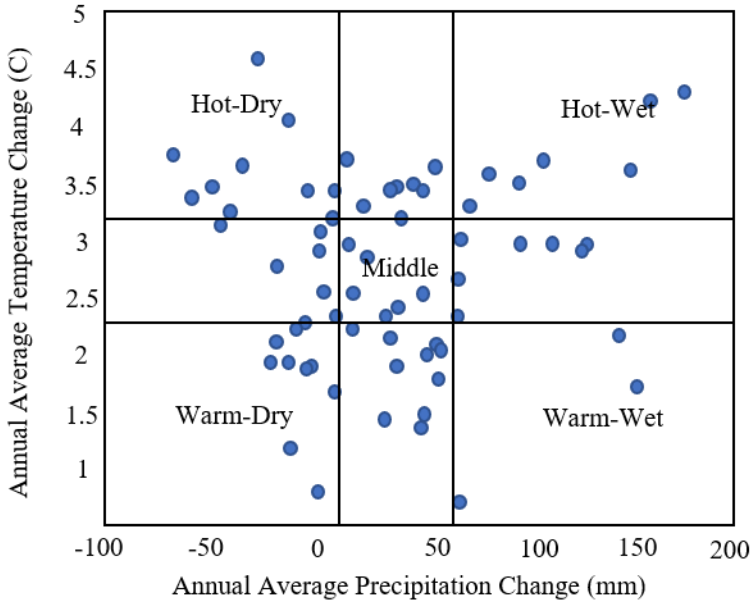

Figure C-3. Classification of downscaled climate scenarios into hot-dry, hot-wet, warm-dry, warm-wet, and median categories based on the difference in current and future temperature and precipitation.

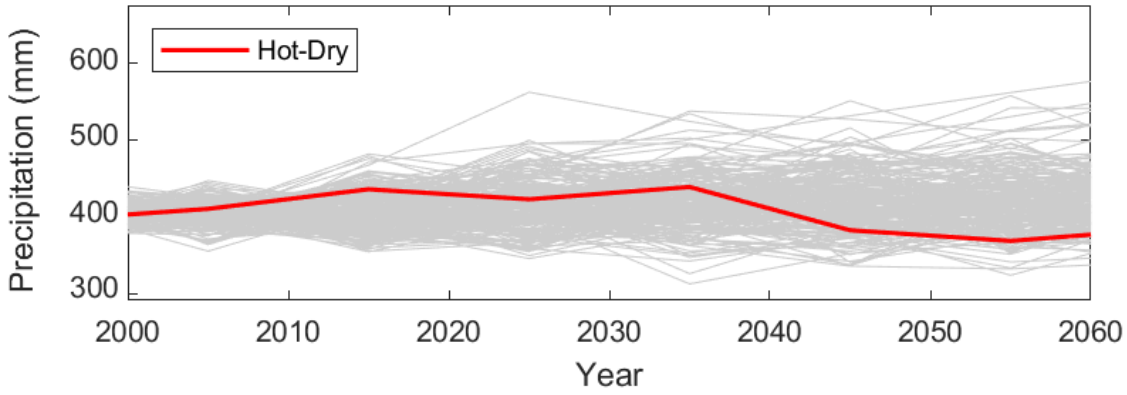

Figure C-4. 30-year normal annual precipitation from the current conditions to the future

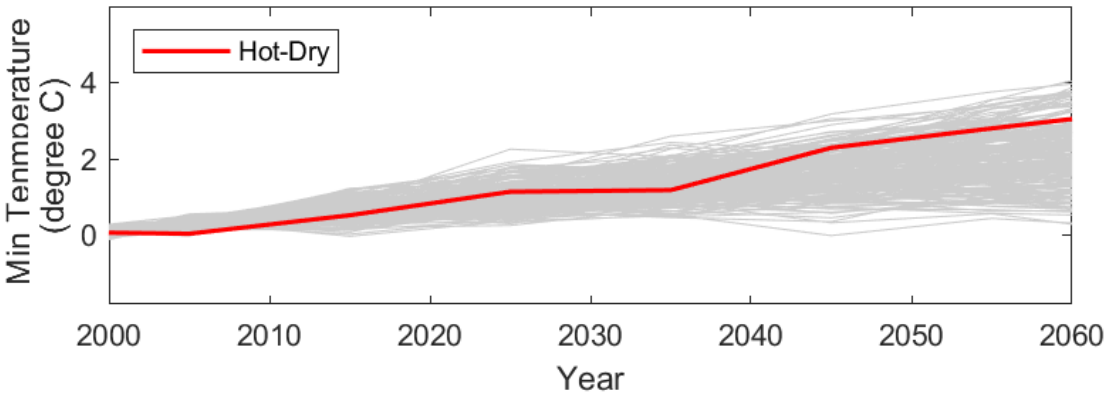

Figure C-5. 30-year normal annual minimum temperature from the current conditions to the future

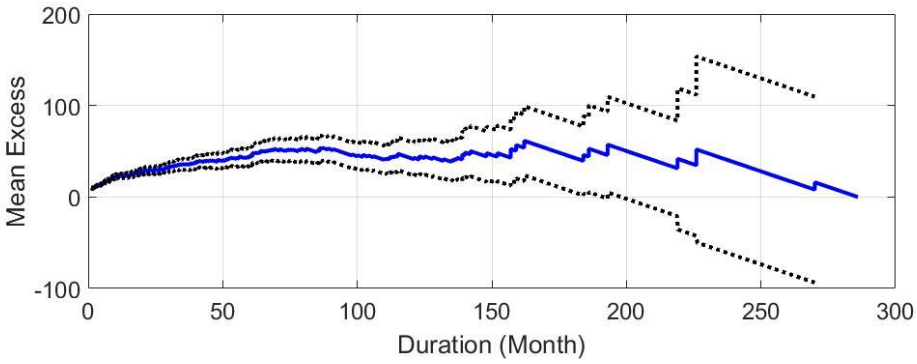

Figure C-6. Mean residual life plot of drought durations

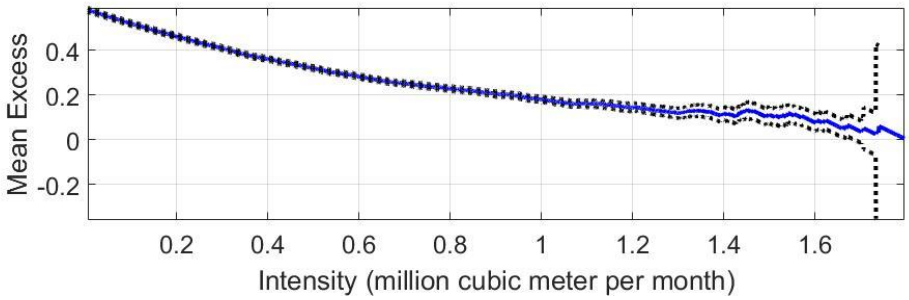

Figure C-7. Mean residual life plot of drought intensities

Table C-1. Boundaries of mixture model parameters

Parameter	Minimum	Maximum
GPD Shape	-0.3	0.3
GPD Scale	0.1	0.3
GPD Location	1	1.3
Gamma Shape	1	2
Gamma Scale	0.2	0.3

Table C-2. First order sensitivity indices of mixture model parameters

	GPD			Gamma		Sum
Intensity	Shape	Scale	Location	Shape	Scale	
0.01	0	0	0	0.978	0.018	0.997
0.5	0	0	0.005	0.735	0.247	0.987
1	0	0	0.514	0.266	0.171	0.685
1.3	0.026	0.17	0.219	0	0	0.415

Table C-3. Total order sensitivity indices of mixture model parameters

	GPD			Gamma		Sum
Intensity	Shape	Scale	Location	Shape	Scale	
0.01	0	0	0	0.991	0.031	1.022
0.5	0	0	0.005	0.759	0.271	1.035
1	0	0	0.568	0.3	0.195	1.063
1.3	0.454	0.72	0.792	0	0	1.966

APPENDIX D

SUPPORTING INFORMATION FOR CHAPTER 6:

VULNERABILITY TO WATER SHORTAGE UNDER CURRENT AND FUTURE WATER SUPPLY-DEMAND CONDITIONS ACROSS U.S. RIVER BASINS

Figure D-1. The 204 HUC4 river basins across the CONUS

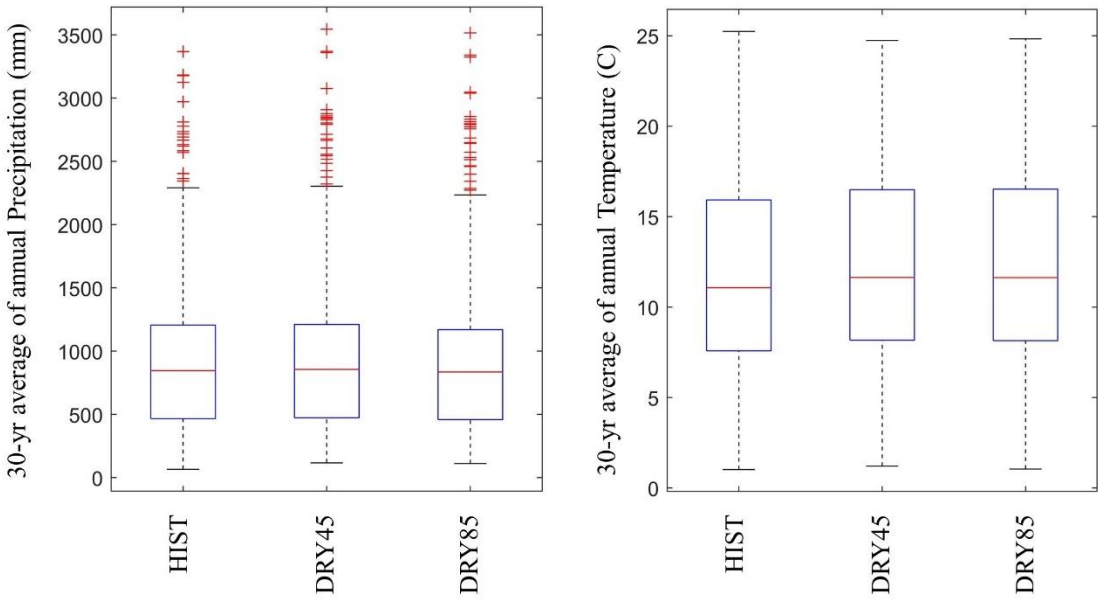

Figure D-2. The comparison of baseline climate model (HIST) and the driest MACA climate model over the historical (1986-2015) period.

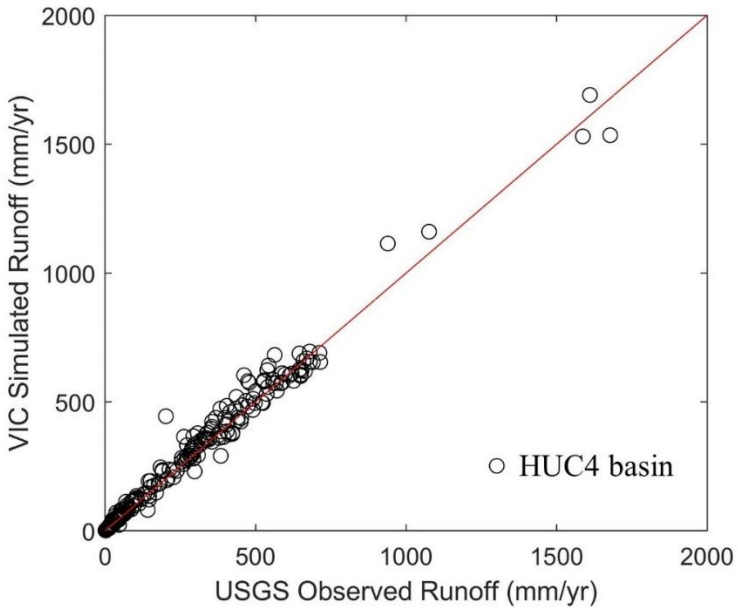

Figure D-3. The comparison of VIC simulated runoff and USGS observed runoff over the historical period

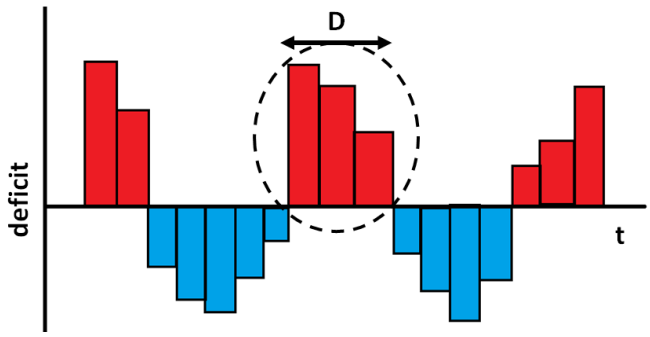

Figure D-4. Schematic of drought characteristics (Heidari et al, 2020)

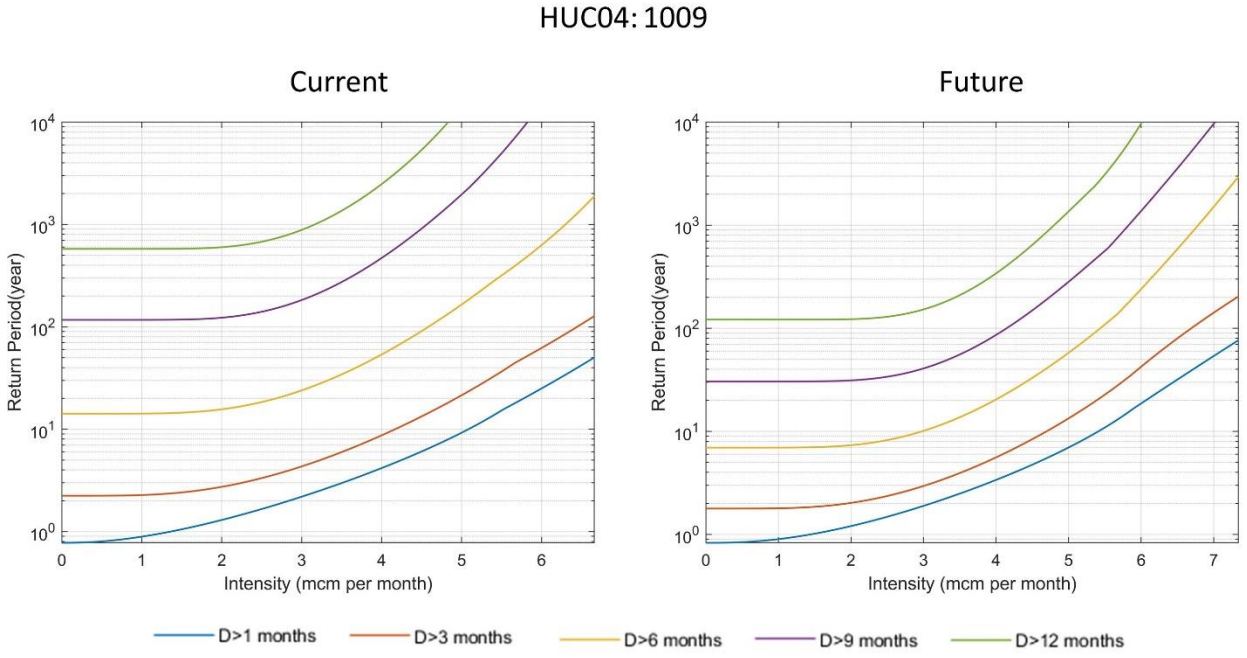

Figure D-5. Intensity-duration-frequency curves for current (left-panel) and future conditions (right-panel)

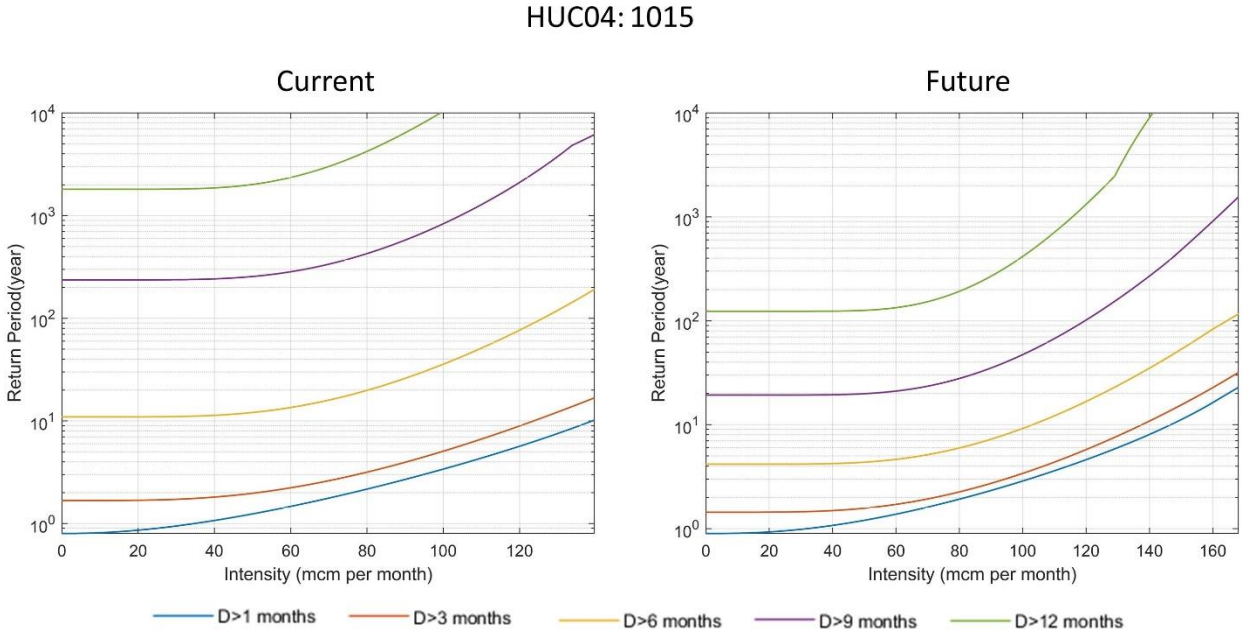

Figure D-6. Intensity-duration-frequency curves for current (left-panel) and future conditions (right-panel)

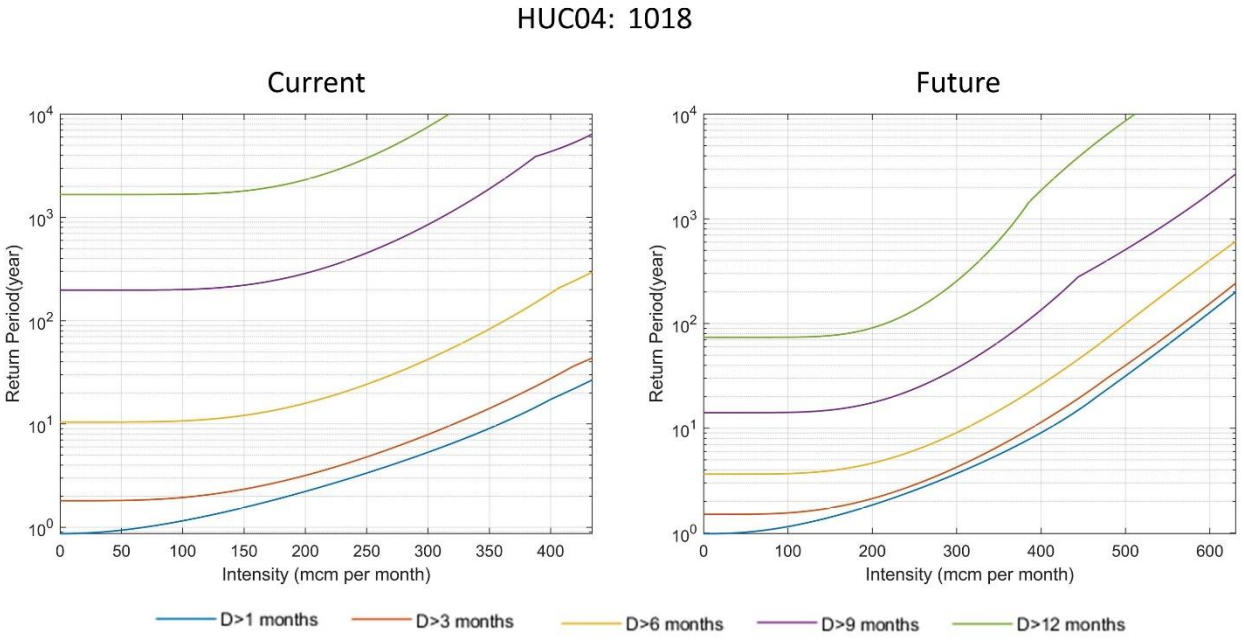

Figure D-7. Intensity-duration-frequency curves for current (left-panel) and future conditions (right-panel)

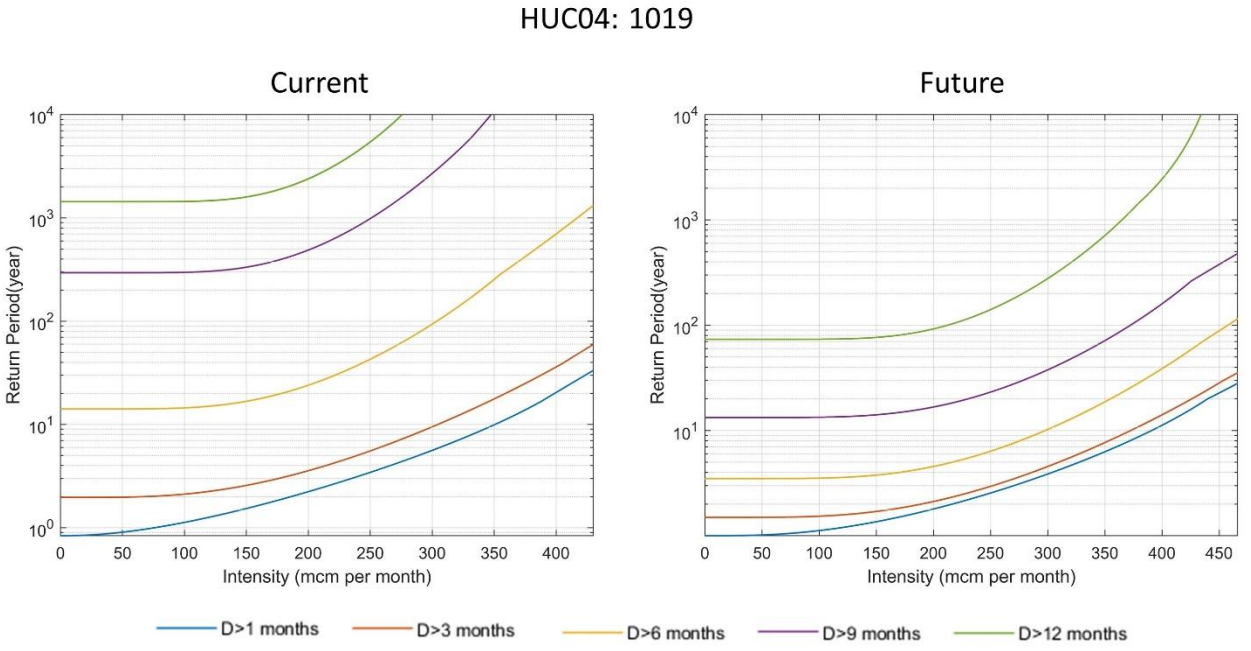

Figure D-8. Intensity-duration-frequency curves for current (left-panel) and future conditions (right-panel)

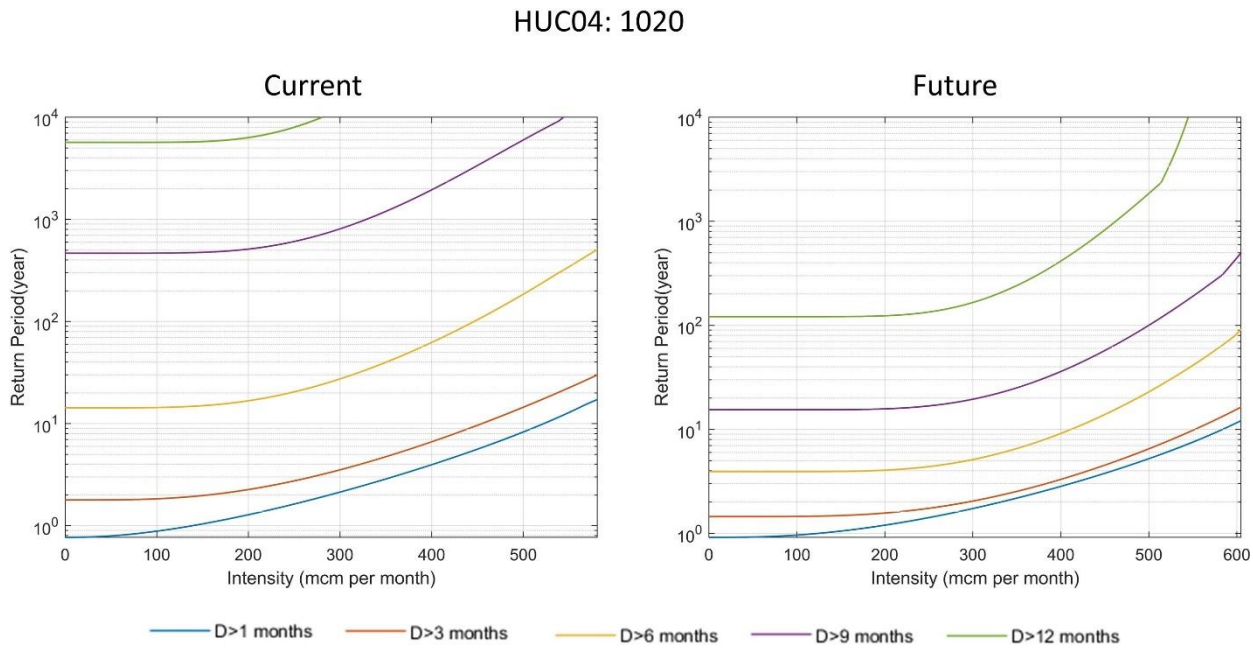

Figure D-9. Intensity-duration-frequency curves for current (left-panel) and future conditions (right-panel)

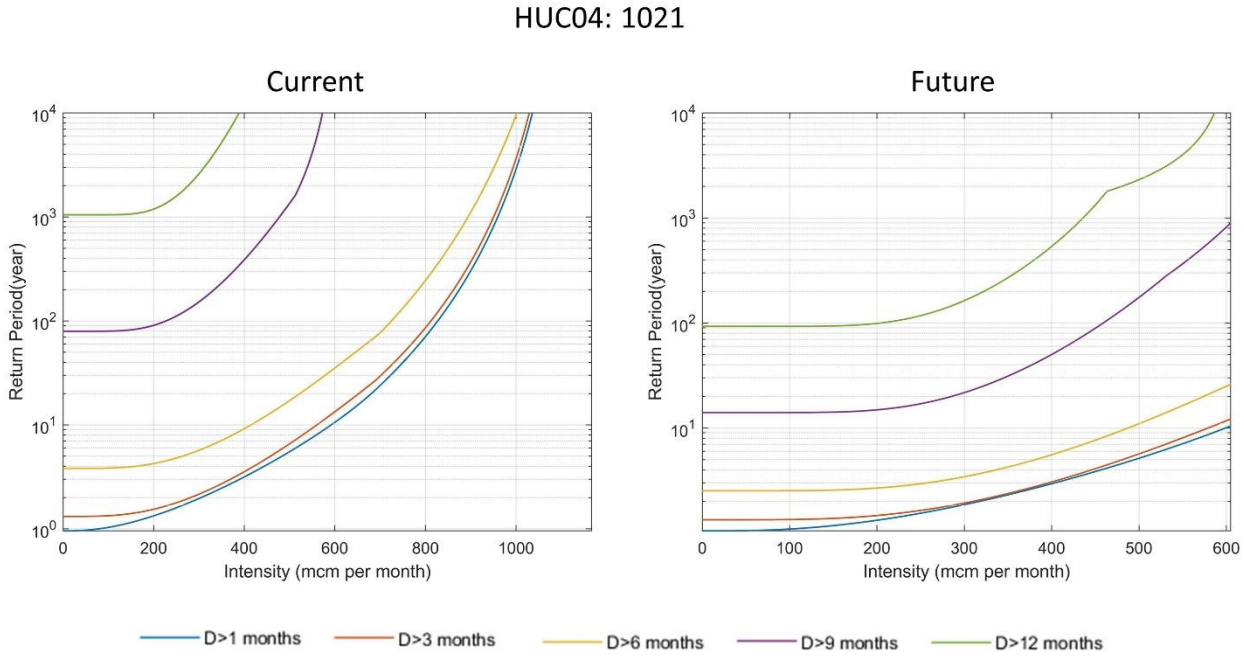

Figure D-10. Intensity-duration-frequency curves for current (left-panel) and future conditions (right-panel)

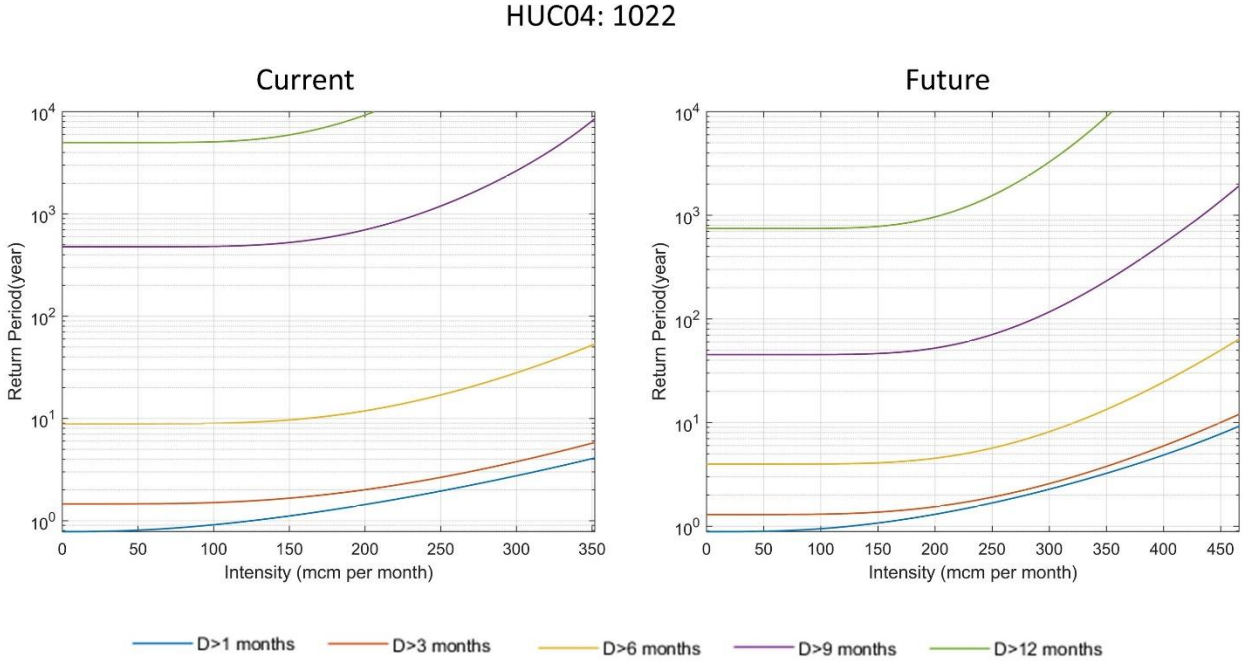

Figure D-11. Intensity-duration-frequency curves for current (left-panel) and future conditions (right-panel)

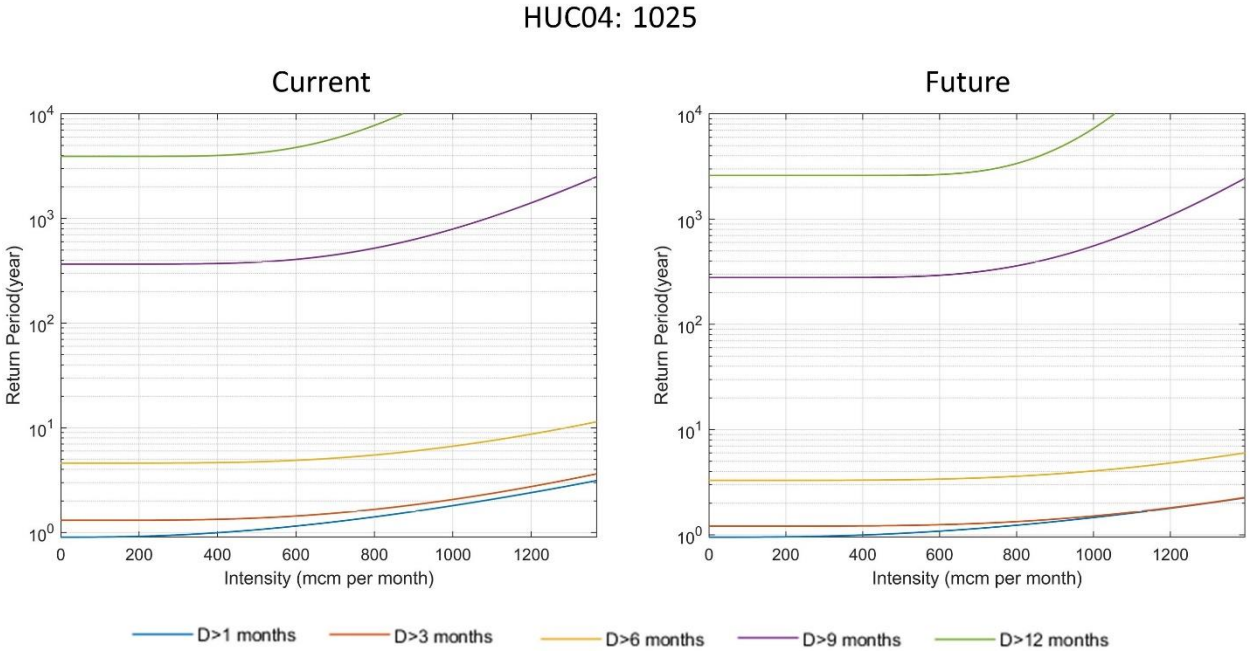

Figure D-12. Intensity-duration-frequency curves for current (left-panel) and future conditions (right-panel)

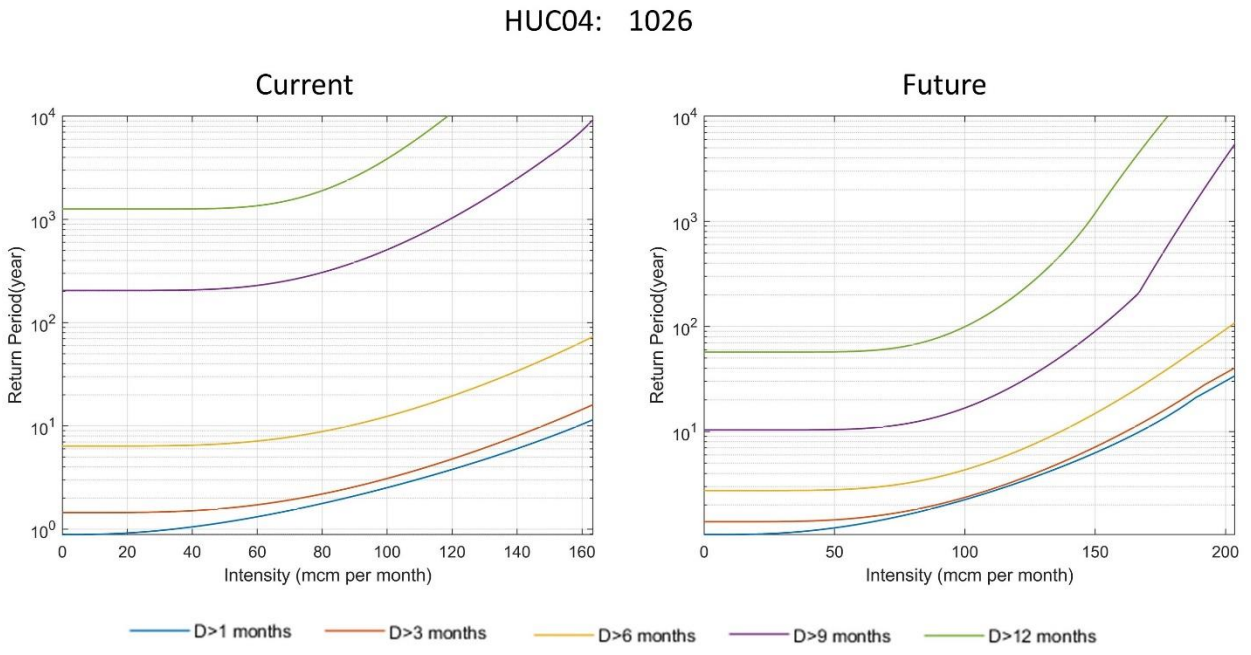

Figure D-13. Intensity-duration-frequency curves for current (left-panel) and future conditions (right-panel)

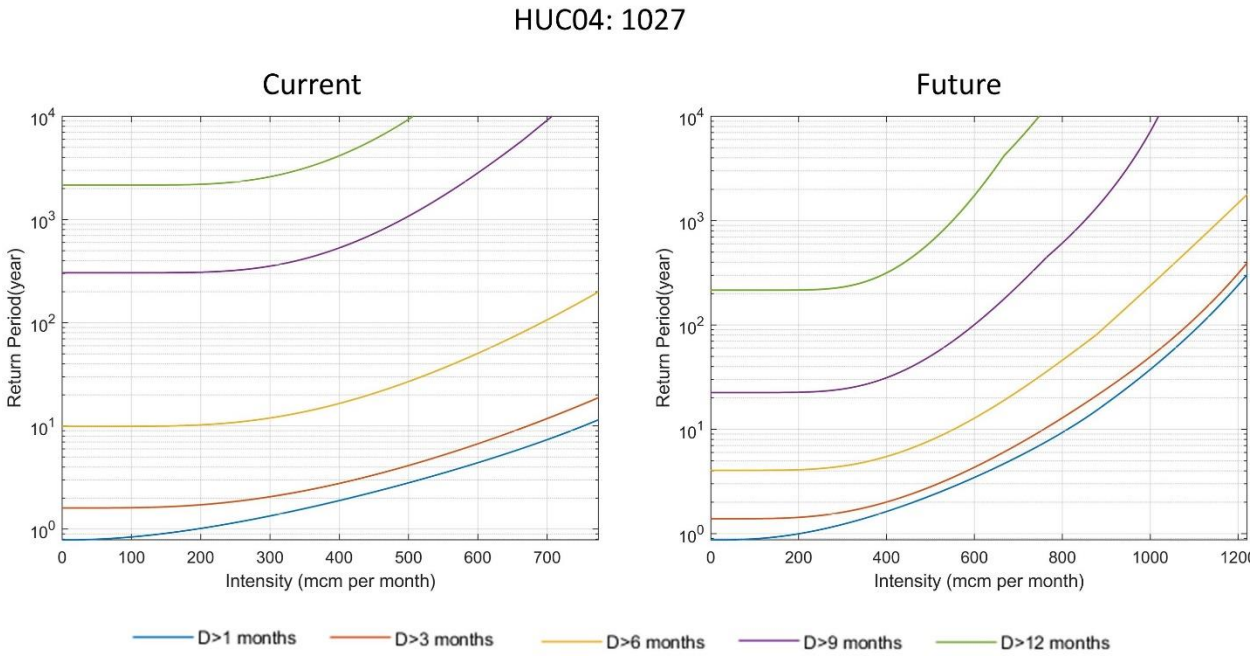

Figure D-14. Intensity-duration-frequency curves for current (left-panel) and future conditions (right-panel)

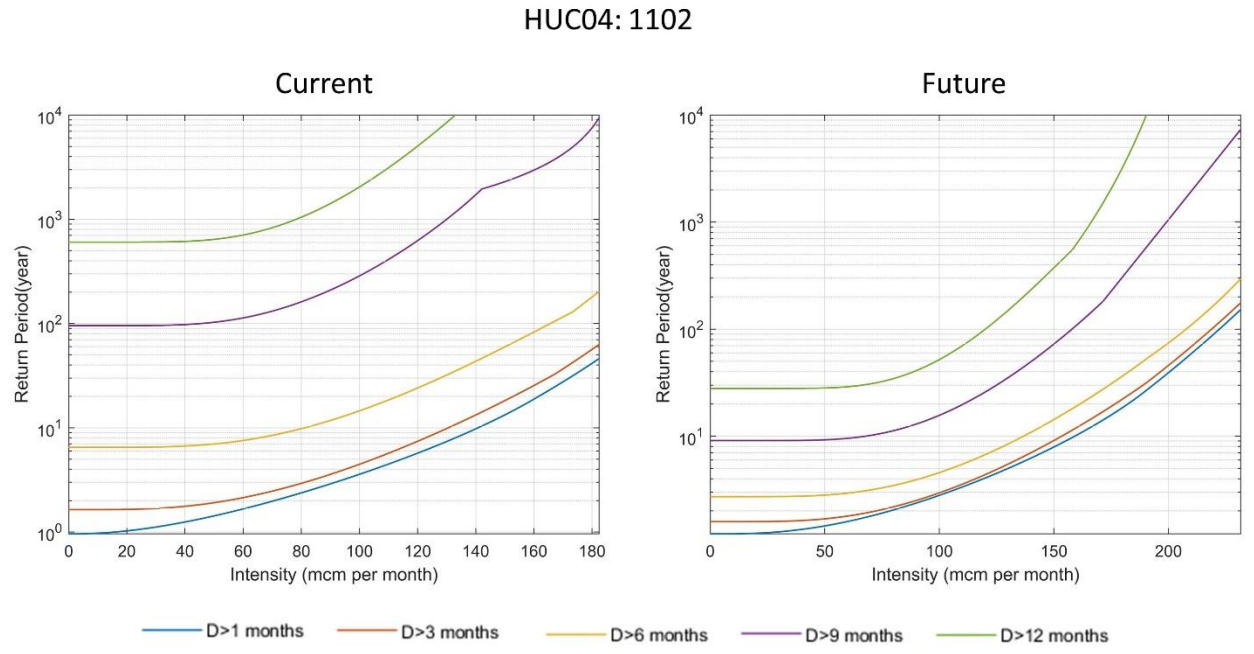

Figure D-15. Intensity-duration-frequency curves for current (left-panel) and future conditions (right-panel)

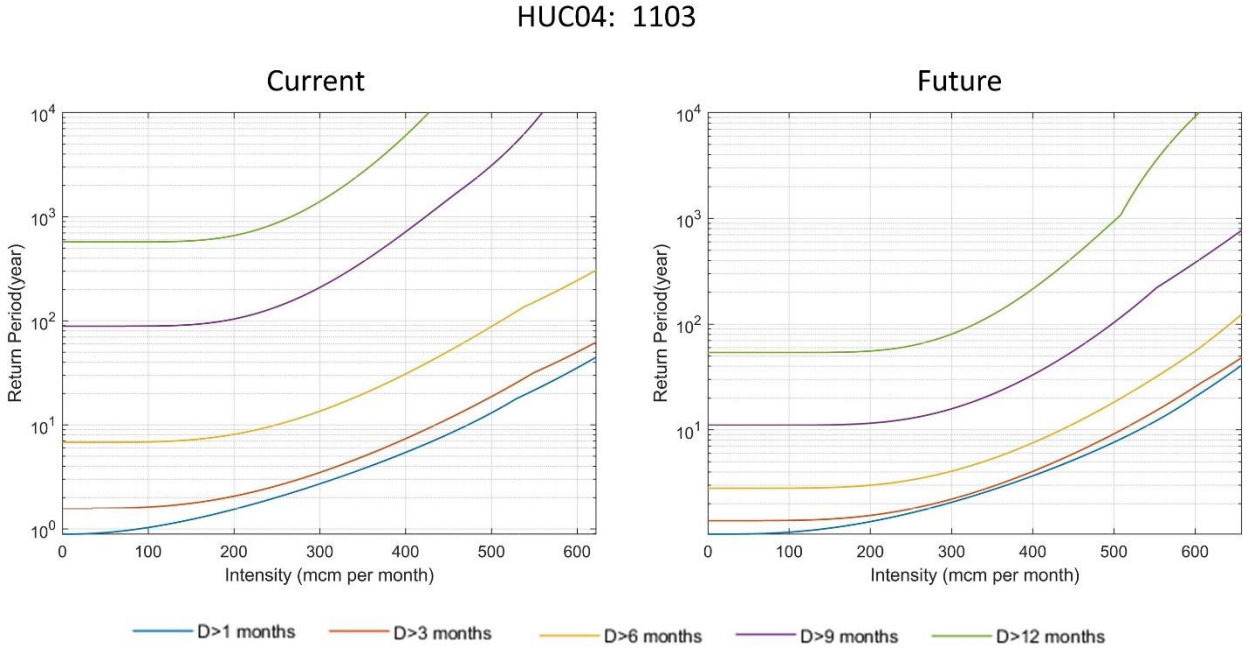

Figure D-16. Intensity-duration-frequency curves for current (left-panel) and future conditions (right-panel)

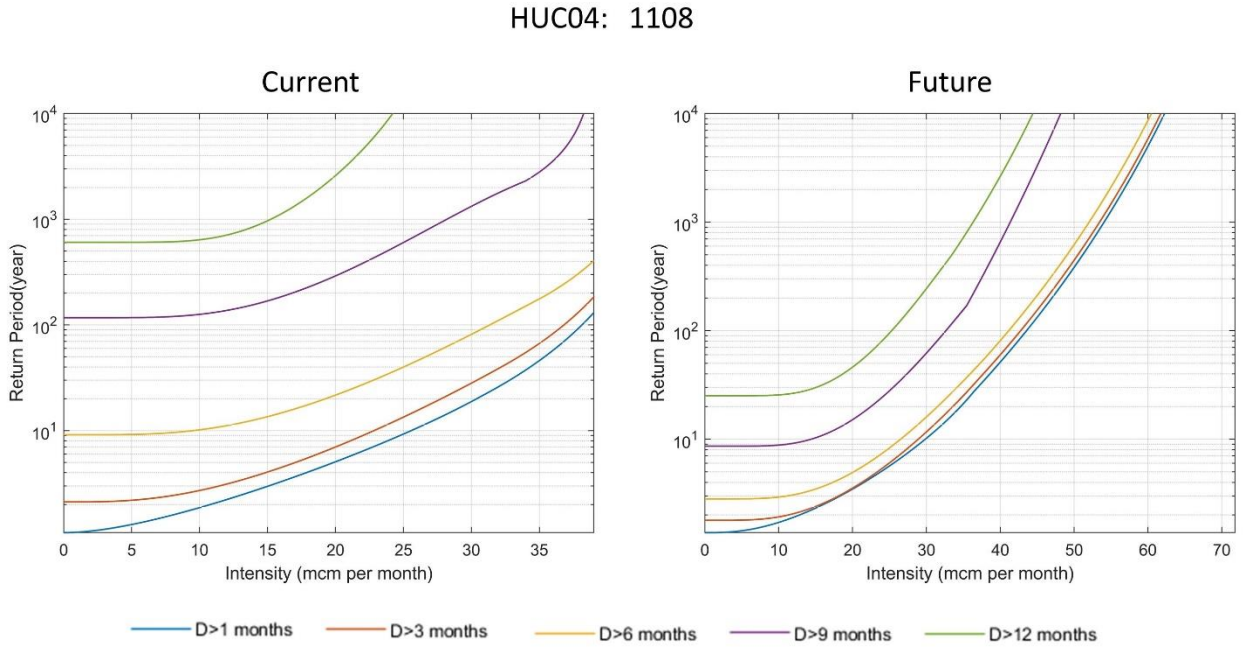

Figure D-17. Intensity-duration-frequency curves for current (left-panel) and future conditions (right-panel)

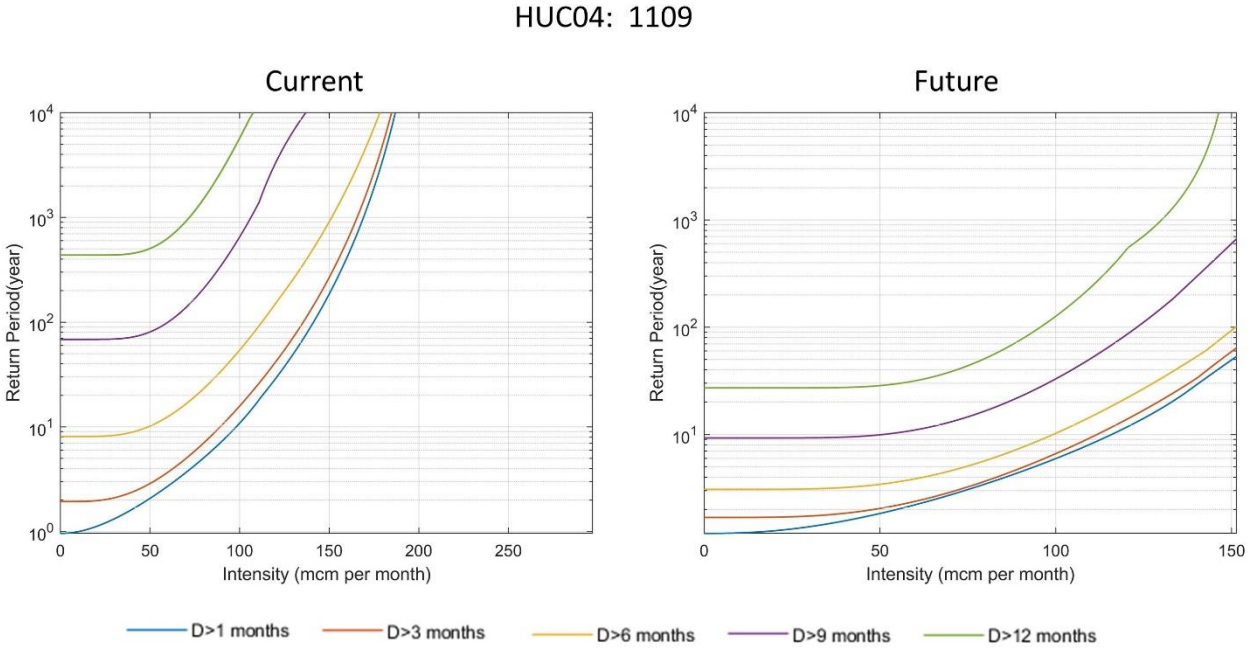

Figure D-18. Intensity-duration-frequency curves for current (left-panel) and future conditions (right-panel)

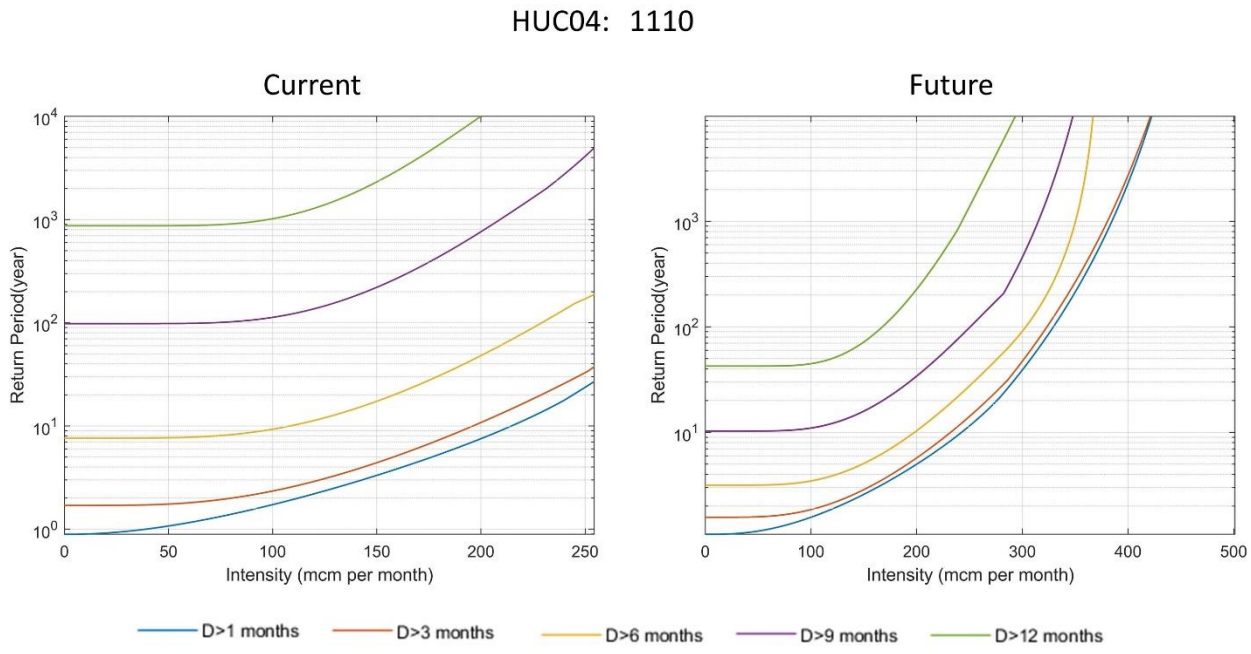

Figure D-19. Intensity-duration-frequency curves for current (left-panel) and future conditions (right-panel)

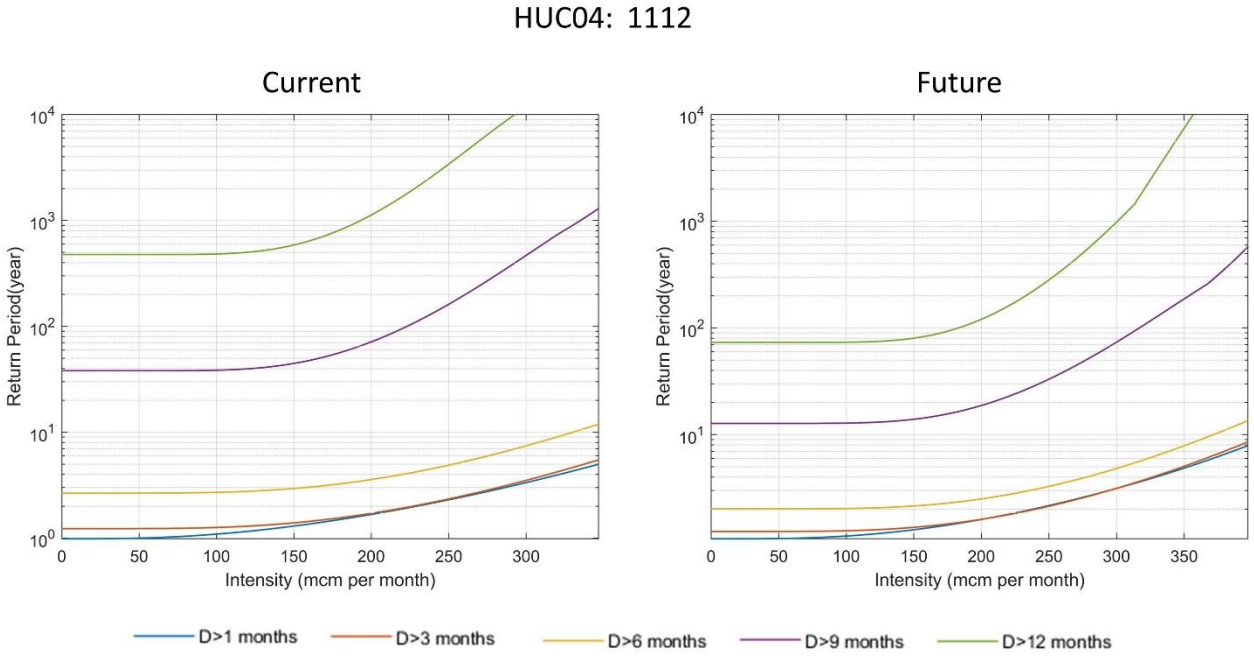

Figure D-20. Intensity-duration-frequency curves for current (left-panel) and future conditions (right-panel)

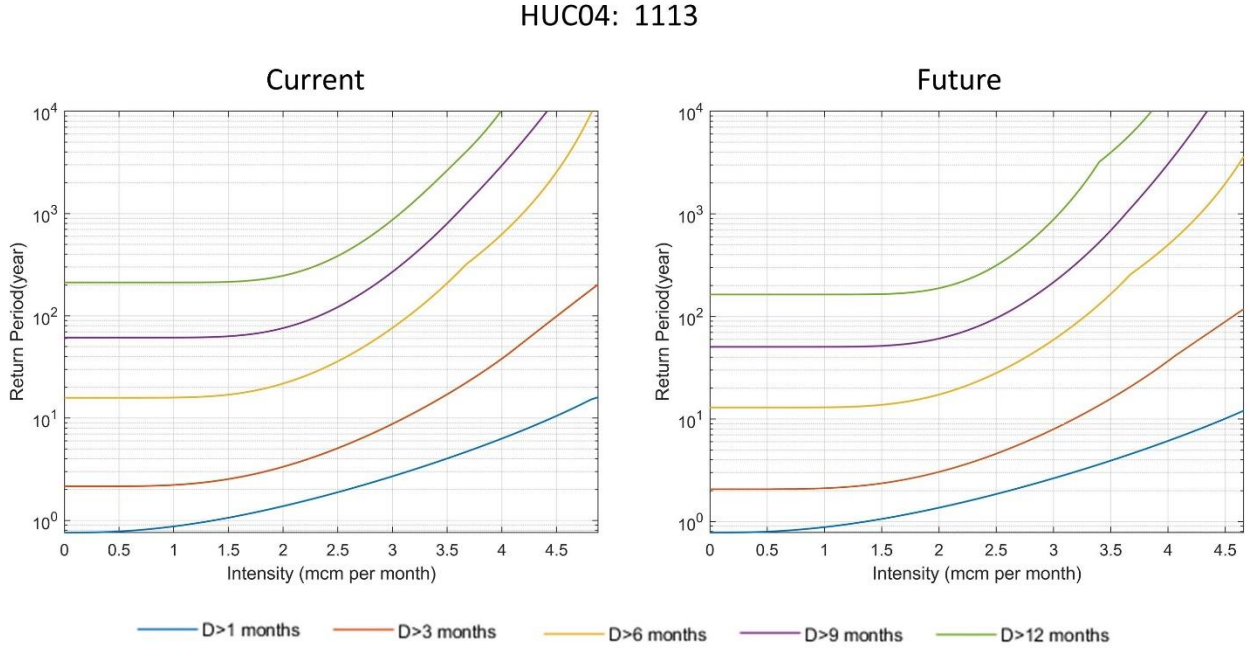

Figure D-21. Intensity-duration-frequency curves for current (left-panel) and future conditions (right-panel)

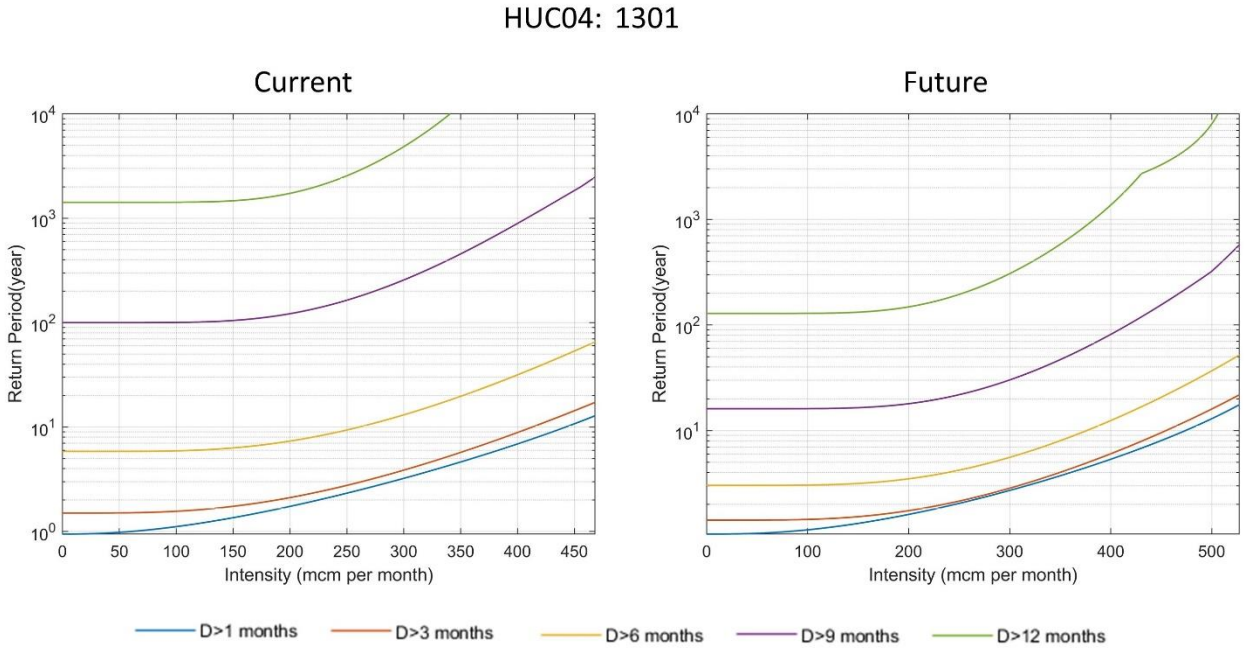

Figure D-22. Intensity-duration-frequency curves for current (left-panel) and future conditions (right-panel)

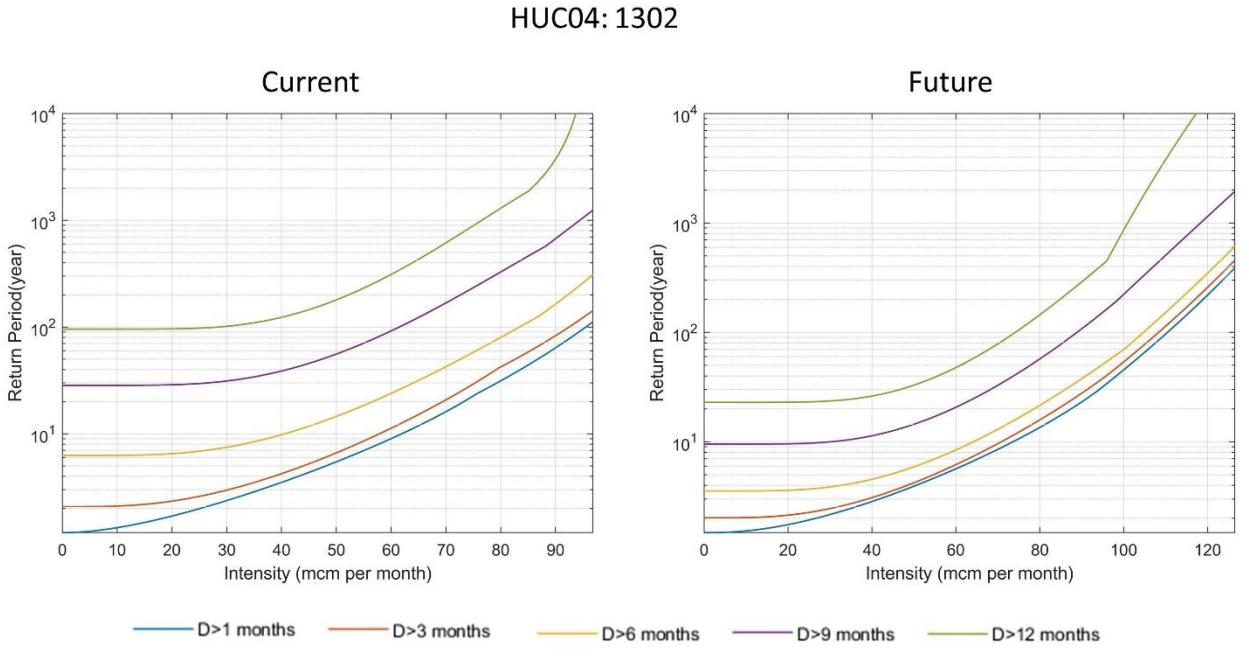

Figure D-23. Intensity-duration-frequency curves for current (left-panel) and future conditions (right-panel)

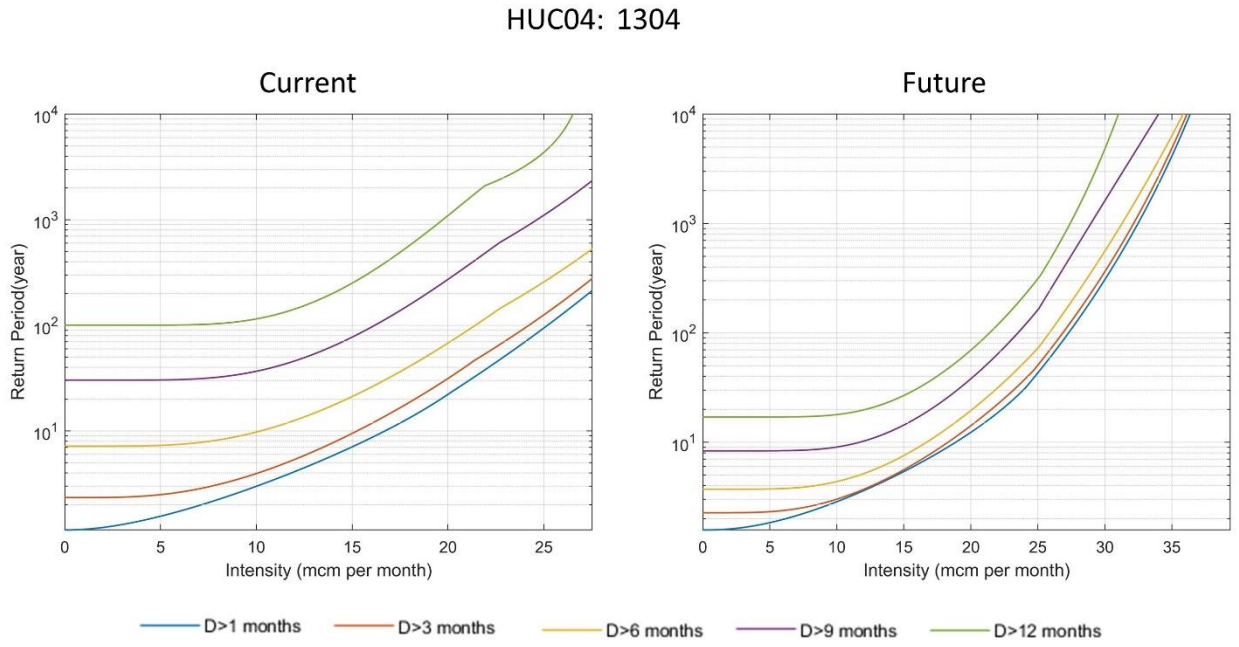

Figure D-24. Intensity-duration-frequency curves for current (left-panel) and future conditions (right-panel)

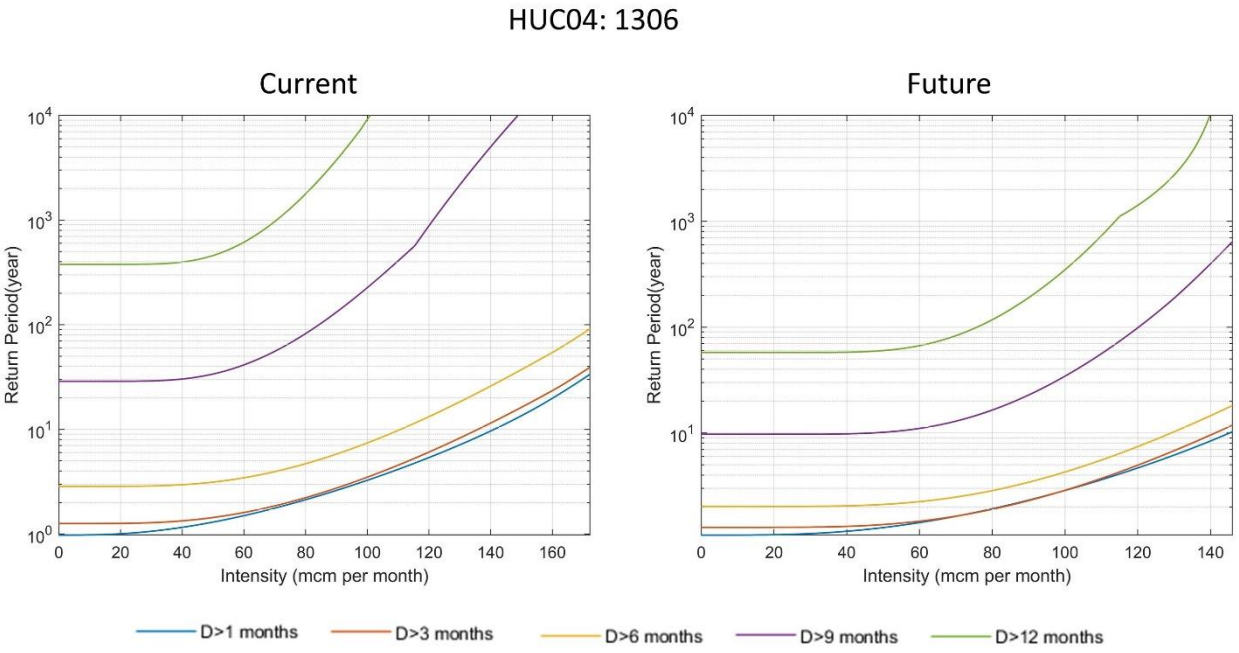

Figure D-25. Intensity-duration-frequency curves for current (left-panel) and future conditions (right-panel)

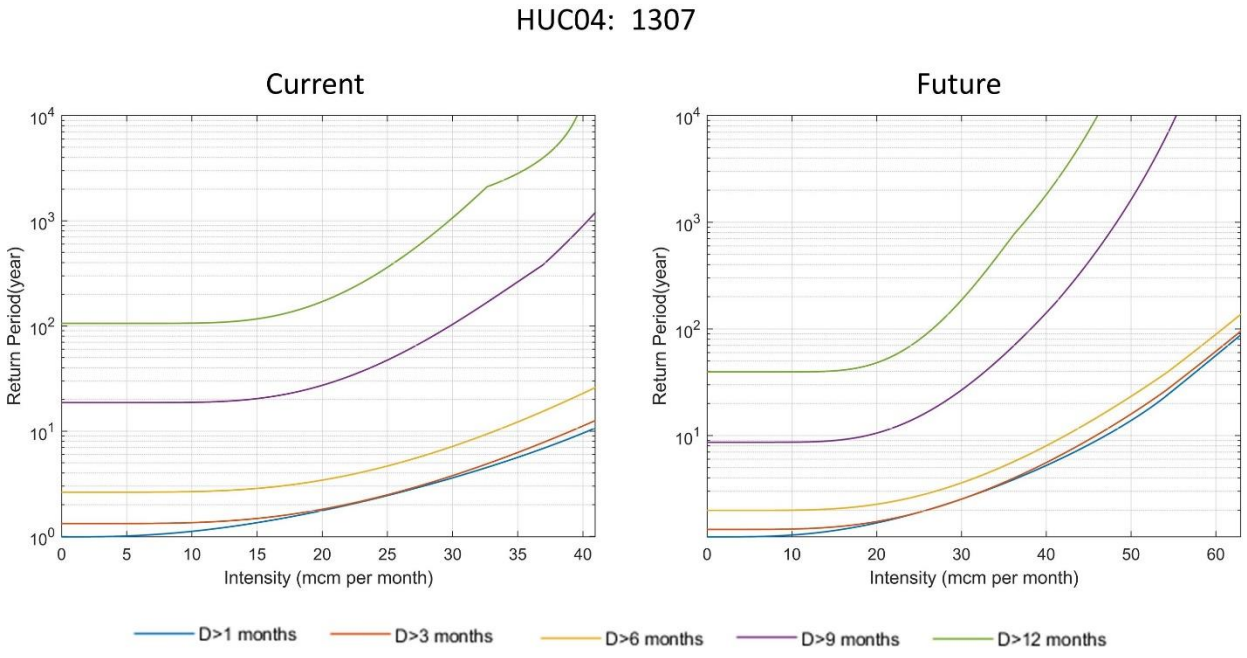

Figure D-26. Intensity-duration-frequency curves for current (left-panel) and future conditions (right-panel)

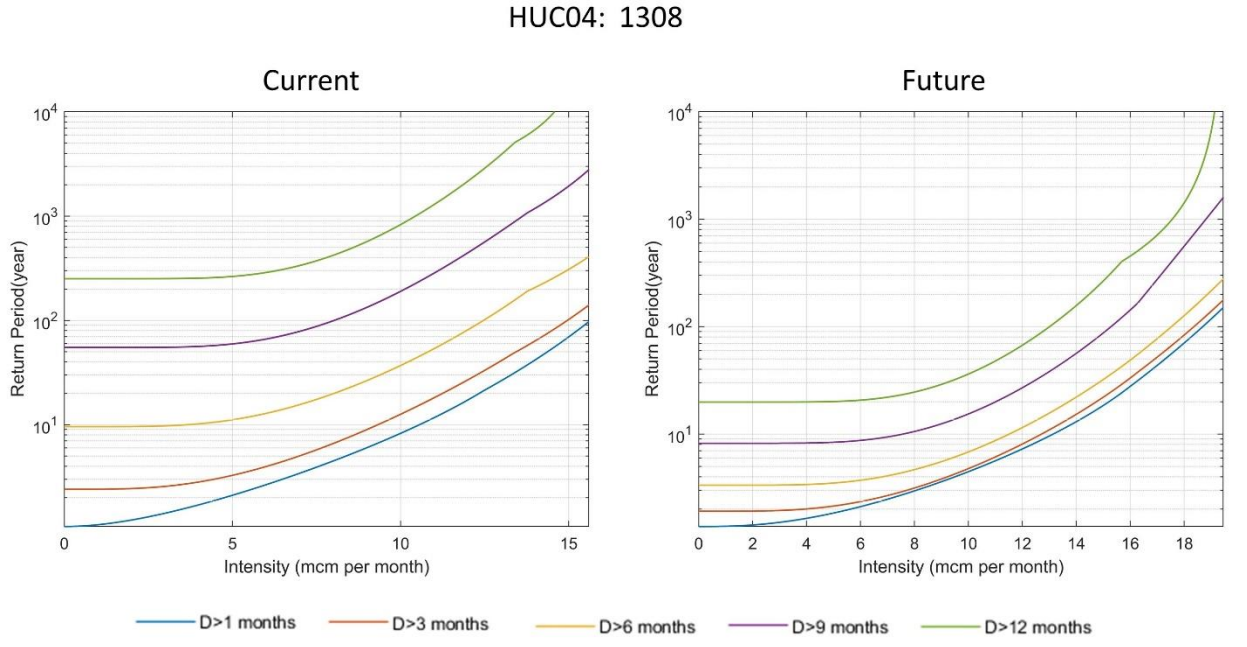

Figure D-27. Intensity-duration-frequency curves for current (left-panel) and future conditions (right-panel)

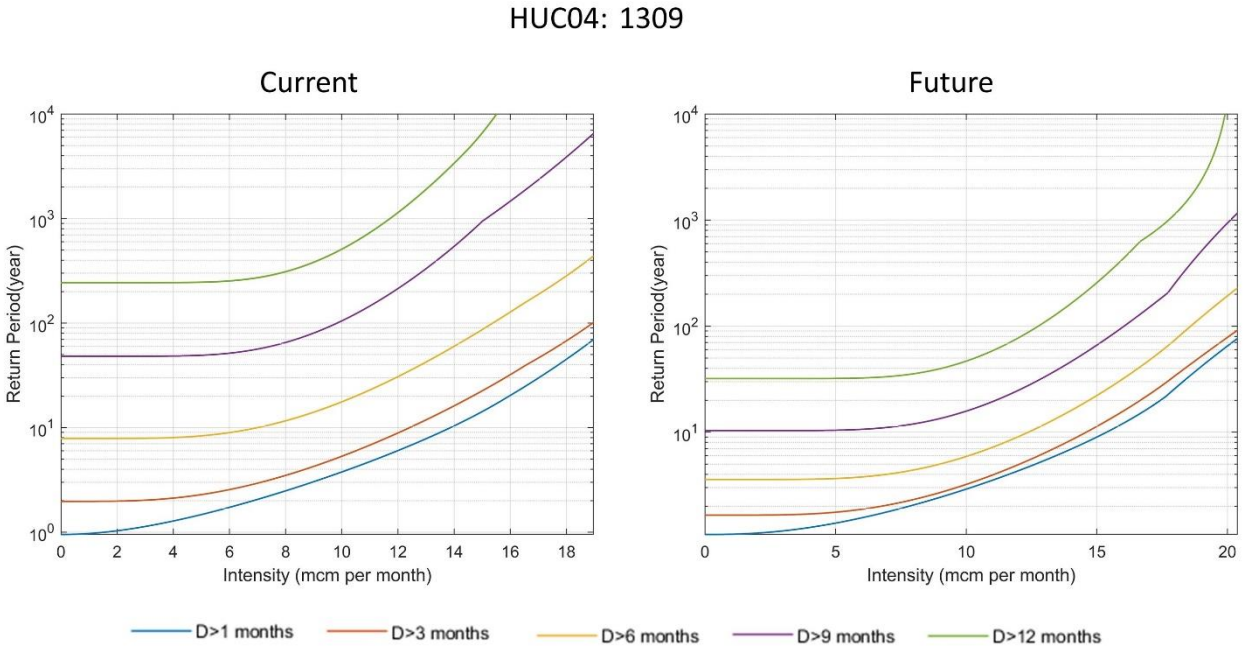

Figure D-28. Intensity-duration-frequency curves for current (left-panel) and future conditions (right-panel)

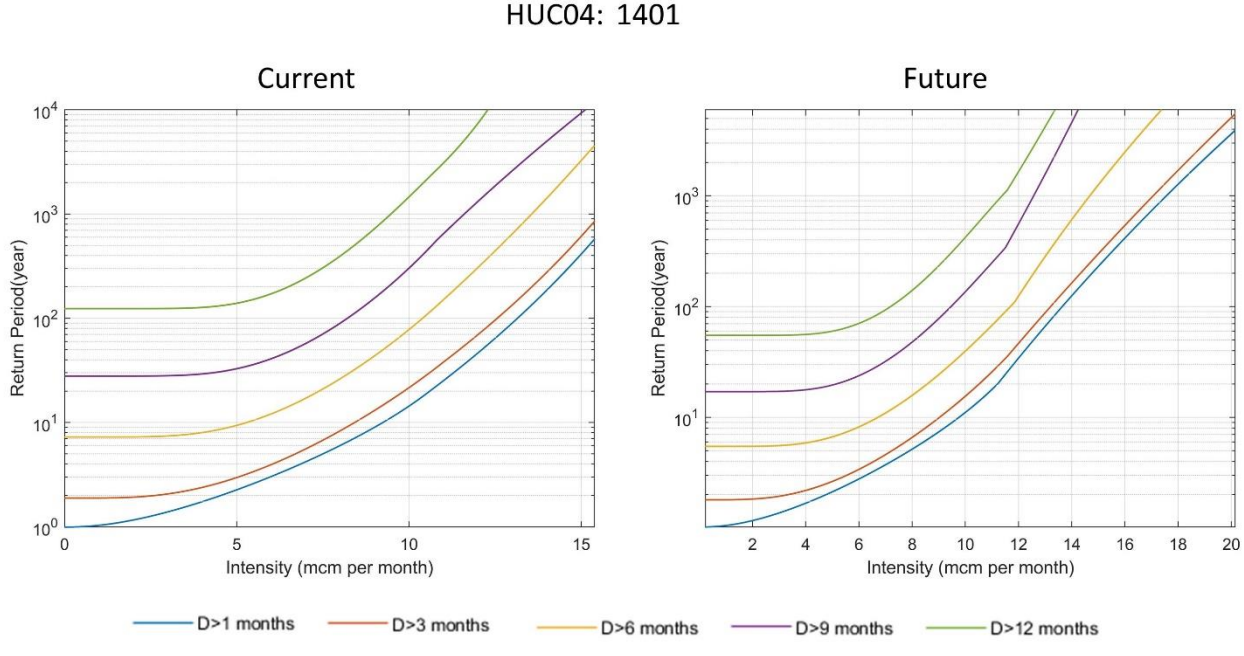

Figure D-29. Intensity-duration-frequency curves for current (left-panel) and future conditions (right-panel)

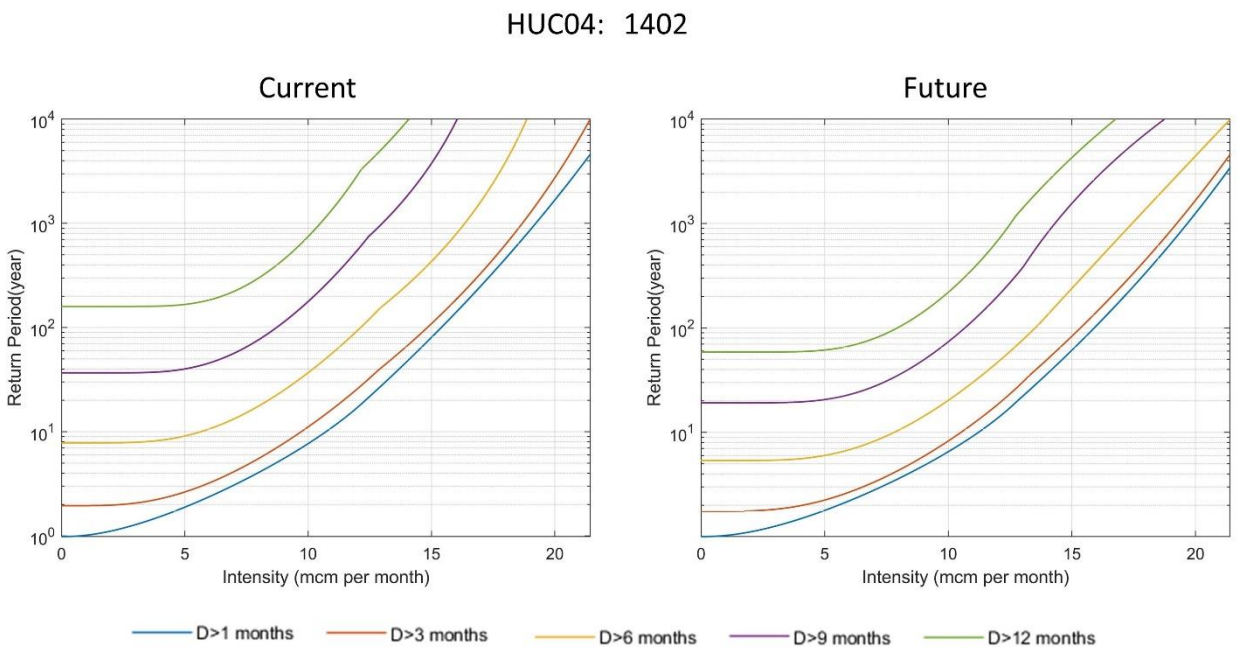

Figure D-30. Intensity-duration-frequency curves for current (left-panel) and future conditions (right-panel)

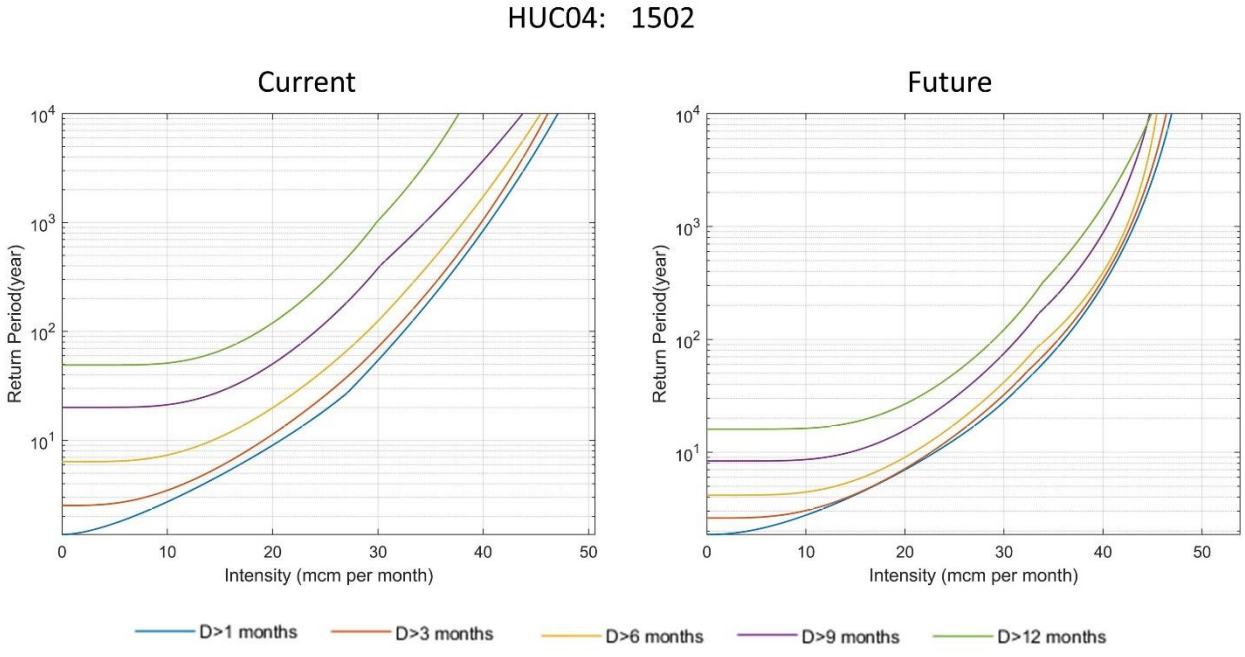

Figure D-31. Intensity-duration-frequency curves for current (left-panel) and future conditions (right-panel)

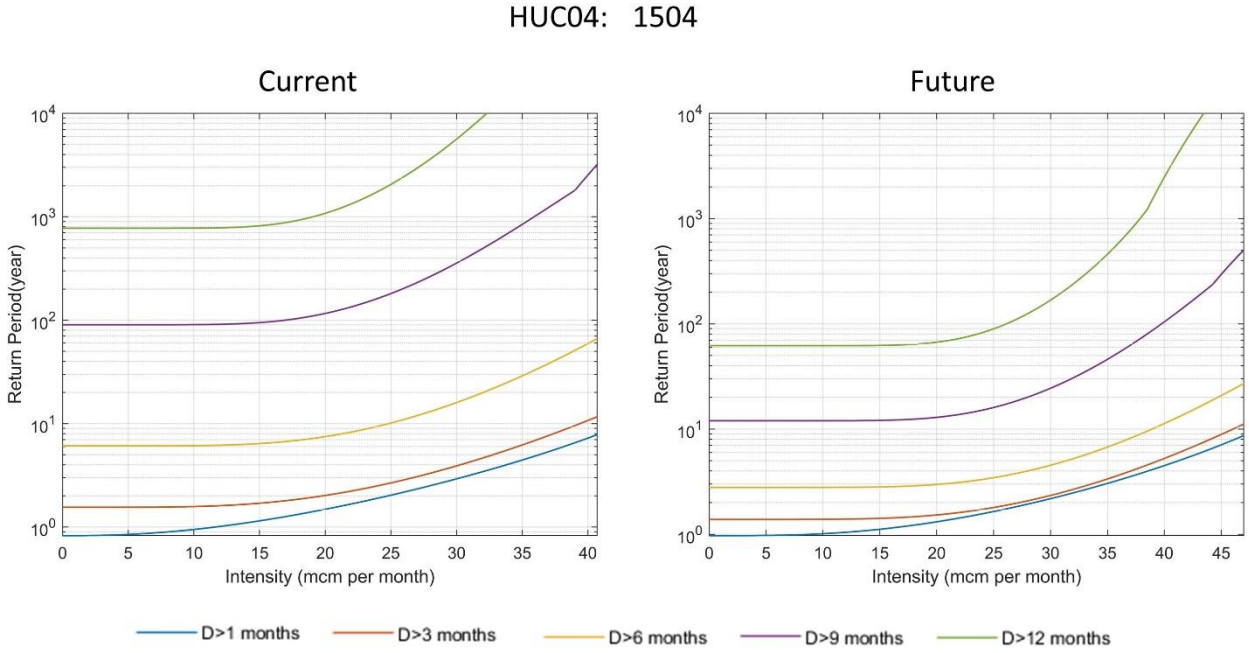

Figure D-32. Intensity-duration-frequency curves for current (left-panel) and future conditions (right-panel)

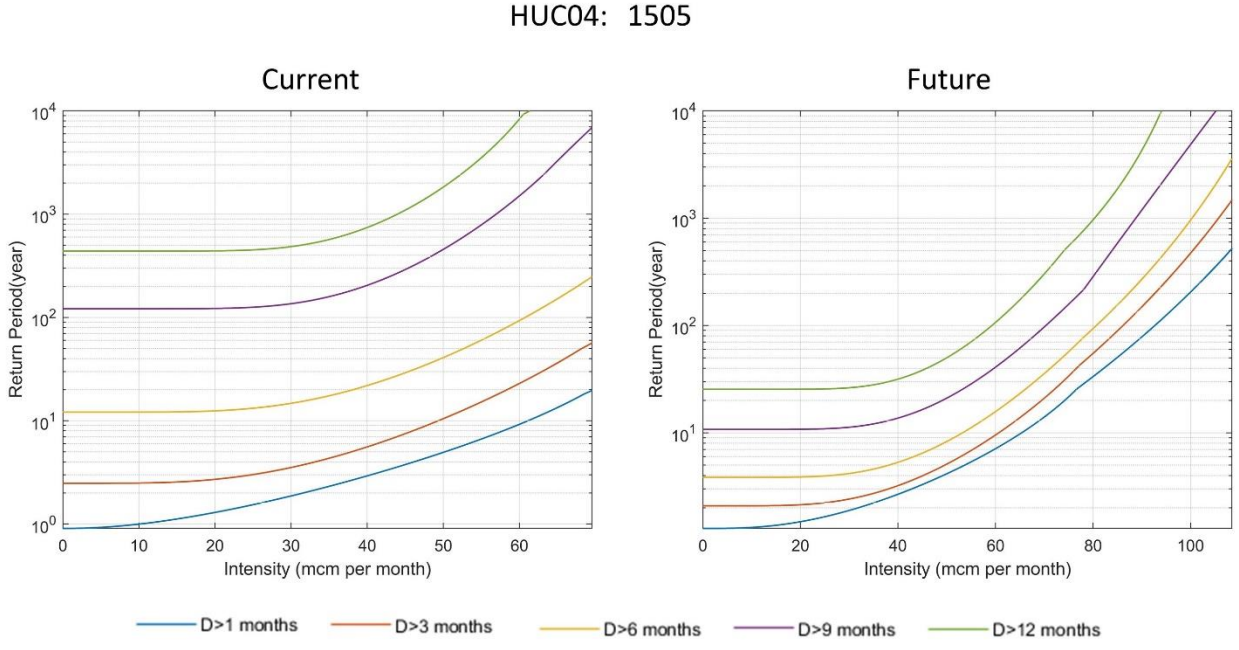

Figure D-33. Intensity-duration-frequency curves for current (left-panel) and future conditions (right-panel)

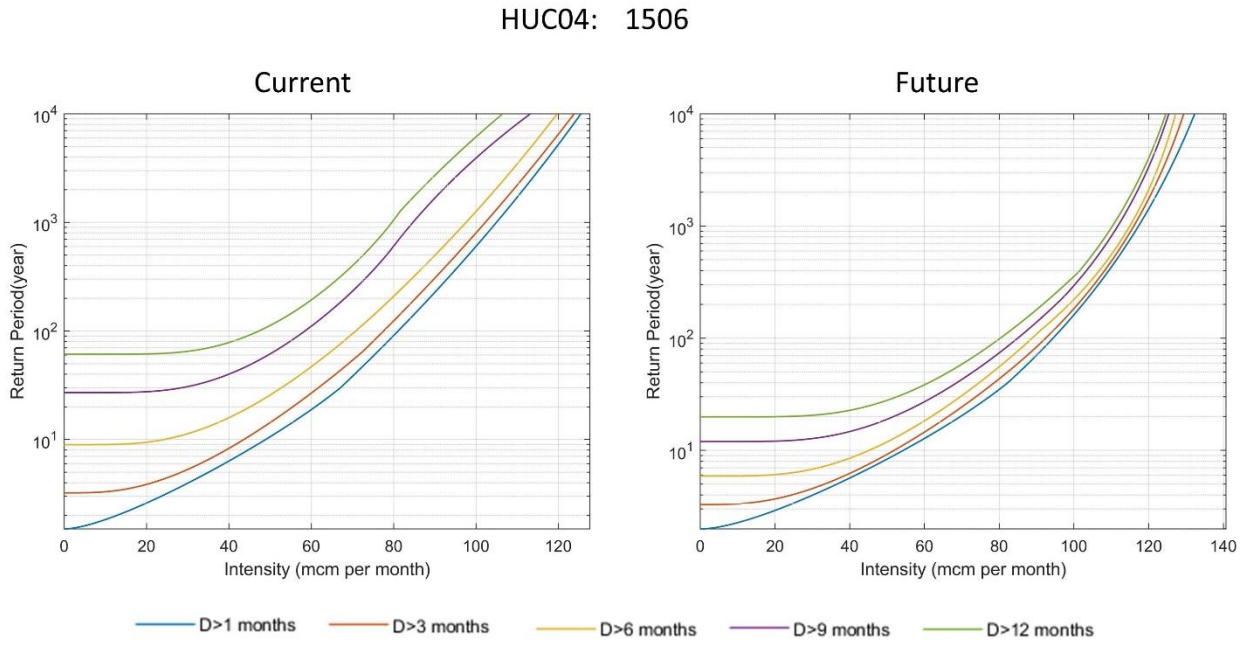

Figure D-34. Intensity-duration-frequency curves for current (left-panel) and future conditions (right-panel)

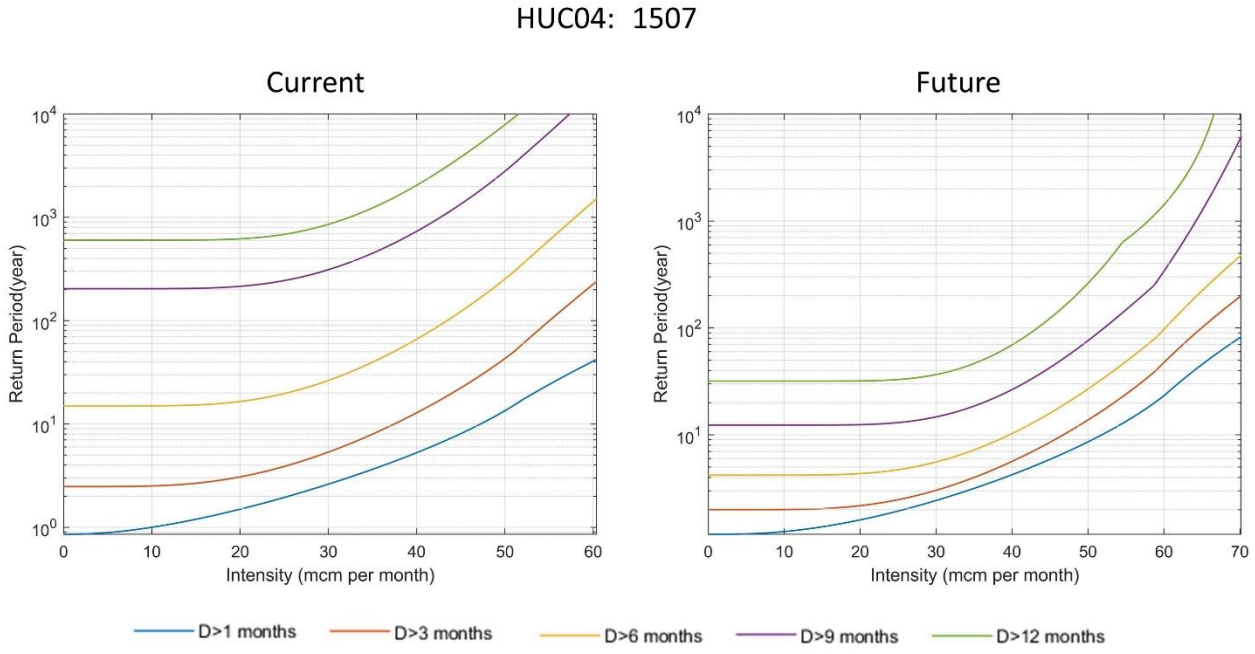

Figure D-35. Intensity-duration-frequency curves for current (left-panel) and future conditions (right-panel)

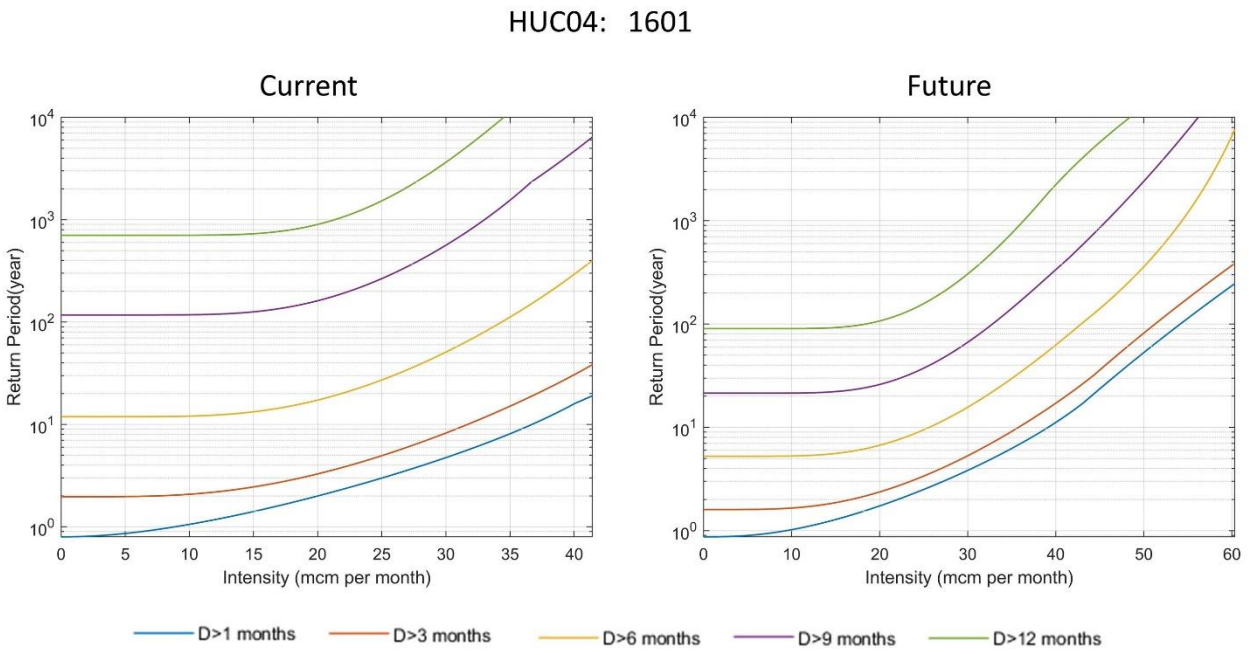

Figure D-36. Intensity-duration-frequency curves for current (left-panel) and future conditions (right-panel)

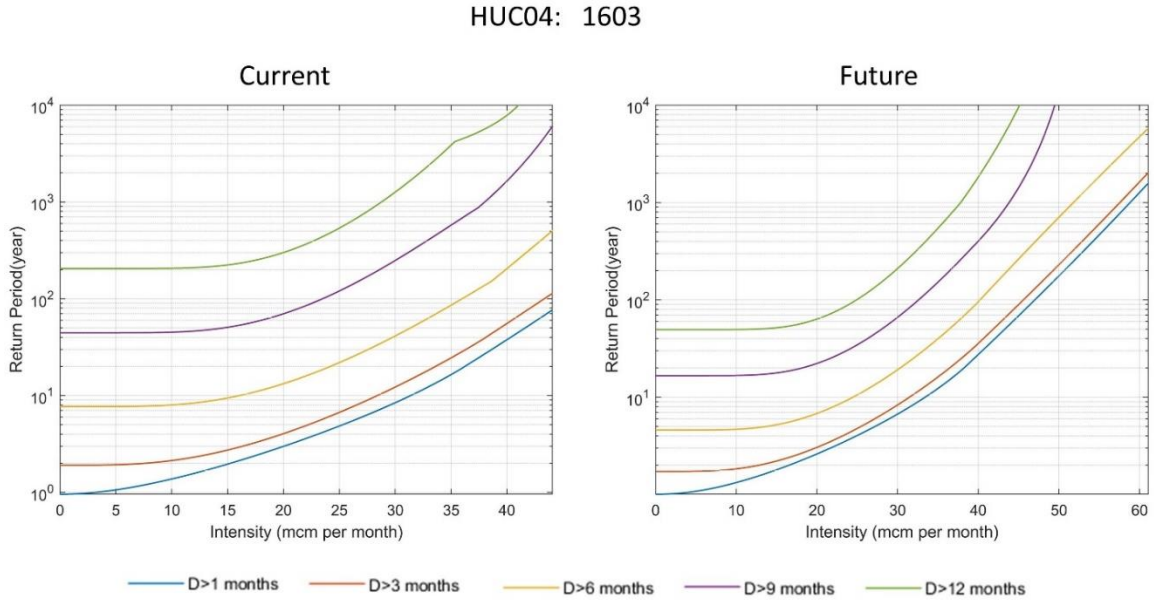

Figure D-37. Intensity-duration-frequency curves for current (left-panel) and future conditions (right-panel)

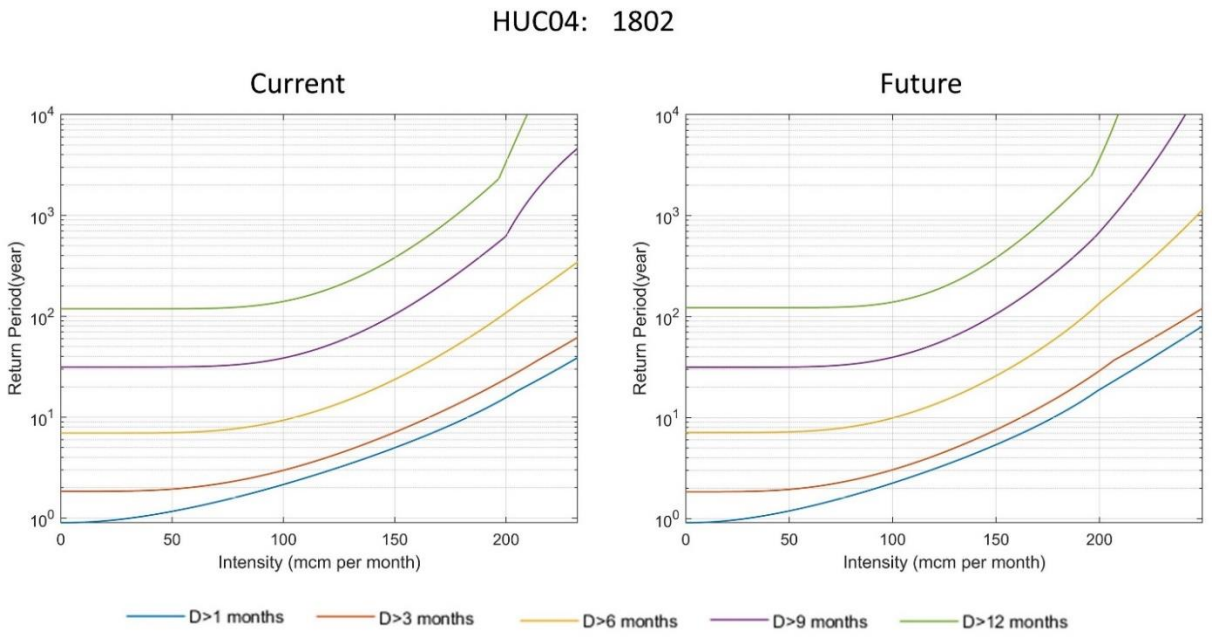

Figure D-38. Intensity-duration-frequency curves for current (left-panel) and future conditions (right-panel)

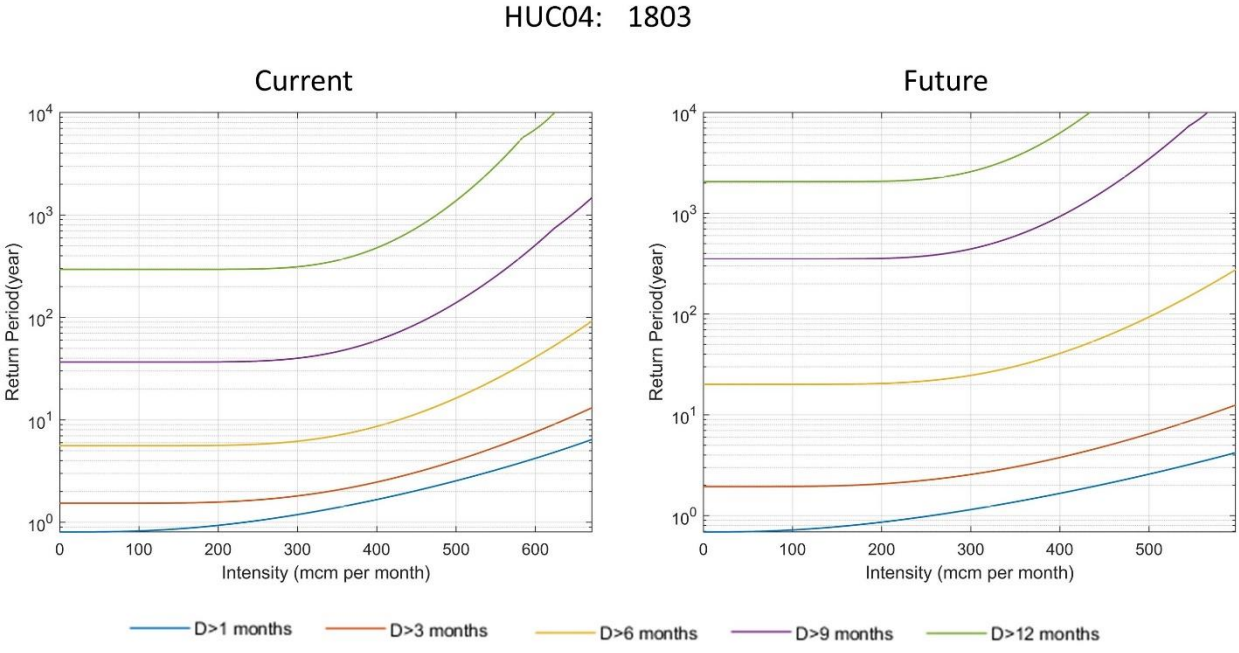

Figure D-39. Intensity-duration-frequency curves for current (left-panel) and future conditions (right-panel)

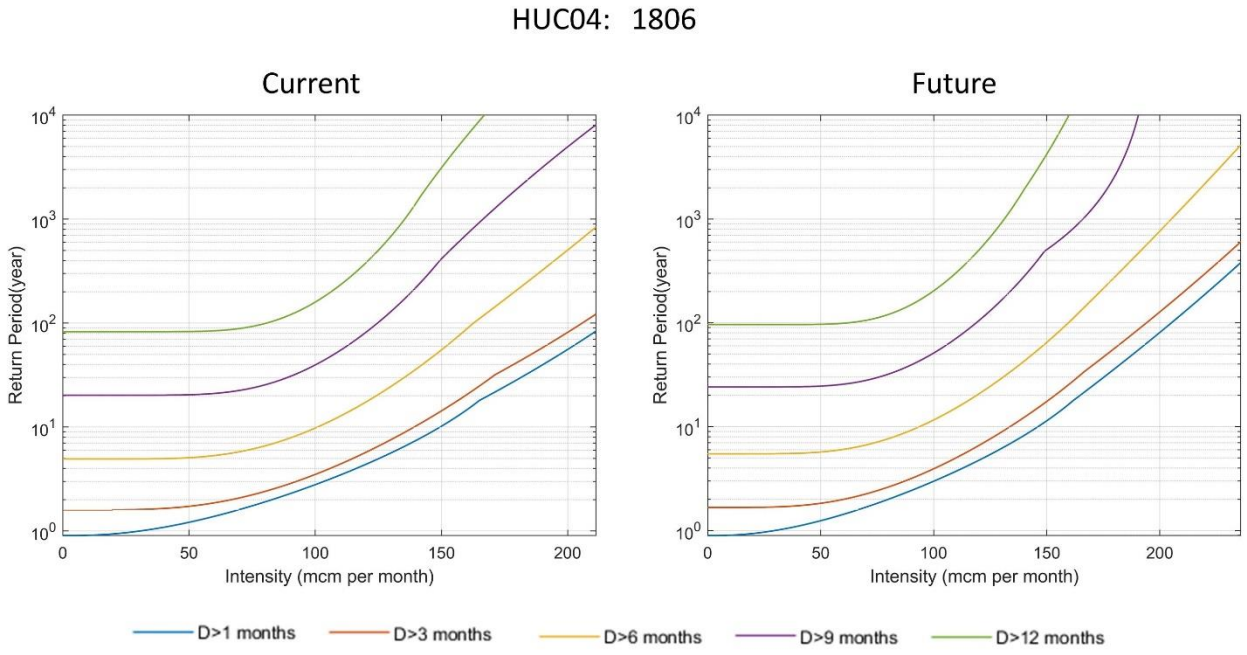

Figure D-40. Intensity-duration-frequency curves for current (left-panel) and future conditions (right-panel)

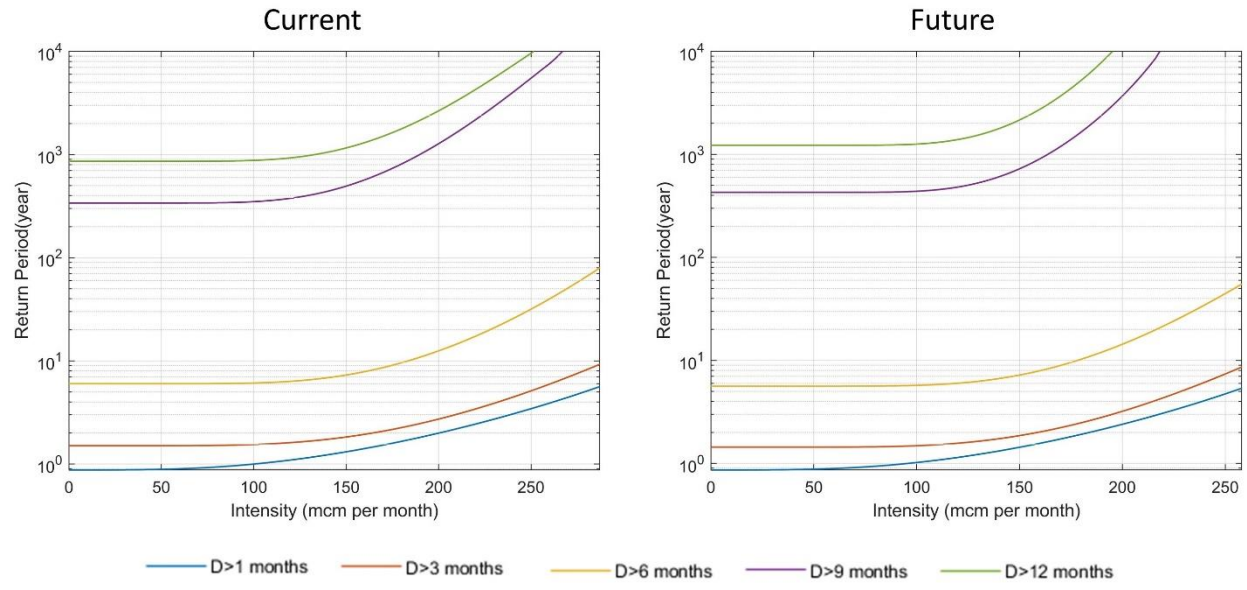

Figure D-41. Intensity-duration-frequency curves for current (left-panel) and future conditions (right-panel)

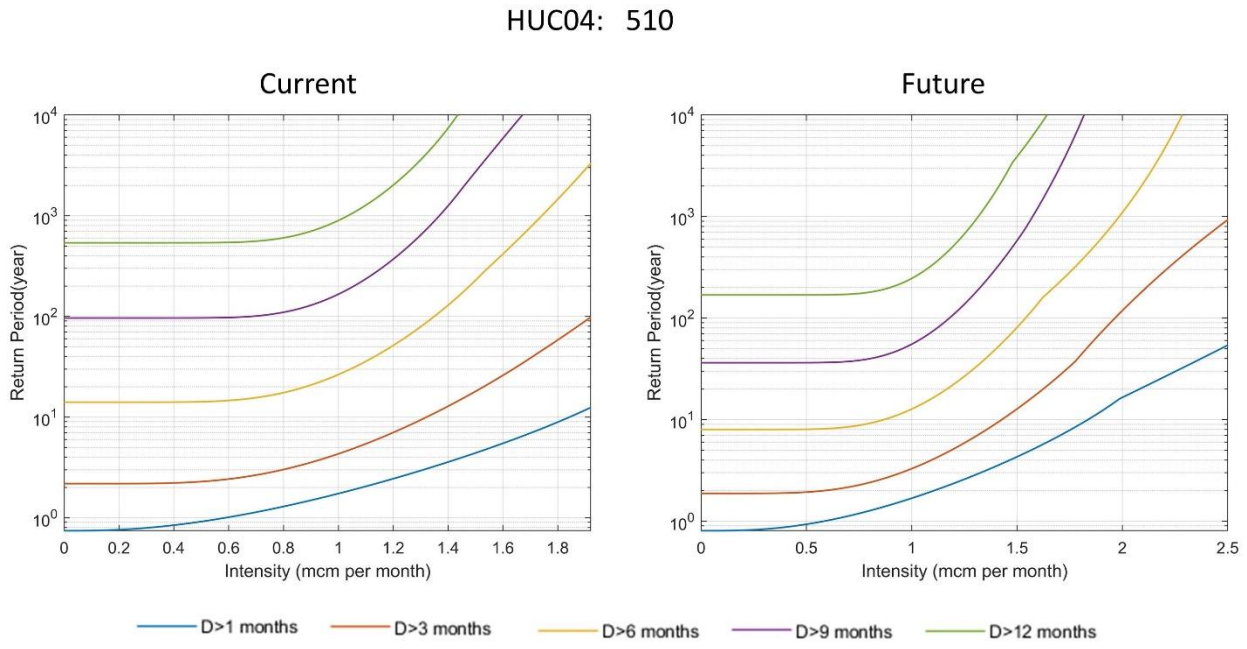

Figure D-42. Intensity-duration-frequency curves for current (left-panel) and future conditions (right-panel)

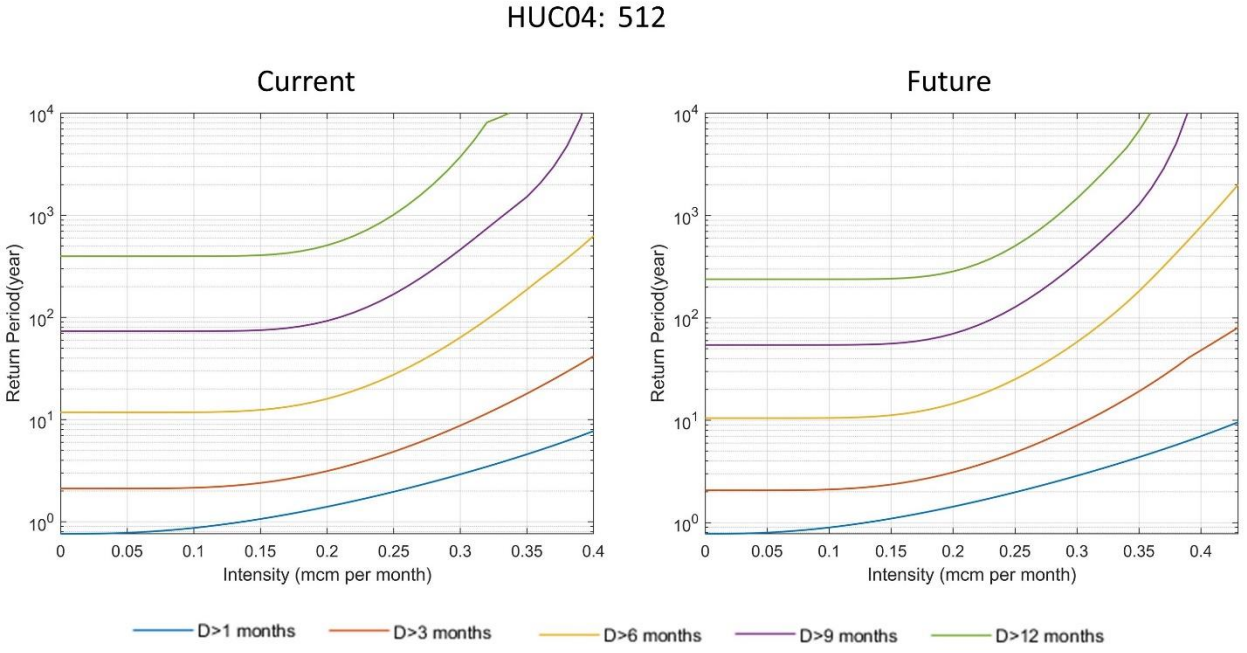

Figure D-43. Intensity-duration-frequency curves for current (left-panel) and future conditions (right-panel)

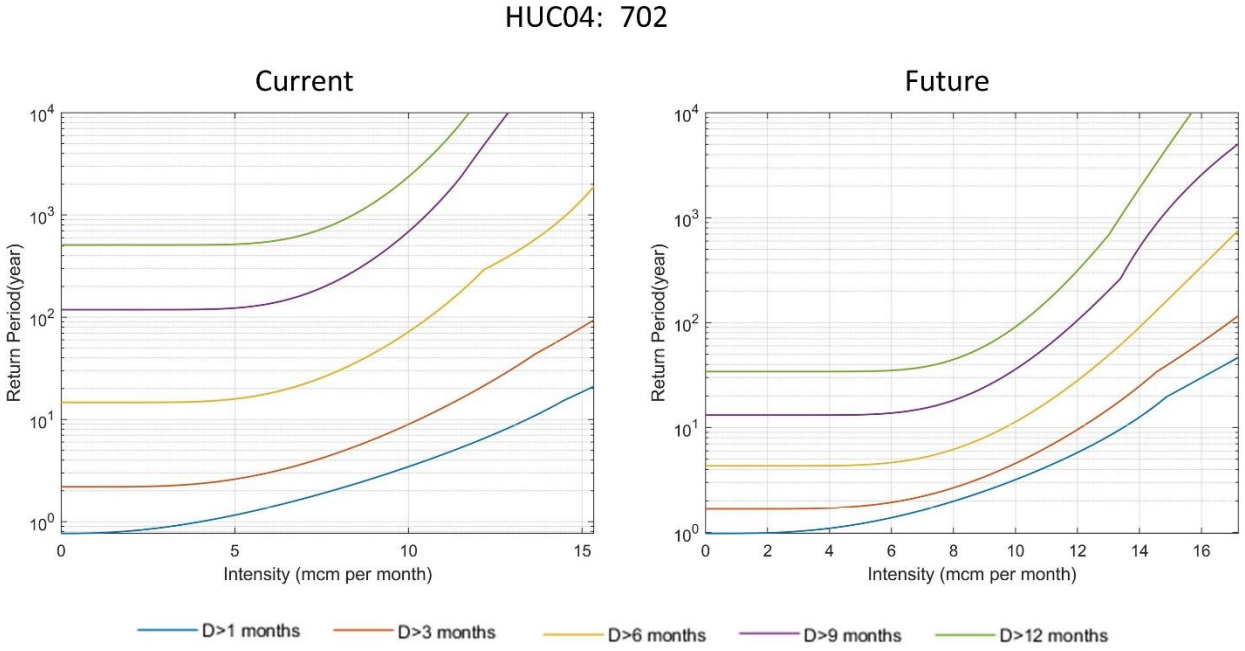

Figure D-44. Intensity-duration-frequency curves for current (left-panel) and future conditions (right-panel)

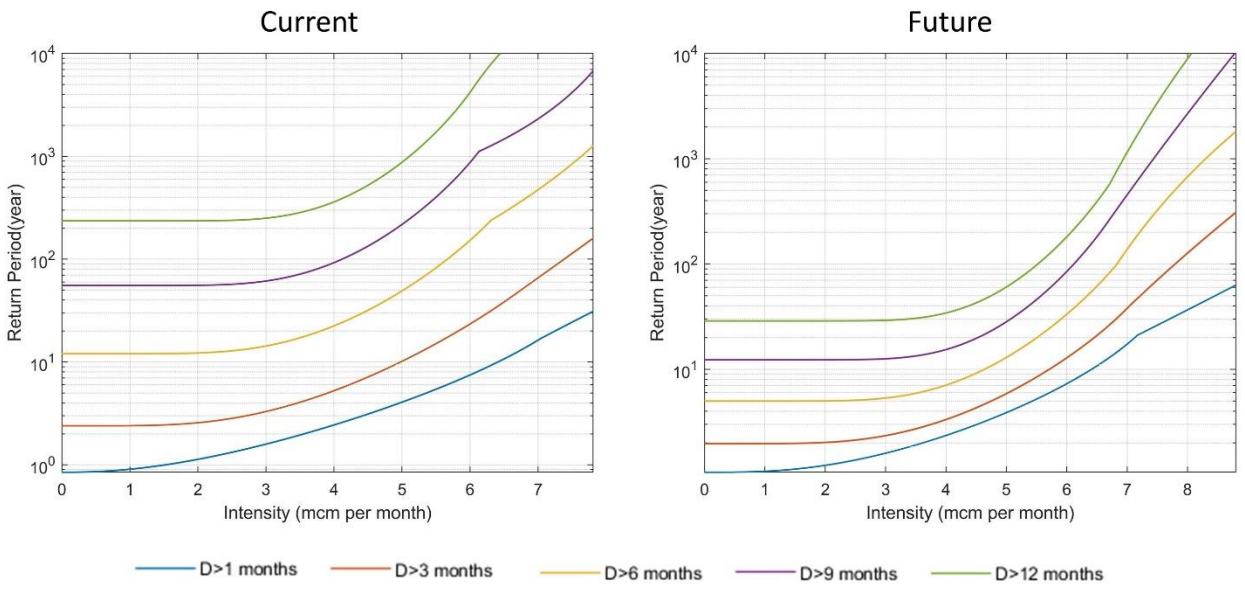

Figure D-45. Intensity-duration-frequency curves for current (left-panel) and future conditions (right-panel)

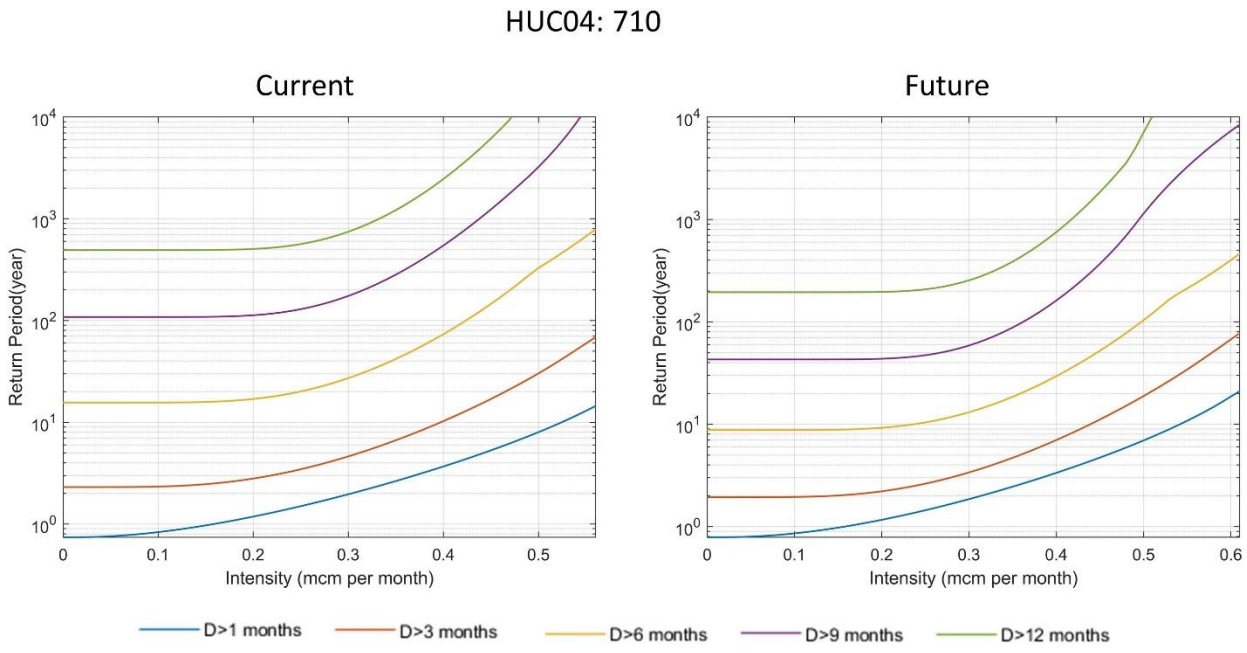

Figure D-46. Intensity-duration-frequency curves for current (left-panel) and future conditions (right-panel)

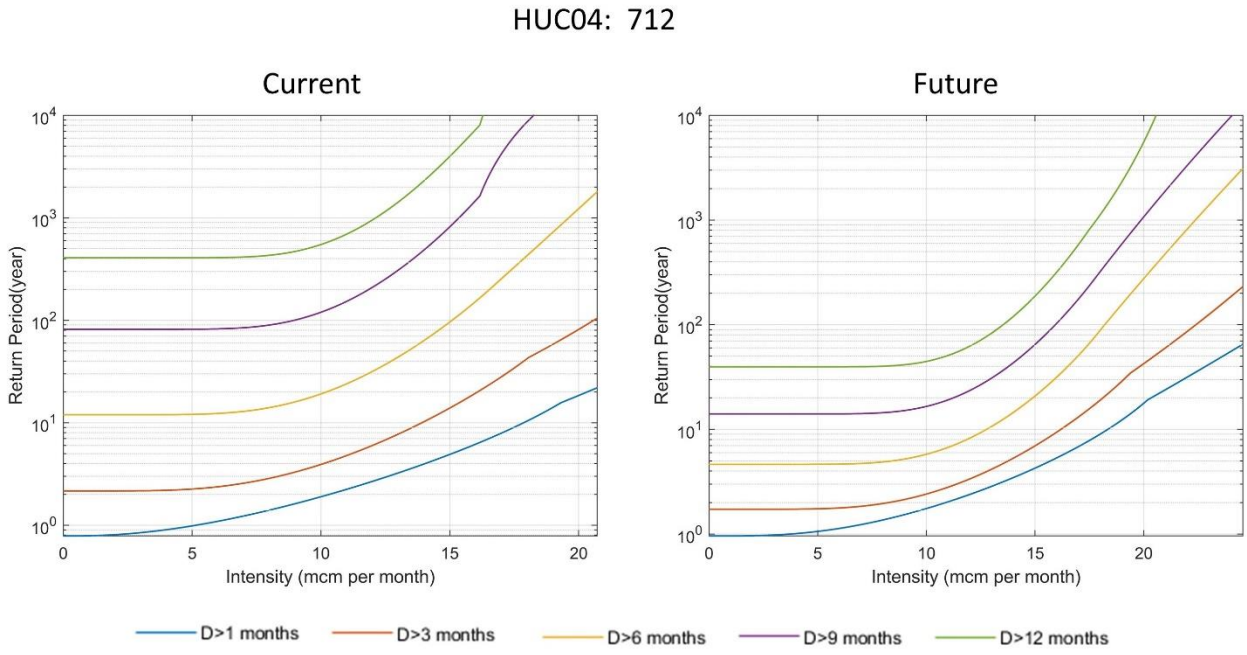

Figure D-47. Intensity-duration-frequency curves for current (left-panel) and future conditions (right-panel)

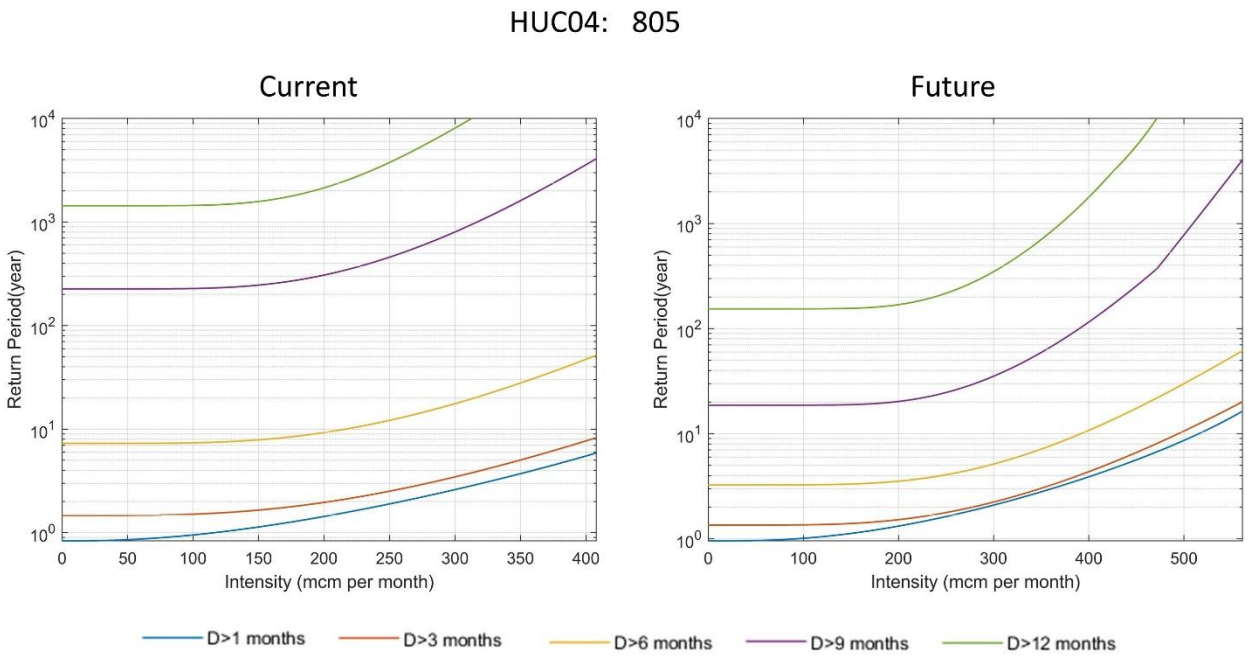

Figure D-48. Intensity-duration-frequency curves for current (left-panel) and future conditions (right-panel)

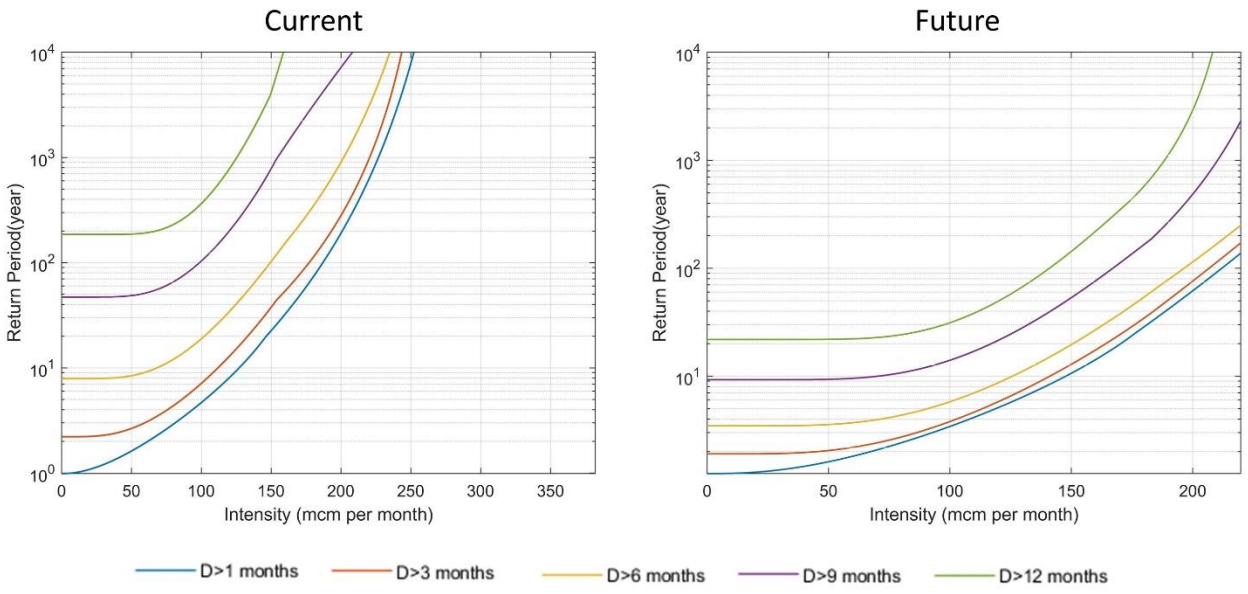

Figure D-49. Intensity-duration-frequency curves for current (left-panel) and future conditions (right-panel)

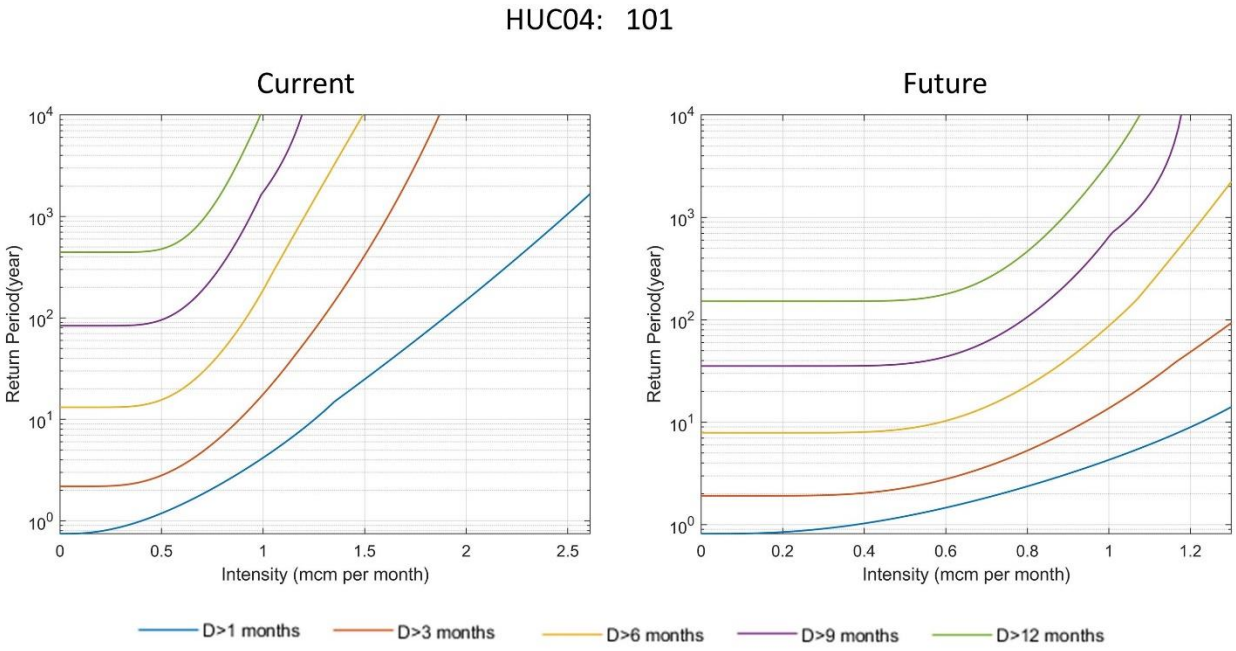

Figure D-50. Intensity-duration-frequency curves for current (left-panel) and future conditions (right-panel)

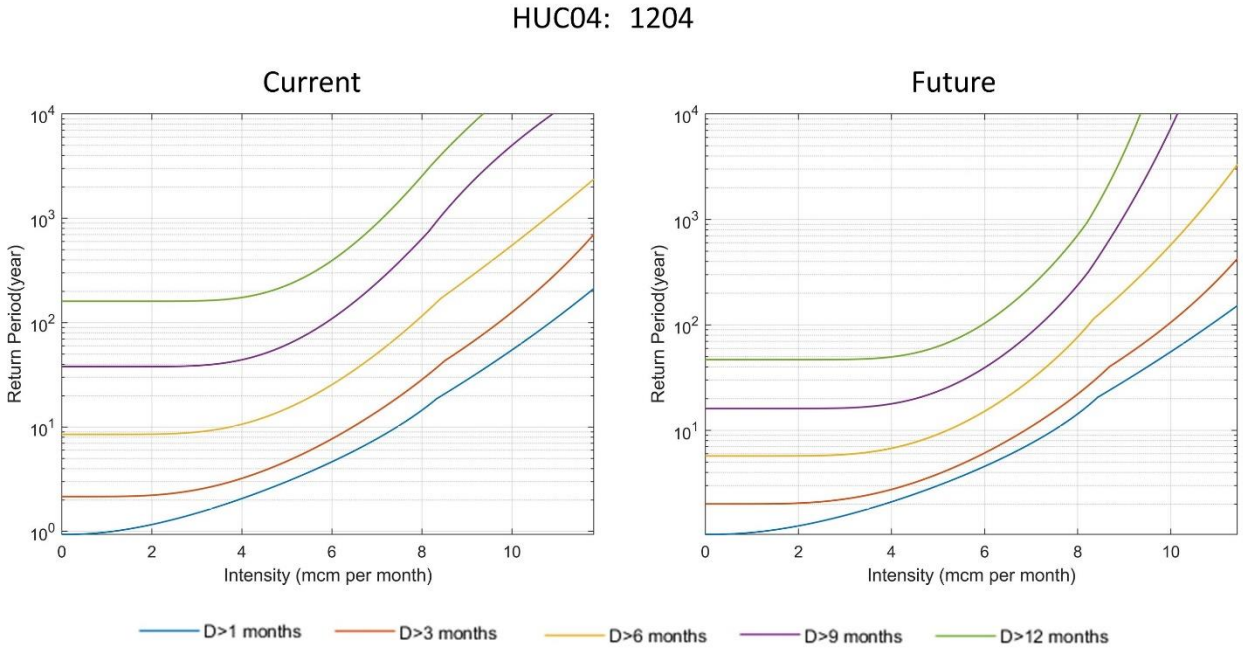

Figure D-51. Intensity-duration-frequency curves for current (left-panel) and future conditions (right-panel)

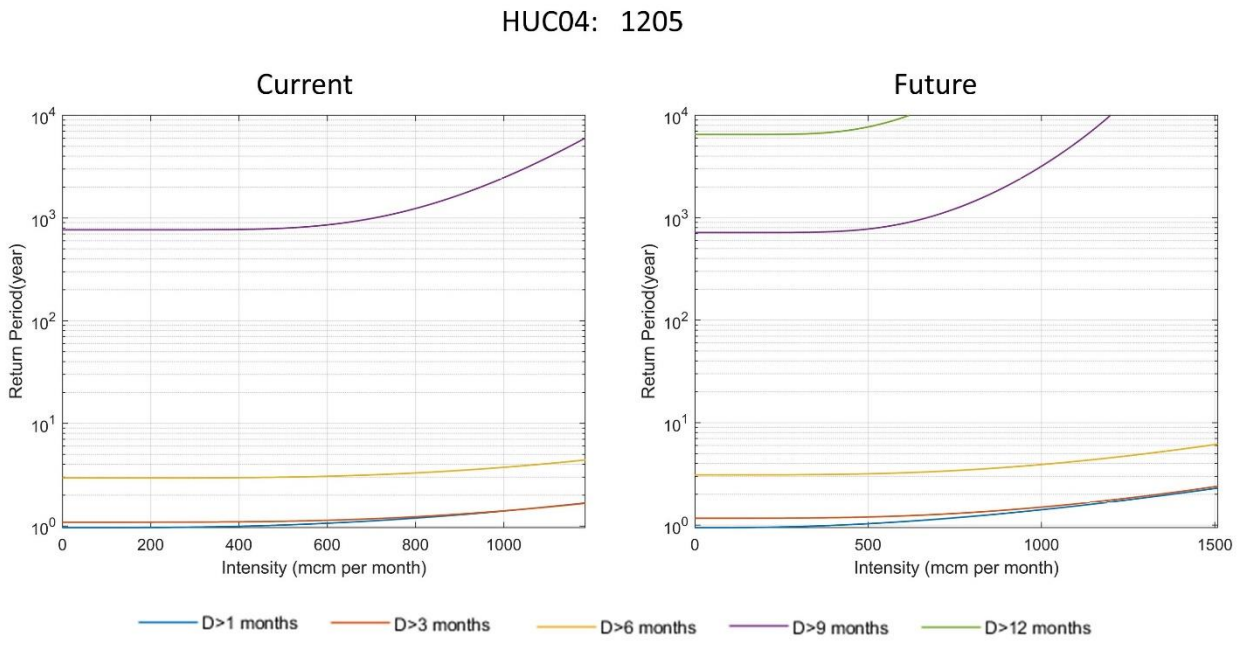

Figure D-52. Intensity-duration-frequency curves for current (left-panel) and future conditions (right-panel)

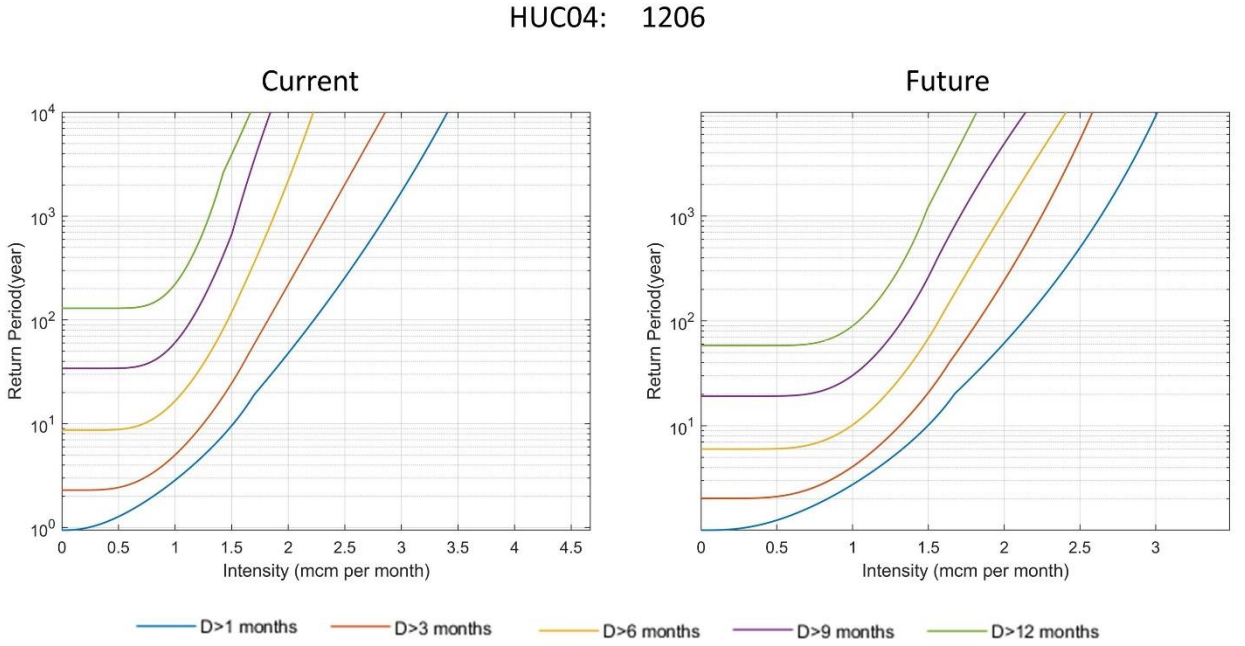

Figure D-53. Intensity-duration-frequency curves for current (left-panel) and future conditions (right-panel)

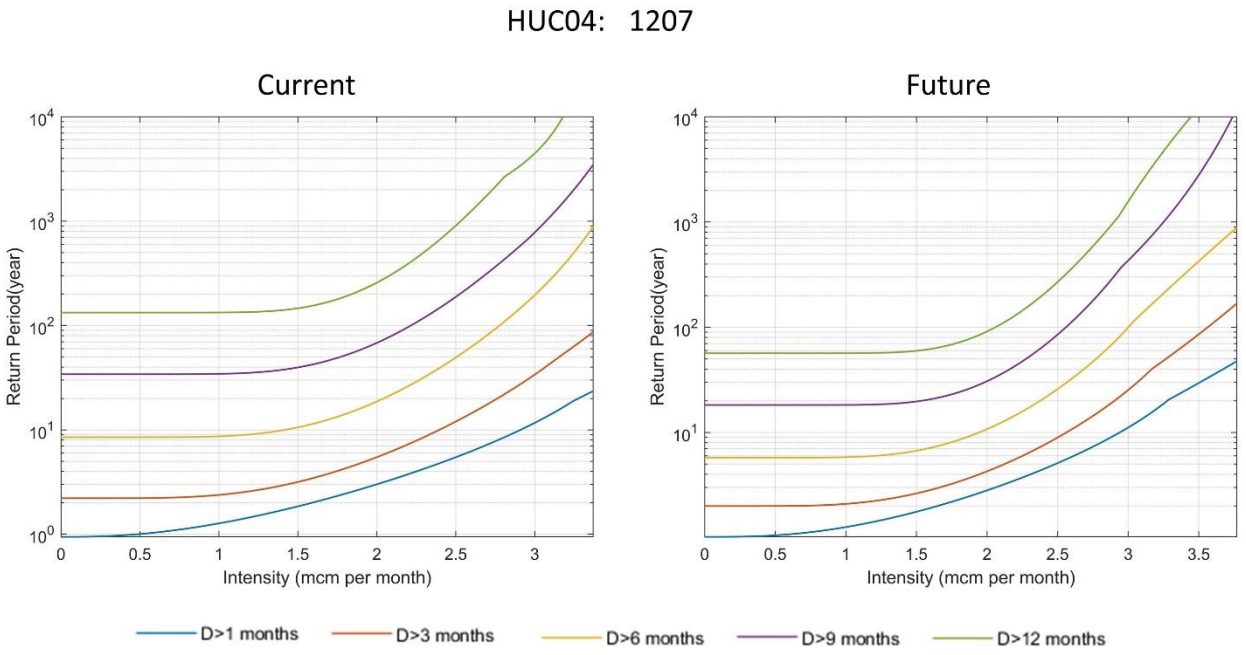

Figure D-54. Intensity-duration-frequency curves for current (left-panel) and future conditions (right-panel)

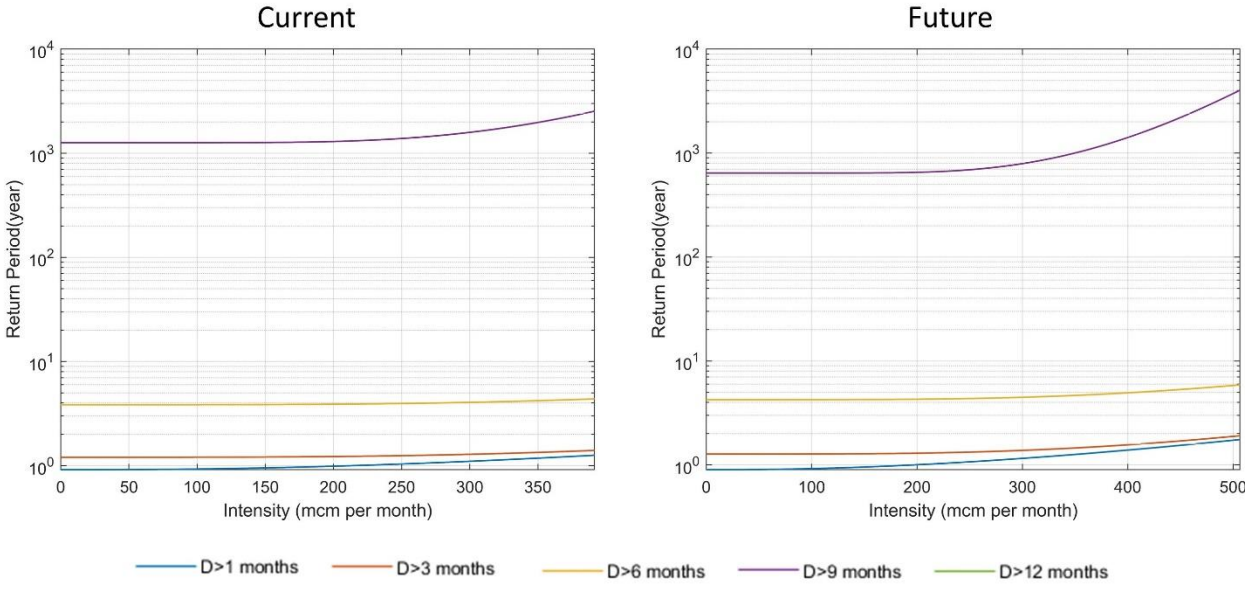

Figure D-55. Intensity-duration-frequency curves for current (left-panel) and future conditions (right-panel)

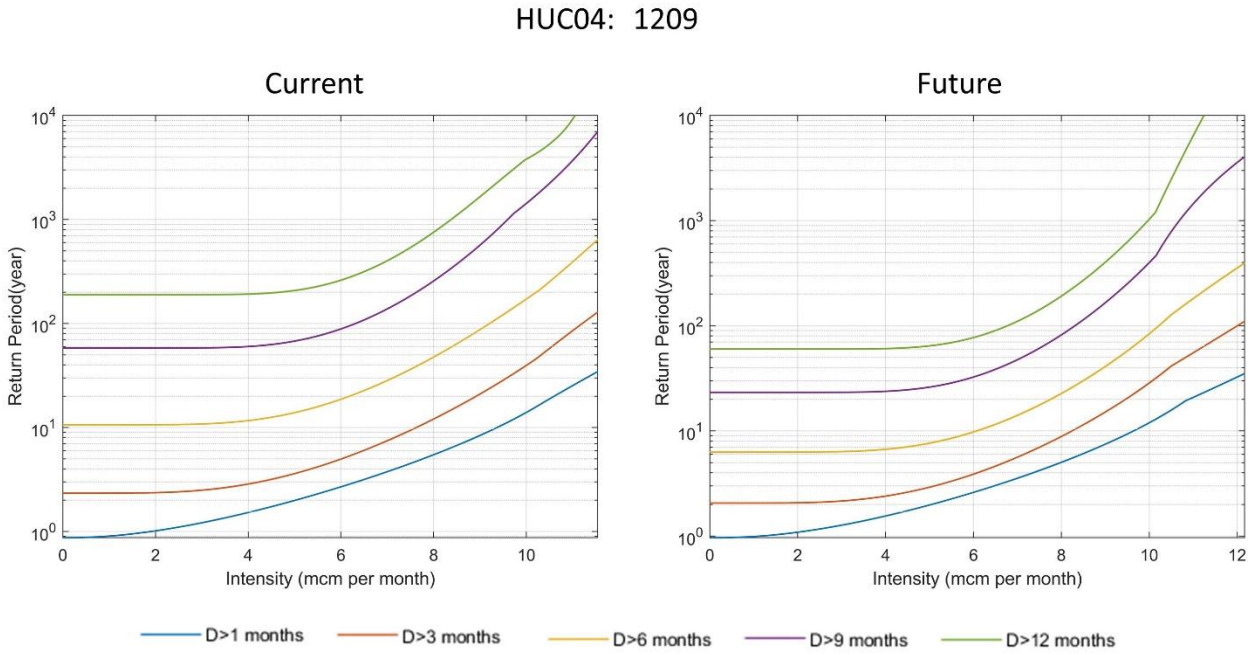

Figure D-56. Intensity-duration-frequency curves for current (left-panel) and future conditions (right-panel)

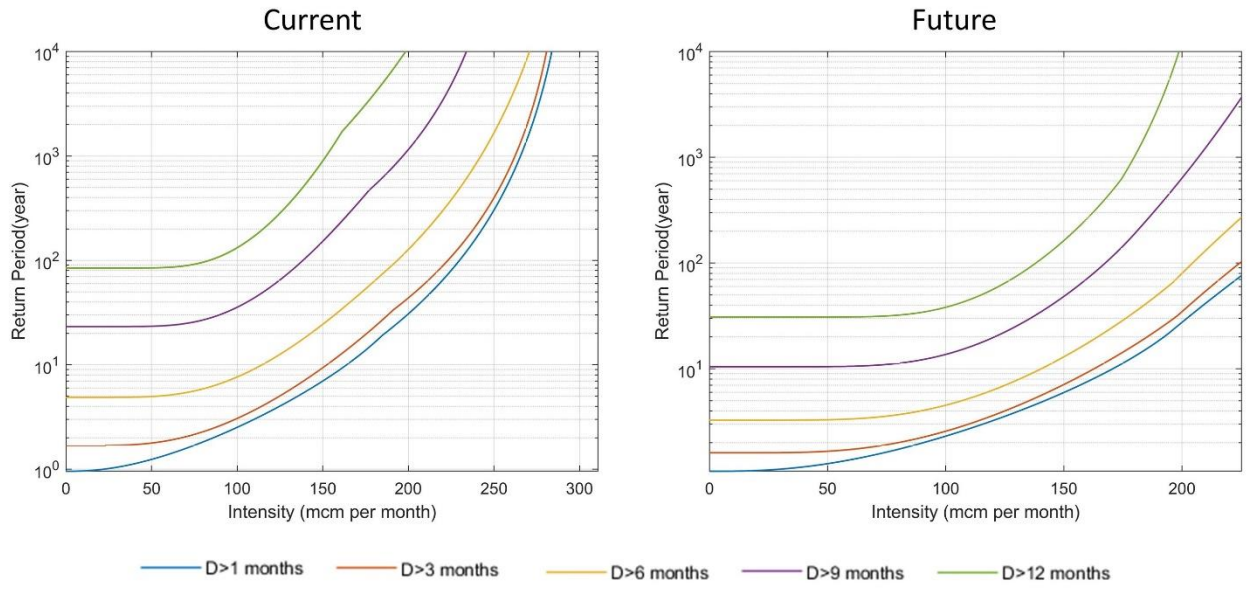

Figure D-57. Intensity-duration-frequency curves for current (left-panel) and future conditions (right-panel)

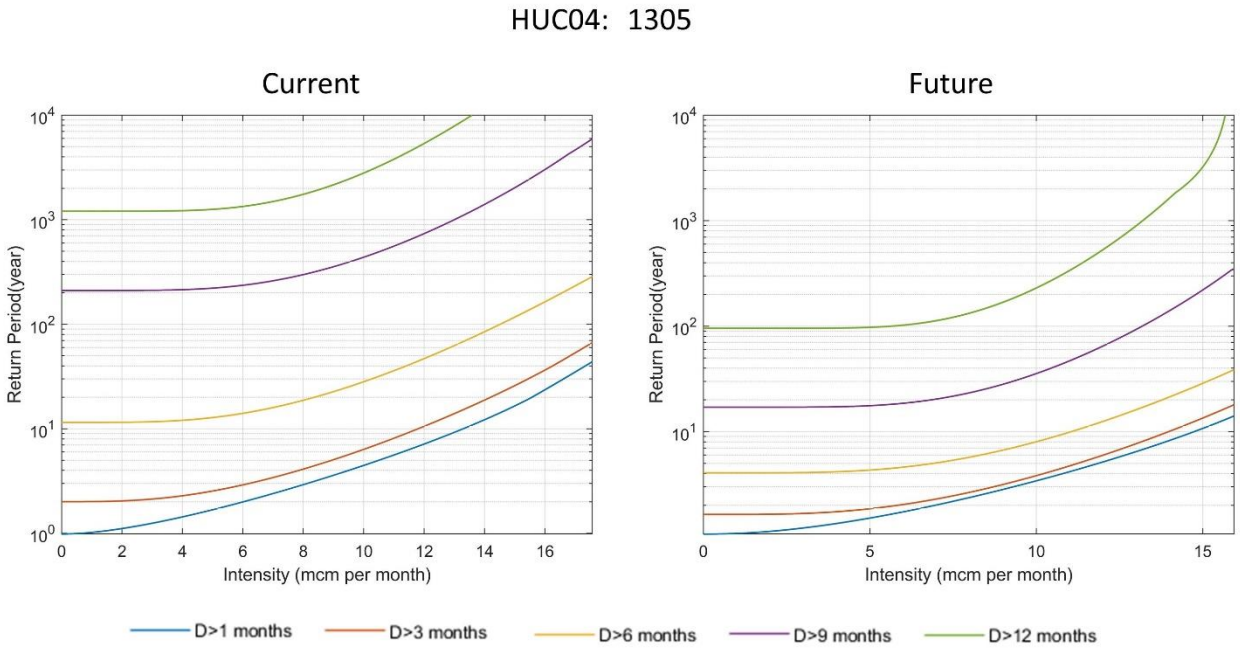

Figure D-58. Intensity-duration-frequency curves for current (left-panel) and future conditions (right-panel)

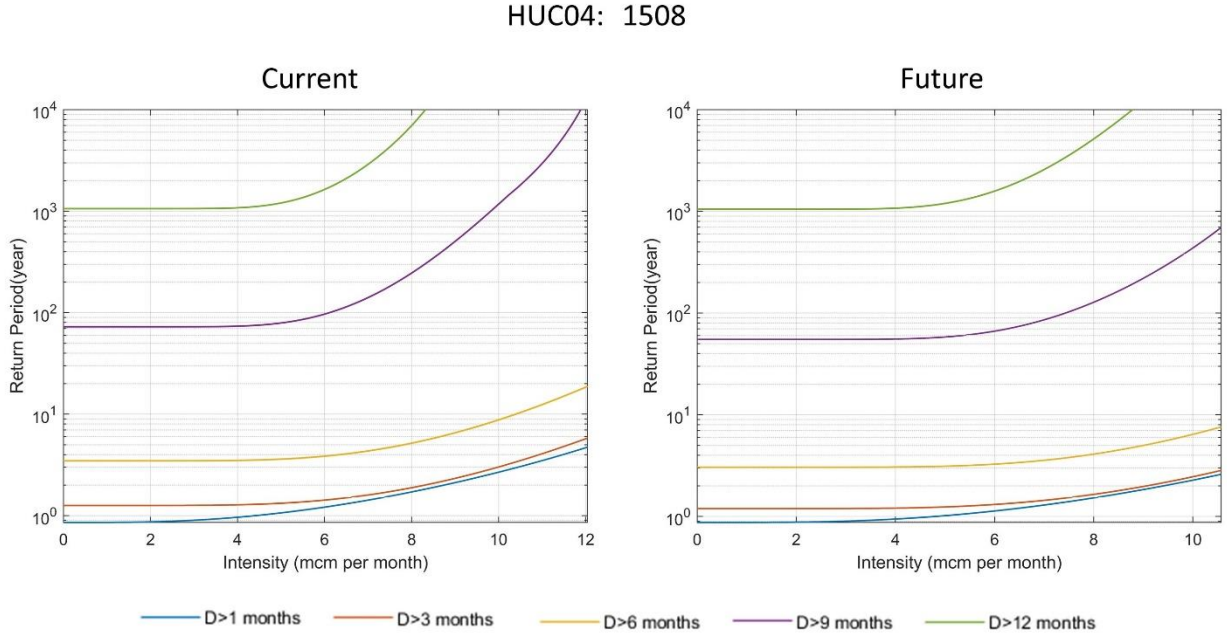

Figure D-59. Intensity-duration-frequency curves for current (left-panel) and future conditions (right-panel)

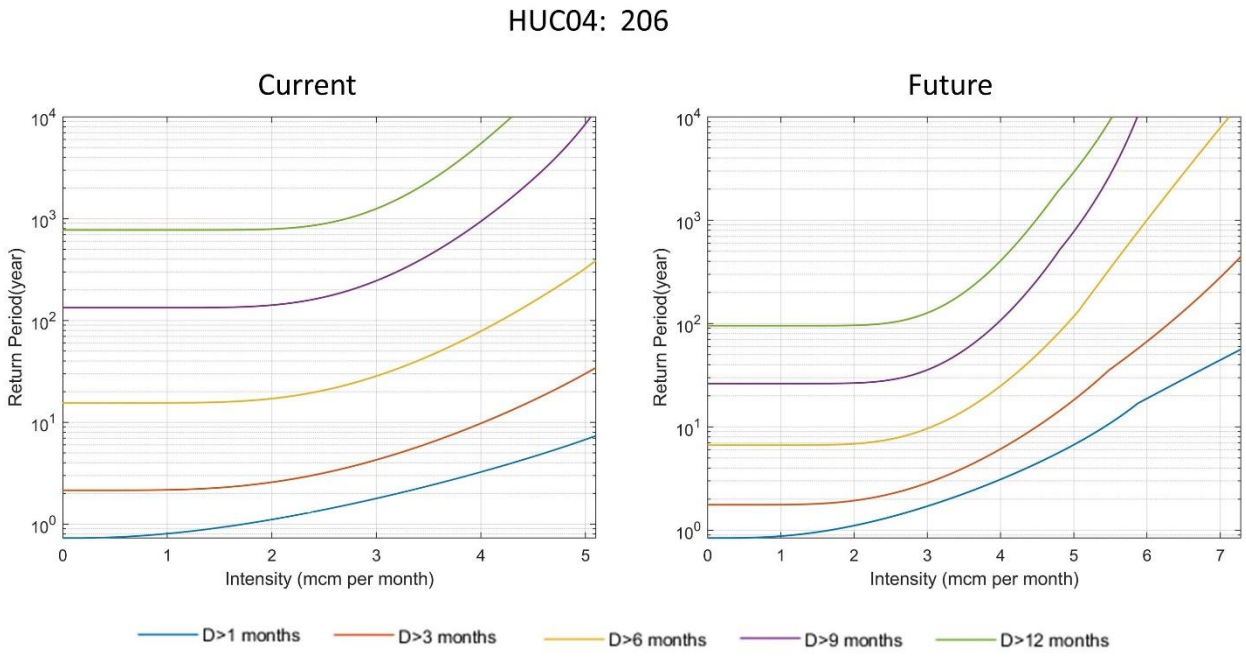

Figure D-60. Intensity-duration-frequency curves for current (left-panel) and future conditions (right-panel)

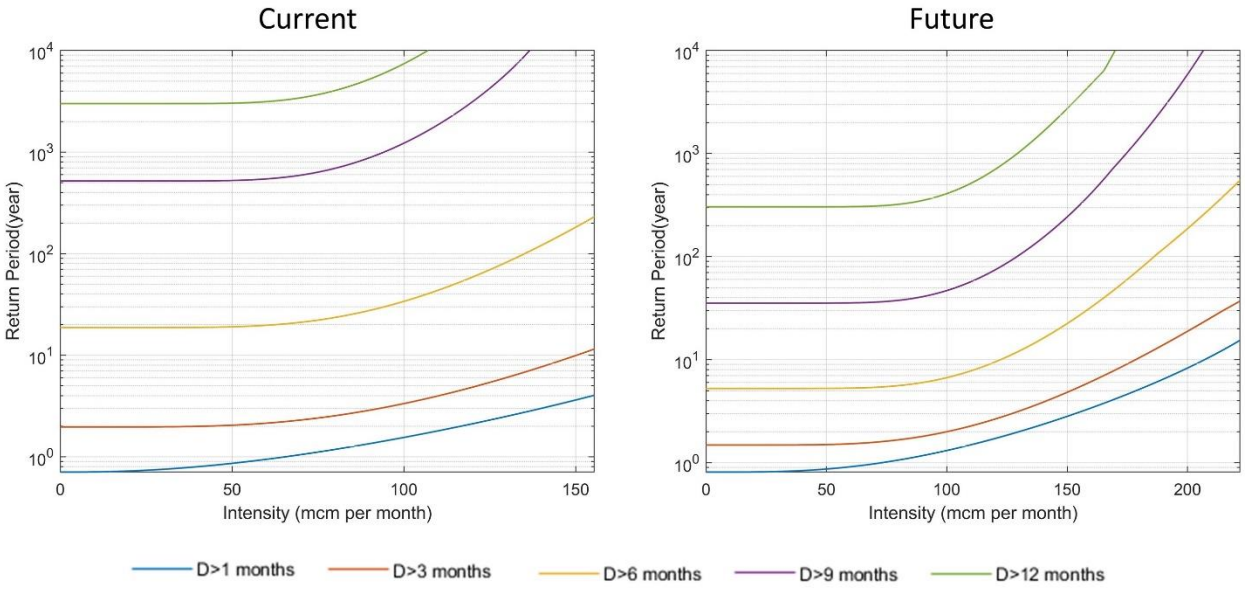

Figure D-61. Intensity-duration-frequency curves for current (left-panel) and future conditions (right-panel)

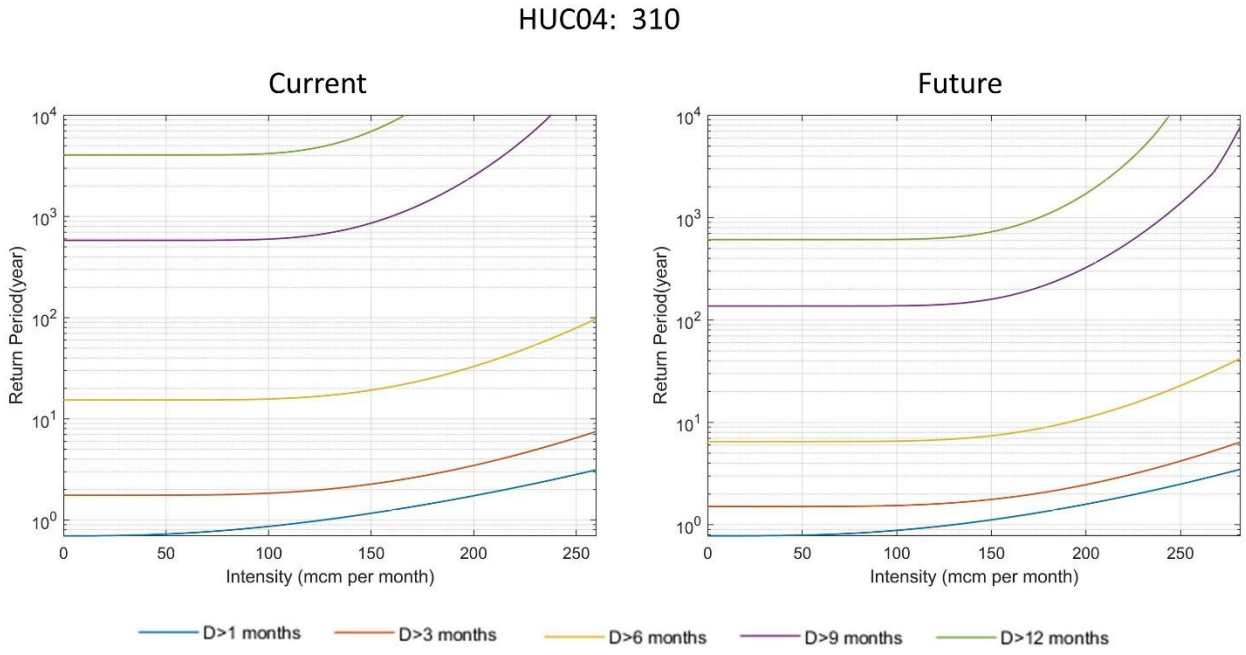

Figure D-62. Intensity-duration-frequency curves for current (left-panel) and future conditions (right-panel)

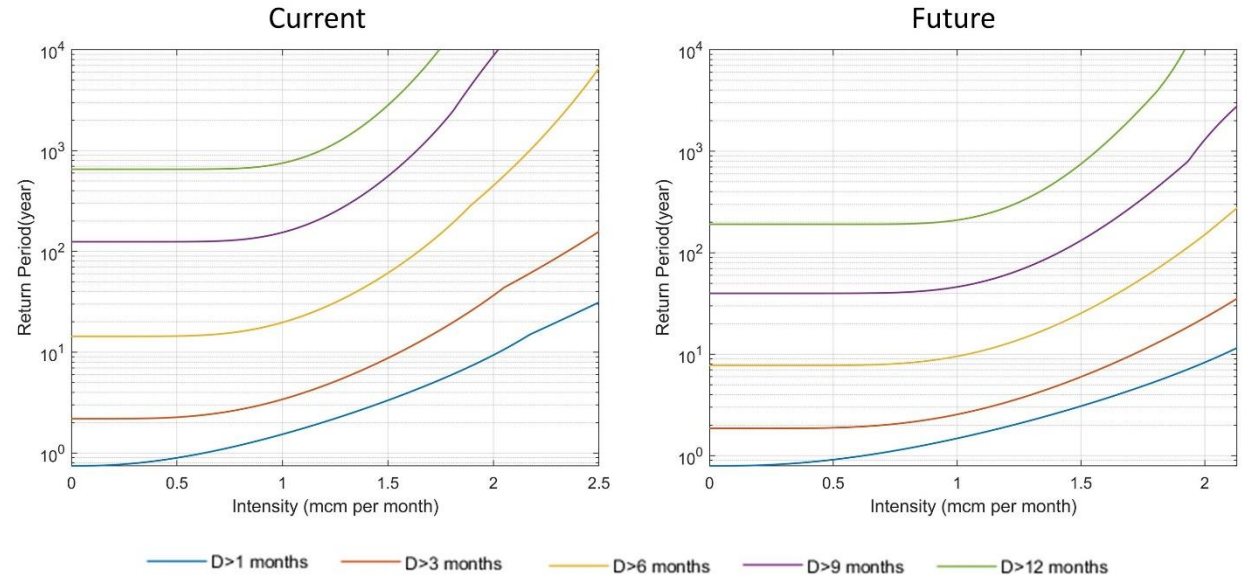

Figure D-63. Intensity-duration-frequency curves for current (left-panel) and future conditions (right-panel)

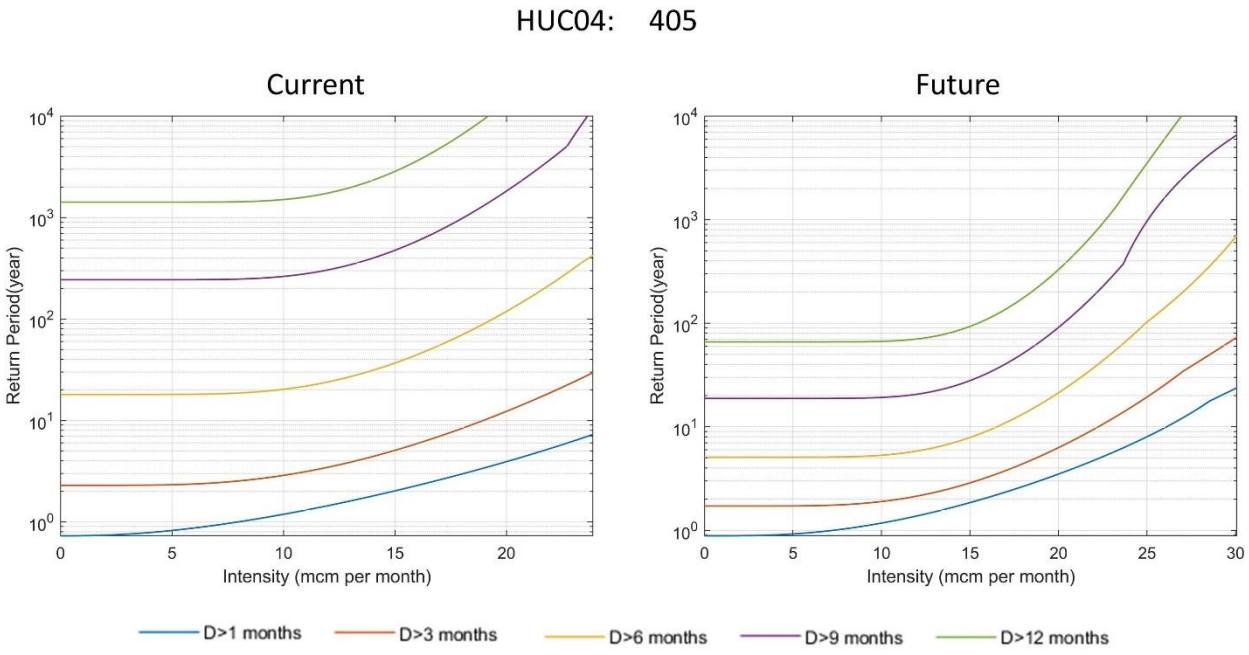

Figure D-64. Intensity-duration-frequency curves for current (left-panel) and future conditions (right-panel)

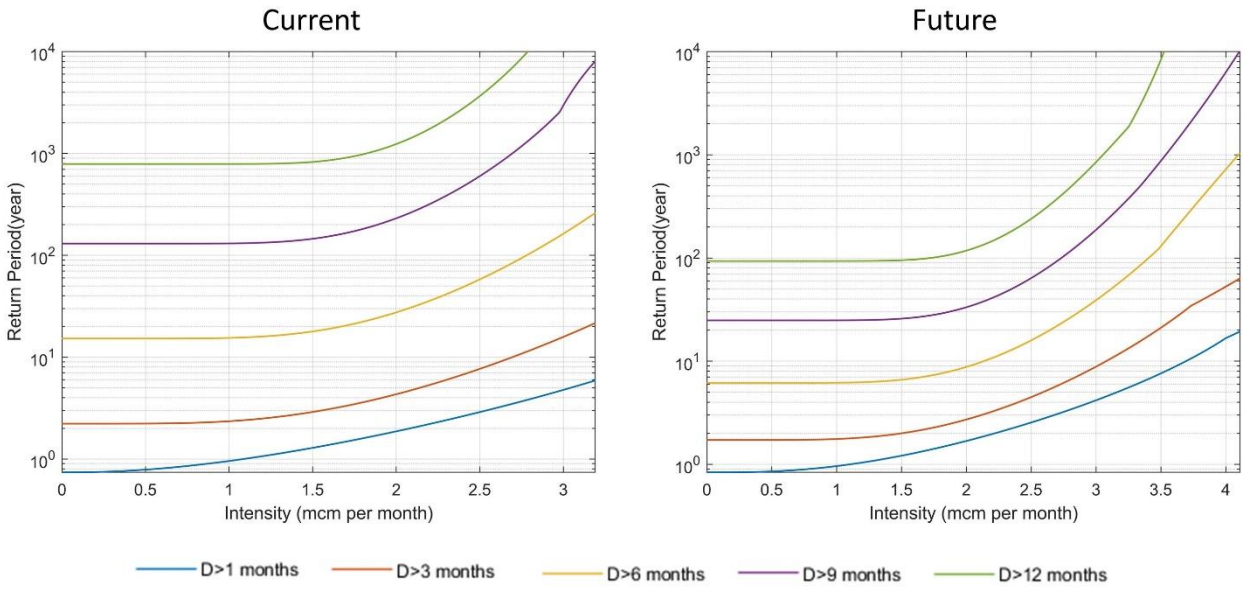

Figure D-65. Intensity-duration-frequency curves for current (left-panel) and future conditions (right-panel)

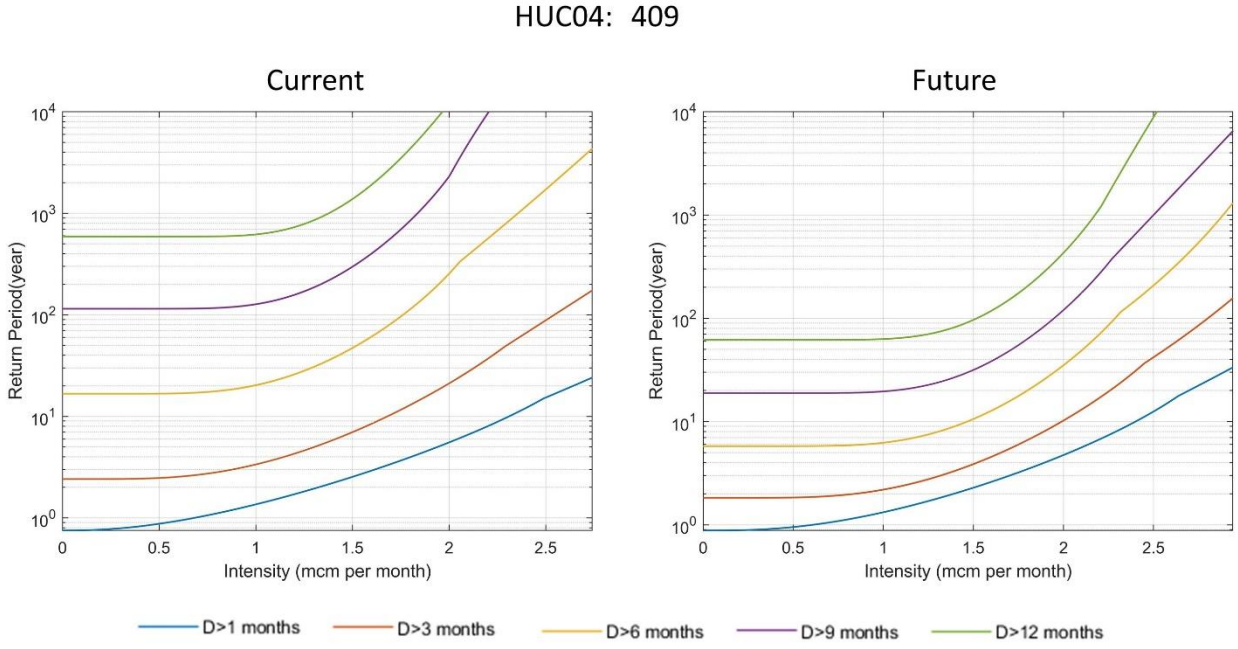

Figure D-66. Intensity-duration-frequency curves for current (left-panel) and future conditions (right-panel)

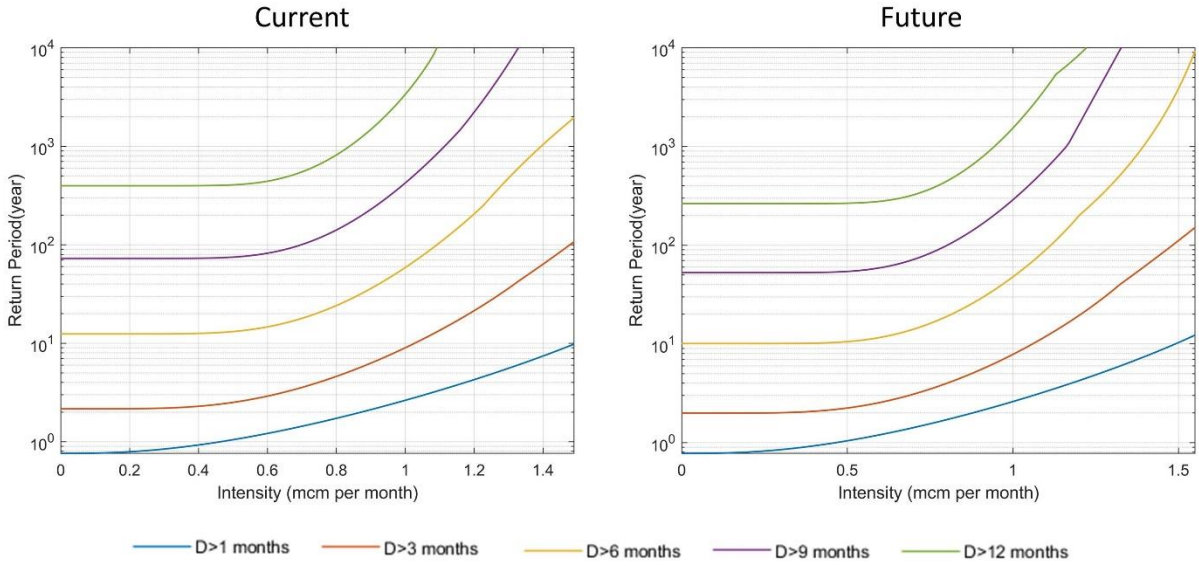

Figure D-67. Intensity-duration-frequency curves for current (left-panel) and future conditions (right-panel)

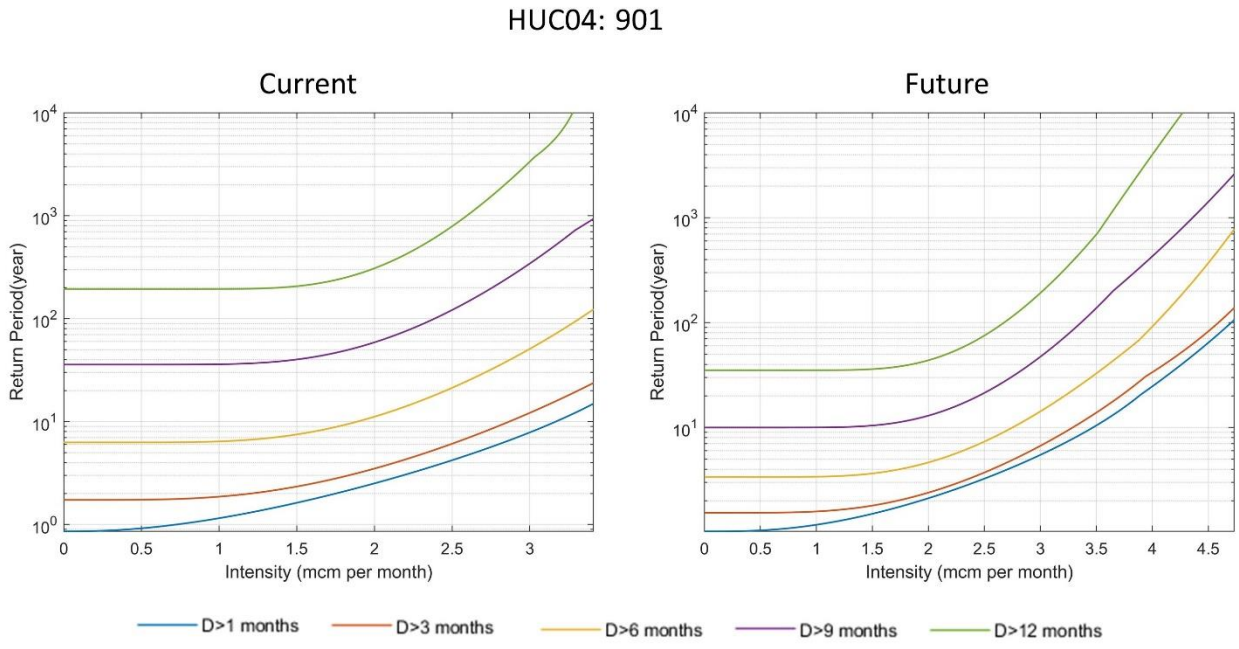

Figure D-68. Intensity-duration-frequency curves for current (left-panel) and future conditions (right-panel)

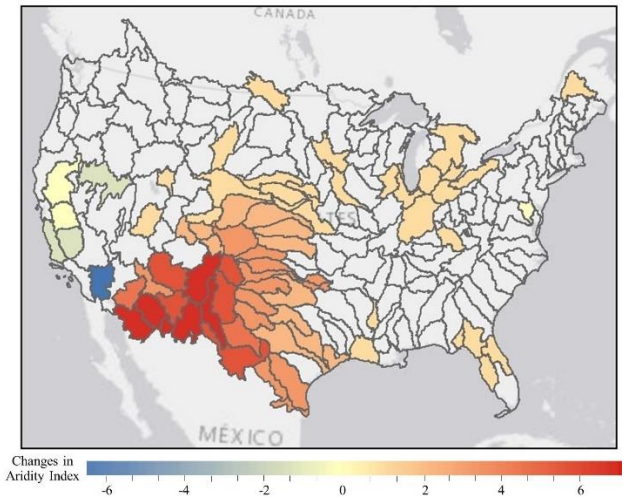

Figure D-69. Changes in the aridity index from current to future conditions under the driest MACA climate model with RCP 8.5.